

https://dspace.org/

Mapping and monitoring urban trees in the City of Johannesburg using remote sensing techniques: the case of Randburg municipal area

Jombo, Simbarashe

2021

https://hdl.handle.net/10539/33073

Downloaded from a DSpace repository. https://dspace.org/



Mapping and monitoring urban trees in the City of Johannesburg using remote sensing techniques: The case of Randburg municipal area

by

Simbarashe Jombo

Submitted to the Faculty of Science, University of the Witwatersrand, Johannesburg, in partial fulfilment of the requirements for the degree of Doctor of Philosophy (Geography and Environmental Science)

Supervisors: Professor Elhadi Adam
Professor Marcus B. Byrne
Professor Solomon W. Newete

Abstract

The precise identification and mapping of urban tree species are vital for the monitoring and management of such ecosystems. Sustainable management of trees requires reliable information about the condition and distribution of the species involved. Municipalities and other stakeholders need such information to facilitate decision making and prioritise resource allocation for effective management of the urban tree ecosystems. Urban tree managers need information on the spatial distribution, status, and changes of urban trees. The heterogeneity and complexity of the urban landscape features, however, make the tree monitoring process challenging. The high structural and spectral intra-species variability and species similarity because of phenology, shadow, and tree age differences limit tree species classification using remote sensing. Traditionally, urban tree classification and mapping were conducted through field-walking surveys which are costly, time-consuming, and labour intensive. However, the technology of remote sensing has overcome such challenges by offering repeatable, time and a cost-effective technique with the advantage of extracting chronological data of the urban trees. The main objective of this study was, therefore, to map and monitor urban trees in Randburg municipal area in the City of Johannesburg (CoJ) using field spectroscopic, WorldView-2 (WV-2), Light Detection and Ranging (LiDAR) and Moderate Resolution Imaging Spectroradiometer (MODIS) data.

First, the study explored the potential of feature selection methods in the classification of urban trees using field spectroscopic data in the Randburg municipal area located in the CoJ. The effectiveness of three feature selection methods, namely, Guided Regularized Random Forest (GRRF), Partial Least Squares Discriminant Analysis (PLS-DA) and Principal Component Analysis Discriminant Analysis (PCA-DA), in selecting key wavelengths in the classification of common urban tree species was investigated and compared. The selected key wavelengths were classified using the Random Forest (RF) and Support Vector Machines (SVM) machine learning algorithms. The feature selection methods reduced the high dimensionality of the field spectroscopic data, with GRRF selecting 13 wavelengths, whilst both PCA-DA and PLS-DA selected 10 wavelengths from the entire dataset (n = 1523). The results indicated that the most key wavelengths were selected from the short-wave infrared (SWIR) region, suggesting that they were the most effective in classifying the common urban tree species. The SVM classifier produced overall accuracy values of 95.3% for the GRRF, 93.3% (PLS-DA) and 86% (PCA-DA). The RF classifier results were 88.7%, 72% and 64% for the GRRF, PLS-DA and PCA-DA methods, respectively. The SVM outperformed RF in the classification of the key wavelengths. The results of this study did not show the desired spatial distribution of the classified urban trees. The results suggested using very high resolution (VHR) multispectral data would better classify, map, and

show the common urban trees spatial distribution in the study area. The results were validated using ground truth data collected in the area of study.

The second part of this study assessed the capability of remote sensing to map and classify urban trees using VHR multispectral data. The WV-2 imagery was used to map the common urban tree species and land use and land cover (LULC) classes in a complex urban environment of the city using pixel-based classification methods. The study tested the utility of WV-2 bands and compared the RF and SVM performance in the classification of common urban trees and LULC classes in the Randburg municipal area. The red, red edge, near-infrared 1 (NIR1), and NIR2 bands played the most important role in classifying the common urban trees and LULC classes. The study produced accuracies of 84.2% using the RF classifier and 81.2% for the SVM classifier. The RF overall accuracy was 3% higher than SVM accuracy in the classification of the common urban trees and LULC classes. There were misclassifications in the study, and these were due to several factors, which include the "mixed pixel problem" and the reference points' location errors. These misclassifications can be dealt with using the object-based classification method. The object-based classification is often indicated as a relatively robust classification method, and therefore, this was investigated in the third part of the study.

The object-based ensemble analysis was examined to classify common urban trees using the WV-2 multispectral imagery. The study tested the object-based method's capability and tested the utility of WV-2 bands and other feature variables in the classification of common urban trees and LULC classes. The performance of the RF and SVM was compared in the object-based classification. The results indicated that the object-based classification is capable of successfully mapping urban trees using WV-2 imagery. The overall classification accuracy was 91.9% for the RF classifier and 87.3% for the SVM classifier. The overall accuracy for the RF improved from 84.2% using the pixel-based classification method to 91.9%, whilst for the SVM algorithm, it increased from 81.2% to 87.3%. The results showed an improvement in the accuracies of the object-based classification of common urban trees and other LULC classes. The near-infrared 1 (NIR1), NIR2 and Normalized Difference Vegetation Index (NDVI) were the most important indices for the trees' effective classification. This study shows that object-based analysis produces better results than the pixel-based approaches because it considers various aspects such as the objects' location, shape, texture, directional pattern and area. It has been noted in previous studies that combining LiDAR data with the VHR multispectral data and vegetation indices can produce higher accuracies using object-based analysis in the classification and mapping of the urban trees. This was investigated in the fourth part of this study.

The effectiveness of LiDAR point-cloud data, WV-2 bands, and vegetation indices were examined to classify and map common urban trees. The study also ranked the importance of the fused dataset (normalised Digital Surface Model (nDSM), WV-2 bands and vegetation indices) in the classification of common urban trees and LULC classes. The results indicate that the fused dataset effectively maps the common urban trees and LULC classes in the study area. This was shown by high accuracies of 97% for the RF classifier and 94% for the SVM classifier. The nDSM was the most effective variable in the classification, as shown by the high Mean Decrease Accuracy (MDA) value of 0.98 and Mean Decrease in Gini (MDG) value of 0.61. The Green Normalised Difference Vegetation Index (GNDVI) was the least important variable with an MDA value of 0.18 and an MDG value of 0.01.

This study provides information to the end-user on the type of data and methods that can be used in the mapping of urban tree species to produce high accuracies. An urban tree inventory and comprehensive urban tree assessment are needed to provide information on the tree distribution and benefits of particular species in an urban environment, including mitigation of air and land temperatures, filtering of gas pollutants, and mitigating consequences of the urban heat island (UHI). This suggested the need to determine the relationship between vegetation and land surface temperature (LST) in the study area.

Finally, the study assessed the spatiotemporal dynamics of vegetation coverage and LST at a city-regional level. The spatial distribution of LST and NDVI was investigated in seven city-regions over five years (2001, 2005, 2010, 2015 and 2020). This study also analysed the mean variances of LST and vegetation cover over the years of study. The study also examined the relationship between LST and NDVI over the period of study. The results indicated an increase in LST in all the city-regions with the highest value of 20.1°C in city-region G, followed by 19.6°C in city-region E. The vegetation cover decreased in all the city-regions over the years of study, with the lowest NDVI value of 0.39 in city-region G, followed by city regions F (0.43) and D (0.48). There was a negative correlation between LST and NDVI values in the study area, ranging from -0.03 to -0.76. This information is useful to urban authorities to find areas that need trees to enforce policies that minimise the cutting down of trees. This study can assist municipalities and other stakeholders involved in urban planning and management of the UHI effects to mitigate local and regional thermal changes.

Overall, this study showed that remote sensing techniques are applicable in the classification and mapping of trees in a heterogeneous urban area. The methodologies in this thesis can be used in

the classification of other tree species in both heterogeneous and homogeneous environments, which adds knowledge to urban tree management. This is important to municipalities, researchers and other stakeholders to develop a comprehensive urban tree inventory, vital in providing sustainable urban tree management.

Declaration

I declare that this work is my original work and has not been previously submitted to obtain any academic qualification. Data and information obtained from published and unpublished work of others have been acknowledged in the text and a list of references is herein provided.

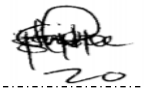
Signature: 

Date: 03 August 2021

Declaration – Plagiarism

I, Simbarashe Jombo, declare that this thesis titled "Mapping and monitoring urban trees in the city of Johannesburg using remote sensing techniques: The case of Randburg municipal area" and the work presented in it are my own. I confirm that:

- This work was done wholly or mainly while in candidature for a research degree at University of the Witwatersrand, Johannesburg.
- Where any part of this thesis has previously been submitted for a degree or any other qualification at this University or any other institution, this has been clearly stated.
- Where I have consulted the published work of others, this is always clearly attributed.
- Where I have quoted from the work of others, the source is always given. With the exception of such quotations, this thesis is entirely my work.
- Where the thesis is based on work done by myself jointly with others, I have made clear exactly what was done by others and what I have contributed myself.

Signature: 

Declaration – Publications and manuscripts

1. Chapter 2 - **Jombo, S.**, Adam, E., Byrne, M.J., Ali, K.A. and Newete, S.W. 2020. Exploring the Potential of Feature Selection Methods in the Classification of Urban Trees using Field Spectroscopy Data. *International Journal of Geospatial and Environmental Research*, 7(3):3. DOI: https://dc.uwm.edu/ijger/vol7/iss3/3
2. Chapter 3 - **Jombo, S.**, Adam, E., Byrne, M.J. and Newete, S.W. 2020. Evaluating the capability of Worldview-2 imagery for mapping alien tree species in a heterogeneous urban environment. *Cogent Social Sciences*, 6(1):1754146. DOI: https://doi.org/10.1080/23311886.2020.1754146
3. Chapter 4 - **Jombo, S.**, Adam, E. and Odindi, J. 2021. Classification of tree species in a heterogeneous urban environment using object-based ensemble analysis and World View-2 satellite imagery. *Applied Geomatics*. DOI: https://doi.org/10.1007/s12518-021-00358-3
4. Chapter 5 - **Jombo, S.**, Adam, E. and Tesfamichael, S. Urban tree classification using point cloud LiDAR data and WorldView-2 satellite imagery in a heterogeneous environment. *International Society for Photogrammetry and Remote Sensing* (Under review).
5. Chapter 6 - **Jombo, S.**, Adam, E., Byrne, M. J and Newete, S. W. Assessing the spatiotemporal dynamics of vegetation coverage and land surface temperature in a heterogeneous urban area. *Remote Sensing* (Under review).

Dedication

This thesis is dedicated to Shamiso Nyakuwa and Dr Robert Nyakuwa. Thank you for giving me your unyielding love, support, and encouragement that inspired me to pursue and complete this research.

This is also dedicated to my late parents: Happy Jabulani Jombo and Marginolia Dorcas Mwandifura. You left us before you could witness this endeavour. God be with you until we meet again.

If you can't explain it simply, you don't understand it well enough."

Albert Einstein

Acknowledgements

I would like to thank Wits for giving me a Merit Award to study for a PhD. My appreciation extends to the City of Johannesburg Corporate Geo-Informatics (DP & UM) department for giving me WorldView-2 satellite imagery and Light Detection and Ranging (LiDAR) data to use in my research. I would also like to thank my supervisors for their assistance in collecting field data and providing the Analytical Spectral Device (ASD) field spectrometer that I used in my research. Without their help, my research could not have been solid. I would also like to thank the Wits School of Governance (WSG) at the University of the Witwatersrand for their financial support during the field data collection through the "Life in City" project (Project number: 2858).

My PhD wouldn't have been complete without assistance from the first supervisor Professor Elhadi Adam. I would also like to thank my co-supervisors, Professor Solomon Newete and Professor Marcus Byrne, for their guidance and support through this study. Thanks to members of the staff and friends who helped me with ideas, namely: Professor Paidamwoyo Mhangara, Natanya Alexander, Professor Stefan Grab, Khanyo Ngubo, Clemence Hlokwa, Nyasha Mureriwa, Dr Patrick "*Pinjo*" Nyamaruze, Baldwin Jenya, Liberty "*Dzvoti*" Mlambo and members of the William Cullen library.

With gratitude, I would like to thank my family, who contributed to my overall well-being. Thanks to Dr Robert Nyakuwa, Shamiso Nyakuwa, Hilary Feruzi, Sithembinkosi Feruzi, Ryan Tinevimbo "*RTN*" Nyakuwa, Celeste Matipa Belva "*CMB*" Nyakuwa, Alana Feruzi, Liam Feruzi, Lorraine Mudzimwa and others, I could not write their full names. Thanks to everyone who played a part in my research for their unequivocal love and support.

Contents

Abstract ..... **i**

Declaration ..... **v**

Declaration – Plagiarism ..... **vi**

Declaration – Publications and manuscripts ..... **vii**

Dedication ..... **viii**

Acknowledgements ..... **x**

List of figures ..... **xvi**

List of tables ..... **xviii**

List of abbreviations ..... **xxi**

Chapter One **1**

General introduction **1**

1.1 Background 2

1.2 The urban environment 3

1.3 Monitoring urban trees 3

1.4 Remote sensing for urban tree mapping 6

1.4.1 Hyperspectral and multispectral sensors in urban tree mapping 6

1.4.2 LiDAR in urban tree mapping 7

1.5 Challenges in urban tree mapping 7

1.6 Research gap and motivation 8

1.7 Research objectives 9

1.8 Scope of the study 9

1.9 Thesis outline 10

Chapter Two **13**

Exploring the potential of feature selection methods in the classification of urban trees using field spectroscopic data **13**

2.1 Introduction 15

2.2 Methodology 18

2.2.1 Study area 18

2.2.2 Identification of common urban trees 19

2.2.3 Field hyperspectral data measurements 21

2.2.4 Feature selection methods 25
2.2.5 Classification techniques 28
2.2.6 Accuracy Assessment 30
2.3 Results 30
2.3.1 PCA-DA wavelength selection results 30
2.3.2 PLS-DA wavelength selection results 32
2.3.3 GRRF wavelength selection results 34
2.3.4 Comparison of the selected wavelengths from the three feature selection techniques (PCA-DA, PLS-DA and GRRF) 36
2.3.5 Accuracy Assessment 37
2.4 Discussion 40
2.4.1 Classification using wavelengths selected by multivariate statistical techniques 41
2.5 Conclusions 41
Chapter Three 43
Evaluating the capability of Worldview-2 imagery for mapping alien tree species in a heterogeneous urban environment 43
3.1 Introduction 45
3.2 Methodology 47
3.2.1 Study area 47
3.2.2 Remote sensing data acquisition 48
3.2.3 Field data collection 49
3.2.4 Data analysis and classification 50
3.3 Results 54
3.3.1 RF parameter tuning 54
3.3.2 SVM parameter tuning 54
3.3.3 RF and SVM in urban tree species mapping 55
3.3.4 Accuracy assessment and validation 59
3.4 Discussion 62
3.5 Conclusions 65
Chapter Four 66
Classification of tree species in a heterogeneous urban environment using object-based ensemble analysis and World View-2 satellite imagery 66
4.1 Introduction 68
4.2 Methodology 70

4.2.1 Study area ... 70
4.2.2 Multispectral remote sensing data and pre-processing ... 71
4.2.3 Ground truth training, test and evaluation samples ... 72
4.2.4 Image classification ... 73
4.3 Results ... 76
4.3.1 Segmentation results ... 76
4.3.2 Shadow index ... 77
4.3.3 Normalized Difference Vegetation Index (NDVI) ... 78
4.3.4 SVM and optimization ... 78
4.3.5 Random forest and optimization ... 79
4.3.6 Classification results ... 80
4.3.7 Accuracy assessment ... 84
4.4 Discussion ... 87
4.5 Conclusions ... 90
Chapter Five ... 91
Urban tree classification using point cloud LiDAR data and WorldView-2 satellite imagery in a heterogeneous environment ... 91
5.1 Introduction ... 93
5.2 Methods ... 96
5.2.1 Study area ... 96
5.2.2 LiDAR data ... 97
5.2.3 Multispectral data ... 99
5.2.4 Vegetation indices ... 100
5.2.5 Reference data ... 101
5.2.6 Image data fusion and classification ... 102
5.2.7 Image segmentation ... 103
5.2.8 Feature selection ... 103
5.2.9 Classification methods ... 104
5.2.10 Accuracy assessment ... 105
5.2.11 McNemar's test ... 106
5.2.12 Variable selection ... 106
5.3 Results ... 107
5.3.1 Segmentation of used dataset ... 107
5.3.2 Classification of the common urban tree species and LULC classes ... 107
5.3.3 Validation ... 108

5.3.4 Statistical comparisons 113
5.3.5 Variable importance and ranking 113
5.4 Discussion 116
5.4.1 Effectiveness of fused data 116
5.4.2 Accuracies and Mcnemar's test 117
5.4.3 Importance of WV-2 bands, vegetation indices and nDSM 118
5.4.4 Importance of the study 119
5.5 Conclusions 119
Chapter Six 121
Assessing the spatiotemporal dynamics of vegetation coverage and land surface temperature in a heterogeneous urban area 121
6.1 Introduction 123
6.2 Materials and methods 126
6.2.1 Study area 126
6.2.2 Multispectral remote sensing data 127
6.2.3 Statistical analysis 129
6.3 Results 130
6.3.1 Spatiotemporal distribution and variations of LST 130
6.3.2 Validation of MODIS LST data 132
6.3.3 Spatiotemporal distribution and variations of NDVI 133
6.3.4 Analysis of variance on MODIS LST and NDVI data 136
6.3.5 Relationship between LST and NDVI 137
6.4 Discussion 138
6.5 Conclusions 141
Chapter Seven 142
Synthesis 142
7.1 Introduction 143
7.2 Summary of the findings 144
7.2.1 The potential of feature selection methods in the classification of urban trees using field spectroscopy data. 144
7.2.2 The capability of remote sensing to classify and map urban alien tree species using high-resolution multispectral data. 145
7.2.3 The ability of object-based ensemble analysis in classifying common urban trees using high-resolution multispectral data. 147

7.2.4 The ability of a combination of airborne LiDAR point-cloud data and very high-resolution imagery in the classification and mapping of common urban trees. 148

7.2.5 The spatiotemporal dynamics of vegetation coverage and LST in a heterogeneous urban area. 148

7.3 Conclusions 149

References 153

List of figures

Figure 2.1 Map of South African provinces, Johannesburg's regions and a basemap showing the Randburg municipal area located in the City of Johannesburg. a) South African provinces b) City of Johannesburg's regions A to G and c) basemap showing Randburg municipal area from QGIS software (version 3.12.0) by QGIS Development Team (2020). 19
Figure 2.2 Tree bouquets of the common urban trees in the study area. The common urban trees are a) *Eucalyptus* spp., b) *Jacaranda mimosifolia*, c) *Platanus* x *acerifolia*, d) *Platanus occidentalis*, e) *Pinus* spp. and f) *Quercus* spp. 20
Figure 2.3 Wavelengths selected using the VIP method for the six urban trees in this study using PCA-DA. The trees are *Eucalyptus* spp. (EC), *Jacaranda mimosifolia* (JC), *Quercus* spp. (QS), *Platanus occidentalis* (PO), *Platanus* x *acerifolia* (PA) and *Pinus* spp. (PN). 32
Figure 2.4 Discriminatory power for PLS-DA components using all hyperspectral wavelengths data (n = 1523). The 10-fold cross-validation resampling method was used to get cross-validation accuracy results for the components. The optimal component with the highest accuracy value is shown in bold. 33
Figure 2.5 Wavelengths selected using the VIP method for the six common urban trees in this study using PLS-DA. The six common urban trees are *Eucalyptus* spp. (EC), *Jacaranda mimosifolia* (JC), *Quercus* spp. (QS), *Platanus occidentalis* (PO), *Platanus* x *acerifolia* (PA) and *Pinus* spp. (PN). 34
Figure 2.6 The mean decrease in Gini index showing the variable of importance for all the variables (n = 1523) for the traditional RF classifier. The important variables have a high mean decrease in Gini index value. 35
Figure 2.7 The wavelengths with the highest importance scores selected by the GRRF as calculated by the traditional RF for the urban trees. 36
Figure 3.1 Maps of South African provinces, Johannesburg's regions and true-colour WorldView-2 satellite imagery (RGB 532 combination) of the Randburg municipal area located in the City of Johannesburg. 48
Figure 3.2 Average spectral reflectance curves extracted from Worldview-2 imagery pixels for the five dominant alien tree species considered in this study. 50
Figure 3.3 RF parameters (*mtry* and *ntree*) after optimization utilizing the 10-fold cross-validation sampling method and OOB estimate of error rate. 54
Figure 3.4 SVM parameters (γ and C) after optimization utilizing the 10-fold cross-validation sampling method and cross-validation error rate. 55
Figure 3.5 Classified maps of the five urban tree species and other classes in the Randburg municipal area using a) RF and b) SVM machine learning algorithms. 56
Figure 3.6 Importance of WV-2 multispectral bands in RF classification using Mean Decrease Accuracy (MDA) values. 58
Figure 3.7 The Mean Decrease Accuracy (MDA) values showing the relationship between each class and WV-2 spectral bands. The classes are bare land (BL), built-up (BU), *Eucalyptus* spp. (EC), Grassland (GL), *Jacaranda* spp. (JC), *Platanus* spp. (PL), *Quercus* spp. (QR), other woody vegetation (OWV), *Pinus* spp. (PN) and Shadow (SW). 59
Figure 4.1 a) South African provinces, b) City of Johannesburg's regions A to F and c) basemap showing Randburg municipal area. 71
Figure 4.2 (a) Subsection of WV-2 true colour image and (b) segmented WV-2 image for the study area. 77

Figure 4.3 (a) Subsection of WV-2 true colour image; (b) Subsection of WV-2 image with shadow areas in black; and (c) binary image with the value 0 indicating shadow and 1 (non-shadow areas) in the study area. 77
Figure 4.4 (a) Subsection of WV-2 true colour image; (b) Subsection of the WV-2 image showing vegetated image objects in green using the NDVI threshold value (> 0.3) in the study area. 78
Figure 4.5 10–fold cross-validation technique in optimizing SVM RBF kernel parameters (C and γ). 79
Figure 4.6 10–fold cross-validation technique in optimizing RF parameters (*mtry* and *ntree*). The error rate was determined using the OOB sample for all different combinations. 80
Figure 4.7 Mapping results of urban trees and other LULC classes using a) SVM and b) RF classifiers. 81
Figure 4.8 MDA for WV-2 bands, NDVI and length (pixels) in the RF model. 83
Figure 4.9 MDA for the LULC classes and variables used in the study. 84
Figure 5.1 The map shows a) South African provinces and b) ESRI's basemap showing Randburg municipal area 97
Figure 5.2 a) Hillshade view of Digital Terrain Model (DTM) and b) Normalised Digital Surface Model (nDSM) for the study area. 99
Figure 5.3 a) Subsection of the fused dataset (WV-2 bands, vegetation indices and nDSM) and b) segmented subsection of the fused dataset. 107
Figure 5.4 Classification maps for common urban trees and land use and land cover (LULC) classes using a) RF and b) SVM classifiers. 108
Figure 6.1 Map of South Africa and the study area with the seven city-regions (A-G) of the City of Johannesburg. 126
Figure 6.2 Maps with mean LST values for city-regions A to G in the city of Johannesburg over the study periods of a) 2001, b) 2005, c) 2010, d) 2015, and e) 2020. 131
Figure 6.3 Mean MODIS LST values for city-regions A to G in the years: 2001, 2005, 2010, 2015 and 2020. 132
Figure 6.4 Ground-based weather station vs MODIS LST values in degrees Celsius (°C) for the years: 2001, 2005, 2010, 2015 and 2020. 133
Figure 6.5 Maps with mean NDVI values for city-regions A to G in the years: a) 2001, b) 2005, c) 2010, d) 2015 and e) 2020. 135
Figure 6.6 The mean NDVI values for city-regions A to G in the study area for the years: 2001, 2005, 2010, 2015 and 2020 136

List of tables

Table 2.1 Spectral reflectance and images for the six urban trees examined in this study..... 23

Table 2.2 Principal Component Analysis (PCA) results showing the proportion of variance (PV) and cumulative proportion (CP) in percentage (%) and eigenvalues for the first 10 principal components (PCs) of reflectance values from six urban tree species. 31

Table 2.3 Wavelengths selected by the PCA-DA, PLS-DA and GRRF techniques. The wavelength that was able to differentiate in both PLS-DA and GRRF is highlighted in grey..... 36

Table 2.4 Confusion matrix obtained using SVM classifier for the selected wavelengths using PCA-DA, PLS-DA and GRRF. The overall accuracy (OA) and kappa values are shown for the urban trees namely; *Eucalyptus* spp. (EC), *Jacaranda mimosifolia* (JC), *Quercus* spp. (QS), *Platanus occidentalis* (PO), *Platanus* x *acerifolia* (PA) and *Pinus* spp. (PN). 38

Table 2.5 Confusion matrix obtained using RF classifier for the selected wavelengths using PCA-DA, PLS-DA and GRRF. The overall accuracy (OA) and kappa values are shown for the urban trees namely; *Eucalyptus* spp. (EC), *Jacaranda mimosifolia* (JC), Quercus spp. (QS), *Platanus occidentalis* (PO), *Platanus* x *acerifolia* (PA) and *Pinus* spp. (PN)..... 39

Table 2.6 Producer's accuracy (PA) and user's accuracy (UA) values for RF and SVM obtained from the optimal wavelengths selected using PCA-DA, PLS-DA and GRRF for the trees used in this study. The trees are *Eucalyptus* spp. (EC), *Jacaranda mimosifolia* (JC), *Quercus* spp. (QS), *Platanus occidentalis* (PO), *Platanus* x *acerifolia* (PA) and *Pinus* spp. (PN)..... 40

Table 3.1 WV-2 spectral resolution and sensor band names used in this study..... 49

Table 3.2 Scientific and common names, code, training, test and total samples used in this study. 50

Table 3.3 Area in hectares (ha) and percentage cover of LULC classes acquired using the RF and SVM classification methods. The classes are bare land (BL), built-up (BU), *Eucalyptus* spp. (EC), Grassland (GL), Jacaranda spp. (JC), Platanus spp. (PL), Quercus spp. (QR), Other woody vegetation (OWV), Pinus spp. (PN) and Shadow (SW)..... 58

Table 3.4 Confusion matrices using a) RF and b) SVM classification algorithms. The classes are bare land (BL), built-up (BU), *Eucalyptus* spp. (EC), Grassland (GL), *Jacaranda* spp. (JC), *Platanus* spp. (PL), *Quercus* spp. (QR), Other woody vegetation (OWV), *Pinus* spp. (PN) and Shadow (SW). The producer's accuracy (PA), overall accuracy (OA), user's accuracy (UA), and kappa coefficient calculated using the 'rasclass' package in R on the test dataset..... 61

Table 3.5 Comparison of Random Forest (RF) and Support Vector Machines (SVM) classification methods using McNemar's test. CC stands for correctly classified, and IC is for incorrectly classified samples. 62

Table 4.1 WorldView-2 spectral band configuration..... 72

Table 4.2 Number of training and test samples used in this study 73

Table 4.3 Variables used in a rule set for all LULC classes in this study. 76

Table 4.4 Area of coverage in hectares (ha) and percentage (%) for the two classified maps using SVM and RF classifiers. The classes are bare land (BL), built-up (BU), *Eucalyptus* spp. (EC), Grassland (GL), *Jacaranda* spp. (JC), *Platanus* spp. (PL), *Quercus* spp. (QS), other woody vegetation (OWV), *Pinus* spp. (PN) and Road (RD). 83

Table 4.5 Confusion matrices for a) SVM and b) RF classifiers. The classes are bare land (BL), built-up (BU), *Eucalyptus* spp. (EC), Grassland (GL), *Jacaranda* spp. (JC), *Platanus* spp. (PL), *Quercus* spp. (QS), other woody vegetation (OWV), *Pinus* spp. (PN) and Road (RD). The overall accuracy (OA), user's accuracy (UA), producer's accuracy (PA) and the kappa value were computed on the test dataset using the 'rasclass' package in R (Version 3.5.2). 86

Table 5.1 Summary of flight and sensor characteristics of the LiDAR survey used in this study. 98

Table 5.2 Vegetation indices used in this study. 101

Table 5.3 Total number of training and test datasets for common trees and land use and land cover (LULC) classes used in this study..... 102

Table 5.6 The comparison of classification accuracies for RF and SVM classifiers using McNemar's test. The McNemar's chi-squared value is represented by $\chi 2$ and Σ is for summation. 113

Table 6.1 Some of the suburbs located in the seven city-regions of the City of Johannesburg (CoJ). 127

Table 6.2 Temperature, wind and humidity readings collected at Johannesburg-Botanical Gardens weather station at the time of MODIS LST imagery overpass..... 129

Table 6.3 Minimum (Min), maximum (Max) and standard deviation (SD) land surface temperature (LST) values for city-region A to G for the years 2001, 2005, 2010, 2015 and 2020 in the study area. 130

Table 6.4 Minimum (Min), maximum (Max) and standard deviation (SD) values for NDVI in city-regions A to F for 2001, 2005, 2010, 2015 and 2020 in the study area. 134

Table 6.5 Two-way ANOVA test results with the Tukey's post hoc test in the city-regions for LST values for the years: 2001, 2005, 2010, 2015 and 2020..... 137

Table 6.6 Two-way ANOVA test results with the Tukey's post hoc test in the city-regions for NDVI values for the years: 2001, 2005, 2010, 2015 and 2020..... 137

Table 6.7 The Pearson correlation coefficients between MODIS LST and NDVI for the seven city-regions over the study periods: 2001, 2005, 2010, 2015 and 2020..... 138

List of abbreviations

ANOVA	Analysis of variance
APEX	Airborne Prism Experiment
ASD	Analytical Spectral Device
BRDF	Bidirectional reflectance distribution
CART	Classification and regression trees
CoJ	City of Johannesburg
CP	Cumulative proportion
CV	Cross-validation
DAFF	Department of Agriculture, Forestry and Fisheries
DEM	Digital Elevation Model
DSM	Digital Surface Model
DTM	Digital Terrain Model
FSO	Feature Space Optimization
GA	Genetic Algorithm
GNDVI	Green Normalized Difference Vegetation Index
GPS	Global Positioning System
GRRF	Guided Regularized Random Forest
IDW	Inverse Distance Weighting
JCP	Johannesburg City Parks
KIA	Kappa index of agreement
LDA	Linear Discriminant Analysis
LIDAR	Light Detection and Ranging
LST	Land surface temperature
LULC	Land use and land cover
MDA	Mean decrease in accuracy
MDG	Mean decrease in Gini
MNF	Minimum Noise Fraction
MODIS	Moderate Resolution Imaging Spectroradiometer
MRS	Multi-resolution segmentation
NASA	National Aeronautics and Space Administration
NCSS	Number Cruncher Statistical System
NDRE	Normalized Difference Red Edge Index
NDRE2	Normalized Difference Red Edge Index 2

nDSM	normalized Digital Surface Model
NDVI	Normalized Difference Vegetation Index
NDVI2	Normalized Difference Vegetation Index2
NDVIGR	Normalized Difference Vegetation Index-Green/Red Ratio
NDVIY	Normalized Difference Vegetation Index-Yellow
NFAP	National Forest Action Programme
NIR	Near-infrared
OBIA	Object-based image analysis
OOB	Out-of-bag
PCA	Principal Component Analysis
PCA-DA	Principal Component Analysis Discriminant Analysis (PCA-DA)
PLS	Least Squares
PLS-DA	Partial Least Squares Discriminant Analysis
PV	Proportion of variance
RBF	Radial basis function
RF	Random Forest
RMSE	Root Mean Square Error
ROC	Receiver Operating Characteristic
RRF	Regularized random forest
SAWS	South African Weather Service
SD	Standard deviation
SI	Shadow Index
SVM	Support Vector Machines
SWIR	Short-wave infrared
UAV	Unmanned aerial vehicles
UHI	Urban heat island
USGS	United States Geological Survey
UV-Vis-NIR	Ultraviolet-visible and near infra-red
VHR	Very high resolution
VHSR	Very high spatial resolution
VIP	Variable importance in the projection
WV	WorldView

Chapter One

General introduction

1.1 Background

The world is encountering accelerating urban growth and urbanisation, which have significantly changed the urban landscape (Li *et al.*, 2019). Urban landscapes are complex mosaics, with varying land use and land cover (LULC) features such as buildings, roads and pavements, and tree species thrive (Czaja *et al.*, 2020). Urban trees are defined as all privately and publicly owned trees in urban areas, and this includes individual trees along the streets and in the backyard, as well as stands of remnant forests (Comas et al., 2010; Dangulla et al., 2020). Tree species are an essential component of the urban ecosystem (Yan *et al.*, 2018). Urban trees provide a range of ecosystem services that benefit humans directly or indirectly, which serves as a basis for social welfare and economic development (Roy *et al.*, 2012; Timilsina *et al.*, 2020).

Urban trees play a vital role in *inter alia*, providing shade that reduces air temperature (Aval *et al.*, 2019), recreation, provide habitat for animals (Scholz *et al.*, 2018) and reduce noise (Ellis and Mathews, 2019). The information on urban tree species is vital to environmentalists, city planners, municipal leaders and urban forest managers to know the location of tree species and implement effective plans and programs that support sustainable urban tree management (Alonzo *et al.*, 2016; Roman *et al.*, 2020). An effective urban tree management plant requires timely, precise and accurate information on the distribution, conditions and patterns of trees at temporal and spatial levels (Li *et al.*, 2019). Despite the huge demand for precise and accurate information on urban trees, recent studies (e.g. Ordóñez *et al.*, 2019; Brabant *et al.*, 2019; Jombo *et al.*, 2020) indicate that urban tree inventories are lacking or incomplete and they need to be updated.

In general, urban tree classification has previously been done using traditional approaches such as ground surveys and field walking surveys (Fassnacht *et al.*, 2014; Wen *et al.*, 2017). However, these approaches are labour intensive, costly and time-consuming due to the heterogeneity of urban landscapes, while remote sensing data have progressively complemented the costly traditional approaches (Cleve *et al.*, 2008). Remote sensing techniques are fast, efficient and provide timely and low-cost information on urban trees (Myeong *et al.*, 2006). More recently developed remote sensing sensors, such as multispectral, hyperspectral and Light Detection and Ranging (LiDAR) systems are effective and a less-costly way of depicting the characteristics of urban trees. They capture structural and spectral signatures that provide important information for mapping urban trees at a large aerial extent (Sothe *et al.*, 2019). For instance, the structure (3D arrangement of trees, e.g. tree height, size of stems and volume) functional characteristics, species richness and diversity or all urban trees can be detected, classified, mapped, inventoried, monitored and

modelled using remote sensing techniques (Li *et al.*, 2019). Over the past decade, studies that have used multispectral and hyperspectral data in urban tree mapping have increased (Alonzo *et al.*, 2014; Puissant *et al.*, 2014; Li *et al.*, 2015; Shojanoori *et al.*, 2016; Liu *et al.*, 2017; Le Louarn *et al.*, 2017), although their application is still limited in heterogeneous urban landscapes. They generally concluded that urban tree mapping can successfully be done using multispectral and hyperspectral data.

1.2 The urban environment

The global urbanisation rates are accelerating, and the proportion of people residing in urban environments is expected to increase from 58% in the year 2018 to 68% by the year 2050 (United Nations Publications, 2019). The rise in urban population around the world calls for proper use and management of resources to support urban dwellers' livelihoods (Nilsson *et al.*, 2013). One way to achieve this is through the management of urban trees and/or forests to maximize the benefits they provide which include improving air quality (Pu and Landry, 2020), mitigating urban heat island effects (Yan *et al.*, 2018), supporting biodiversity (Seiferling *et al.*, 2017) and sequestering carbon (Nowak *et al.*, 2008), among others.

1.3 Monitoring urban trees

Urban trees management is vital for city managers in municipal councils or stakeholders involved in urban tree management (Ajewole, 2010). Municipal councils have introduced urban greening initiatives to meet global environmental challenges (Roman *et al.*, 2020). These initiatives include planting more trees in urban parks, cemeteries and gardens, creating green patches linked by greenways or green corridors and innovation of greening sites (Jim, 2013). Municipalities need to quantify the impact of urban trees on the ecosystems and develop policies for tree planting and conservation to achieve urban tree management goals (Ajewole, 2010).

The metropolitan cities can be harsh environments for tree species due to various factors, and these include their susceptibility to pests and diseases, climatic and air conditions, and soil pollution (Konijnendijk *et al.*, 2005; Thomsen *et al.*, 2016). The presence and distribution of trees in urban areas are also affected by infrastructure and location preferences of the tree planters (Agarwal *et al.*, 2013). Urban trees can grow in soils that are toxic and compacted, impacting the growing space for tree roots and upper branching (Czaja *et al.*, 2020). The increased land need for basic amenities such as housing and road construction reduces the amount of urban green spaces (Schäffler and Swilling, 2013). The reduction in urban green spaces and an increase in impervious surfaces have negative impacts, including the emergence of the urban heat island (UHI) (Alexander, 2020).

The lifespan of trees in urban environments is short due to the amount of stress they are exposed to (Konijnendijk *et al.*, 2005; Ellis and Mathews, 2019; Czaja *et al.*, 2020). There is a loss of urban trees in South Africa, but it has never been accounted for due to a lack of government support or research focus to provide urban tree information (Shackleton, 2006). Comprehensive information on urban trees is required for urban tree management (Escobedo *et al.*, 2011). An urban tree inventory is vital for proper planning and management to promote urban greening (Azeez *et al.*, 2019). A detailed urban tree inventory requires the inclusion of physical parameters such as tree height, spatial distribution, location, crown depth, species type, tree height and age (Zhang and Qiu, 2012). Several methods, such as pixel and object-based classification techniques, can be used in preparing an urban tree or forest inventory (Azeez *et al.*, 2019). The acquisition of data and management of urban tree information faces several challenges, including the data collection method and analysis techniques used (Zhang *et al.*, 2015).

Urban tree inventories have traditionally been carried out using field survey methods, and these include the use of sampling procedures and plot data collection approaches (Nowak *et al.*, 2008). Nonetheless, the field survey methods cannot replicate the amount of information required for a detailed urban tree inventory desirable for planning and management purposes (Roy *et al.*, 2012). Several techniques have been used to collect data for single-tree inventories, and these include the use of a Global Positioning System (GPS) receiver and aerial photographs (Yuan *et al.*, 1991; Hartling *et al.*, 2019). These techniques are tedious, costly and cannot be used over large areas (Hartling *et al.*, 2019). Moreover, these methods cannot be used to obtain information on the age, structure, extent and diversity of urban tree species (Alonzo *et al.*, 2014).

Urban forest managers and other stakeholders involved in urban tree management do not only need information on the current state of urban trees but also need data on the trends of tree cover change which is vital in urban tree governance and policymaking (Ordóñez *et al.*, 2019; Li *et al.*, 2019). Acquisition of data in urban environments is challenging, given the land cover heterogeneity and complexity of features in these areas (Li *et al.*, 2015). The monitoring and management of urban trees require data integration from multiple sources and knowledge of urban vegetation in the area of interest (Wang *et al.*, 2018).

In South Africa, more than 66% of the human population reside in urban areas (World Bank, 2019), and forests cover around 1.3 million hectares (ha) which is about 1% of the country's land area of 122.3 million ha (Department of Agriculture Forestry and Fisheries, 2011). South Africa

has managed urban trees using the National Forest Action Programme (NFAP) under the Department of Agriculture, Forestry and Fisheries (DAFF). The NFAP states the objectives and role of stakeholders, such as municipalities, in the management of urban trees (Shackleton, 2006). Municipalities in the country manage and maintain urban trees and their activities include tree planting in public spaces, parks and along sidewalks in the main streets (Shackleton, 2006).

The DAFF implements policies towards managing urban trees in the country, which include planning and carrying out urban greening programmes (Department of Agriculture Forestry and Fisheries, 2011). The management of urban trees in Johannesburg is founded on the principles of the South African Constitution in Chapter 2: Bill of Rights, the Environment section (24), which states that "Everyone has the right – a) to an environment that is not harmful to their health or wellbeing; and b) to have the environment protected, for the benefit of present and future generations" (Republic of South Africa, 1996). The management of urban trees involves using science, information and technology, promotion of a diverse, healthy and sustainable urban forest (Ajewole, 2010). Communities are also involved in the management and protection of urban trees in the City of Johannesburg (CoJ), enhancing the city's urban greening programmes (Schäffler and Swilling, 2013). Several programs have been implemented in the management of urban trees in the CoJ. For instance, the Johannesburg City Parks (JCP) carried out the "Greening of the City of Johannesburg" program in 2006, and it involved the planting of tree species to turn the city into a green hub (Motsatsi, 2010). The program involved regreening suburbs and other disadvantaged areas in the city, such as informal settlements (Motsatsi, 2010). In 2010, approximately 200 000 trees were planted in the CoJ (Motsatsi, 2010). The program used field-based methods to identify areas that needed more trees to be planted, which was costly (Motsatsi, 2010). There have been several developments in urban tree management that can address the limitations of field-based methods, and these involve the use of various technologies and methods to support sustainable urban tree management (Nilsson *et al.*, 2013).

In response to recent developments, the academic, scientific, and private communities are interested in identifying and developing approaches for providing applicable information on the state of urban trees. This research was sponsored through the "Life in City" project to assist in developing a road map and action plan to guide, inform and enact urban tree management in the CoJ.

1.4 Remote sensing for urban tree mapping

A wide range of geospatial and remote sensing methods have been adopted by urban forest managers and other stakeholders involved in urban tree management (Li *et al.*, 2019). Remote sensing has received a lot of attention and has been successfully used in mapping urban tree species in several studies (Pu, 2011; Agarwal *et al.*, 2013; Le Louarn *et al.*, 2017; Seiferling *et al.*, 2017; Matasci *et al.*, 2018; Pu *et al.*, 2018). Urban tree managers in municipalities and other stakeholders in various areas such as academia and research institutions have considered remote sensing techniques to provide comprehensive, timely and less costly information on urban trees (Li *et al.*, 2019). With the introduction of remote sensing in tree management, practitioners saw the opportunity of replacing difficult and costly traditional field surveying methods with remotely sensed data (Fassnacht *et al.*, 2016). In the 1940s, tree inventories were created using aerial photographs (Holmström, 2002). The use of remote sensing has developed over the years, and this has been done using improved spatial and spectral resolutions on remotely sensed data (Fassnacht *et al.*, 2014). Among some of the advantages of this technology includes providing a synoptic view of large areas which is less costly compared to traditional field survey methods that require substantial time and money to collect an equivalent amount of data (Immitzer *et al.*, 2012). In recent times, the use of multispectral and hyperspectral remote sensing sensors have successfully been used in urban tree classification and mapping (Alonzo *et al.*, 2014).

1.4.1 Hyperspectral and multispectral sensors in urban tree mapping

Passive optical sensors can be divided into multispectral and hyperspectral (also called imaging spectroscopy) systems (Asner, 1998). Most of the multispectral sensors have 4 to 8 bands, whereas hyperspectral sensors have numerous narrow contiguous bands that cover the visible, near-infrared (NIR) and shortwave-infrared (SWIR) ranging from 400 to 2500nm (Asner, 1998). Both hyperspectral and multispectral sensors provide information to distinguish trees by measuring the spectral response of electromagnetic radiation emitted by the sun after being reflected by the tree canopies and other land cover features in different wavelength regions (Fassnacht *et al.*, 2016). The amount of radiation that is reflected at the tree canopy level is due to several factors which include the chemical properties of the plant tissue (e.g. structural carbohydrates and water), leaf morphology (e.g. cell-wall thickness and airspaces), the structure of the canopy (e.g. leaf density and angular distribution) and the size of a tree in comparison to neighbouring tree species (Leckie *et al.*, 2005). Several factors make these properties vary, for example, the health status of the species and their leafage and density (Fassnacht *et al.*, 2016).

Remote sensing sensors are also used to derive land surface temperature (LST) and vegetation indices such as the Normalized Difference Vegetation Index (NDVI), which help understand the emergence of the UHI (Huang and Ye, 2015). The data from remote sensing sensors have been widely used in UHI studies because they are cost-effective and provide data at various spatial resolutions, and dependable compared to field survey techniques (Odindi *et al.*, 2015; Huang and Ye, 2015; Adeyeri *et al.*, 2017; Alexander, 2020).

1.4.2 LiDAR in urban tree mapping

The classification and mapping of urban tree species have evolved over the years, and the advent of the LiDAR systems helps capture their three-dimensional (3D) information (Hartling *et al.*, 2019). LiDAR systems produce satisfactory results because they provide radiometric and geometric information, which is more robust for urban tree classification (Korpela *et al.*, 2010). The radiometric information comprises the precise echo parameters derived from the received waveform, whilst geometric information includes the structure of trees such as the branching, shape, height and crown volume of tree species (Fassnacht *et al.*, 2016). These radiometric and geometric properties can differ between and within tree species, and they can be supported by information acquired using remote sensing instruments (Alonzo *et al.*, 2014).

1.5 Challenges in urban tree mapping

The application of remotely sensed data for mapping trees in a complex urban environment has widely been reported (Ke and Quackenbush, 2011; Richardson and Moskal, 2014; Li *et al.*, 2015; Shojanoori *et al.*, 2016). However, there are some limitations, including, *inter alia*, the low/medium spatial resolution of the most commonly available and accessible satellite sensors and among these are the Landsat OLS/TIRS and Moderate Resolution Imaging Spectroradiometer (MODIS) with a spatial resolution of ≥30m (Yan *et al.*, 2018). This makes it challenging to map many of the tree species with a crown diameter of < 5m. The introduction of Very High Resolution (VHR) satellite imagery such as WorldView (WV), RapidEye, GeoEye, Quickbird and SPOT has, however, resolved such challenges of spatial resolution for mapping urban trees at the species level (Richardson and Moskal, 2014).

Mapping urban forests is often complicated by the high level of heterogeneity and complex environment (Jombo *et al.*, 2020). There might be higher spectral variation within rather than between the species (Hill *et al.*, 2010). This challenge is caused by shadowing effects, natural variability of tree crowns, tree health, differences in view angles and illumination (Leckie *et al.*,

2005). These could, however, be reduced by using multisource data sources such as LiDAR intensity data, vegetation indices and effective classification techniques such as object-based image analysis (Azeez *et al.*, 2019).

Moreover, urban tree mapping's poor spectral separability with other vegetation features is a problem in urban tree mapping (Clark *et al.*, 2005). Most classification techniques depend on the statistical clustering of pixels in a multivariate feature space (Cocchi *et al.*, 2018). However, the spectral separability of tree species is poor compared to other vegetation features such as shrubs and grass in the optical and NIR range (Calviño-Cancela and Martín-Herrero, 2016). This leads to low overall accuracy values and high producer's and user's accuracies in the confusion matrices even on VHR imageries (Cocchi *et al.*, 2018).

1.6 Research gap and motivation

Municipalities and urban authorities must promote sustainable development by avoiding *inter alia,* overcrowding spaces with humans, increase pavements and buildings, land degradation, deforestation, land and air pollution (Li *et al.*, 2019). Urban areas of the future need to be planned and developed, and existing ones have to be improved where possible. The use of remote sensing techniques and spatial data analysis plays a vital role in the planning, developing, and managing of urban areas (Dizdaroglu *et al.*, 2009). However, the dearth of accurate and up to date urban tree information is an issue in many countries, especially those in Africa, which slows down sustainable urban planning, development and management (United Nations Publications, 2019). Local authorities, urban forest managers, urban planners, researchers, and other stakeholders involved in urban trees management are interested in several kinds of spatial data such as tree distribution, LULC and their spatiotemporal change, distribution of the UHI, land statistics and population spread (Jombo *et al.*, 2020; Ngie, 2020). However, these spatial data are often unavailable and sometimes have to be purchased from third parties or collected using traditional, costly, labour-intensive, and timeous methods. Several methods have been used to extract urban tree information automatically from spaceborne and airborne sensors in recent decades, with varying accuracy (Le Louarn *et al.*, 2017; Liu and An., 2019 Jombo *et al.*, 2020). This thesis aims to map and monitor urban trees using remote sensing techniques. The resulting maps or data can assist the local municipality, local authorities, researcher, policy makers, urban planners and other stakeholders involved in urban tree management for sustainable urban planning and management.

1.7 Research objectives

This research aims to map and monitor urban trees in the CoJ using remote sensing techniques. The focus was on the Randburg municipal area. The specific objectives of this study were to:

1. Explore the potential of feature selection methods in the classification of urban trees using field spectroscopic data.
2. Assess the capability of remote sensing to map and classify urban alien tree species using high-resolution multispectral data.
3. Examine the ability of object-based ensemble analysis in classifying common urban trees using high-resolution multispectral data.
4. Evaluate the ability of a combination of airborne LiDAR point-cloud data and very high-resolution imagery in the classification and mapping of common urban trees.
5. Assess the spatiotemporal dynamics of vegetation coverage and LST in a heterogeneous urban area.

1.8 Scope of the study

The study was aimed at mapping and monitoring urban trees in Randburg municipal area in the CoJ in South Africa, using remote sensing techniques. The study highlights the potential of field spectroscopic data in classifying the common urban trees in the study area. The study further evaluates the potential of very high spatial resolution (VHSR) WV-2 imagery in mapping the common urban trees and LULC classes in the study area. The effectiveness of the WV-2 bands in the classification of the common urban trees and LULC classes was also highlighted. The study compared the performance of two robust machine learning algorithms, Random Forest (RF) and Support Vector Machines (SVM). The study also used object-based ensemble analysis on the WV-2 dataset and fused data (WV-2 bands, LiDAR-derived normalised Digital Surface Model (nDSM) and vegetation indices to classify the common urban trees and LULC classes. The study indicated that a fused dataset produces high accuracies in the classification and mapping of the common urban trees and LULC classes using the RF and SVM classification algorithms. The study finally assessed the spatiotemporal dynamics of vegetation coverage and LST in the seven city-regions of the CoJ. The mapping of urban trees and assessing the relation between vegetation mapping is crucial to urban authorities and other stakeholders to draft and implement programmes that can assist in urban greening for sustainable urban tree management.

1.9 Thesis outline

This research consists of seven chapters, of which chapters 2 to 4 have already been published in International Scientific Indexing (ISI) rated peer-reviewed journals. Chapters 5 and 6 are still in preparation for publication in ISI rated peer-reviewed journals. The chapters are presented in a standalone scientific article format with aims, objectives, results, discussion and conclusion. The conclusions in each chapter address the main aim of this research study. Little or no changes were made to the chapters that have been published. Therefore, the previously mentioned approach involves some reiterations in various sections such as the data used, samples taken and species examined, which is unavoidable in some of the chapters. However, this drawback is considered insignificant considering that each chapter gets peer-reviewed as a standalone paper after submission to international journals, and it can be read independently without losing its meaning. This research is organized as follows:

Chapter 1 - Highlights the general introduction of the research. It introduces urban trees and the urban environment, the use of remote sensing in mapping urban trees using hyperspectral and multispectral sensors and the challenges encountered in urban tree mapping. The research objectives and questions of this research were also outlined in this chapter.

Chapter 2 - Explores the potential of feature selection methods in the classification of urban trees using field hyperspectral data. This aimed to show the optimal wavelengths and reduce the high dimensionality of hyperspectral data in the classification of common urban trees. The effectiveness of three feature selection methods, namely, Principal Component Analysis Discriminant Analysis (PCA-DA), Partial Least Squares Discriminant Analysis (PLS-DA), and Guided Regularized Random Forest (GRRF), was compared in identifying the optimal wavelengths. The high accuracies in this chapter show the potential of hyperspectral data in the classification of urban trees. Although the accuracies were high, the chapter did not show the spatial distribution of the tree species in the study area. Therefore, it was necessary to use multispectral imageries such as WV to improve accuracies and show the common urban trees' distribution. The following chapter evaluates the capability of WV-2 in mapping the common urban trees in the study area.

Chapter 3 - Assesses remote sensing ability in classifying and mapping common urban tree species and other LULC classes using pixel-based classification techniques. The chapter evaluated the capability of WV-2 imagery in mapping the common urban tree species and other LULC classes in the study area. The chapter also tested the utility of the WV-2 bands in the classification and

the RF and SVM algorithms' feasibility in mapping the common urban trees and other LULC classes. There were misclassifications in this chapter, and it was due to several factors such as the "mixed pixel problem" and the reference points' location errors. The challenges encountered require consideration of different classification approaches such as the object-based classification method to improve the accuracies. The applicability of the object-based ensemble analysis was tested in the classification of the common urban trees and LULC classes in the following chapter.

Chapter 4 - Examines object-based ensemble analysis capability in classifying and mapping common urban tree species and other LULC classes using VHR multispectral imagery. The study tested the utility of WV-2 bands and other feature variables (NDVI and length) to classify common urban trees and LULC classes in the study area. The utility of the RF and SVM algorithms was compared in the classification. The results showed that the NDVI, NIR1 and NIR2 bands were vital in the classification of the common urban trees and LULC classes in the study area. Chapter 4 recommended using object-based classification methods using WV-2 with other non-spectral data such as LiDAR point cloud data in the classification of the common urban trees and LULC in the study to increase the accuracies. This was done as LiDAR point-cloud data incorporates tree height, measurement of the crown spread, which can increase the accuracies that were obtained in this chapter. The LiDAR-derived nDSM was fused with WV-2 imagery in the next chapter.

Chapter 5 - Evaluates the ability of a combination of airborne LiDAR point-cloud data and VHR multispectral imagery in mapping common urban trees and other LULC classes. The chapter examined the effectiveness and ranked the importance of the nDSM, WV-2 bands, and vegetation indices in mapping common urban trees and other LULC classes in the study area. The study indicated the effectiveness of data fusion in the classification of urban trees and LULC classes, which is important to municipalities for urban tree management, including reducing problems such as the growth of urban heat islands. The next chapter focussed on the spatiotemporal dynamics of vegetation coverage and LST in the seven city-regions of the CoJ.

Chapter 6 - Determines the spatiotemporal dynamics of vegetation coverage and LST. This was done at a city-region level using MODIS satellite data. The study determined the spatial distribution of NDVI and LST in the seven city-regions of the CoJ over five years (2001, 2005, 2010, 2015 and 2020). The study also analysed the variances of mean NDVI and LST and examined the relationship between NDVI and LST in the study area to provide information to urban authorities that can assist to increase and maintain existing vegetation coverage. The study

indicated that areas with a high amount of vegetation cover had low LSTs and vice versa. This chapter assists the municipalities and other stakeholders involved in urban planning and urban tree management related to UHI mitigation.

Chapter 7 - Summarises the outcomes of this research and answers the research questions. It outlines the main contributions of this research to the identification, classification and mapping of urban trees. In this chapter, the limitations of the current study are outlined, and it also gives an outlook into other research aspects that can be considered in further studies. This study seeks to assist municipalities and other urban authorities with knowledge of the data and techniques used in urban tree classification mapping. This is vital for urban greening programmes which promote sustainable urban tree management.

At the end of the thesis, a single reference list from all the chapters is provided.

Chapter Two

Exploring the potential of feature selection methods in the classification of urban trees using field spectroscopic data

This chapter is based on **Jombo, S**., Adam, E., Byrne, M. J., Ali, K. A. and Newete, S. W. (2020) Exploring the Potential of Feature Selection Methods in the Classification of Urban Trees using Field Spectroscopy Data. *International Journal of Geospatial and Environmental Research*, 7, 3. Available at: https://dc.uwm.edu/ijger/vol7/iss3/3

Abstract

Discriminating vegetation at the species level using hyperspectral data can be effective and accurate because of its high spectral and spatial resolutions that can detect detailed information of a target object. Its wide application, however, not only is restricted by its high cost and large data storage requirements but its processing is also complicated by challenges of what is known as the Hughes effect. The Hughes effect is where classification accuracy decreases once the number of features or wavelengths passes a certain limit. This study aimed to explore the potential of feature selection methods in the classification of urban trees using field hyperspectral data. We identified the best feature selection method of key wavelengths that respond to the target urban tree species for effective and accurate classification. The study compared the effectiveness of Principal Component Analysis Discriminant Analysis (PCA-DA), Partial Least Squares Discriminant Analysis (PLS-DA) and Guided Regularized Random Forest (GRRF) in feature selection of the key wavelengths for classification of urban trees. The classification performance of Random Forest (RF) and Support Vector Machines (SVM) algorithms were also compared to determine the importance of the key wavelengths selected for the detection of the target urban trees. The feature selection methods managed to reduce the high dimensionality of the hyperspectral data. Both the PCA-DA and PLS-DA selected 10 wavelengths and the GRRF algorithm selected 13 wavelengths from the entire dataset (n = 1523). Most of the key wavelengths were from the short-wave infrared region (1300-2500nm). SVM outperformed RF in classifying the key wavelengths selected by the feature selection methods. The SVM classifier produced overall accuracy values of 95.3%, 93.3% and 86% using the GRRF, PLS-DA and PCA-DA techniques, respectively, whereas those for the RF classifier were 88.7%, 72% and 64%, respectively.

2.1 Introduction

Urban forests provide several ecosystem services, such as reducing the effects of the urban heat island by providing shade (Brabant *et al.*, 2019), promoting biodiversity, decreasing air temperature and promoting urban aesthetic values (Aval *et al.*, 2019). In this way, urban trees improve the quality of urban life and reduce stormwater runoff, decrease air pollution and maintain environmental health (Li *et al.*, 2019). The ecosystem services provided by urban trees vary with tree type, structure, density and location (Pretzsch *et al.*, 2015). Trees such as *Platanus* spp., *Quercus* spp. and *Eucalyptus* spp. are often selected as urban forest trees because of their height and broad leaves which can suppress noise, provide shade and act as windbreaks (Love *et al.*, 2009). Proper planning, monitoring and use of sustainable management practices such as urban greening are crucial measures for ensuring a balance between the natural environment and human developments through careful use of such long-lived resources, caring for the inheritance of future generations (Dizdaroglu *et al.*, 2009). An effective urban forest management plan requires precise and timely information on the patterns, distribution and conditions of the trees at both spatial and temporal levels, and remote sensing could be an effective tool to accomplish such mapping and assessment (Li *et al.*, 2019).

Although used for decades, traditional approaches such as field walking surveys have been used to collect information for urban tree inventories, the advent of advanced remote sensing tools have revolutionized the mapping of forest trees, progressively complementing the labour-intensive field tree surveys (Fassnacht *et al.*, 2014). Multispectral images, for instance, SPOT, Landsat TM and ETM+ satellite data have been widely utilized because of their low cost for mapping urban trees (Fassnacht *et al.*, 2014). They are the most applicable for general land use and land cover (LULC) classifications, but not for mapping trees at the species level (Abbasi *et al.*, 2019). This is associated with their low spectral resolution, making it particularly difficult for mapping individual trees in a highly complex and heterogeneous environment such as a forest in an urban setup, often resulting in spectral confusion between individual tree species and low accuracy levels (Dalponte *et al.*, 2012; Ghiyamat *et al.*, 2013). Although there has been progressive improvement in the spectral and spatial resolutions of some multispectral sensors making them relatively more suitable for mapping individual trees, hyperspectral data is better (Liu *et al.*, 2017). Whether from airborne sources, space platforms or hyperspectral sensors, the system records the electromagnetic energy of target objects across hundreds of contiguous narrow spectral bands (Adam and Mutanga, 2009). These can accurately classify and map urban tree species better than the standard multispectral bands (Adam and Mutanga, 2009; Jombo *et al.*, 2020). Hyperspectral data have shown great success in urban

forest classifications (Alonzo *et al.*, 2014; Liu *et al.*, 2017; Brabant *et al.*, 2019; Aval *et al.*, 2019), urban land cover mapping (Bartesaghi-Koc *et al.*, 2019) and monitoring tree biophysical parameters (Jarocińska *et al.*, 2018).

However, due to its exorbitant cost (Degerickx *et al.*, 2019), and high data dimensionality because of the "Hughes effects" (Liu *et al.*, 2017), the application of hyperspectral data for vegetation mapping and classification is limited. The "Hughes effects" occur when the number of samples is less than the number of features in the dataset resulting in low accuracies when using classification algorithms designed for low-dimensional data (Kiala *et al.*, 2019). The classification of urban trees using hyperspectral data has often been overlooked in South Africa and only a few studies have used a hand-held field spectrometer to discriminate between plant species (Mutanga *et al.*, 2004; Adam and Mutanga, 2009; Mureriwa *et al.*, 2016). The high-data volume and data dimensionality problems of field spectroscopic can be overcome by reducing the number of spectral bands used whilst keeping vital information through selecting key wavelengths to improve classification accuracy (Serpico and Bruzzone, 2001). Dimensionality reduction methods are grouped into feature extraction and feature selection (Guyon and Elisseeff, 2003). Feature extraction (e.g. Principal Component Analysis (PCA)) and Minimum Noise Fraction (MNF) use new features derived from a combination of the original bands after transforming the data into a lower dimension (Aval *et al.*, 2019). Feature selection methods such as Support Vector Machines (SVM) wrapper, Partial Least Squares Discriminant Analysis (PLS-DA), Guided Regularized Random Forest (GRRF) and Genetic Algorithm (GA), however, preserve the physical interpretation of the data using a subset of the original bands (Mureriwa *et al.*, 2016; Gholizadeh *et al.*, 2018; Aval *et al.*, 2019).

The methods used to reduce the number of features by choosing the relevant ones and removing those with redundant information include Principal Component Analysis Discriminant Analysis (PCA-DA), PLS-DA and GRRF. Several researchers (Calviño-Cancela and Martín-Herrero, 2016; Abbasi *et al.*, 2019; Xu *et al.*, 2020) have successfully used PCA-DA to produce a reduced set of features from hyperspectral data of vegetation and obtained high accuracies. For instance, Abbasi *et al.* (2019) used PCA-DA to identify key wavelengths with the highest sensitivity and performance to separate orchard tree species using a handheld Analytical Spectral Device (ASD) FieldSpec® 3 spectroradiometer. Peerbhay *et al.* (2013) successfully used the PLS-DA for feature selection and classification of trees in a commercial forest using AISA Eagle hyperspectral imagery and obtained high accuracies of 88.78%. Peerbhay *et al.* (2013) highlighted that the PLS-DA alone can neither

clearly identify the key wavelengths nor redundant wavelengths. The PLS-DA was used with the variable importance in the projection (VIP) method to identify the optimal wavelengths, precisely discriminate and classify commercial trees in the Hodgsons Sappi plantation in KwaZulu –Natal, South Africa. Mureriwa *et al.* (2016) used the GRRF method to identify key wavelengths that could discriminate *Prosopis glandulosa* from other species with a handheld Spectral Evolution® RS-3500 spectroradiometer bundle in the Northern Cape, South Africa. High overall accuracies of 88.59% were obtained using the 11 wavelengths selected by the GRRF method. Thus, these feature selection methods have performed well in dimensionality reduction and classification of hyperspectral data. However, the superiority of one of the three feature selection methods (PCA-DA, PLS-DA and GRRF) is yet to be established, especially in classifying urban trees. The use of the feature selection methods on hyperspectral data in classifying urban trees in Southern African urban landscapes has not been well examined. To the best of our knowledge, these feature selection methods have not been compared in a heterogeneous urban environment for the classification of trees.

There is a general paucity of urban tree inventory data in South Africa (Schäffler and Swilling, 2013). This impedes municipalities and urban forest managers to reach sustainable management goals in urban greening or controlling pests such as the polyphagous shot hole borer (Paap *et al.*, 2018). The mapping of urban trees using pixel-based approaches or field spectra provides important information for researchers, urban and municipal managers on the spatial distribution of trees, which is vital in drafting policies for effective urban green management (Fassnacht *et al.*, 2016). The mapping of urban trees in a heterogeneous area is affected by a spectral variation that can be reduced using field spectroscopy data, requiring feature selection of key wavelengths for high accuracy (Aval *et al.*, 2019). Contradictory findings have been retrieved for different vegetation species in various environments and the utilization of one feature selection method and data dimensionality reduction technique has not produced results that are acceptable at operational levels (Adam and Mutanga, 2009). To overcome the abovementioned issues, this study aims to explore the potential of feature selection methods in the classification of urban trees using field hyperspectral data. The objectives of this study were to: i) identify the optimal wavelengths (i.e. from 350 to 2500 nm) for the common urban trees using the PCA-DA, PLS-DA and GRRF ii) compare the effectiveness of PCA-DA, PLS-DA and GRRF methods in identifying key wavelengths that precisely classify common urban trees in the study area and iii) assess the performance of RF and SVM algorithms in classifying the selected key wavelengths.

2.2 Methodology

2.2.1 Study area

The study was conducted in Randburg municipal area, covering 167.98km^2 in Region B of the City of Johannesburg (CoJ) (longitude 28°0´23" E, latitude 26°5´36" S) (Figure 2.1). The area is characterized by a subtropical climate, with an annual rainfall of around 750mm per annum and possible evaporation of approximately 1600mm per annum (Tyson and Wilcocks, 1971). The climatic conditions are characterized by warm to hot conditions, and rain mainly falls in the summer season. The summer season runs from October to March with a mean daily temperature of around 21ºC (Abiye, 2015).

In the 19th century, fast-growing trees were introduced in the study area, and these include Pepper trees, jacaranda, oaks and black wattle (Schäffler and Swilling, 2013). Most non-indigenous trees, including the fast-growing species in the study area, were planted during the colonial period, resulting in the heterogeneity of species in the area (Turton *et al.*, 2006). These urban trees form an ecological space that is fairly uncommon in the whole world, especially looking at space-constrained urban environments (Schäffler and Swilling, 2013).

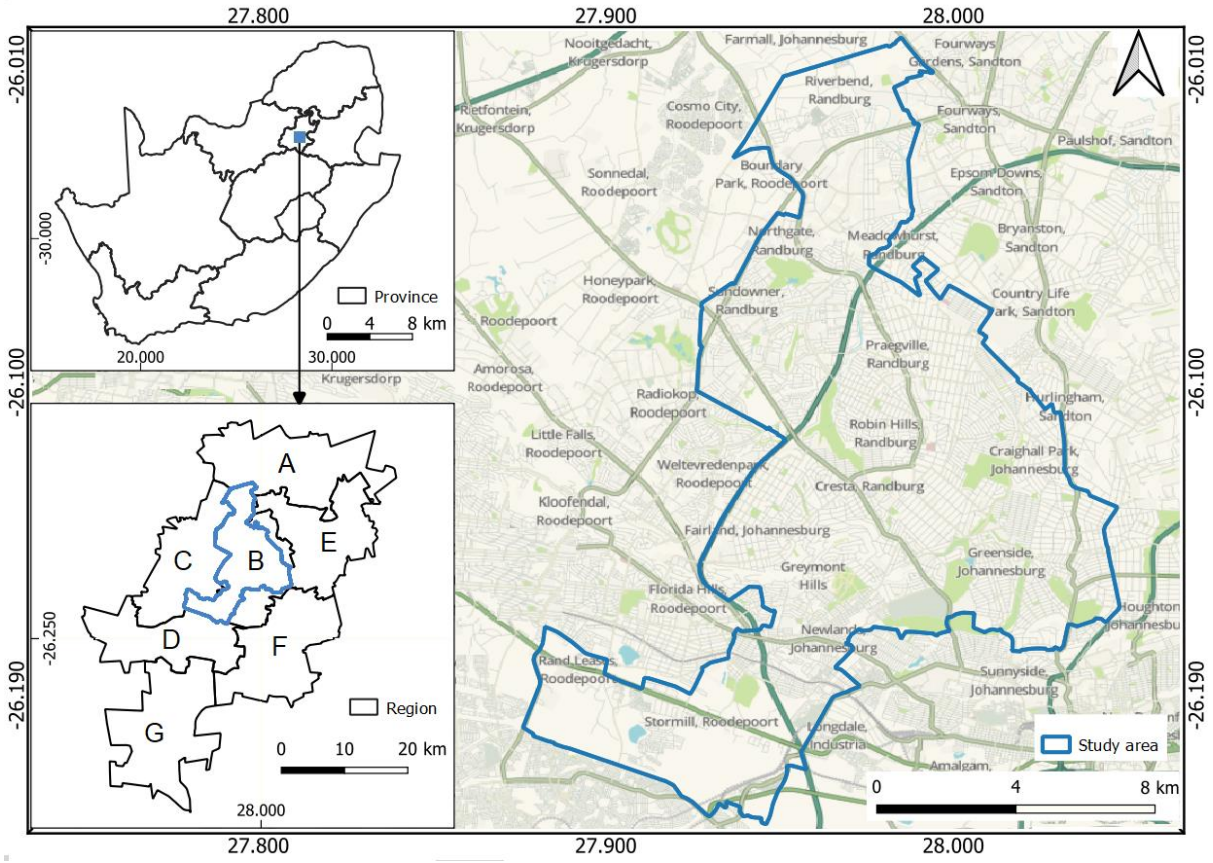


Figure 2.1 Map of South African provinces, Johannesburg's regions and a basemap showing the Randburg municipal area located in the City of Johannesburg. a) South African provinces b) City of Johannesburg's regions A to G and c) basemap showing Randburg municipal area from QGIS software (version 3.12.0) by QGIS Development Team (2020).

2.2.2 Identification of common urban trees

In this study, stratified purposeful sampling was applied to identify areas with the common urban trees. The study area was divided into 40 stands (strata) measuring around 4.2km^2 each. The stratified purposeful sampling method was used because it enables a comparison of differences across sub-groups in an easy way (Farrugia, 2019). The zigzag sampling procedure as described by Almeida and Tomé (2009) was used to sample the common urban trees. The stands with the most common urban trees were selected, and 84 to 86 bouquets were cut from the canopy for each of the six common tree classes. The six identified common urban trees were *Eucalyptus* spp., *Jacaranda mimosifolia*, *Platanus* x *acerifolia*, *Platanus occidentalis*, *Quercus* spp. and *Pinus* spp. (Figure 2.2).



Figure 2.2 Tree bouquets of the common urban trees in the study area. The common urban trees are a) *Eucalyptus* spp., b) *Jacaranda mimosifolia*, c) *Platanus* x *acerifolia*, d) *Platanus occidentalis*, e) *Pinus* spp. and f) *Quercus* spp.

Eucalyptus spp. originated from Australia and was introduced into the study area mainly for commercial pulpwood production (Henderson, 2001). They are generally evergreen with wide leaves and deep roots (Odebiri *et al.*, 2020). *Eucalyptus* spp. use huge amounts of water, and they are mainly found on roadsides, forest gaps and waterways (Henderson, 2001; Forsyth *et al.*, 2004).

Jacaranda mimosifolia originated from North West Argentina, and they are shade and ornamental trees with wide and rounded crowns (Henderson, 2001). *Jacaranda mimosifolia* trees have dark green leaves that turn yellow during the autumn or winter season (Henderson, 1990). They are deciduous or semi-deciduous and invade riverbanks and wooded kloofs (Henderson, 2001). *Platanus* spp. originated from Greece and Asia Minor, and they are deciduous with large leaves, often 25cm in width (Henry and Flood, 1919). *Platanus* spp. produce fragrant flowers in the spring season and are mainly located in parks and roadsides (Love *et al.*, 2009). *Quercus* spp. originated from Britain, the Mediterranean and West Asia (Love *et al.*, 2009). They have bright green leaves turning dark green and are mainly grown for shelter, shade, and to act as windbreaks due to their wide canopies (Love *et al.*, 2009). They are deciduous and mainly found in riverbanks, roadsides, forest margins, grassland and fynbos (Henderson, 2001). Most *Pinus* spp. are native to Central America and have needle-shaped bright green leaves, and are mostly found on roadsides, forest margins and gaps (Henderson, 2001). They were planted in the study area mainly for timber and recreation shade for urbanites (van Wilgen, 2012).

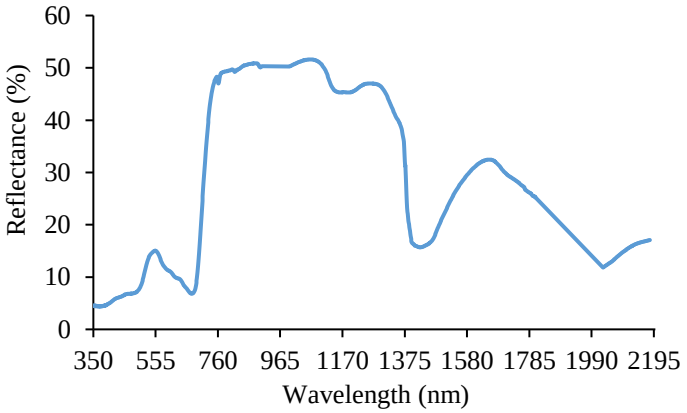
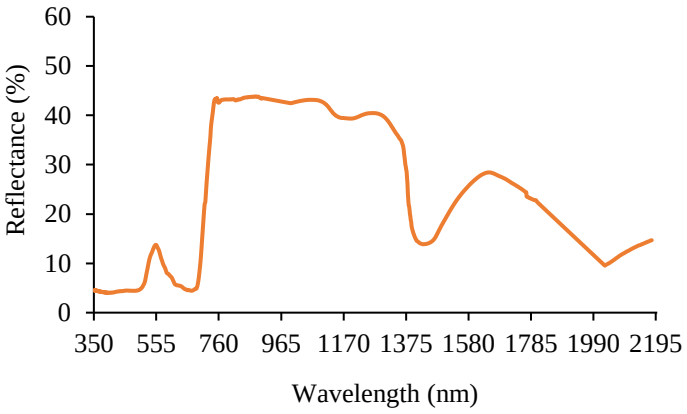
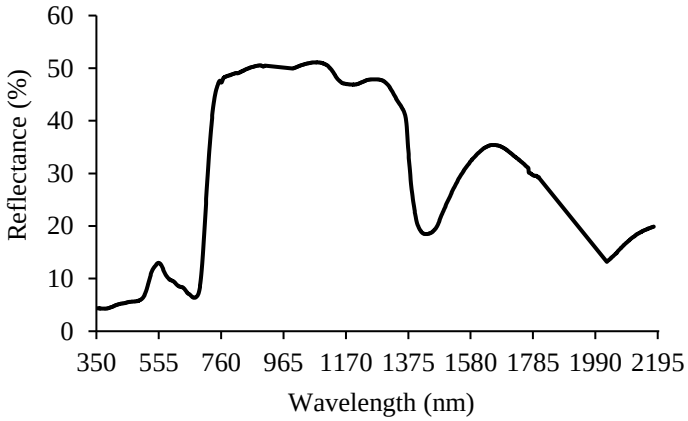
2.2.3 Field hyperspectral data measurements

Field spectral measurements of the six common urban trees (*Eucalyptus* spp., *Jacaranda mimosifolia*, *Platanus* x *acerifolia*, *Platanus occidentalis*, *Quercus* spp. and *Pinus* spp.) were taken in the field between 10.00 and 14.00 hours (local time) from 18 to 22 March 2019, under a clear sky and sunny conditions. The spectral measurements were collected using a portable ASD FieldSpec® 4 optical sensor. The ASD offers fast and full-spectral measurements covering the ultraviolet-visible and near infra-red (UV-Vis-NIR) wavelengths from 350 to 2500 nm with wavelength reproducibility of 0.1nm and 2151 channels are reported (Malvern Panalytical, 2019).

In total, 508 scans were taken from tree bouquets of the six tree types (Table 2.1). The tree bouquets (84 to 86) from each of the six trees were randomly arranged on a thick black panel. The leaf reflectance measurements were taken at a nadir-looking angle that was roughly 25cm above the bouquets. Spectral measurements were calibrated every 10 to 15 readings using a white reference panel to reduce the effects of sun irradiance and changes in atmospheric conditions. The spectral curves obtained were reviewed, and the inconsistent spectral reflectance curves were discarded and replaced by repeating the measurements. This study's total number of wavelengths was 2050 in the spectral range starting from 350nm to 2500nm. A total of 1523 wavelengths were used in the analysis as 627 wavelengths (ranging from 904 to 994nm, 1808 to 2027nm and 2183 to 2500nm) were removed. These regions of the electromagnetic spectrum were removed because

they are noisy and the reflectance spectra are affected by water absorption in the atmosphere (Mureriwa *et al.*, 2016). The spectral data collected from the tree bouquets were averaged to represent the spectral reflectance of each of the six tree species (Table 2.1). The reference data (n = 508) was split into 70% (training) and 30% (test) datasets. The reference data were randomly sampled to select training and test datasets.

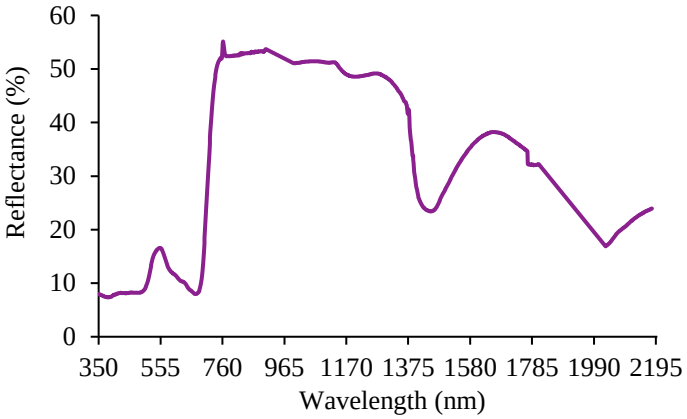
Table 2.1 Spectral reflectance and images for the six urban trees examined in this study.

Class	Reflectance curve
Eucalyptus spp. (EC)  Total sample size = 84	
Jacaranda spp. (JC)  Total sample size = 84	
Platanus x *acerifolia* (PA)  Total sample size = 84	

Platanus occidentalis (PO)



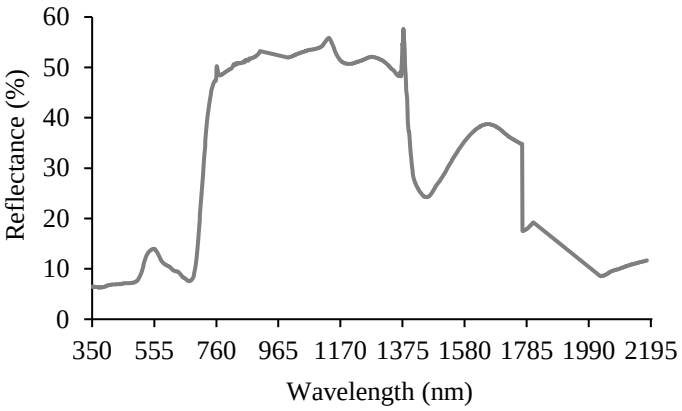
Total sample size = 85



Quercus spp. (QS)



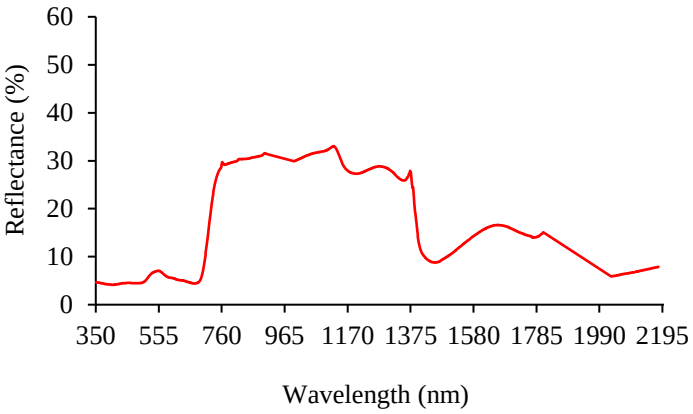
Total sample size = 86



Pinus spp. (PN)

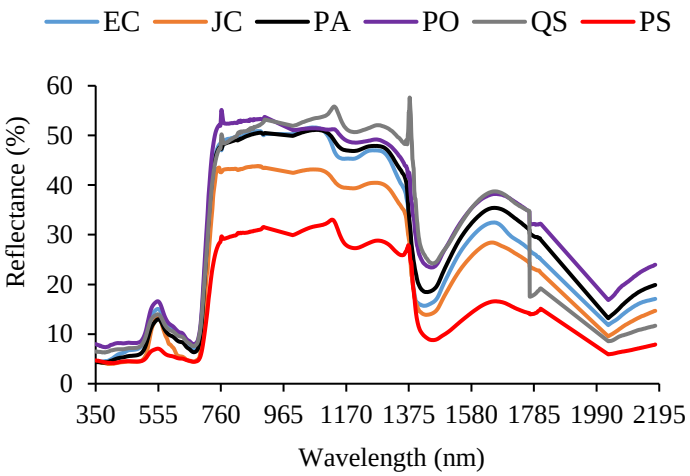


Total sample size = 85



Average spectra for the common urban tree species (*Eucalyptus* spp. (EC), *Jacaranda* spp. (JC), *Platanus* x *acerifolia* (PA), *Platanus occidentalis* (PO), *Quercus* spp. (QS) and *Pinus* spp. (PN)).

Total sample size = 508



2.2.4 Feature selection methods

The PCA-DA, PLS-DA and GRRF were used for feature selection and reduction of the high dimensionality of hyperspectral data in this study. The wavelengths were first standardized to have a mean value of zero and a standard deviation value of one before the feature selection methods were used.

2.2.4.1 Principal Component Analysis – Discriminant Analysis (PCA-DA)

The PCA was used in combination with Linear Discriminant Analysis (LDA) to select features of the common urban trees surveyed. The algorithm generated a set of new bands with non-correlated features, providing maximum visual separability to distinguish them (Nordin *et al.*, 2018). The PCA algorithm provided a variance value for each hyperspectral band enabling the selection of the useful ones for analysis of a covariance matrix made from the whole data distribution (Tochon *et al.*, 2015). The LDA was used to extract principal components (PCs) that had eigenvalues above 1. The PCA algorithm is used to eliminate the correlation between features and eigenvalues above one were chosen as they represent the same amount of information as a single feature (Brabant *et al.*, 2019). In this study, the LDA used ten principal components as predictor variables.

The variable importance in projection (VIP) was used for variable selection and classification of data. In classifying data, the VIP shows the importance of a feature which is a function of its impact on the PCA embedding's outline and its value in the prediction of class labels (Ginsburg *et al.*, 2015). The PCA-DA provided scores resulting in identifying important features that gave good class discrimination (Ginsburg *et al.*, 2015). The features which contributed the most to the PCA embedding were the ones with high VIP scores.

With consideration of the size of the sample (n = 1523), 10-fold cross-validation (CV) repeated 10 times was used to assist in reducing high variance (Cocchi *et al.*, 2018).

2.2.4.2 Partial Least Squares-Discriminant Analysis (PLS-DA)

The Partial Least Squares (PLS) algorithm was used first for regression tasks and only later developed into a classification technique, known as the Partial Least Squares-Discriminant Analysis (PLS-DA) (Lee *et al.*, 2018). The PLS-DA is a multivariate supervised statistical method that models the class parameters and measured spectra figures to assess their relationship (Barker and Rayens, 2003). Moreover, this method employs a training routine where variables are assigned

with class membership based on statistical parameters that are known and projected into latent features (Chivasa *et al.*, 2019). The PLS-DA method performed in this study can be represented as:

$$X = TP' + E, \quad \text{Equation 2.1}$$

$$Y = UQ' + F, \quad \text{Equation 2.2}$$

where *X* stands for the matrix of the predictors (wavelengths); *Y* represents the matrix response (common urban trees); *T* stands for scores for *X*; *P* represents the *X*-loadings; *E* stands for the noise terms or residuals for *X*; *U* represents scores for *Y*; *Q* stands for loadings for *Y* and *F* represents the residuals for *Y*.

The VIP scores were used in this study to select relevant spectral regions with a cut-off point of 1, i.e. important variables to the model are the ones with a value of 1 or more (Zovko *et al.*, 2019). The accuracies of the PLS-DA in discriminating variables from the selected training data sets were done using the 10-fold CV. This technique tests the significance of the model for each component, and it is efficient and reliable (Chivasa *et al.*, 2019). The 10-fold CV technique optimized the PLS-DA model parameters using the whole dataset (n = 1523).

2.2.4.3 Guided Regularized Random Forest (GRRF)

The GRRF algorithm put forward by Deng and Runger (2013) was also used in this study to select features that do not carry similar information to the ones already selected at every single node. The GRRF is a feature selection method that uses a regularisation parameter applied to various types of decision tree models to select feature subsets (Jovanovic *et al.*, 2019). The scores of feature importance guide the regularization in GRRF, and it is measured using the Gini index in the traditional RF (Izquierdo-Verdiguier *et al.*, 2017). The level of impurity for each variable is assessed using the Gini importance, where amongst a small subset of variables, the optimal split at every single node is selected (Deng and Runger, 2013). The Gini index for node z is calculated as follows:

$$Gini\ (z) = \sum_{h=1}^{h} P_h^z\ (1 - P_h^z), \quad \text{Equation 2.3}$$

where P_h^z denotes the proportion of class *h* observations at node z. The Gini information gain (K_i, z) is calculated as the difference between the weighted average of impurities for each child node

of z and the impurity at node z. The gain information for the feature K_i at node z can be calculated as follows:

$$Gain\ (K_i, z) = Gain\ (z) - w_L\ Gini\ (z_L) - w_R\ \text{Gini}\ (z_R), \quad \text{Equation 2.4}$$

where *Gini* (z_L) and *Gini* (z_R) denotes the impurities whereas w_R and w_L represents the weights for the right and left nodes, respectively.

In GRRF, the regularization parameter is used to keep gain from the regularized RF, and a penalty coefficient is given to the gain new features (Izquierdo-Verdiguier *et al.*, 2017). The definition of the feature importance of the GRRF is as follows:

$$Gain_{K_i,z} = \begin{cases} \lambda_i .\ Gain\ (K_i, z), & K_i\ \notin F, \\ Gain\ (K_i, z), & K_i\ \notin F, \end{cases} \quad \text{Equation 2.5}$$

where F represents the set of indices that are utilized to split in the previous nodes whilst $\lambda_i\ \notin$ (0,1) denotes the coefficient for K_i ($i \in \{1, \ldots\ldots, P\}$, computed based on the importance score of K_i from the traditional RF, and it is calculated using the formula:

$$\lambda_i\ =\ (1 - \gamma) +\ \gamma Imp_i, \quad \text{Equation 2.6}$$

where Imp_i, is the importance score from the traditional RF. It should be considered that weight for the normalized importance is represented by $\gamma \in [0, 1]$, and the GRRF lowers to the random forest technique if $\gamma = 0$. The features are chosen by the GRRF method in an easy procedure, as stated in Equation (6). The first step is attaining the feature importance after training the random forest, and this is followed by the calculation of the best weight parameter (γ^*) as well as the regularization parameter λ_i . The final step involves training a new random forest using the selected features (Izquierdo-Verdiguier *et al.*, 2017).

The algorithm guides the feature selection process of regularized random forest (RRF) centred on the random forest's importance scores, and it is an ensemble machine learning method (Jovanovic *et al.*, 2019). The GRRF algorithm was used in this study as it is computationally effective, produces high accuracies, and is firm compared to RRF (Deng and Runger, 2013). Furthermore, the algorithm chooses the compact subsets (small set with features of high importance) from the

variable interactions whilst preventing the action of analysing redundant features hence reducing the course of data dimensionality (Jovanovic *et al.*, 2019).

The PCA-DA, PLS-DA and GRRF were run using R (Version 4.0.0) on a desktop computer, and the processor was Intel ® Core ™ i7-4790 CPU @ 3.60 GHz, installed ram of 8 GB, with a 64-bit system type and x64-based processor. The key wavelengths selected by PCA-DA, PLS-DA and GRRF algorithms were input variables in SVM and the traditional RF classifiers to discriminate the urban trees.

2.2.5 Classification techniques

The features selected by the three multivariate statistical analysis methods (PCA-DA, PLS-DA and GRRF) were used as input variables to classify the tree species using RF and SVM. The performance of the two classifiers on the selected features was compared. The RF and SVM were used in this study because they have been widely used in tree species classification, and good accuracies were achieved in most of the previous studies (Dalponte *et al.*, 2012; Cao *et al.*, 2018; Brabant *et al.*, 2019).

2.2.5.1 Support Vector Machines (SVM)

The SVM classification method developed by Vapnik (1995) is non-parametric, designated to search for a hyperplane that separates classes. The side on which the samples end up on the hyperplane is how test data is separated from the overall dataset (Suppers *et al.*, 2018). Support vectors are the points that are closest to the hyperplane, and they measure the margin (Vapnik, 1995). If two classes are non-linearly separable, the SVM finds a suitable hyperplane that maximises the margin whilst reducing misclassification errors (Pal, 2005). In a high dimensional space, SVM has kernel functions that convert nonlinear boundaries into linear ones (Marcinkowska-Ochtyra *et al.*, 2017). The most common SVM kernel functions are radial basis function (RBF), polynomial, linear and sigmoidal kernels (Brabant *et al.*, 2019). Polynomial and RBF kernels using the SVM algorithm have been applied in various remote sensing studies and produced different results (Zhu and Blumberg, 2002; Mountrakis *et al.*, 2011). The RBF kernel function has produced better results than the polynomial function in previous studies (Foody and Mathur, 2004; Marcinkowska-Ochtyra *et al.*, 2017). Hence, the RBF kernel function was used to classify the selected wavelengths in this study. The RBF function has two parameters, the gamma (γ) and the cost (C) parameter which have to be optimized in a SVM algorithm (Sun *et al.*, 2019). The optimization in this study was done using a 10-fold CV and grid search on a log scale. The SVM algorithm tests different

pairs of γ and *C* and select the ones with the highest CV values (Zhou *et al.*, 2019). The optimization of the RBF parameters was done using the *e1071* library of R statistical software (Version 4.0.0).

2.2.5.2 Random Forest (RF)

The random forest (RF) classification method, developed by Breiman (2001), merges numerous tree predictors where each tree is dependent on a value belonging to a vector that is randomly chosen and equally distributed in a forest amongst all trees (Masetic and Subasi, 2016). The RF classifier is a supervised method consisting of numerous decision trees where each tree is grown on a bootstrap sample from the overall training dataset (Deng and Runger, 2013). The numerous decision trees are joined, and each tree gives a vote to assign the most common class to the overall input dataset (Breiman, 2001). The number of binary classification trees (*ntree*) in RF is built using numerous bootstrap samples where replacements are derived from the input dataset. The other parameter required in the RF classifier is the *mtry*, which is a random set of variables from the original data that are used to split at each node (Breiman, 2001). The optimization of the *mtry* and *ntree* values was done with the use of the *randomForest* package in R statistical software (Version 4.0.0). In RF modelling using the *randomForest* package, the *ntree* default value for the *ntree* is 500 and √P for *mtry*, where P represents the total number of the predictor variables (Karlson *et al.*, 2016). The grid search method was applied to figure out optimal *ntree* and *mtry* parameters. The parameters varied from 500 to 10000 with an interval of 1000 for *ntree* and the *mtry* values ranged from 2 to 10 for both the PCA-DA and PLS-DA and 2 to 13 for the GRRF method.

The RF classification algorithm can be summarized as follows: i) *ntrees* bootstrap sets are drawn from the overall training data with bagging, also known as a replacement. The tree is grown using two-thirds (70%) of the overall training data, and the remaining one-third (30%) is utilized in performing CV, which will be done in correspondence with the training procedure (Breiman, 2001). The following step ii) involves the growing of an unpruned tree for each bootstrap. However, *mtry* values are chosen randomly in each node, and the best split is selected, and it is the one that offers the minimum Gini index outcome. When the tree is grown, it will stop when there are no additional splits possible (Breiman, 2001). The final step iii) is where the user can repeat the aforementioned steps (i and ii) until the *ntrees* are grown (de Santana *et al.*, 2019).

The RF classification has been effectively used in mapping urban trees (Liu *et al.*, 2017; Brabant *et al.*, 2019) and the classification of trees using Light Detection and Ranging (LiDAR) and

hyperspectral data (Shi *et al.*, 2018). The wavelengths selected for the hyperspectral data were analysed using the RF classification algorithm in R (Version 4.0.0).

2.2.6 Accuracy Assessment

The effectiveness of the RF and SVM classification methods in classifying the selected wavelengths using feature selection techniques (PCA-DA, PLS-DA and GRRF) was validated. A holdout dataset from the wavelengths selected by the feature selection techniques was randomly divided into test (30%) and training (70%) datasets before classification. The accuracy assessment was done using confusion matrices where the overall accuracy (OA), kappa statistic, user's and the producer's accuracy (PA) values were calculated (Chivasa *et al.*, 2019). The overall accuracy (OA) represents the overall number of correctly classified grids divided by the total number of all the grids (Bartesaghi-Koc *et al.*, 2019). The PA ascertains the possibility of a class being appropriately classified, whilst the user's accuracy (UA) represents the possibility that a sample belongs to a particular class and is correctly assigned to it by the classifier (Bartesaghi-Koc *et al.*, 2019). The kappa value was also calculated in this study, and it looks at the agreement between ground truth and classified samples, ranging from 0 (no agreement) to 1 (perfect agreement) (Bartesaghi-Koc *et al.*, 2019).

2.3 Results

2.3.1 PCA-DA wavelength selection results

The PCA-DA algorithm was run on all the wavelengths (n = 1523), and the results indicated that the maximum variation was shown by the first principal component (PC1) with a cumulative proportion (CP) of 77.81%, followed by PC2 (85.98%) with a proportion of variance (PV) of 8.18% (Table 2.2). The first ten PCs gave a CP total of 99.80% (Table 2.2). The first 10 PCs were retained as the common urban trees' reflectance data offering large data variance in comparison to lower-order PCs. It can be noted that there is a decline in the eigenvalues from higher to lower order PCs (Table 2.2).

Table 2.2 Principal Component Analysis (PCA) results showing the proportion of variance (PV) and cumulative proportion (CP) in percentage (%) and eigenvalues for the first 10 principal components (PCs) of reflectance values from six urban tree species.

PC	PV (%)	CP (%)	Eigenvalues
1	77.81	77.81	1185.1
2	8.18	85.98	124.6
3	7.52	93.51	114.5
4	3.08	96.58	46.9
5	1.72	98.29	26.1
6	0.59	98.89	9.0
7	0.48	99.37	7.4
8	0.24	99.61	3.7
9	0.11	99.72	1.7
10	0.08	99.80	1.2

The variable of importance in the projection (VIP) was used to determine the 10 best wavelengths with high scores. The significant wavelengths were selected from the 10 PCs with eigenvalues greater than 1.

The ten selected wavelengths using the PCA-DA had the highest VIP percentage values of 100% for both the Quercus *spp*. and *Jacaranda mimosifolia* (Figure 2.3). The lowest VIP percentage values were for Pinus *spp*. which ranged from 34% (1796) to 50% (2152) (Figure 2.3).

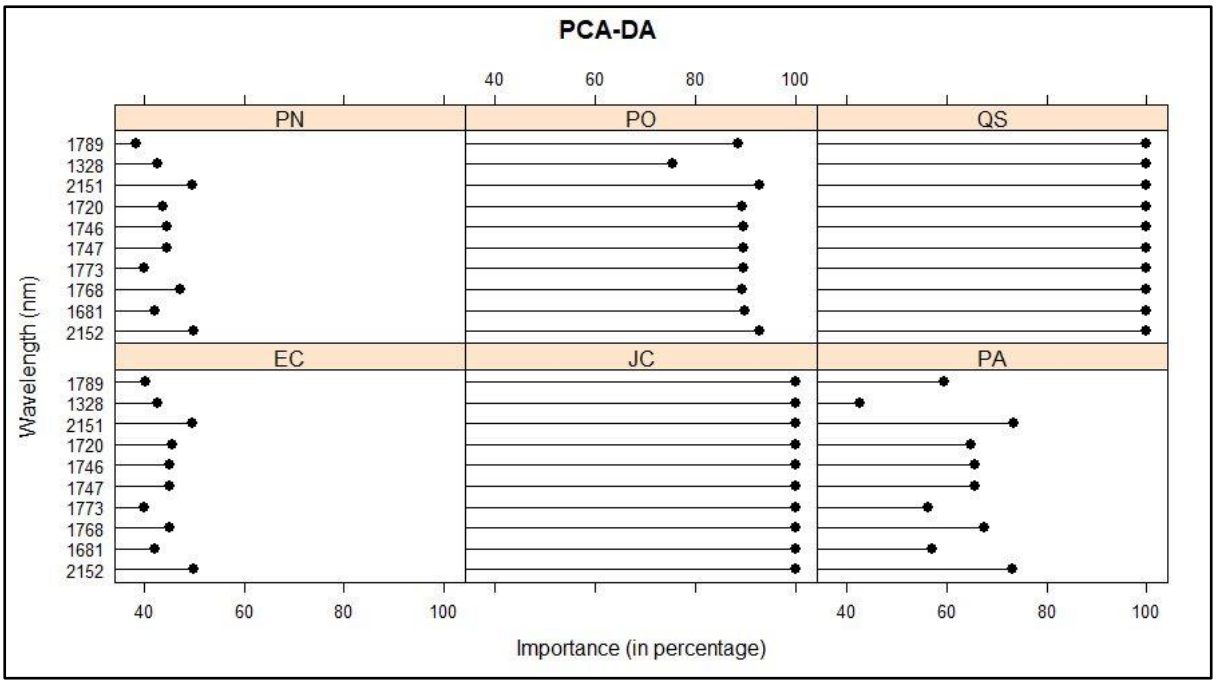


Figure 2.3 Wavelengths selected using the VIP method for the six urban trees in this study using PCA-DA. The trees are *Eucalyptus* spp. (EC), *Jacaranda mimosifolia* (JC), *Quercus* spp. (QS), *Platanus occidentalis* (PO), *Platanus* x *acerifolia* (PA) and *Pinus* spp. (PN).

2.3.2 PLS-DA wavelength selection results

The PLS-DA model was applied on all the hyperspectral wavelengths (n = 1523) to select the important variables to classify the common urban trees. The optimal value used for the model was component number 10 (Figure 2.4), which had a CV accuracy value of 98.6%. This value increases with the number of components, where 28.5% was obtained for the 1st component and 98.6% for the 10th component (Figure 2.4). The 10 principal components were used in developing the PLS-DA model in this study, and VIP scores for the individual wavelengths were calculated.

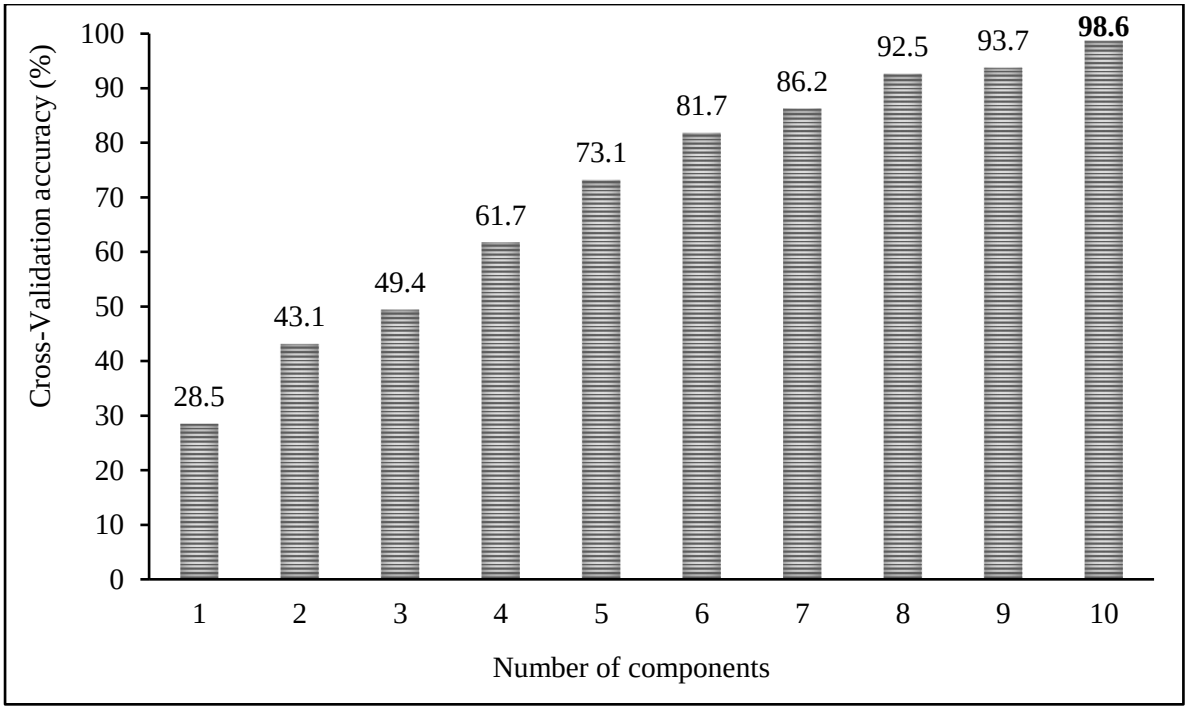


Figure 2.4 Discriminatory power for PLS-DA components using all hyperspectral wavelengths data (n = 1523). The 10-fold cross-validation resampling method was used to get cross-validation accuracy results for the components. The optimal component with the highest accuracy value is shown in bold.

The ten wavelengths selected by the PLS-DA algorithm had low VIP percentage values for *Pinus* spp., with the highest being 5% for the 1378nm, 1377nm, 1376nm and 1375nm wavelengths (Figure 2.5). The highest VIP values for all the common urban trees wavelengths using the PLS-DA algorithm were obtained on the Platanus x acerifolia ranging from 44% (762nm) to 100% (1378nm), as shown in Figure 2.5.

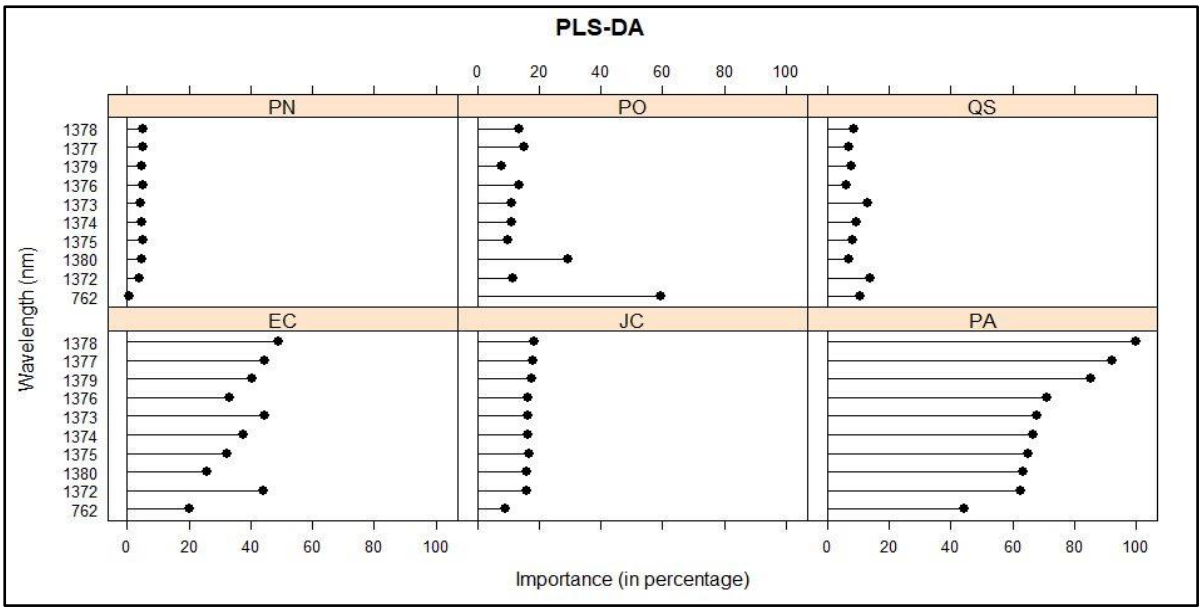


Figure 2.5 Wavelengths selected using the VIP method for the six common urban trees in this study using PLS-DA. The six common urban trees are *Eucalyptus* spp. (EC), *Jacaranda mimosifolia* (JC), *Quercus* spp. (QS), *Platanus occidentalis* (PO), *Platanus* x *acerifolia* (PA) and *Pinus* spp. (PN).

2.3.3 GRRF wavelength selection results

The RF method was utilised to select the most relevant features from the overall hyperspectral data (n = 1523) collected using the ASD field spectrometer. The mean decrease in Gini index was used to select the most important wavelengths in differentiating the common urban trees. The importance scores were derived using the mean decrease in Gini index. The mean decrease in Gini index values in the visible region (350–700nm) ranged from 0.03 (595nm) to 5.86 (587nm) (Figure 2.6). The mean decrease in Gini values in the NIR region (700-1300nm) were from 0 (885, 890, 898, 1171, 1199, 1203, 1206, 1208 and 1259, 1281nm) to 1.86 (713nm). The red-edge region (680-750nm) had a mean decrease in Gini index values ranging from 0.12 (690nm) to 1.86 (713nm). The mean decrease in index values in the SWIR (1300–2500nm) ranged from 0 (1618nm) to 5.29 (2174nm) (2174nm) (Figure 2.6).

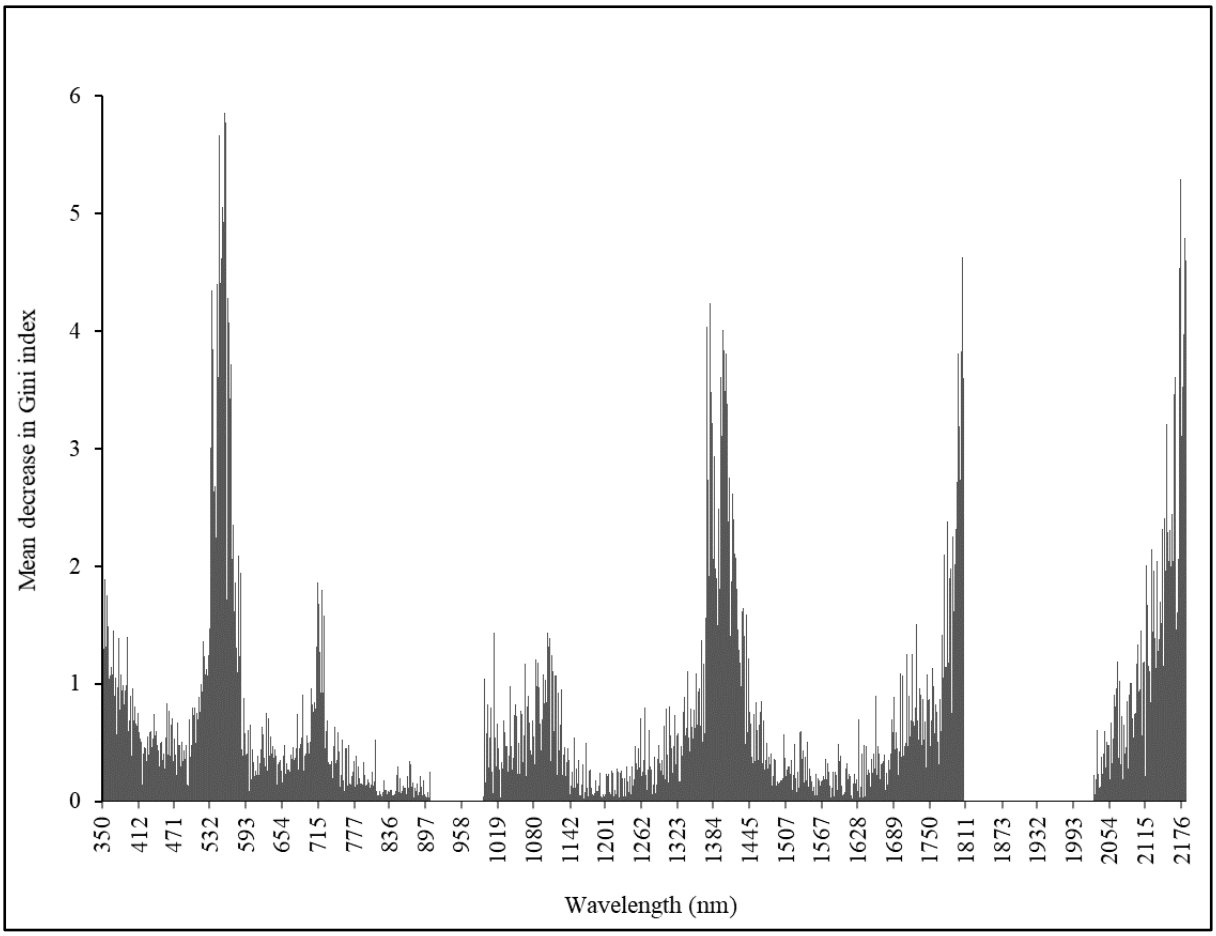


Figure 2.6 The mean decrease in Gini index showing the variable of importance for all the variables (n = 1523) for the traditional RF classifier. The important variables have a high mean decrease in Gini index value.

The GRRF was used to select the important wavelengths from the importance scores obtained using the traditional RF classifier. The GRRF technique selected 13 optimal wavelengths where five wavelengths (360nm, 409nm, 513nm, 562nm, 618nm) were in the visible region whilst the rest were in the SWIR region (Figure 2.7). These optimal wavelengths were then utilized as input variables in distinguishing common urban trees using the SVM and RF classification methods.

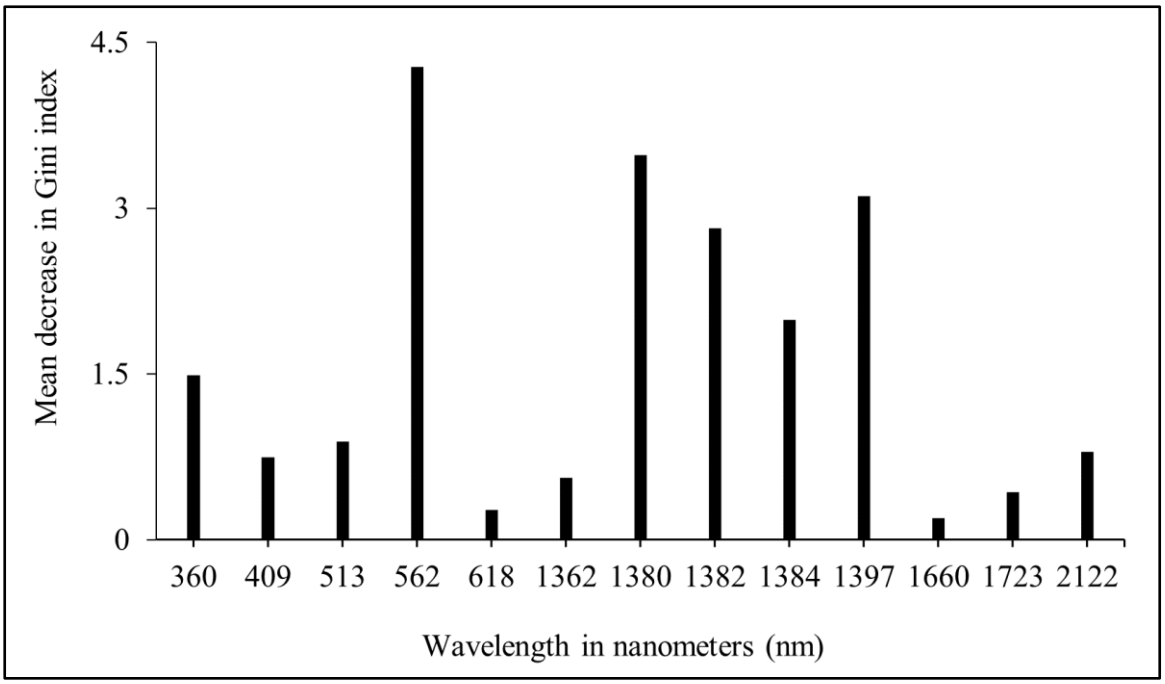


Figure 2.7 The wavelengths with the highest importance scores selected by the GRRF as calculated by the traditional RF for the urban trees.

2.3.4 Comparison of the selected wavelengths from the three feature selection techniques (PCA-DA, PLS-DA and GRRF)

The wavelengths selected by the three feature selection techniques (PCA-DA, PLS-DA and GRRF are shown in Table 2.3. Both the PCA-DA and PLS-DA selected 10 wavelengths, while the GRRF selected 13 wavelengths from the total number of wavelengths (n = 1523) used in this study (Table 2.3). One wavelength (1380nm) appeared in both the PLS-DA and GRRF, illustrating that it could potentially discriminate tree species using both feature selection techniques.

Table 2.3 Wavelengths selected by the PCA-DA, PLS-DA and GRRF techniques. The wavelength that was able to differentiate in both PLS-DA and GRRF is highlighted in grey.

Variable selection method	Selected wavelengths (nm)	Number of selected wavelengths
PCA-DA	1328, 1681, 1720, 1746, 1747, 1768, 1773, 1789, 2151, 2152	10
PLS-DA	762, 1372, 1373, 1374, 1375, 1376, 1377, 1378, 1379, 1380	10
GRRF	360, 409, 513, 562, 618, 1362, 1380, 1382, 1384, 1397, 1660, 1723, 2122	13

2.3.5 Accuracy Assessment

The random splitting of the selected data into 70% for training and 30% for accuracy assessment was randomly repeated seven times to ensure the model's stability. The accuracies were tested, and they showed no significant differences. The optimal wavelengths selected by PCA-DA (n = 10), PLS-DA (n = 10) and GRRF (n = 13) were classified using the SVM and the traditional RF classifier. As shown in Table 2.4, the SVM classifier had the highest overall accuracy values as compared to RF for all the feature selection techniques (PCA-DA, PLS-DA and GRRF). The GRRF produced the highest overall accuracy value (95.3%) with a kappa coefficient of 94.4% compared to the PCA-DA's overall accuracy (86%) and kappa coefficient (83.2%) and PLS-DA's overall accuracy (93.3%) and kappa coefficient (92%) using the SVM classifier (Table 2.4). The selected wavelengths using the GRRF technique also produced the highest overall accuracy value (88.7%) and kappa coefficient (86.4%) as compared to PCA-DA's accuracy value (64%) and kappa coefficient (56.8%), and PLS-DA's accuracy value (72%) using the RF classifier (Table 2.5).

Table 2.4 Confusion matrix obtained using SVM classifier for the selected wavelengths using PCA-DA, PLS-DA and GRRF. The overall accuracy (OA) and kappa values are shown for the urban trees namely; *Eucalyptus* spp. (EC), *Jacaranda mimosifolia* (JC), *Quercus* spp. (QS), *Platanus occidentalis* (PO), *Platanus* x *acerifolia* (PA) and *Pinus* spp. (PN).

PCA-DA							
Class	EC	JC	QS	PO	PA	PN	Total
EC	20	2	1	0	0	0	23
JC	5	20	1	0	3	0	29
QS	0	0	22	1	2	0	25
PO	0	3	0	23	1	0	27
PA	0	0	1	1	19	0	21
PN	0	0	0	0	0	25	25
Total	25	25	25	25	25	25	150
OA =86%							
Kappa = 83.2%							

PLS-DA							
Class	EC	JC	QS	PO	PA	PN	Total
EC	21	2	0	0	0	0	23
JC	2	23	0	1	0	0	26
QS	1	0	22	0	0	0	23
PO	0	0	1	24	0	0	25
PA	1	0	2	0	25	0	28
PN	0	0	0	0	0	25	25
Total	25	25	25	25	25	25	150
OA = 93.3%							
Kappa = 92%							

GRRF							
Class	EC	JC	QS	PO	PA	PN	Total
EC	24	0	1	0	0	0	25
JC	0	25	0	0	0	0	25
QS	1	0	23	0	1	0	25
PO	0	0	0	23	1	0	24
PA	0	0	1	2	23	0	26
PN	0	0	0	0	0	25	25
Total	25	25	25	25	25	25	150
OA = 95.3%							
Kappa = 94.4%							

Table 2.5 Confusion matrix obtained using RF classifier for the selected wavelengths using PCA-DA, PLS-DA and GRRF. The overall accuracy (OA) and kappa values are shown for the urban trees namely; *Eucalyptus* spp. (EC), *Jacaranda mimosifolia* (JC), Quercus spp. (QS), *Platanus occidentalis* (PO), *Platanus* x *acerifolia* (PA) and *Pinus* spp. (PN).

PCA-DA							
Class	EC	JC	QS	PO	PA	PN	Total
EC	13	3	0	1	3	0	20
JC	6	13	3	0	6	0	28
QS	2	1	16	0	2	0	21
PO	2	5	3	17	2	0	29
PA	2	3	3	7	12	0	27
PN	0	0	0	0	0	25	25
Total	25	25	25	25	25	25	150
OA = 64%							
Kappa = 56.8%							

PLS-DA							
Class	EC	JC	QS	PO	PA	PN	Total
EC	14	1	0	0	0	0	15
JC	3	20	2	3	6	0	34
QS	0	0	22	4	0	0	26
PO	4	0	0	17	2	0	23
PA	4	4	1	1	17	0	27
PN	0	0	0	0	0	25	25
Total	25	25	25	25	25	25	150
OA = 76.7%							
Kappa = 72%							

GRRF							
Class	EC	JC	QS	PO	PA	PN	Total
EC	19	1	1	1	1	0	23
JC	1	23	0	0	0	0	24
QS	1	1	22	1	0	0	25
PO	1	0	2	20	1	0	24
PA	3	0	0	3	23	0	29
PN	0	0	0	0	0	25	25
Total	25	25	25	25	25	25	150
OA = 88%							
Kappa = 86.4%							

Table 2.6 shows the PA and UA results from the selected wavelengths after being classified using the traditional RF classifier.

Table 2.6 Producer's accuracy (PA) and user's accuracy (UA) values for RF and SVM obtained from the optimal wavelengths selected using PCA-DA, PLS-DA and GRRF for the trees used in this study. The trees are *Eucalyptus* spp. (EC), *Jacaranda mimosifolia* (JC), *Quercus* spp. (QS), *Platanus occidentalis* (PO), *Platanus* x *acerifolia* (PA) and *Pinus* spp. (PN).

	PCA-DA				PLS-DA				GRRF			
	RF		SVM		RF		SVM		RF		SVM	
Class	PA	UA	PA	UA	PA	UA	PA	UA	PA	UA	PA	UA
EC	52	65	80	87	56	93	84	91	84	84	96	92
JC	52	46	80	69	80	59	92	88	88	88	100	100
PA	48	44	76	90	68	63	100	89	84	88	92	88
PO	68	59	92	85	68	74	96	96	84	78	92	96
QS	64	76	88	88	88	85	88	96	92	96	92	96
PN	100	100	100	100	100	100	100	100	100	100	100	100

2.4 Discussion

There has been a wide use of field spectral data for discriminating and classifying trees. This study shows the ability of hyperspectral data in the classification of six urban trees in the Randburg municipal area. This is in line with several studies: for example, Raczko and Zagajewski (2017) used hyperspectral data in mapping tree species in Poland; Cao *et al.* (2018) used field hyperspectral data in identifying eight mangrove species in Qi'ao Island of Zhuhai, China. Adam and Mutanga (2009) and Mureriwa *et al.* (2016) used hyperspectral data in the spectral discrimination and classification of vegetation species in South Africa. Due to the huge data volume and high dimensionality of hyperspectral data, removing redundant data and identifying key wavelengths is vital for the classification of urban trees (Aval *et al.*, 2019). Various techniques have been applied in reducing the high dimensionality of hyperspectral data, and it is vital to minimize the loss of information.

In this study, it was difficult to use a single feature selection method as no technique has been universally proven to be superior over others in selecting the optimal wavelengths for the classification of vegetation species (Adam and Mutanga, 2009). Hence three feature selection methods (PCA-DA, PLS-DA and GRRF) were used for feature selection and dimensionality reduction of field hyperspectral data. This is a key prerequisite for mapping urban tree species using remote sensing airborne and hyperspectral sensors as a small number of selected wavelengths give detailed information for classification purposes (Abbasi *et al.*, 2019).

2.4.1 Classification using wavelengths selected by multivariate statistical techniques

Most of the optimal bands selected by the three feature selection techniques (PCA-DA, PLS-DA and GRRF) in classifying the urban trees (*Eucalyptus* spp., *Jacaranda mimosifolia*, *Platanus* x *acerifolia*, *Platanus occidentalis*, *Quercus* spp. and *Pinus* spp.) were in the SWIR region. This is in line with other studies (Dalponte *et al.*, 2012; Alonzo *et al.*, 2014; Ferreira *et al.*, 2015), which observed wavelengths in the SWIR region as the most suitable bands for classifying trees. In the classification of tree species, the significance of the SWIR bands may be due to their capability in discriminating the subtle variations in the moisture content from one species' type to the other (Cherrington, 2016). Although there were no biochemical features directly assessed in this study, it assumed that varying levels of lignin and the amount of cellulose available in foliar and plant matter that is non-photosynthetic might have driven the separability of trees in the SWIR region (Alonzo *et al.*, 2014).

None of the wavelengths was selected from the NIR region when the PCA-DA algorithm was applied. The PLS-DA algorithm selected only a single wavelength (762nm) in the NIR region of the electromagnetic spectrum. The results are in line with previous studies (Alonzo *et al.*, 2014; Oldeland *et al.*, 2017), which found the NIR region less important in discriminating tree species. Alonzo *et al.* (2014) used hyperspectral data to map 29 tree species (including the six tree species used in this study) in Santa Barbara, California, while Oldeland *et al.* (2017) classified 16 other tree and shrub species in central Namibia. Oldeland *et al.* (2017) found that the high variation within the classes and the reflectance might have been influenced by metabolites (e.g. proteins) and water, resulting in the SWIR playing a critical role in discriminating tree species. The GRRF algorithm selected five significant wavelengths in the visible region, from 360nm to 618nm (Figure 2.7). The reflectance from the visible region in this study was mainly associated with the absorption traits of the trees' leaf pigments (Aval *et al.*, 2019). These results also agree with those in the literature (Mureriwa *et al.*, 2016; Abbasi *et al.*, 2019), which showed a correlation between wavelength absorption in the visible region and leaf chlorophyll content in the tree leaves.

2.5 Conclusions

The focus of this study was to identify the key wavelengths for classifying urban trees (*Eucalyptus* spp., *Jacaranda mimosifolia*, *Platanus* x *acerifolia*, *Platanus occidentalis*, *Quercus* spp. and *Pinus* spp.) using feature selection methods on field hyperspectral data. Our main findings include: (1) The use of various feature selection techniques such as PCA-DA, PLS-DA, and GRRF can reduce the high dimensionality associated with field hyperspectral data in a heterogeneous area (2) The selected wavelengths by GRRF produced the highest classification accuracies, followed by PLS-DA and

lastly, PCA-DA feature selection methods. The selected wavelengths were classified using RF and SVM classification methods. The GRRF can be regarded as the most effective and efficient feature selection tool compared to PCA-DA and PLS-DA in reducing the high dimensionality of field hyperspectral data. The selected key wavelengths were mainly in the SWIR region of the electromagnetic spectrum showing that they can be used to classify urban trees (3) The SVM classifier proved to be more reliable than RF in classifying the selected wavelengths of the urban trees.

Overall, this study shows the potential of feature selection methods in reducing the high dimensionality and classification of urban trees using field hyperspectral data. Although this study was conducted using field hyperspectral data on urban trees with data collected using stratified purposeful sampling, the results do not show the spatial distribution of the species in the whole study area. The use of very high spatial resolution (VHSR) hyperspectral images such as Airborne Prism Experiment (APEX) and Hyperion or multispectral images such as Worldview and Sentinel-2 can assist in providing information on the spatial distribution of the urban trees in the study area which can be of great importance to the municipality and stakeholders involved in greenspace or urban tree management.

Chapter Three

Evaluating the capability of Worldview-2 imagery for mapping alien tree species in a heterogeneous urban environment

This chapter is based on Jombo, S., Adam, E., Byrne, M. J. and Newete, S. W. (2020) Evaluating the capability of Worldview-2 imagery for mapping alien tree species in a heterogeneous urban environment. *Cogent Social Sciences,* 6**,** 1754146.
DOI: https://doi.org/10.1080/23311886.2020.1754146

Abstract

Street trees in urban planning have a long history as providers of an amicable environment for urban dwellers. Nevertheless, street trees are not always without a challenge, their ecosystem disservices include, *inter alia*, cracking pavements and foundations due to wandering tree roots that destroy concrete or asphalt surfaces. Thus, effective mapping of street trees assists in planning a suitable urban environment to improve city life. The traditional method for urban tree mapping is costly, time-consuming, and labour intensive. However, commercially operated multi-spectral sensors, such as WorldView (WV), provide a more viable way to map trees at the species level. This study investigates the use of WV-2 imagery in the classification and mapping of five common alien street trees in a complex urban environment. It also examined the feasibility of Random Forest (RF) and Support Vector Machines (SVM) classifiers in mapping street trees in a heterogeneous urban environment. The classifiers produced an overall accuracy of 84.2% for RF and 81.2% for SVM. This study provides a detailed understanding of urban tree species to the municipality of Johannesburg and offers environmental managers an insight into classification methods for mapping trees using satellite imagery to comprehend their spatial distribution.

3.1 Introduction

The mapping of tree species in an urban environment is vital for planning through strengthening our knowledge of their ecological functions in these environments (Liu *et al.*, 2017). Urban trees provide ecosystem services such as mitigating urban heat island effects (Yan *et al.*, 2018), reducing air and noise pollution, as well as potential flooding, and they support biodiversity (Seiferling *et al.*, 2017). Urban tree species also offer essential social, economic and psychological amenities to human beings, such as increased property values and improved physical/mental health (Tyrväinen *et al.*, 2005). Even though urban trees offer various advantages, there is a debate about alien tree species use in cities. The major debate over the usefulness of alien vs indigenous tree species necessitates precise identification and mapping of alien trees, which is important for city or metropolis managers to develop and sustain urban planning strategies (Li *et al.*, 2015). Alien tree species were introduced into South African cities for recreation parks, soil stabilisation, erosion control, timber use, shelter, beekeeping, ornamental use, firewood and commercial purposes, amongst other reasons (Henderson, 2001; Zengeya *et al.*, 2017). Alien tree species in South Africa originated from Europe, Australia, Central America, and North-West Argentina (Henderson, 2001). Accurate spatial data on urban trees are required to assess tree species' extent and distribution to estimate their ecosystem services and disservices (Nowak *et al.*, 2008).

Urban tree inventories based on spatial data have long been established using field-based surveys and visual interpretation of aerial photography (Myeong *et al.*, 2006). These techniques work well on local and small-scale levels (Alonzo *et al.*, 2014). However, the process is time-consuming, labour intensive and costly, especially at large scales and heterogeneous environments (Alonzo *et al.*, 2016). Remote sensing technologies offer a solution to these problems (Fassnacht *et al.*, 2016; Liu *et al.*, 2017) because they are efficient, robust, repeatable and rapid in monitoring urban tree dynamics (Myeong *et al.*, 2006). The use of hyperspectral imagery has overcome time and labour challenges in mapping urban tree species (Liu *et al.*, 2017). These challenges are because of the complexity of features in urban areas and the heterogeneity of land covers (Li *et al.*, 2015), diversity of the species and variations in the spatial characteristics (Alonzo *et al.*, 2014). On the other hand, hyperspectral data usage is also constrained by availability, the high dimensionality of data, computer processing time and cost (Adam *et al.*, 2017).

Commercially operated sensors such as RapidEye and WorldView provide multispectral and panchromatic imagery globally, at a high spatial resolution (<7m) for analysing tree species (Ke and Quackenbush, 2011; Richardson and Moskal, 2014). Their efficiency in classifying trees in a

complex urban setting justify their continued use (Novack *et al.*, 2011). WorldView-2 (WV-2) satellite imagery with good radiometric, spectral and geometric resolution (up to eight bands) has produced satisfactory results in urban tree species mapping. In earlier studies by Li *et al.* (2015), Yan *et al.* (2018) and Shojanoori *et al.* (2016), urban tree species were mapped using WV-2 satellite data and produced high accuracy values. The accuracy of WV-2 satellite data to provide a precise thematic map depends on the selected remote sensing data characteristics (landscape complexity), as well as the methods used for processing and classifying the images (Lu and Weng, 2007).

Image appropriateness and the classification method used are essential requirements to obtain optimal accuracies (Lu and Weng, 2007). Previous studies utilized different machine algorithms such as random forest (RF), decision trees, support vector machines (SVM) and k-Nearest Neighbors (Knn) to classify satellite imagery (Thanh Noi and Kappas, 2017). Machine learning algorithms, in particular, RF, have been used in previous studies (Puissant *et al.*, 2014; Li *et al.*, 2015) and performed well in classifying tree species in urban environments. Support Vector Machines (SVM) have also increasingly been utilized in natural vegetation classification (Pal, 2005; Niska *et al.*, 2010; Krahwinkler and Rossman, 2011; Li *et al.*, 2015; Thanh Noi and Kappas, 2017). Furthermore, RF and SVM classification methods have mostly classified images based on pixels, and few studies have used object-based image analysis (OBIA) in which objects are used to depict features (Li *et al.*, 2015). Previous research studies (Li *et al.*, 2015; Mustafa *et al.*, 2015; Yan *et al.*, 2018) have mapped urban trees using OBIA and produced satisfactory results.

The City of Johannesburg (CoJ) is considered the largest man-made forest in the world (Schäffler and Swilling, 2013). CoJ is predominantly planted with alien trees that appeared with the Europeans' arrival in the 19th century (Schäffler and Swilling, 2013). Improved classification accuracy can provide us with a better understanding of the health of all trees planted in the CoJ. The alien tree species are subject to many stresses, which include: soil, water and air pollution, soil sealing and compaction (Pautasso *et al.*, 2015; Paap *et al.*, 2017). These stresses make trees susceptible to pathogens and insects (Paap *et al.*, 2017). For example, the polyphagous shot hole borer, *Euwallacea fornicatus*, an ambrosia beetle that is affecting urban alien trees in the CoJ, including *Platanus* spp., (Paap *et al.*, 2018), *Jacaranda* spp., *Quercus* spp. and *Eucalyptus* spp. (Forestry and Agricultural Biotechnology Institute, 2019). Data capture via WV-2 satellite imagery can be used to identify such affected areas, which prove invaluable for urban planners and other research groups.

The CoJ is believed to have over 10 million trees, with over 4.5 million in private gardens and about 2.5 million trees in conservation areas, parks, nature reserves, city's pavements and cemeteries (Johannesburg City Parks and Zoo, 2018). Nevertheless, the management of these trees depends on anecdotal information on the urban tree species in the CoJ. To address this issue, this study assesses the ability of remote sensing to map and classify urban alien tree species in the Johannesburg area using high-resolution multispectral data. In this study, the specific objectives were i) to examine the effectiveness of RF and SVM in mapping urban alien tree species and other land use and land cover (LULC) classes with the use of WV-2 imagery in a suburb of Johannesburg; ii) test the utility of the spectral bands of WV-2 in mapping urban alien tree species and LULC classes, and iii) compare the performance of RF and SVM classification methods in mapping urban alien tree species and LULC classes using high-resolution WV-2 image.

3.2 Methodology

3.2.1 Study area

Randburg municipal area (167.98km^2) is where this study was conducted, in Region B of the CoJ (Figure 3.1). The annual rainfall in CoJ is approximately 750mm per annum, with potential evaporation of around 1600 mm/annum (Tyson and Wilcocks, 1971). The rain mostly falls in the summer season, which runs from October to February and temperature averages reaches around 15ºC in winter and 20ºC in summer (Naicker *et al.*, 2003). The mean altitude in CoJ is 1512m, with altitudes ranging between 1081m and 1899m (Grobler *et al.*, 2002). The soil in this area is composed of Glenrosa and Mispah soil forms (Grobler *et al.*, 2002), and the rocks are crystalline of Archean age, which underlies the whole of Johannesburg (Abiye *et al.*, 2018). The rocks in the area are mainly granitic gneiss, meta-volcanic and metasedimentary rocks (Abiye *et al.*, 2018).

The most common and fast-growing alien trees in the study area are black wattle, jacaranda, eucalyptus, pepper trees, oaks and London planes which were introduced in the 19th century (Turton *et al.*, 2006). There are indigenous trees in the CoJ but primarily non-indigenous tree species were planted during Johannesburg's colonial era, resulting in the city's spatial diversity (Schäffler and Swilling, 2013).

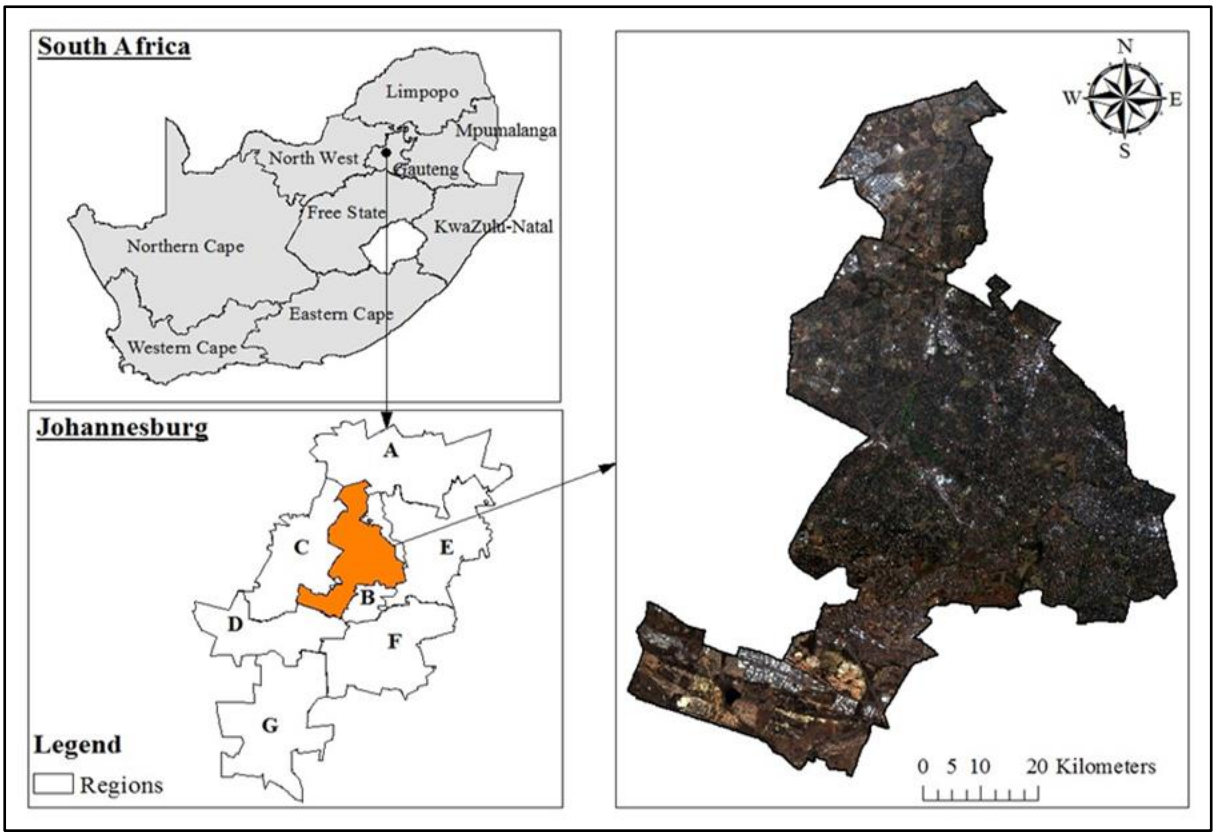


Figure 3.1 Maps of South African provinces, Johannesburg's regions and true-colour WorldView-2 satellite imagery (RGB 532 combination) of the Randburg municipal area located in the City of Johannesburg.

3.2.2 Remote sensing data acquisition

This study is based on remote sensing and field data obtained in spring 2017. A total number of 36 scenes of WV-2 satellite imagery, captured on 15 September 2017, and field data collected in November of the same year were used. The scenes were supplied by the CoJ Corporate Geo-Informatics, Development Planning and Urban Management (DP&UM) department, free of charge with radiometric and geometric corrections already done. To combine the scenes for the WV-2 image, they were mosaicked using ArcMap 10.5 software. The WV-2 image provides high spatial resolution data, with a swath width of 16.4km at nadir, eight multispectral bands, and a 2m spatial resolution. Moreover, the WV-2 multispectral sensor's eight multi-spectral bands cover the NIR1, NIR2, red edge, red, yellow, green, blue and coastal wavelength region (Table 3.1). Furthermore, the panchromatic sensor band has a spatial resolution of 0.46m and lies within a spectral range of 450 – 800nm. The WV-2 image was provided in Hartebeeshoek WGS84 coordinates (Central Meridian-29, Projection-Transverse Mercator).

Table 3.1 WV-2 spectral resolution and sensor band names used in this study

Band number and name	Centre wavelength (nm)	Spectral resolution (nm)	Spatial resolution (m)
1. (Coastal blue)	425	400-500	1.85
2. (Blue)	480	450-510	1.85
3. (Green)	545	510-580	1.85
4. (Yellow)	605	585-635	1.85
5. (Red)	660	630-690	1.85
6. (Red edge)	725	705-745	1.85
7. (NIR1)	833	770-895	1.85
8. (NIR2)	950	860-1040	1.85

3.2.3 Field data collection

A handheld outdoor Global Positioning System (G.P.S) receiver (Garmin eTrex 20 X) was used to collect field data and determine the coordinates for the dominant alien tree species. Due to the dearth of precise data on the spatial distribution of urban trees in South Africa, stratified purposive sampling was used to visit areas dominated by five dominant alien tree species (*Eucalyptus spp.*, *Jacaranda spp.*, *Platanus spp.*, *Quercus spp.* and *Pinus spp.*). The study area was divided into zone segments and samples taken, ensuring that every block has an equal chance of being selected. Stratification permits accuracy by combining the results from random samples in the chosen zone segments (Jaenson *et al.*, 1992). In addition, this method captures major differences rather than identifying a common species even though the latter may appear in the analysis (Palinkas *et al.*, 2015). The zigzag sampling method was used to provide a uniform distribution of the sampling sites (Ryan *et al.*, 2007), and it identified the urban alien tree species that were planted mostly along the streets in the study area. Additional ground truth points were also collected for the common land use/cover classes (Table 3.2).

The sample size for the five urban alien tree species and additional LULC classes was 1369 (Table 3.2). The sample was divided into a training set (70%) of 964 and a test set (30%) of 405.

Table 3.2 Scientific and common names, code, training, test and total samples used in this study.

Name	Code	Common name	Training samples	Test samples	Total samples
Eucalyptus spp.	EC	Eucalyptus	73	31	104
Jacaranda spp.	JC	Jacaranda	64	27	91
Pinus spp.	PN	Pine	97	41	138
Platanus spp.	PL	London plane	49	20	69
Quercus spp.	QR	Oak	34	14	48
Bare land	BL	N/A	87	36	123
Built-up	BU	N/A	198	84	282
Grassland	GL	N/A	152	64	216
Other woody vegetation	OWV	N/A	177	75	252
Shadow	SW	N/A	33	13	46
Total			964	405	1369

The spectral characteristics of the five dominant alien tree species considered in this study are shown in Figure 3.2. The average spectrum was extracted from WV-2 imagery pixels, with $n = 40$ for each dominant alien tree species.

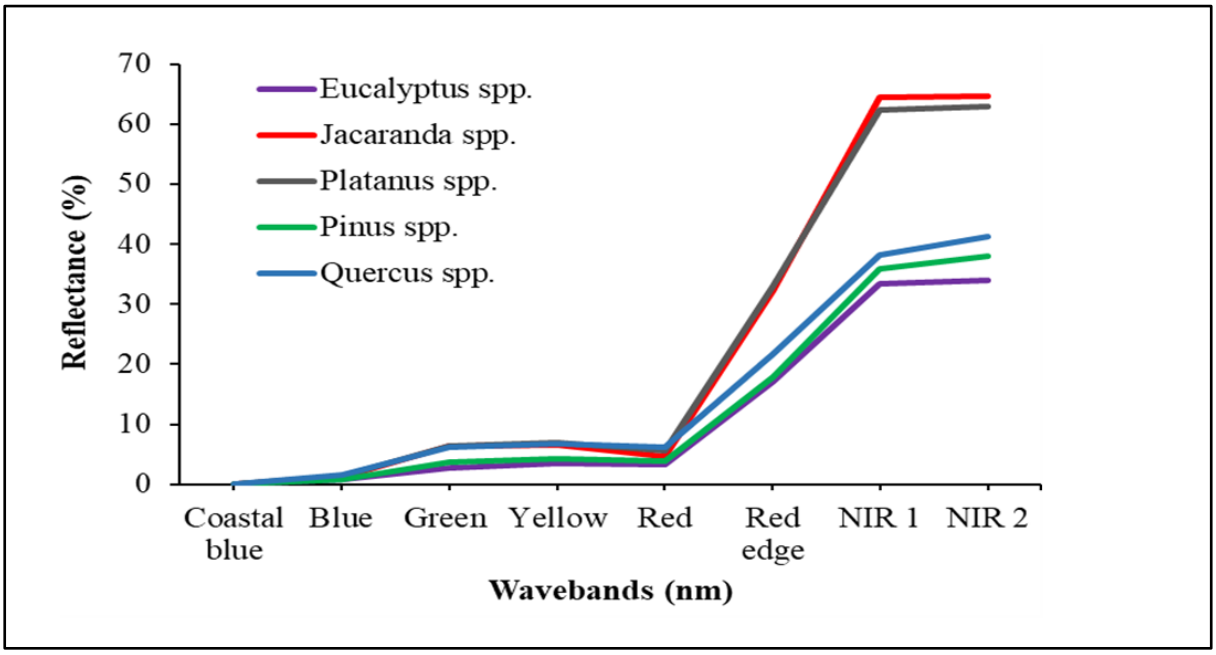


Figure 3.2 Average spectral reflectance curves extracted from Worldview-2 imagery pixels for the five dominant alien tree species considered in this study.

3.2.4 Data analysis and classification

The ability of RF and SVM machine learning algorithms to map urban alien trees was assessed in this study. The pixel-based classification techniques were used to map urban alien trees using the

RF and SVM machine learning algorithms. Both classifiers (RF and SVM) were trained with the training sample set, while the test set was used to measure the classification maps' accuracy. The training and test data obtained from the WV-2 image in the study area are shown in Table 3.2. The RF and SVM classifiers' parameters for both algorithms were analysed with the open-source statistical software R for the classification of the WV-2 imagery.

3.2.4.1 Random Forest (RF) classifier

The RF machine learning algorithm for statistical data analysis was put forward by Breiman (2001) for the improvement of classification and regression trees (CART). RF builds up numerous unpruned trees (*ntree*) on the original data's bootstrap sample, where the default ntree value in the "random forest" package in R statistical software is 500, specifically assigned for large datasets. The user defines *ntree* value, and trees with low bias and high diversity are created by the RF algorithm (Breiman, 2001). A bootstrap sample, which is a two-thirds majority of the original data, known as "in-bag" samples, are utilized in the training of trees, and the rest of them (one-third) is "out-of-the-bag" samples (Belgiu and Drăguţ, 2016). The "out-of-the-bag" samples estimate how well the RF classifier performs in a cross-validation approach, and the resulting estimate value is known as the out-of-bag (OOB) error (Belgiu and Drăguţ, 2016).

Furthermore, in the RF machine learning algorithm, random subsets of variables are used to split trees into nodes, referred to as *mtry* and its default value is the √P, which is the predictor variables' total number (Breiman, 2001). Based on the chosen variables of the *mtry* (default value is 500 trees), the variable yielding the greatest decrease in impurity is selected for the splitting of samples at each node (Breiman, 2001). Both the *ntree* and *mtry* parameters need to be put together to generate forest trees, and the optimization of these parameters can improve the classification accuracy values (Mutanga *et al.*, 2012; Belgiu and Drăguţ, 2016).

In this study, a 10-fold cross-validation technique dependant on the OOB error was used to identify the best *ntree* and *mtry* parameters. The *ntree* parameter tested in this study varied from 500 to 10 000 with 1000 intervals, and the *mtry* values ranged from 1 to 8. If the OOB error is low, this shows that the RF classification method performed well, whereas high OOB error values show poor performance.

In addition, the RF algorithm sets out the variable importance (VI) measurement and is calculated in different ways, which include making use of the Mean Decrease in Accuracy (MDA), or else the

Mean Decrease in Gini (MDG) (Breiman, 2001). In the RF model establishment, the computing time required is calculated using Equation 3.1 below:

$$\mathrm{T}\sqrt{MN\log(N)} \qquad \text{Equation 3.1}$$

where *M* illustrates the specific number of variables applied in each split, whereas *N* represents the total number of the training samples, and T stands for the total number of trees (Breiman, 2001; Belgiu & Drăguţ, 2016).

RF classifier has been used in other studies to successfully map urban buildings (Belgiu and Drăguţ, 2016), boreal forest habits (Räsänen *et al.*, 2013), tree, biomass and crown cover (Karlson *et al.*, 2015) as well as urban tree species (Puissant *et al.*, 2014; Li *et al.*, 2015; Liu *et al.*, 2017). This illustrates the usefulness of the RF classifier to map urban alien tree species for the current study. In this study, the RF classifier in R was utilized in mapping urban alien tree species in the study area.

3.2.4.2 Support Vector Machines (SVM) classifier

The Support Vector Machines (SVM) classifier does not require an assumption concerning data distribution and does not overfit the new or test data samples by applying viable principles (Abdel-Rahman *et al.*, 2014). The SVM machine-learning algorithm initially proposed by Vapnik (1995) focuses on the training sites, which are closest to the optimal boundary amid classes in the attribute space (Maxwell *et al.*, 2018). In addition, SVM is a supervised classification approach that is non-parametric and non-linear broadly employed in remote sensing research because of its precise capacity to derive results even using a small number of training samples or sites (Mountrakis *et al.*, 2011). The data points that lie on the supporting hyperplanes are known as support vectors, and the optimal hyperplane is positioned in the middle of the margin. Additionally, the machine-learning algorithm has kernel and mapping functions derived from the original input space to the high dimensional feature space (Mountrakis *et al.*, 2011).

In recent years, SVM's four most commonly utilized kernel functions are the polynomial, sigmoid, linear and radial basis function (RBF) kernels (Qian *et al.*, 2014). The current study makes use of the radial basis function (RBF) kernel since it lends itself to successfully classify urban land cover (Qian *et al.*, 2014) and tree species (Raczko and Zagajewski, 2017). The RBF kernel consists of two

significant parameters, which are the "gamma" (γ), and "cost" (C), which play an essential role in determining the overall classification accuracy value (Qian *et al.*, 2014).

Eight WV-2 bands and the RBF kernel were used to find an optimal hyperplane that could distinguish all the LULC classes, including the five-target tree species of this study. More so, the optimization of γ and C parameters of the RBF function was done using the LIBSVM library to obtain the best parameter values. The SVM classifier was run in R statistical software version 3.4.4, and the "e1071" library was used in the optimization of SVM parameters.

3.2.4.3 Accuracy assessment and validation

The accuracy of any classification algorithm in remote sensing is judged by the prediction performance testing results (Odindi *et al.*, 2016). Thus, the RF and SVM machine-learning algorithms were utilized to assess their efficiency using the test dataset (30%) in confusion matrices, where the kappa coefficient, user's, overall and producer's accuracy values were derived on the classified maps to ascertain the level of reliability and accuracy (Jombo *et al.*, 2017).

Moreover, the significant difference between the results from the SVM and RF classifiers was tested in this study using McNemar's test. The test is non-parametric, based on a normal test statistic, and calculated out of the two classification methods' error matrices. It is measured as follows (Equation 3.2):

$$Z = \frac{\not{f}\,12 - \not{f}\,21}{\sqrt{\not{f}\,12 + \not{f}\,21}} \qquad \text{Equation 3.2}$$

where $\not{f}\,12$ represents the misclassified number of samples by the RF yet classified correctly by the SVM classifier, and $\not{f}\,21$ represents a number in a total of samples classified correctly by RF although not classified correctly by SVM (Abdel-Rahman *et al.*, 2014). Additionally, the Z value was obtained in this study, and it shows the RF and SVM classifiers' difference in accuracy results. In McNemar's test, at 95% confidence level, the z score is regarded as statistically significant if it is > 1.96 (Adelabu *et al.*, 2013).

3.3 Results

3.3.1 RF parameter tuning

The best-input parameters for the classification of the five urban trees species and LULC classes were determined through optimization for training in the RF machine-learning algorithm. Consequently, the 10-fold cross-validation sampling method was utilized in this study, and a combination of the best parameters had *mtry* and *ntree* values of 2 and 6500, respectively (Figure 3.3). Additionally, this combination produced the lowest OOB error rate of 19.2% and the highest OOB error rate of 21.2% (*mtry* of 8 and *ntree* of 3500).

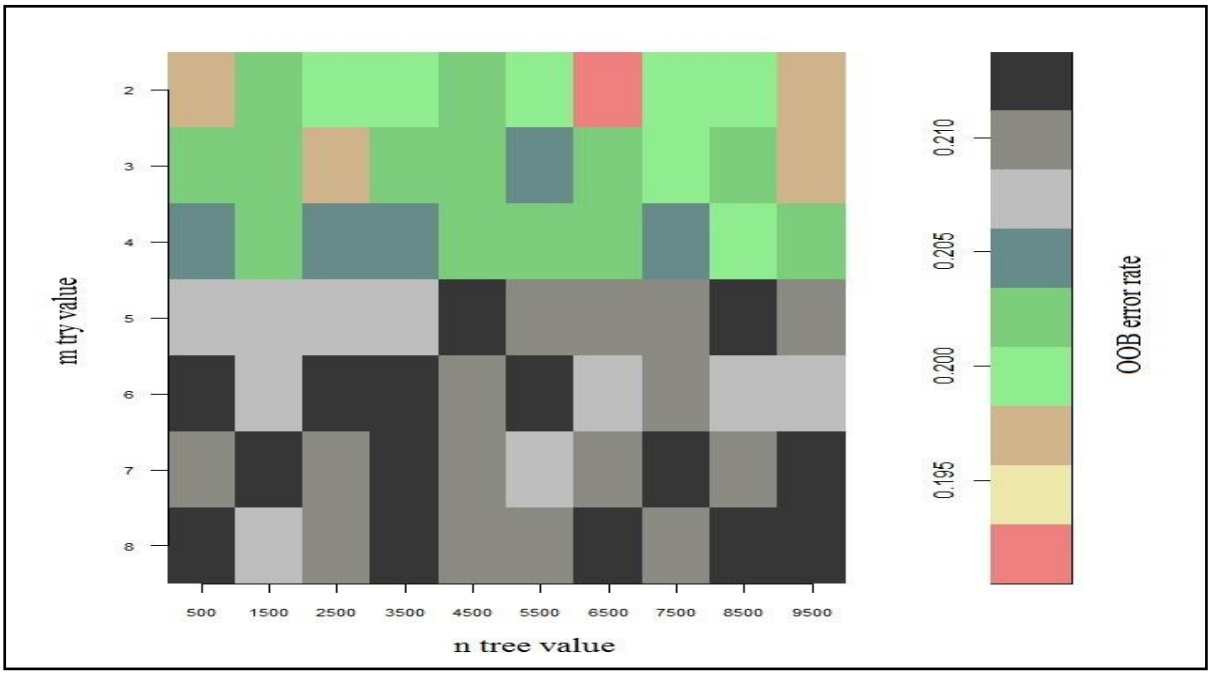


Figure 3.3 RF parameters (*mtry* and *ntree*) after optimization utilizing the 10-fold cross-validation sampling method and OOB estimate of error rate.

3.3.2 SVM parameter tuning

The best parameters of the γ and C RBF kernel parameters were found through optimization for classification using the SVM method. Therefore, the best γ and C parameters were obtained with the use of the 10-fold cross-validation sampling technique. Figure 3.4 illustrates that the best parameters for γ and C were 1 and 100, respectively, using the radial SVM-kernel and 521 support vectors.

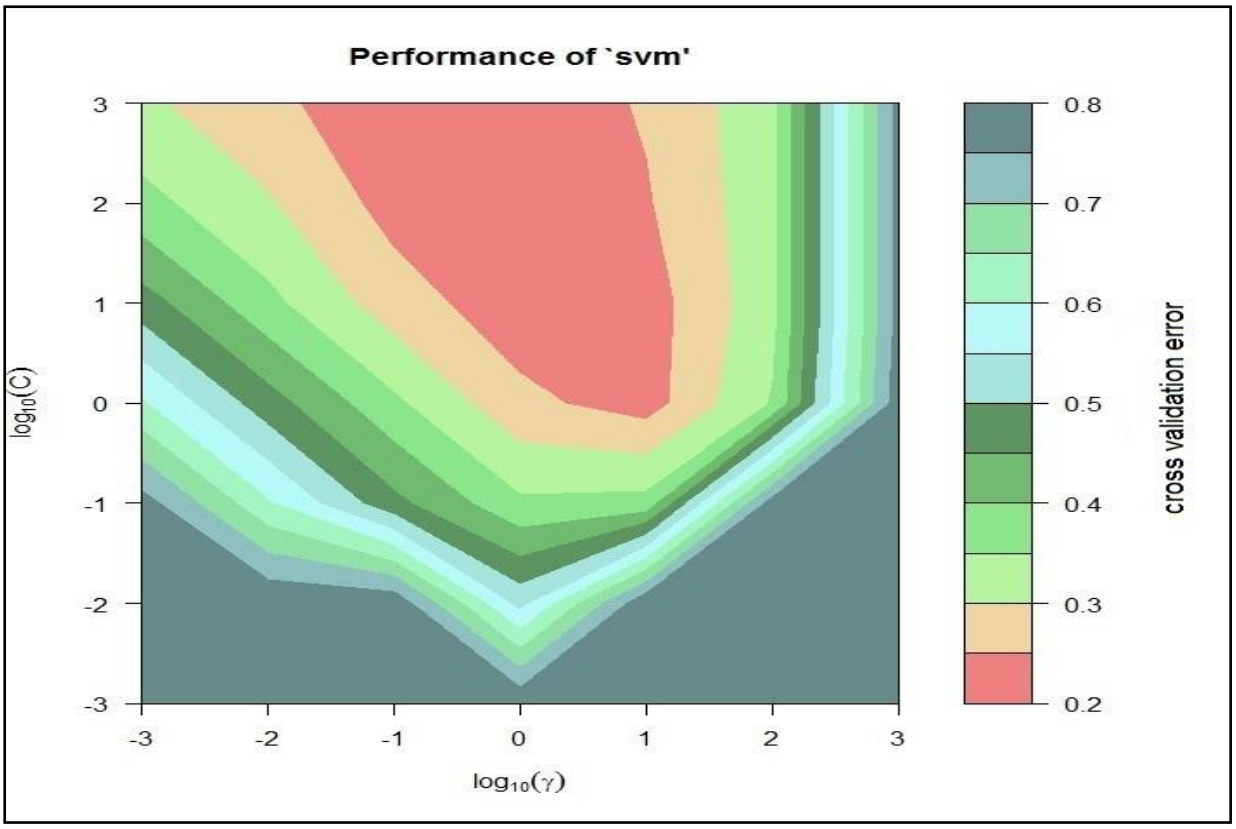


Figure 3.4 SVM parameters (γ and C) after optimization utilizing the 10-fold cross-validation sampling method and cross-validation error rate.

3.3.3 RF and SVM in urban tree species mapping

The maps showing other LULC classes and urban alien tree species' spatial distribution were produced for both the RF and SVM classifiers (Figure 3.5). The classified maps showed that other woody vegetation covers the largest land area compared to other classes. The other woody vegetation class covers mostly the southern part of the area of study (Figure 3.5). The *Platanus* spp. covered the largest area as compared to all the other urban alien trees classes with values of 8.38% and 8.11% using the RF and SVM classifiers, respectively (Table 3.3). The *Platanus* spp. were mainly found in Pine Park and Linden suburbs, situated on the southern side of the study area (Figure 3.5).



Figure 3.5 Classified maps of the five urban tree species and other classes in the Randburg municipal area using a) RF and b) SVM machine learning algorithms.

Furthermore, most of the *Eucalyptus* spp. are situated in the northern part of the area of study in places like suburbs such as Bloubosrand and Fleurhof, while most of the *Jacaranda* spp. were in the southern part of the area of study in the suburbs like Randpark ridge, Fairland and Windsor East. The *Pinus* spp. and *Quercus* spp. were mostly located in the Greenside and Parkview suburbs (southern part). All the LULC classes (bare land, built-up, grassland, other woody vegetation and shadow) were spread across all regions of the study area.

The two classifiers (RF and SVM) showed some minor inconsistencies in the size of each class. The differences in the areas covered by the five alien tree species classified using the two models were less than 1% (Table 3.3). However, the area of coverage (ha) between each of the species showed some substantial differences; for example, when looking at *Eucalyptus* spp., SVM shows an area of 737.96ha and RF, 576.54ha (Table 3.3). This gives a difference of 161.42ha between the total area of coverage between the two classifiers for the *Eucalyptus* spp. *Quercus* spp. had a difference of 164.08ha as SVM shows a total coverage area of 409.80ha and RF, 245.71ha (Table 3.3). The values for the SVM classifier were generally higher than the ones for the RF classifier. There are also differences in the area covered by other LULC classes; for example, the built-up area showed a difference of 769.19ha as RF showed total coverage of 5489.70ha, whilst SVM showed 4720.51ha for the same class. The RF classifier showed that the built-up and other woody vegetation were the dominant classes in the study area (Figure 3.5), whereas *Quercus* spp. and *Eucalyptus* spp. were the least dominant classes (Table 3.3). Shadow and *Quercus* spp. were the least dominant classes from the classified map using the SVM classifier (Table 3.3).

Table 3.3 Area in hectares (ha) and percentage cover of LULC classes acquired using the RF and SVM classification methods. The classes are bare land (BL), built-up (BU), *Eucalyptus* spp. (EC), Grassland (GL), *Jacaranda* spp. (JC), *Platanus* spp. (PL), *Quercus* spp. (QR), Other woody vegetation (OWV), *Pinus* spp. (PN) and Shadow (SW).

Class	RF in ha	Percentage (%)	SVM in ha	Percentage (%)
BL	807.72	4.81	1 060.74	6.31
BU	5 489.70	32.66	4 720.51	28.08
EC	576.54	3.43	737.96	4.39
GL	1 879.92	11.18	1 966.44	11.70
JC	884.77	5.26	921.85	5.48
PL	1408.23	8.38	1 362.96	8.11
QR	245.71	1.46	409.80	2.44
OWV	3 939.82	23.44	4 359.35	25.93
PN	866.03	5.15	865.77	5.15
SW	710.33	4.23	403.39	2.40
Total	16808.77	100.00	16 808.77	100.00

The RF classifier presented the variable of importance (Figure 3.6), indicating the part each band played in the classification procedure. More importantly, the more essential bands are the ones with the uppermost MDA values.

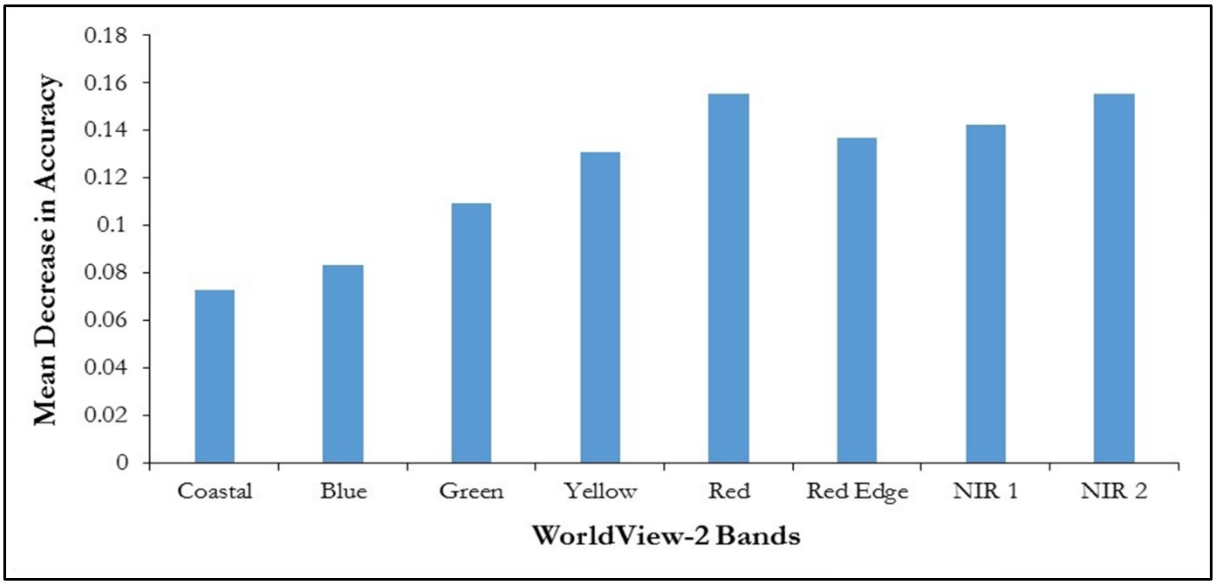


Figure 3.6 Importance of WV-2 multispectral bands in RF classification using Mean Decrease Accuracy (MDA) values.

The utility of every single WV-2 spectral band was evaluated in mapping all the classes in the study (Figure 3.7). As shown by the high level of MDA in Figure 3.7, the NIR and red edge bands were the most imperative in the classification of the five urban alien tree species (*Eucalyptus* spp.,

Jacaranda spp., *Platanus* spp., *Quercus* spp. and *Pinus* spp.). Similarly, areas with trees or vegetation predominantly fell on the red edge and NIR bands, which are valuable in the discrimination of plant species in classification, biomass and vegetation analysis. As illustrated in Figure 3.7, the green, red and yellow bands were the most imperative in mapping bare land areas. The red, yellow, and coastal bands were more significant in the built-up class classification, whereas the red edge and NIR bands were important in classifying the grasslands (Figure 3.7). The blue and two red bands were the most important bands for the other woody vegetation, whilst the NIR and red edge bands were the imperative bands for detecting the shadow class.

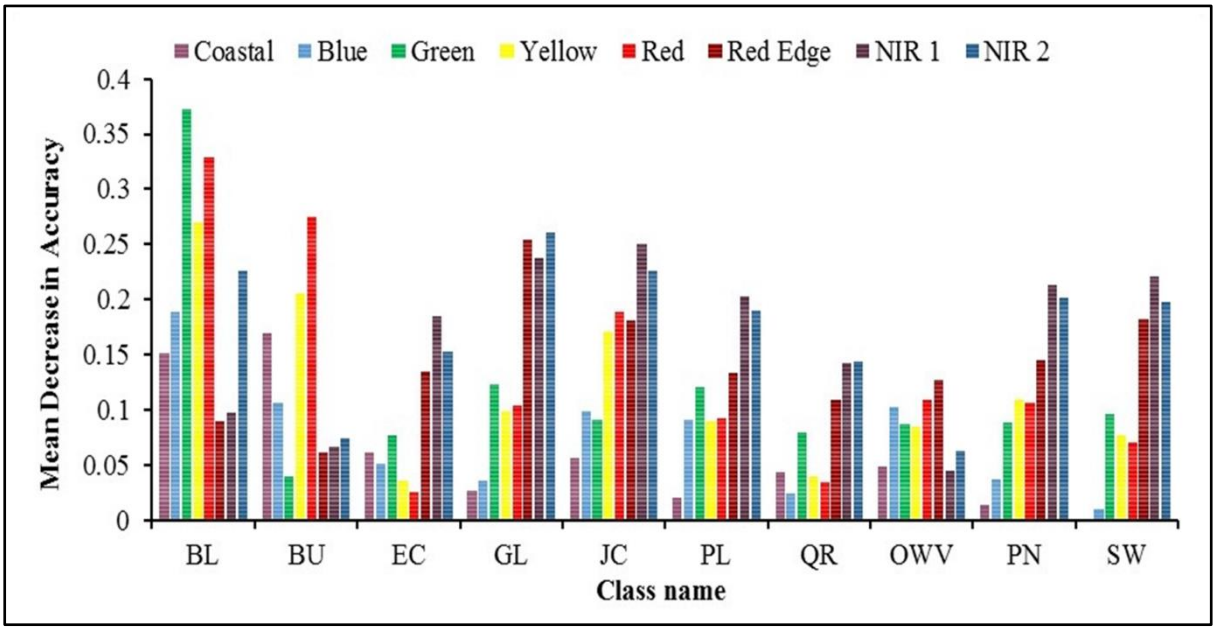


Figure 3.7 The Mean Decrease Accuracy (MDA) values showing the relationship between each class and WV-2 spectral bands. The classes are bare land (BL), built-up (BU), *Eucalyptus* spp. (EC), Grassland (GL), *Jacaranda* spp. (JC), *Platanus* spp. (PL), *Quercus* spp. (QR), other woody vegetation (OWV), *Pinus* spp. (PN) and Shadow (SW).

3.3.4 Accuracy assessment and validation

The accuracy levels for both RF and SVM classifiers were attained utilizing a 30% test set of data on the WV-2 imagery, and the confusion matrices for both classifiers are shown in Table 3.4. The range for the user's accuracy values for RF was between 61.11% (*Platanus* spp.) and 100% for the grassland class (Table 3.4a), while the producer's accuracy ranged from 55% (*Platanus* spp.) to 100% for the *Quercus* spp. class. Moreover, the RF values for the user's and producer's accuracy were lowest on the *Platanus* spp. at 61.11% and 55%, respectively (Table 3.4-a) whereas the same

accuracy levels for the SVM classifier ranged from 50% (shadow) to 100% (grassland) and 42.86% (*Quercus* spp.) to 98.81% (built-up) (Table 3.4-b).

The user's accuracy for the five urban alien trees (*Eucalyptus* spp., *Jacaranda* spp., *Platanus* spp., *Quercus* spp. and *Pinus* spp.) produced by the RF classifier ranged from 61.11% (*Platanus* spp.) to 85.71% for the *Eucalyptus* spp. class (Table 3.4-a), while the producer's accuracy ranged from 55% (*Platanus* spp.) to 100% (*Quercus* spp.). Similarly, the SVM accuracy results for these five alien trees ranged from 54.55% (*Quercus* spp.) to 68.89% (*Pinus* spp.), while the producer's accuracy values ranged from 42.86% (*Quercus* spp.) to 85.19% (*Jacaranda* spp.).

The overall accuracy assessment based on the independent test dataset was 84.2% for RF, with a 0.82 kappa coefficient value (Table 3.4-a), while that of the SVM classifier was 81.2%, and 0.78 as the kappa coefficient value (Table 3.4-b).

Table 3.4 Confusion matrices using a) RF and b) SVM classification algorithms. The classes are bare land (BL), built-up (BU), *Eucalyptus* spp. (EC), Grassland (GL), *Jacaranda* spp. (JC), *Platanus* spp. (PL), *Quercus* spp. (QR), Other woody vegetation (OWV), *Pinus* spp. (PN) and Shadow (SW). The producer's accuracy (PA), overall accuracy (OA), user's accuracy (UA), and kappa coefficient were calculated using the 'rasclass' package in R on the test dataset.

a. RF classification

Class	BL	BU	EC	GL	JC	PL	QR	OWV	PN	SW	Row total	UA
BL	27	7	0	0	0	0	0	0	0	0	34	79.41
BU	9	77	0	0	0	0	0	1	0	0	87	88.51
EC	0	0	24	0	0	0	0	3	1	0	28	85.71
GL	0	0	0	62	0	0	0	0	0	0	62	100.00
JC	0	0	0	0	17	2	0	5	0	0	24	70.83
PL	0	0	0	0	2	11	0	5	0	0	18	61.11
QR	0	0	0	0	0	0	14	1	0	2	17	82.35
OWV	0	0	0	2	8	7	0	59	0	0	76	77.63
PN	0	0	6	0	0	0	0	1	40	1	48	83.33
SW	0	0	1	0	0	0	0	0	0	10	11	90.91
Column Total	36	84	31	64	27	20	14	75	41	13	405	
PA	75	91.67	77.42	96.88	62.96	55	100	78.67	97.56	76.92		
OA	84.2%											
Kappa coefficient		0.82										

b. SVM classification

Class	BL	BU	EC	GL	JC	PL	QR	OWV	PN	SW	Row total	UA
BL	30	1	0	0	0	0	0	0	0	0	31	96.77
BU	6	83	0	0	0	0	0	0	0	0	89	93.26
EC	0	0	20	0	0	0	0	3	10	0	33	60.61
GL	0	0	0	62	0	0	0	0	0	0	62	100.00
JC	0	0	0	1	23	3	0	7	0	0	34	67.65
PL	0	0	0	0	1	10	1	4	0	0	16	62.50
QR	0	0	0	0	0	0	6	1	0	4	11	54.55
OWV	0	0	1	1	3	7	0	57	0	1	70	81.43
PN	0	0	10	0	0	0	0	3	31	1	45	68.89
SW	0	0	0	0	0	0	7	0	0	7	14	50.00
Column total	36	84	31	64	27	20	14	75	41	13	405	
PA	83.33	98.81	64.52	96.88	85.19	50	42.86	76	75.61	53.85		
OA	81.2%											
Kappa coefficient		0.78										

The results from McNemar's test showed that at a 5% significance level, the RF and SVM's confusion matrices show no significant difference (Table 3.5). The z value obtained was -1.64 (Table 3.5), which was less than 1.96. Some of the classified areas using the RF classifier were almost similar to those obtained using the SVM classifier (Figure 3.5).

Table 3.5 Comparison of Random Forest (RF) and Support Vector Machines (SVM) classification methods using McNemar's test. CC stands for correctly classified, and IC is for incorrectly classified samples.

Classifier		RF		
SVM		CC	IC	Total
	CC	304	25	329
	IC	38	38	76
	Total	342	63	405
	Z-value		-1.64	

3.4 Discussion

Worldview-2 satellite imagery was used to map five common alien urban trees using RF and SVM classification algorithms. The classifiers bands for mapping these alien tree species and LULC classes in this study were the red and the NIR bands (Figure 3.6). Thus, areas with vegetation cover predominantly fall in the NIR and red regions of the WV-2 imagery. Mean decrease in accuracy (MDA) for each variable is obtained during OOB calculation (Liu *et al.*, 2017). Although remote sensing data have been used in studying ecological and environmental phenomena for many years, beneficial information has not been successfully given at fine spatial extent and temporal measures (Anderson and Gaston, 2013). Nevertheless, the traditional photointerpretation methods used in the past were time and labour-intensive, and costly, especially for data acquisition over large geographical areas, and more importantly, such aerial photographs and pixel-based image classification approaches are not well suited for LULC mapping in a heterogeneous urbanized landscape (Cleve *et al.*, 2008). But, Zhang *et al.* (2015) indicated that a problem of mixing various impervious surface areas and vegetation in one pixel for medium spatial resolution images might exist, for example, Landsat TM imagery. However, very high-resolution WV-2 images have solved this problem.

The study has shown that *Eucalyptus* spp. were mostly found in the southern part of the area of study in places such as Robertville, where the mining sites such as Rand Leases and Main Reef are located. These trees were planted to stabilize the soil and reduce soil erosion. *Eucalyptus* spp. in other areas were also planted for timber, pulp, poles (van Wilgen and Richardson, 2014), mine props and excavation (Turton *et al.*, 2006). *Jacaranda* spp., *Platanus* spp. and *Quercus* spp. were found in areas such as Randpark ridge, Fairland, Pine Park, Linden and Windsor East, which are situated in the southern part of the area of study. In addition, it is significant to bear that these areas were among the affluent suburbs of Johannesburg inhabited by the white community during the apartheid era before 1994, many of which were planted in these neighbourhood streets for

beautification and settling dust (Turton *et al.*, 2006). The *Pinus* spp. were situated in areas such as Parkview and Greenside, especially in and around open spaces such as Parkview Golf Club and Johannesburg Botanical Gardens and were introduced in these areas for ornamental or recreational values.

Our results indicate that the multispectral WV-2 sensor is suitable for urban tree species mapping using RF and SVM classifiers with overall accuracies of 84.2% and 81.2%, respectively. The RF user accuracy values for the *Eucalyptus*, *Jacaranda*, *Pinus* and *Quercus* species were higher than those in the SVM classifier (Table 3.4a and 3.4b). The RF user accuracy value for *Platanus* spp. (61.11%) was less than the one for SVM (62.50%). This was mainly due to the misclassifications of *Platanus* spp. as other woody vegetation, *Jacaranda* spp. or *Quercus* spp. classes (Table 3.4a and 3.4b). The misclassifications of the *Platanus spp*. were maybe due to errors in the reference dataset as it was challenging to find these tree species of concern in the area of study as they are not usually found in pure stands. This resulted in differences in the area of coverage, with the SVM classifier having *Platanus* spp. covering 4.68% of the total area whilst RF had 4.98% (Table 3.3). The misclassifications due to errors in the reference dataset were one of the reasons leading to the dissimilarities in the area of coverage for all classes classified by the RF and SVM. The RF producer's accuracy values for four of the five urban tree species (*Eucalyptus* spp., *Platanus* spp., *Pinus* spp. and *Quercus* spp.) were higher than those for SVM. For example, SVM's producer's accuracy value for *Jacaranda spp*. (85.19%) was higher than the one for RF (62.96%). Moreover, the low producer's and user's accuracy values for *Platanus* spp. and *Quercus* spp. for both algorithms (RF and SVM) could be due to a small number of reference polygons for these classes, as illustrated in Table 3.2. It has been conclusively shown that a small number of reference polygons make it challenging in characterizing spectral variability of individual tree species due to their unique phenological ages or stages all along the slope (Le Louarn *et al.*, 2017). In addition, misclassifications were also due to tree species' variety in this urbanized area of study, which leads to a "mixed pixel problem" where some pixels are not entirely occupied by one homogeneous class (Salih *et al.*, 2017).

The RF user accuracies for the LULC classes were between 77.36% and 100%, while those of SVM was between 50% and 100% (Table 3.4a and 3.4b). The RF had producer's accuracy values ranging from 75% to 96.88% for all LULC classes, whereas those for the SVM classifier for the same classes were between 53.85% and 98.81%. The low SVM producer's accuracy value of 53.85% (shadow) was due to misclassifications between this class and the *Quercus* spp., *Pinus* spp.

and other woody vegetation classes (Table 3.4b). The misclassifications may be due to errors in the reference dataset where some points for shadow class were classified to some of the urban tree species. It might have been the case that the values for the user's and producer's accuracy could be high if there were low tree species diversity in the area of study. The identification, classification and mapping of tree species in an urban area at an individual level nowadays have been restricted to airborne Light Detection and Ranging (LiDAR) and hyperspectral data as they produce high accuracy values due to their higher spectral and spatial resolutions as compared to multispectral data (Fassnacht *et al.*, 2016; Liu *et al.*, 2017; Raczko and Zagajewski, 2017). However, hyperspectral data are costly, time-consuming for processing, require huge storage space and also suffer from multi-collinearity (Odindi *et al.*, 2016). Recently, multispectral remote sensing imagery characterised by finer resolutions (i.e. spectral and spatial) has improved classification results (Odindi *et al.*, 2016). In this vein, the advent of the new age WV-2 satellites imageries which cost relatively less, offers new perspectives due to the increased radiometric, geometric and spectral (8 bands) resolutions and can map trees at the species level (Waser *et al.*, 2014).

Our study showed that the RF marginally outperformed the SVM classifier by 3%. This result ties well with previous studies (Puissant *et al.*, 2014; Le Louarn *et al.*, 2017) where the RF outperformed the SVM machine learning algorithms in mapping urban tree species. The high accuracy values achieved by the RF and SVM classifiers may be attributed to the utilization of WV-2 satellite imagery captured in the spring season, a period when the urban trees' new leaves start to expand, and the buds begin to open. The tree leaves assisted in showing spectral differences amongst the species enhancing their separability in mapping urban trees in this study. The development of tree leaves between the spring and summer seasons cause an increase in the content of leaf chlorophyll (Le Louarn *et al.*, 2017). The difference in the MDA values showed high NIR values and low blue and red bands for the five urban tree species (Figure 3.7). The high accuracy values for the urban tree species may be due to the strength of the RF classifier to handle unbalanced datasets, computational efficiency and having no distributional assumptions on the input data set (Odindi *et al.*, 2016). The SVM classifier also produced high accuracy values as a high "cost" (C) value of 100 was used, and the training error is penalized, forcing the misclassification of points to be lowered by the algorithm in the course of the training operation (Abdel-Rahman *et al.*, 2014). It is noteworthy that a non-linear RBF kernel for the SVM classifier was utilized in this study as it solves the inseparability problems that may arise in the vegetation species mapping (Mountrakis *et al.*, 2011). However, the high accuracy values in this study remain unclear as to whether they were

found due to the RF and SVM classifiers used, WV-2's high spatial resolution or the absence of complications in the landscape.

3.5 Conclusions

The ability of the high-resolution multispectral WV-2 satellite imagery, utilizing RF and SVM classification algorithms, was assessed in the mapping of urban tree species at Randburg municipality in the CoJ. The current study demonstrates the enormous ability of WV-2 satellite imagery and machine learning classifiers (RF and SVM) in detecting and mapping urban tree species in a complex urban environment. This study provides an insight to the municipality's urban forest and environmental managers on monitoring the urban tree species. Such spatial information will assist urban forest managers in the current urban tree inventory and urban greening program.

We caution, however, that this conclusion is based on the fact that there are misclassification errors which might be due to many factors such as the image registration error, the spectral and spatial resolution limitations and the spectral signature overlap. Future studies should consider testing different classification approaches such as object-based image analysis to minimize misclassification errors.

Overall, we believe, based on our relatively high accuracies, ease of use, low cost, it is worth considering the WV2 image for urban tree species classification.

Chapter Four

Classification of tree species in a heterogeneous urban environment using object-based ensemble analysis and World View-2 satellite imagery

Jombo, S., Adam, E. and Odindi, J. (2021) Classification of tree species in a heterogeneous urban environment using object-based ensemble analysis and World View-2 satellite imagery. *Applied Geomatics*.

DOI: https://doi.org/10.1007/s12518-021-00358-3

Abstract

Urban trees are valuable in, *inter alia*, ameliorating air pollution and mitigating the effects associated with urban heat islands. The dearth of tree cover maps is a major challenge for urban planners in the management of urban trees. This work adopts remote sensing approaches to provide urban tree cover maps, which can strengthen urban landscape management. Whereas traditional pixel-based classification approaches have been commonly used in image classification, they are not well-suited for urban tree mapping due to their failure to fully explore the image's spatial and spectral characteristics. Object-based classification techniques produce improved accuracies using additional variables. This study depicts the capability of object-based image analysis (OBIA) in mapping common urban trees using very high resolution (VHR) WorldView-2 (WV-2) imagery. The study tests the utility of WV-2 bands and other feature variables in the object-based mapping of common urban trees and other land use and land cover (LULC) classes. Furthermore, the study compares the utility of Support Vector Machine (SVM) and Random Forest (RF) in the object-based mapping of common urban trees and other LULC classes. The results show that the Normalized Difference Vegetation Index (NDVI), near-infrared 1 (NIR1) and near-infrared 2 (NIR2) bands were important in the classification of common urban trees and other LULC classes. The RF classifier performed better than SVM, with an overall accuracy of 91.9% as compared to 87.3% for SVM. The results of this study offer insight to urban authorities providing information on the segmentation parameters, classification methods and feature variables for mapping urban trees, valuable in urban tree management.

4.1 Introduction

Urban green infrastructure, especially trees, provide several ecosystem services, which include thermal regulation and ameliorating water and air pollution (Yan *et al.*, 2018). Specifically, urban trees filter gaseous pollutants and particulate matter, reduce soil contamination, provide habitat for animal species and mitigate consequences associated with urban heat islands (Scholz *et al.*, 2018). According to Zhou *et al.* (2017), urban trees reduce both land surface and air temperature, mitigate against natural stresses such as wind and tropical storms (Duryea and Kampf, 2007) and reduce noise and energy consumption (Ellis and Mathews, 2019). However, increasing urbanisation, especially in developing countries, has been identified as a major threat to urban ecosystems (Yan *et al.*, 2018).

Urban trees are grown for various landscape and ecological functions (Wen *et al.*, 2017). Commonly, urban trees are grown for amenity or ornamental purposes in landscape schemes, streets, private yards and gardens (Rossi *et al.*, 2015). Tall-wide canopy trees are particularly essential in urban areas for the provision of shade, resulting in transpiration cooling near the ground (Manickathan *et al.*, 2018). They also offer efficient animal habitats and effective nutrient cycling due to their deep-rooting system (Kuser, 2006). Tree species such as *Jacaranda* are commonly preferred due to their wide canopy and high tolerance to physical and environmental stress, such as low soil fertility and polluted air (Rani, 2019). *Quercus* and *Pinus* trees, on the other hand, are mostly favoured due to their tall height and wider canopies that act as windbreaks (Love *et al.*, 2009).

Ecosystem services provided by urban trees depend on planting configuration and density (Pretzsch *et al.*, 2015). However, the general paucity of literature on urban tree spatial distribution impedes the assessment of the species' contribution to landscape connectivity and patchiness (Rossi *et al.*, 2015). Hence, up to date, urban tree species maps offer reliable information on their distribution, composition and diversity, valuable for sustainable management of urban ecosystems (Ajewole, 2010). Urban trees mapping has previously been done using visual interpretation of aerial photography and field surveys, whose shortcomings are widely documented in remote sensing literature (Hartling *et al.*, 2019). Recently, high spatial-resolution active sensing such as Light Detection and Ranging (LiDAR) has been successfully used in mapping urban trees (Liu *et al.*, 2017; Matasci *et al.*, 2018; Hartling *et al.*, 2019). However, the use of LiDAR is hindered by significant labour inputs, high acquisition and software licensing costs (Seiferling *et al.*, 2017). Hence, passive sensors with a high spatial resolution like WorldView, Quickbird, GeoEye and

IKONOS have recently gained popularity in classifying complex urban landscapes (Pu *et al.*, 2011; Agarwal *et al.*, 2013; Liu *et al.*, 2017). Compared to four-spectral band high spatial resolution imagery such as GeoEye and IKONOS, WorldView-2 (WV-2) consists of four additional bands (near-infrared 2, yellow, coastal and red-edge) valuable in classifying trees (Hartling *et al.*, 2019).

Pixel-based classification methods have been used in previous studies (Immitzer *et al.*, 2012; Liu and An, 2019; Jombo *et al.*, 2020) to map urban trees using WV-2 satellite imagery. Immitzer *et al.* (2012), for instance, used pixel-based approaches to map ten urban trees in Burgenland Province, East of Austria with overall accuracies of 72.8% for Random Forest (RF) and 70% for Linear Discriminant Analysis (LDA). Liu and An (2019) classified urban greening tree species in Hohhot, China and produced overall accuracies of 74.07% for maximum likelihood classification and 71.79% for Support Vector Machine (SVM). In addition, Jombo *et al.* (2020) evaluated the potential of WV-2 multispectral imagery in mapping alien trees in the Randburg municipal area, Johannesburg using nonparametric RF and SVM machine-learning classifiers. The overall accuracies were 84.2% for RF and 81.2% for the SVM classifier.

Although pixel-based classification methods have been employed in mapping urban trees, the approaches are limited by, among others, "mixed pixel problem", shadow effect and urban complexity, resulting in lower classification accuracies (Jombo *et al.*, 2020). Object-based image analysis (OBIA) on the other hand, has proven to overcome the above-named limitations as it considers among others, an objects' location, shape, texture, directional pattern and area (Agarwal *et al.*, 2013). In previous studies (Mustafa *et al.*, 2015; Li *et al.*, 2015; Yan *et al.*, 2018; Hartling *et al.*, 2019), OBIA has been successfully used in mapping urban trees on WV-2 satellite imagery. Mustafa *et al.* (2015), for instance, mapped urban trees in the city of Duhok, Iraq and obtained an overall accuracy of 88.92%, while Li *et al.* (2015) classified urban trees on bitemporal WV-2 and WV-3 imagery in Beijing, China, with overall accuracies of 92.4% for SVM and 90.2% for RF classifiers. The observed high accuracies may be due to the classifiers' ability to handle any numerical data and their independence to data distribution assumptions. Moreover, Yan *et al.* (2018) mapped vegetation functional types in Beijing using WV-2 images from the summer season and two imagery from the summer-early winter season. The study achieved overall accuracies of 82.3% (summer season) and 91.1% (summer-early winter season). The study identified the additional bands (red edge and NIR2) as most influential in the classification of urban trees due to their high vegetation reflectivity. The previous studies by Li *et al.* (2015) and Yan *et al.* (2018) were carried out in Beijing which has a sub-humid north-temperate continental monsoon climate

whereas this study was conducted in a sub-tropical climate. Despite the high overall accuracies attained, the performance of object-based classification techniques depends on several factors which include site-specific variables such as the size and density of sample objects, elevation and the spatial composition of the landscape (Yu *et al.*, 2008).

The metropolitan City of Johannesburg (CoJ) has the biggest urban forest area in the world, whose heterogeneous landscape includes high-rise buildings, grasslands and roads (Schäffler and Swilling, 2013). This heterogeneity impedes landscape delineation using pixel-based classification approaches. Several studies have successfully mapped trees using OBIA in different urban environments (Puissant *et al.*, 2014; Li *et al.*, 2015; Liu *et al.*, 2017; Wen *et al.*, 2017; Le Louarn *et al.*, 2017). However, few studies (e.g. Schäffler and Swilling, 2013; Mavimbela *et al.*, 2018; Jombo *et al.*, 2020) have been conducted in Southern African urban ecosystems using pixel-based classification methods. No studies to the best of our knowledge have compared the use of SVM and RF classifiers in the object-based mapping of the common urban trees using very high resolution (VHR) WV-2 multispectral imagery. Subsequently, the present study assesses the capability of OBIA in classifying common trees in the Randburg municipal area using VHR WV-2 multispectral imagery. The objective of this study was to examine the performance of SVM and RF classification algorithms in the object-based mapping of common urban trees and other land use and land cover (LULC) classes using VHR WV-2 multispectral imagery. The study seeks to reliably account for common urban trees to facilitate informed decisions and sustainable urban management.

4.2 Methodology

4.2.1 Study area

The Randburg municipal area is found in Region B of the City of Johannesburg (CoJ) and covers 167.98 km^2 (Figure 4.1). The Randburg municipal area's annual rainfall is approximately 750 millimetres per year and normally falls in the summer season (Tyson and Wilcocks, 1971). The mean average temperature is approximately 20ºC in summer and 15ºC in the winter season (Naicker *et al.*, 2003). The geology of the municipal area is dominated by crystalline rocks of the Archean age (Abiye *et al.*, 2018). Granitic gneiss and melta-volcanic rocks are also present in the study area (Abiye *et al.*, 2018).

Randburg municipal area has a total population of approximately 337 053 (Statistics South Africa, 2011). The municipality is complex with various LULC classes, which include the urban trees, water bodies as well as industrial, residential and office buildings (African Green City Index, 2011).

The city has a green infrastructure, which includes effective ecosystem management and green consciousness structures which have been perfected over time (Schäffler and Swilling, 2013). The urban forest in the study area is an essential ecological feature resultant of the city's integration of both ecological and industrial backgrounds (Schäffler and Swilling, 2013). The area of study has indigenous and non-native tree species brought to Johannesburg during the colonial era (Schäffler and Swilling, 2013).

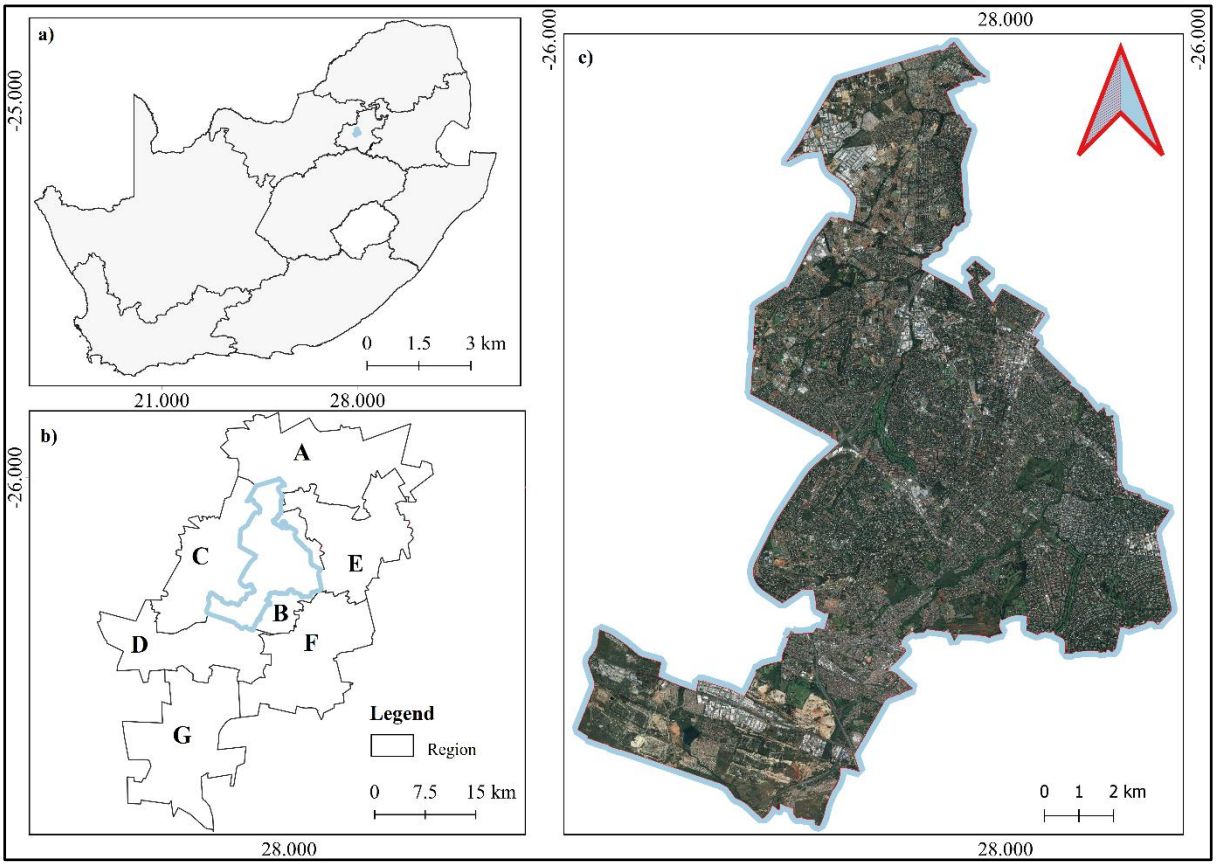


Figure 4.1 a) South African provinces, b) City of Johannesburg's regions A to F and c) basemap showing Randburg municipal area.

4.2.2 Multispectral remote sensing data and pre-processing

The study used very high resolution (VHR) WV-2 multispectral imagery acquired on the 15th of September 2017 for classification and analysis. The image acquisition date was selected based on the availability of the satellite imagery acquired in the vegetation growing season. The WV-2 multispectral image was made of 36 scenes, mosaicked using ArcMap 10.6 software. The multispectral image was provided by the CoJ's Corporate Geo-Informatics, Development Planning and Urban Management (DP&UM) division already corrected for geometric and radiometric anomalies. The WV-2 image was orthorectified using a georeferenced high resolution

(0.5m) aerial photograph of the study area. A total of 30 ground control points were evenly distributed in the study area, and the first-order polynomial transformation technique in ArcMap 10.6 software was used to georeference the WV-2 imagery. An overall Root Mean Square Error (RMSE) of 0.24 of a pixel was achieved and through visual assessment, it was confirmed that the WV-2 image was perfectly aligned to the aerial photograph. WV-2 satellite imagery has eight multispectral imaging bands, a 16.4 km swath width (nadir range), and a dynamic range of 11-bits per pixel with a 1.1-day revisit time. The sensor gathers 1.84m multispectral and 0.46m panchromatic imagery (Table 4.1). The horizontal accuracy of WV-2 satellite imagery is between 5 and 10m. The image has eight multispectral bands, which include the blue, yellow, red edge, and Near-Infrared 1 (NIR1) bands (Table 4.1). The eight multispectral imaging bands are precisely chosen to meet the modern remote sensing application requirements, which include environmental monitoring and vegetation quality and quantity mapping (Odindi *et al.*, 2014). In this study, the imagery projection used was in Hartebeeshoek WGS84 coordinates (Central Meridian-29, Projection-Transverse Mercator).

Table 4.1 WorldView-2 spectral band configuration

Spectral band number and name	Spatial resolution	Spatial range
Panchromatic	0.46 cm	450 – 800 nm
B1. Coastal blue	1.85 m	400 – 450 nm
B2. Blue	1.85 m	450 – 510 nm
B3. Green	1.85 m	510 – 580 nm
B4. Yellow	1.85 m	585 – 625 nm
B5. Red	1.85 m	630 – 690 nm
B6. Red-edge	1.85 m	795 – 745 nm
B7. NIR1	1.85 m	770 – 895 nm
B8. NIR2	1.85 m	860 – 1040 nm

4.2.3 Ground truth training, test and evaluation samples

Ground data were collected in September 2017. The dominant trees were uploaded into a handheld Garmin eTrex 20 X Global Positioning System (GPS) receiver with ± 3m accuracy. To reduce the low accuracy of the positioning of the dominant trees collected using a GPS receiver, the points for the tree species were delineated manually on the high-resolution georeferenced aerial photograph, ensuring that the pixels selected belonged to the trees of interest. The dominant trees were uploaded based on a stratified purposeful sampling approach. The stratified purposeful

sampling method can capture significant differences instead of identifying the most common samples where a fairly homogenous sample is in each stratum (Patton, 2002). The field data gathered was utilized in establishing Image Object (IO) samples for the training and testing sites (Table 4.2). The study area was divided into four equal zone segments measuring approximately 42 km^2 each. Samples from zone segments in the study area were chosen using the zigzag sampling method. The sampling method involves the definition of a zigzag transect that covers the area of interest (Paulo *et al.*, 2005). The sampling method was used mostly on the streets where urban trees coordinates were delineated on the WV-2 satellite imagery. The zigzag sampling approach was used as described by Almeida and Tomé (2009). Using this approach, five dominant urban tree samples were identified; *Eucalyptus* spp., *Jacaranda* spp., *Platanus* spp., *Quercus* spp. and *Pinus* spp. The reference samples for the five dominant urban trees and other LULC classes were collected in the study area. The total dataset samples (n = 1364) were randomly partitioned into training samples (70%) and test samples (30%), as shown in Table 4.2. The training samples were used to train both RF and SVM classifiers, while the test samples validated the accuracy of the two classification models (Adam *et al.*, 2013).

Table 4.2 Number of training and test samples used in this study

Class name	Abbreviation	Number of samples (Training)	Number of samples (Test)	Total number of samples
Bare land	BL	91	39	130
Built-up	BU	187	80	267
Eucalyptus spp.	EC	86	37	123
Grassland	GL	145	62	207
Jacaranda spp.	JC	70	30	100
Platanus spp.	PL	56	24	80
Quercus spp.	QS	33	14	47
Other woody vegetation	OWV	163	70	233
Pinus spp.	PS	84	36	120
Road	RD	40	17	57
Total		955	409	1364

4.2.4 Image classification

The classification and mapping of the common urban trees and other LULC classes in this study were done using OBIA and image objects (IOs) created by segmenting the WV-2 satellite image.

4.2.4.1 Image segmentation

A multi-resolution segmentation (MRS) approach was used to segment the image. A similar image segmentation used in Pu *et al.* (2018) was adopted in the creation of IOs. The MRS algorithm of Definiens eCognition Developer 9.3.2 (Copyright © 2018 Trimble Germany GmbH) is a bottom-up merging method and through various iterative measures, smaller IOs from among single pixels are combined to generate larger IOs (Li *et al.*, 2015). Parameters essential as input for MRS include color/shape ratio, scale parameter, the weight of each input layer and smoothness/compactness ratio (Li *et al.*, 2015). Consequently, optimal image segment parameters are set based on the nature and size of the objects to be identified, for example, how the IOs correspond to object boundaries on the satellite imagery for a specific exercise (e.g. tree crown) (Pu *et al.*, 2018). All the eight multispectral imaging bands for WV-2 satellite image were used in this study as proposed by Li *et al.* (2015) and Mustafa *et al.* (2015). The weights of compactness and color were put at 0.5 and 0.8, respectively, for balancing the spectral/shape dissimilarities between other LULC classes and the tree species.

All WV-2 bands were given a weight value of one while, the NIR1, NIR2, red and red edge bands were given a value of two, as they are essential in the identification and classification of trees. Vegetated and non-vegetated areas were differentiated using a Normalized Difference Vegetation Index (NDVI) threshold value of 0.25 as suggested by Pu *et al.* (2018). To establish the final image segmentation parameters, evaluation of the segmentation results was done using 646 outlined tree crowns. The delineated tree crowns were for all common urban trees (*Eucalyptus* spp., *Jacaranda* spp., *Pinus* spp., *Platanus* spp. and *Quercus* spp.) and other woody vegetation classes. The selection of segmentation parameters was done based on the location of most test IOs collected during field trips in the study area. The present study used eight image segmentation rule sets testing nine different scale settings (20, 30, 40, 50, 60, 70, 80, 90 and 100). The final segmentation with the best scale parameter was chosen by visually checking the extent to which the IOs correspond to the collected coordinates from field visits and the dominant urban trees' boundaries.

4.2.4.2 Feature selection

The use of shape indices and spectral measures are useful in defining the heterogeneity of features (Tzotsos and Argialas, 2006). Shape and spectral variables were used to select the IOs in this study due to their potential in differentiating classes for the common urban trees and other LULC classes. The feature variables utilized in this study for the OBIA were Shadow Index (SI), NDVI, length (*pixel*) and mean (Table 4.3). The incorporation of these feature variables is in line with

previous work (Salehi *et al.*, 2012; Mustafa *et al.*, 2015) where they contributed to distinguishing urban trees resulting in the attainment of high classification accuracies.

4.2.4.3 Object-based shadow index (SI)

The SI is defined as a function of the total amount of tree crowns, i.e., if there are many trees, then there is more shadow. Consequently, SI rises as tree cover increases and it has high values in areas with high tree density and low for areas with bare land, built up and grass (Godinho *et al.*, 2016). It has been observed in previous studies (Mustafa *et al.*, 2015; Hartling *et al.*, 2019) that a major problem in the classification of urban trees is the existence of shadow and shadow masking can eliminate spectral confusion. Accordingly, in this study, shadows were removed from the urban trees using the equation proposed by Mustafa *et al.* (2015) as follows:

$$SI = \sqrt{(256\text{-Red})(256\text{-NIR1})} \qquad \text{Equation 4.1}$$

where the Red and NIR1 are band 5 and 7, respectively on WV-2 imagery (Table 4.1). The regions that were determined as shadows were masked out on the satellite imagery.

The SI was calculated and used after image segmentation and the creation of IOs for all the trees and LULC classes. A binary map was created with a value of 0, representing shadow and 1 for areas without shadow.

4.2.4.4 Normalized Difference Vegetation Index (NDVI)

A threshold value for Normalized Difference Vegetation Index (NDVI) together with brightness values were used to classify the study area into vegetated and non-vegetated areas. The areas with vegetated IOs were identified using the NDVI threshold value (> 0.3). The IOs chosen in this study were for tree crowns and other LULC classes (bare land, built-up, grassland, other woody vegetation and road). The vegetated areas (e.g. *Eucalyptus* spp. and grassland classes) were discriminated from non-vegetated areas (bare land, built-up and road classes) using the NDVI formula (Equation 2) calculated as follows:

$$NDVI = \frac{NIR1\text{-}Red}{NIR1+Red} \qquad \text{Equation 4.2}$$

where the Red and NIR1 are band 5 and 7, respectively on WV-2 imagery. NDVI is calculated based on reflectance values for the infrared and red band (Jebur *et al.*, 2014). High NDVI values show healthy vegetation and low values designate stressed, diseased or a non-vegetated area (Xiao and McPherson, 2005). In this study, all the dominant urban trees and LULC classes were extracted, classified and mapped using SVM and RF classifiers.

The last step was to classify built-up areas and roads using the hierarchical rule-based classifier in eCognition software. The *length (Pxl)* feature variable was utilized to make a distinction between roads and built-up areas, by comparing the linear shape of roads to the concise building structures. The length variable was used due to its importance in the classification and mapping of the road class focussing on the Mean Decrease in Accuracy (MDA) values. The classification and mapping of the WV-2 image were done using variables illustrated in Table 4.3.

Table 4.3 Variables used in a rule set for all LULC classes in this study.

Variable	Feature name	Description
Spectral	Mean	Average of the intensity of values of all pixels that form an object
	SI	Shadow Index
	NDVI	Normalized Difference Vegetation Index
Shape	Length (Pixel)	Multiplication between the length-to-width ratio and number of pixels of an IO

4.3 Results

4.3.1 Segmentation results

The MRS algorithm using a scale parameter of 20 yielded 15 457 579 objects. A subsection of WV-2 imagery and the segmented portion of the Randburg municipal area using a scale parameter of 20 is shown in Figure 4.2.

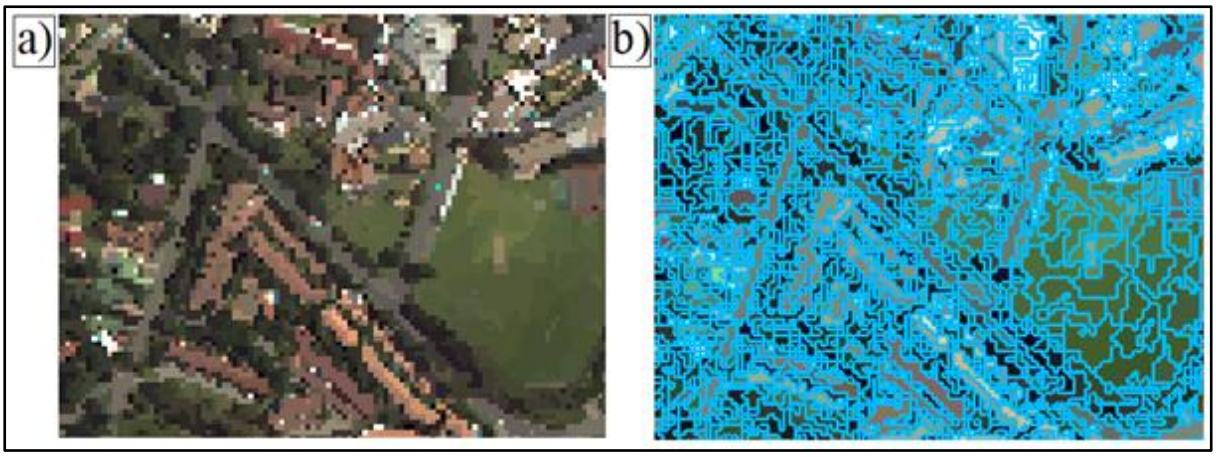


Figure 4.2 (a) Subsection of WV-2 true colour image and (b) segmented WV-2 image for the study area.

4.3.2 Shadow index

The shadow index equation was input into eCognition and yielded areas with shadows, which were mostly near trees and built-up areas (Figure 4.3). A binary map was produced showing areas with shadow represented with the value of 0 and non-shadow indicated by 1 (Figure 4.3c). The areas with shadow were masked out from images for the classification process.

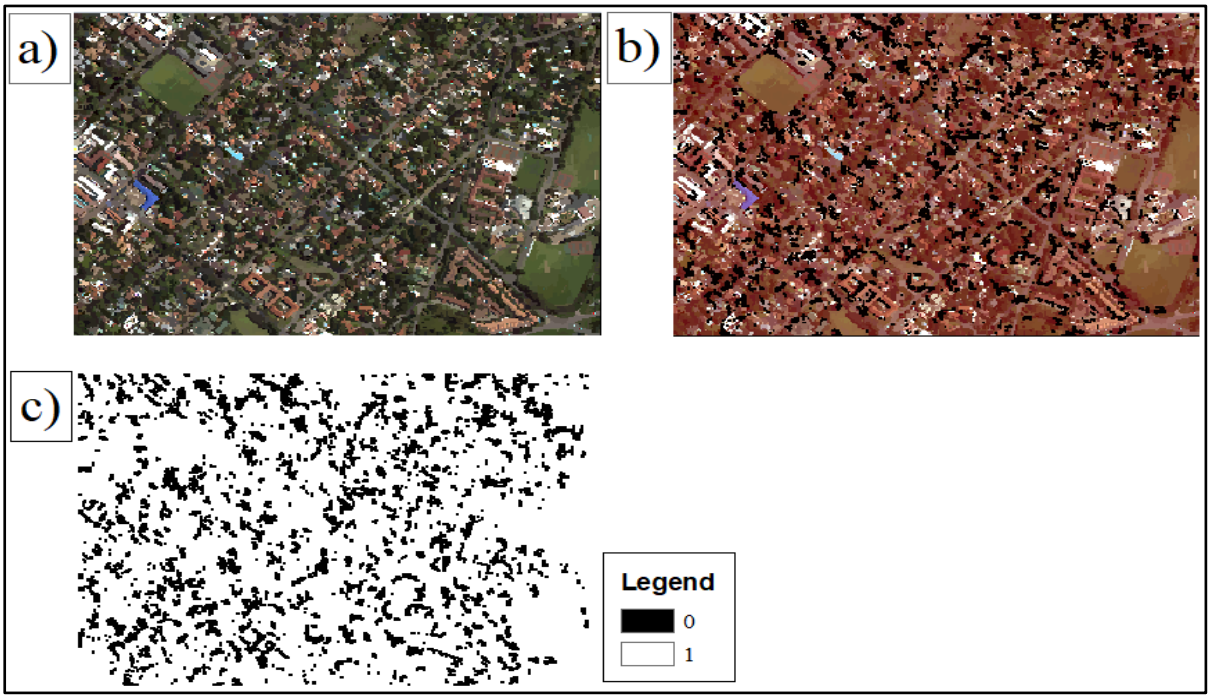


Figure 4.3 (a) Subsection of WV-2 true colour image; (b) Subsection of WV-2 image with shadow areas in black; and (c) binary image with the value 0 indicating shadow and 1 (non-shadow areas) in the study area.

4.3.3 Normalized Difference Vegetation Index (NDVI)

The NDVI analysis was processed on the WV-2 image of the study area using eCognition software (Figure 4.4). Areas in green have tree crowns for the five common urban trees, grassland and other woody vegetation (Figure 4.4).

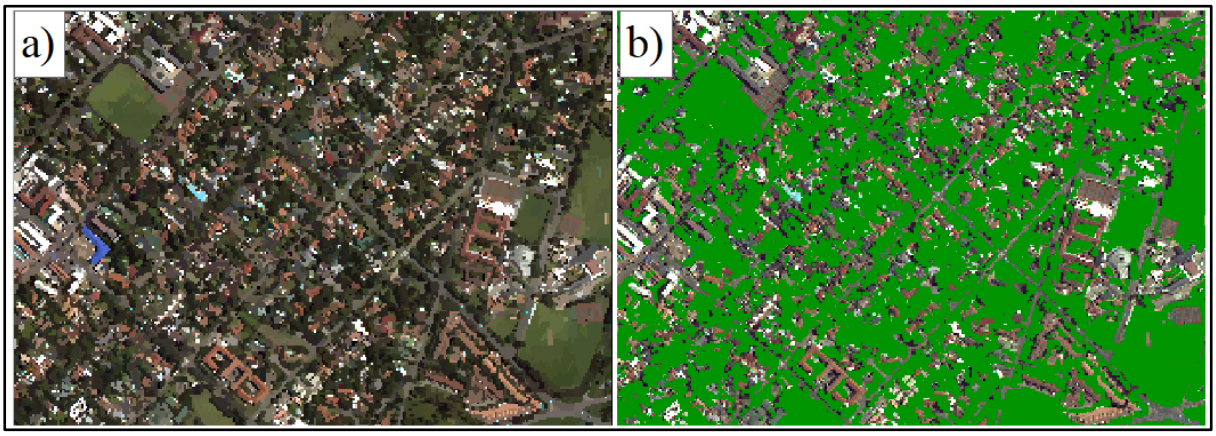


Figure 4.4 (a) Subsection of WV-2 true colour image; (b) Subsection of the WV-2 image showing vegetated image objects in green using the NDVI threshold value (> 0.3) in the study area.

4.3.4 SVM and optimization

Using the SVM algorithm, the best parameters were selected based on a 10-fold cross-validation technique. In this study, the SVM algorithm used 495 support vectors, the best C and γ RBF kernel parameters were 1000 and 1, respectively (Figure 4.5).

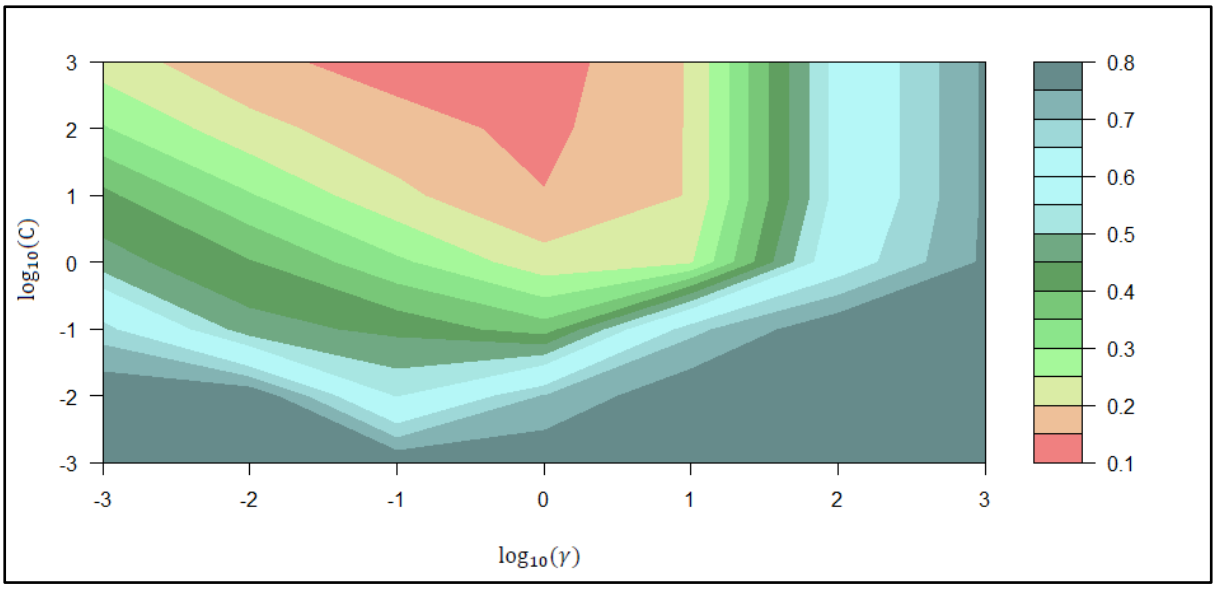


Figure 4.5 10–fold cross-validation technique in optimizing SVM RBF kernel parameters (C and γ).

4.3.5 Random forest and optimization

Using a 10-fold cross-validation (CV) method, the best *mtry* and *ntree* values were 7 and 500, respectively (Figure 4.6). The method yielded a minimum OOB error rate of 4.1% and a maximum of 8.6% with *mtry* and *ntree* values of 2 and 1500, respectively. The *mtry* value of 2 had the highest OOB error rate values ranging from 8.1% (*ntree* = 5500) to 8.6% (*ntree* = 1500) (Figure 4.6). The *mtry* value of 7 had the lowest OOB error rate values ranging between 4.1% (*ntree* = 500) and 4.6% (*ntree* = 1500) (Figure 4.6). The *mtry* values from 5 to 10 had OOB error rate values between 4.1 and 5.1%, whilst the *mtry* values from 2 to 4 had high OOB error rate values between 6.2 and 8.6% (Figure 4.6).

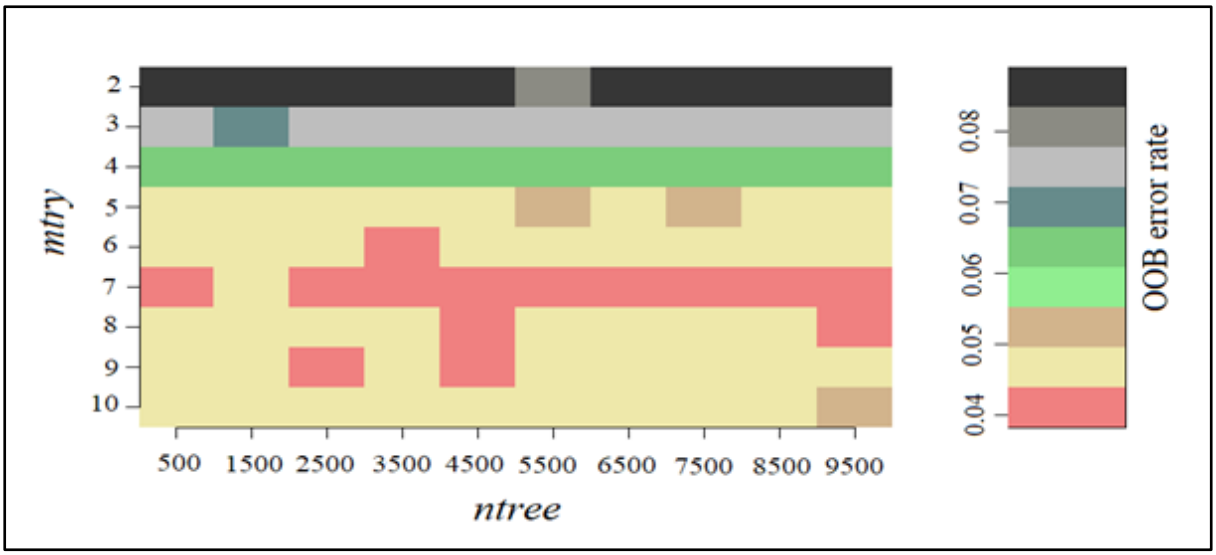


Figure 4.6 10–fold cross-validation technique in optimizing RF parameters (*mtry* and *ntree*). The error rate was determined using the OOB sample for all different combinations.

4.3.6 Classification results

The IOs on the WV-2 VHR satellite imagery were classified into ten classes, five for urban trees and the remaining five as other LULC classes. Segmentation and the extraction of training and validation samples were done in eCognition Developer 9.3.2 (Copyright © 2018 Trimble Germany GmbH). The segments, training and validation samples were modified in QGIS software (V. 2.8.3-Wien). SVM and RF classifiers were used to classify the image in R statistical software (Version 3.5.2). The classification maps from both SVM and RF are shown in Figure 4.7.

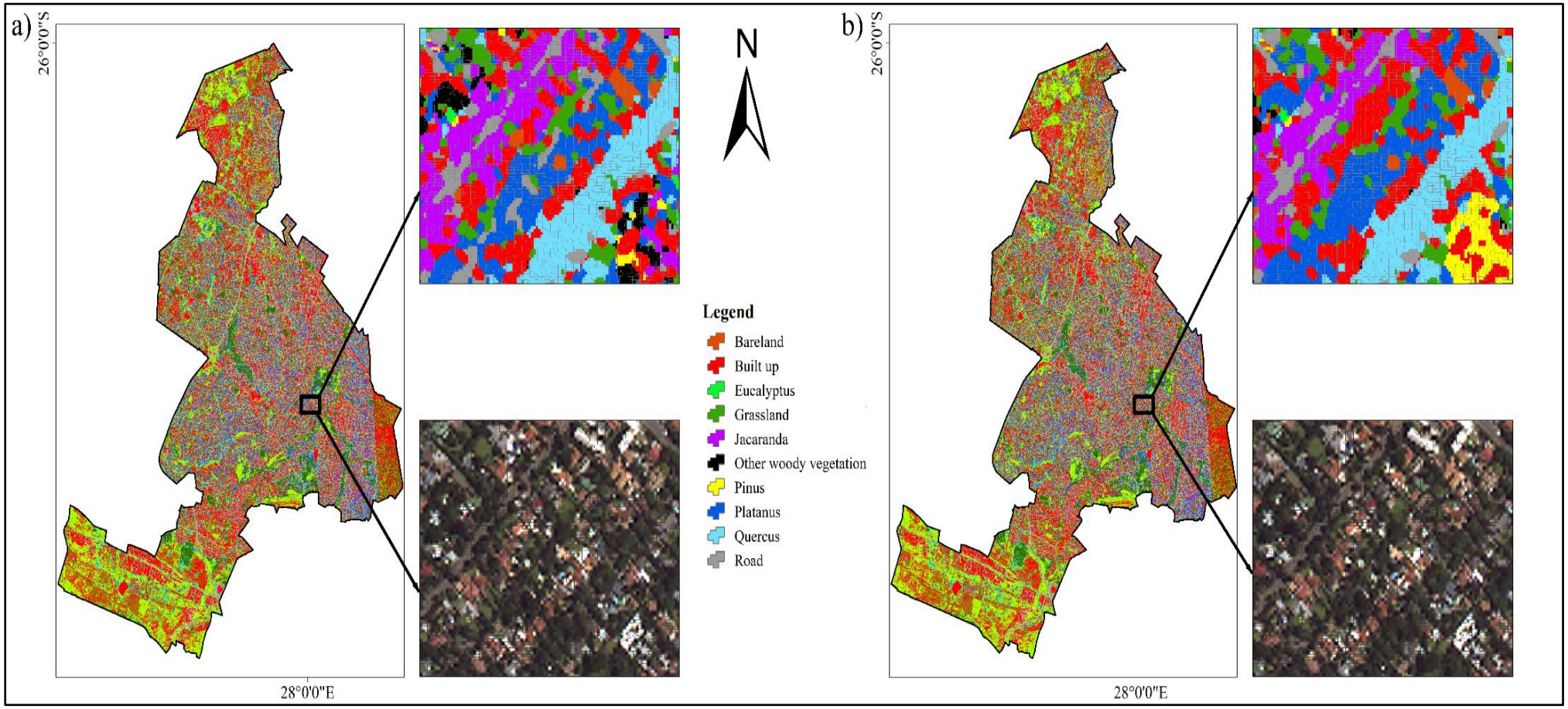


Figure 4.7 Mapping results of urban trees and other LULC classes using a) SVM and b) RF classifiers.

The classified maps (Figure 4.7) show that most *Quercus* spp. and *Pinus* spp. were commonly located in the south. The *Eucalyptus* and *Jacaranda* spp. were mainly located in the northern and southern parts of the study area, respectively (Figure 4.7). As shown in Figure 4.7, all the LULC classes (bare land, built up, grassland, other woody vegetation and road) were spread all over the study area.

The areal coverage for all the classes using the SVM and RF classifiers showed minor inconsistencies. *Quercus* spp. had the highest difference of 0.9% from the image classified by SVM (6.8%) and RF (7.7%) as shown in Table 4.4. *Quercus* spp. also had a different value of 0.3%, where the percentage value for SVM (6.8%) and 7.7% for the RF classifier. *Eucalyptus* spp., *Platanus* spp. and *Pinus* spp. had differences of 0.2%, 0.7% and 0.3%, respectively, with the SVM having more area of coverage than the RF classifier (Table 4.4). The less dominant urban trees classes were *Eucalyptus* spp., which had a total coverage area of 4.0 ha (SVM) and 3.8 ha (RF) (Table 4.4). Other LULC classes (bare land, built-up, grassland, other woody vegetation and road) also had minor differences in the area of coverage using the two classifiers (Table 4.4). The highest difference was for bare land where SVM had a value of 998.6 ha (5.9%) whereas RF had 1119.4 *ha* (6.7%). As shown in table 4.4, the difference in the area of coverage between the two classifiers was 120.8 *ha* (0.8%). The lowest difference for the other LULC classes was 0.2% for grassland (Table 4.4).

Table 4.4 Area of coverage in hectares (ha) and percentage (%) for the two classified maps using SVM and RF classifiers. The classes are bare land (BL), built-up (BU), *Eucalyptus* spp. (EC), Grassland (GL), *Jacaranda* spp. (JC), *Platanus* spp. (PL), *Quercus* spp. (QS), other woody vegetation (OWV), *Pinus* spp. (PN) and Road (RD).

Class	RF in hectares (ha)	Percentage (%)	SVM in hectares (ha)	Percentage (%)
BL	1119.4	6.7	998.6	5.9
BU	3799.1	22.6	3836.7	22.8
EC	631.8	3.8	672.3	4.0
GL	1884.6	11.2	1919.1	11.4
JC	737.8	4.4	723.7	4.3
PL	1381.0	8.2	1497.3	8.9
QS	1291.5	7.7	1141.3	6.8
OWV	2958.9	17.6	2885.8	17.2
PS	1142.1	6.8	1201.1	7.1
RD	1858.9	11.1	1929.2	11.5
Total	16805.1	100.0	16805.1	100.0

The MDA was used to show the variable importance in the RF classification (Figure 4.8).

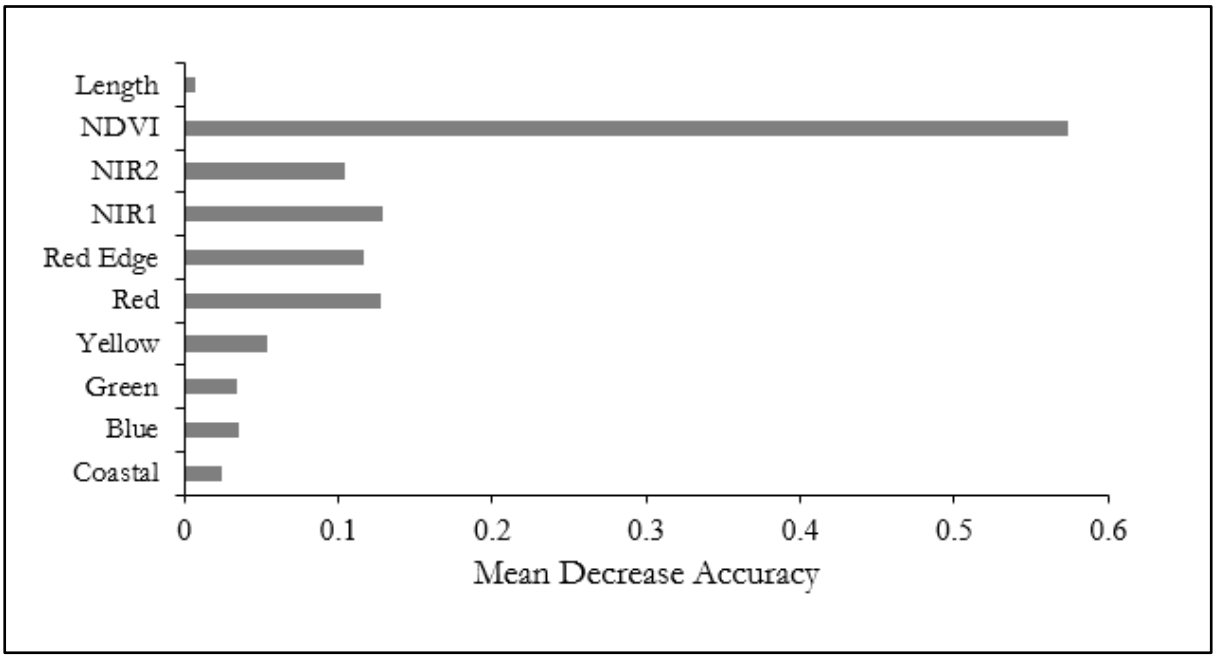


Figure 4.8 MDA for WV-2 bands, NDVI and length (pixels) in the RF model.

The effectiveness of each variable and WV-2 bands was further evaluated in mapping common urban trees and the LULC classes in this study using the MDA (Figure 4.9). The most effective variables in the classification and mapping of the five urban trees were the NDVI, red, NIR1 and NIR2 bands, as shown by high MDA values (Figure 4.9). The NDVI variable was vital in classifying all the classes in this study as it could differentiate vegetated areas from non-vegetated areas. The red band was the most important of all the eight WV-2 bands in the classification of bare land and road classes (Figure 4.9). The NIR1 band was important in the classification of the *Eucalyptus*, *Jacaranda*, *Oak* and *Pinus* spp. classes (Figure 4.9).

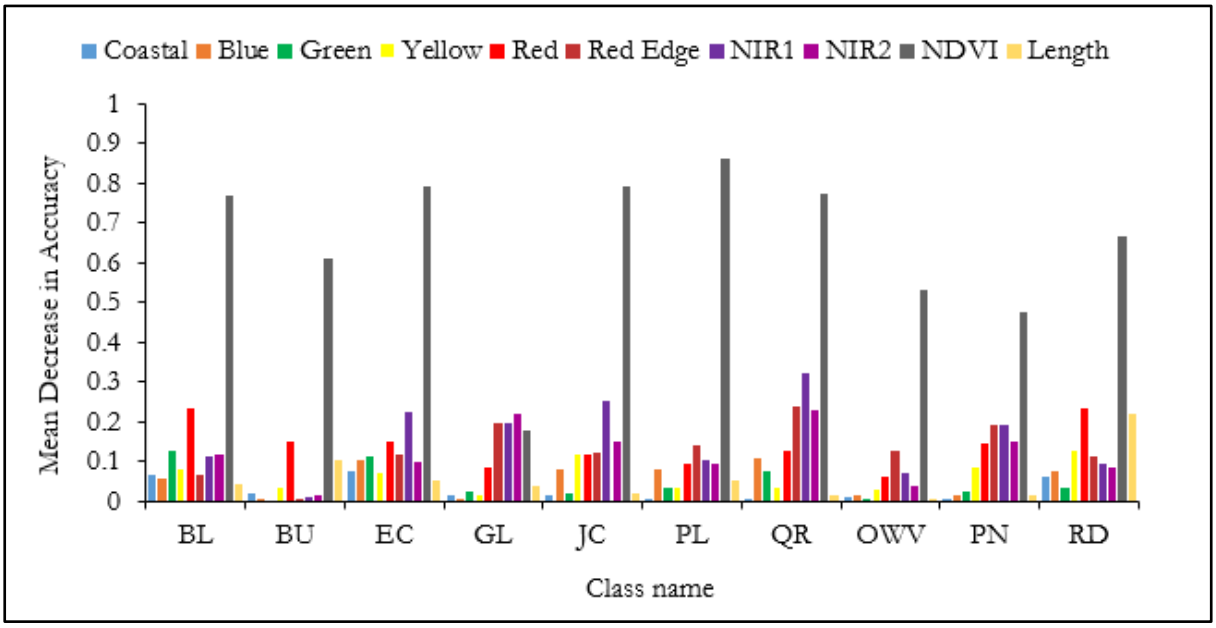


Figure 4.9 MDA for the LULC classes and variables used in the study.

4.3.7 Accuracy assessment

The overall accuracy results and the kappa values for all the urban trees and LULC classes were calculated. As shown in Table 4.5, the RF classifier outperformed SVM in mapping urban trees and other LULC classes, with 91.9% overall accuracy as compared to 87.3% for SVM. The kappa value for RF (0.91) was also higher than the one for SVM (0.85).

Confusion matrices for both the classifiers showing the user's and producer's accuracies for all the classes are shown in Table 4.5. Differences in both the producer's and user's accuracies for urban trees (*Eucalyptus* spp., *Jacaranda* spp., *Pinus* spp., *Platanus* spp. and *Quercus* spp.) were observed for both classifiers. The SVM classifier had user's accuracies ranging from 64% (*Quercus* spp.) to 91% (*Platanus* spp.) for the urban trees (Table 4.5a). The SVM classifier had producer's accuracies

ranging from 64% (*Quercus* spp.) to 100% (*Platanus* spp.) for the urban trees (Table 4.5a). The user's accuracy for the other LULC classes (built up, bare land, road, grassland and other woody vegetation) ranged from 86% to 100% for the SVM classifier (Table 4.5a). The producer's accuracy for other LULC classes ranged from 75% (bare land) to 100% (road) for the SVM classifier (Table 4.5a).

The RF classifier produced the user's and producer's accuracy values which were higher than the ones for the SVM classifier. The user's accuracies for the five urban trees ranged from 81% for both *Eucalyptus* and *Pinus* spp. to 100% (*Quercus* spp.) for the RF classifier (Table 4.5b). The producer's accuracies for the urban trees ranged from 71% (*Pinus* spp.) to 100% for the *Platanus* spp., *Quercus* spp. and *Jacaranda* spp. for the RF classifier (Table 4.5b). The other LULC classes had user's accuracy ranging from 87% (bare land) to 100% for both grassland and road classes, using the RF classifier (Table 4.5b). The producer's accuracy values for other LULC classes ranged from 85% (other woody vegetation) to 100% (road) for the RF classifier (Table 4.5b).

Table 4.5 Confusion matrices for a) SVM and b) RF classifiers. The classes are bare land (BL), built-up (BU), *Eucalyptus* spp. (EC), Grassland (GL), *Jacaranda* spp. (JC), *Platanus* spp. (PL), *Quercus* spp. (QS), other woody vegetation (OWV), *Pinus* spp. (PN) and Road (RD). The overall accuracy (OA), user's accuracy (UA), producer's accuracy (PA) and the kappa value were computed on the test dataset using the 'rasclass' package in R (Version 3.5.2).

a) Confusion Matrix for SVM

OA = 87.3% Kappa value = 0.85

Class	BL	BU	EC	GL	JC	PL	QS	OWV	PS	RD	Total	UA (%)
BL	27	3	0	0	0	0	0	0	0	0	30	90
BU	9	81	0	1	0	0	0	0	0	0	91	89
EC	0	0	29	0	0	0	0	2	8	0	39	74
GL	0	0	0	62	0	0	0	1	0	0	63	98
JC	0	0	0	1	25	0	0	4	0	0	30	83
PL	0	0	0	0	0	20	0	2	0	0	22	91
QS	0	0	0	0	0	0	9	4	1	0	14	64
OWV	0	0	1	0	2	0	2	60	5	0	70	86
PS	0	0	1	0	0	0	3	2	27	0	33	82
RD	0	0	0	0	0	0	0	0	0	17	17	100
Total	36	84	31	64	27	20	14	75	41	17	**409**	
PA (%)	75	96	94	97	93	100	64	80	66	100		

b) Confusion Matrix for RF

OA = 91.9% Kappa value = 0.91

Class	BL	BU	EC	GL	JC	PL	QS	OWV	PN	RD		
BL	34	5	0	0	0	0	0	0	0	0	39	87
BU	2	79	0	0	0	0	0	0	0	0	81	98
EC	0	0	30	0	0	0	0	0	7	0	37	81
GL	0	0	0	62	0	0	0	0	0	0	62	100
JC	0	0	0	0	27	0	0	2	0	0	29	93
PL	0	0	0	1	0	20	0	3	0	0	24	83
QS	0	0	0	0	0	0	14	0	0	0	14	100
OWV	0	0	0	1	0	0	0	64	5	0	70	91
PS	0	0	1	0	0	0	0	6	29	0	36	81
RD	0	0	0	0	0	0	0	0	0	17	17	100
Total	36	84	31	64	27	20	14	75	41	17	**409**	
PA (%)	94	94	97	97	100	100	100	85	71	100		

4.4 Discussion

The study assessed the capability of OBIA in classifying and mapping common urban trees and other LULC classes using SVM and RF classifiers on VHR WV-2 satellite imagery. The classified maps for both SVM (Fig. 7a) and RF (Fig. 7b) classifiers show a reasonably correct depiction of the LULC classes, which include the five common urban trees. The ability and performance of the two classifiers (SVM and RF) were investigated in the object-based mapping of common urban trees and other LULC classes using VHR WV-2 multispectral image.

The size and density of the sample objects were considered in this study. With the segmentation parameter of 20, the size of the IOs was small to reduce the spectral variability on the common urban trees and other LULC classes. In this study, the total number of IOs (n = 1364) were spread across the whole study area. The study obtained high accuracies due to various factors which include the size and density of the IOs. This is in line with previous studies (Wang *et al.*, 2004; Yu *et al.*, 2008) which state that objects of smaller size in the segmentation and higher density of IOs across the study area results in higher accuracies in vegetation mapping.

The results show that the use of NDVI, SI and the length (*pixel*) variables obtained from the WV-2 imagery can produce high classification accuracies, which is consistent with previous studies (Mustafa *et al.*, 2015; Yan *et al.*, 2018). In this study, NDVI was valuable in the classification of common urban trees and other LULC classes, followed by the NIR bands (band 7 and 8) as shown in Fig. 9. This finding is consistent with previous studies (Mustafa *et al.*, 2015; Qin *et al.*, 2016; Vidhya *et al.*, 2017) which used NDVI to distinguish vegetated from non-vegetated areas. The SI used in this study also increased the accuracies of both the SVM and RF classifiers as the shadow of the trees and buildings was masked out before classification. Removal of shadow from trees before classification removed the confusing spectral problem between spectra of tree leaves and shadows (Mustafa *et al.*, 2015). The use of the *length (pxl)* variable was useful in distinguishing roads from other LULC classes such as built-up and bare land, which were spectrally similar. These findings are in agreement with Shackelford and Davis (2003) who found that the incorporation of object features such as length and texture measures have a positive impact in discriminating the often spectrally similar building and road classes. The use of NDVI and SI were useful in providing information on the spatial distribution of trees, useful in providing urban tree inventory data. This finding corresponds to Jovanović and Milanović (2017) who evaluated the use of NDVI in the management of local forests in the municipality of Topola, Serbia.

In addition to WV-2 imagery's high spatial resolution, the additional bands were useful in facilitating urban trees. Some of the additional bands such as NIR2 and the red edge on WV-2 satellite imagery played an important role in mapping common urban trees (*Eucalyptus*, *Jacaranda*, *Pinus*, *Platanus* and *Quercus* spp.). The NIR1, NIR2, red and red-edge bands played an important role in classifying urban trees and other LULC classes (such as grassland and other woody vegetation) as shown by high MDA values (Fig. 9). These results are consistent with Jombo *et al.* (2020) who highlighted the importance of the subdivided NIR bands (NIR1 and NIR2) and the red edge band on WV-2 imagery in classifying urban trees in the Randburg municipal area, Johannesburg. Spectrally similar classes like trees and other woody vegetation, bare land and impervious surfaces can be better distinguished if the additional bands of the WV2 image are used throughout the OBIA process (Zhou *et al.*, 2012).

The use of VHR WV-2 imagery in this study produced high overall classification accuracies. With the advantages of high accuracy results and high spatial resolution, remote sensing technology can be utilized to effectively obtain and show the urban trees spatial distribution and evaluate the ecosystem services of various trees (Chen *et al.*, 2018). In a previous study by Jombo *et al.* (2020), overall accuracies of 81.2% using SVM classifier and 84.2% (RF classifier) were produced for mapping the same urban trees and the LULC classes used in this study. This study produced overall accuracies of 87.3% for the SVM and 91.9% for the RF classifier using OBIA, showing an improvement from the previous study which used pixel-based classification methods. The improvement of the overall accuracy values was due to the use of spatial information which includes shape, directional pattern, area and location of the IOs used in OBIA (Agarwal *et al.*, 2013). In agreement with other studies (Le Louarn *et al.*, 2017; Pu *et al.*, 2018), the RF outperformed the SVM classifier by over 4.6%. The high accuracy value for RF in comparison to SVM in this study could be due to the ability of the classifier to handle a high number of training samples. The SVM classifier is known to have low accuracy results as compared to RF if used in an area that requires a high number of training samples, such as a heterogeneous urban environment (Campomanes *et al.*, 2016).

The accuracy results for both RF and SVM were high, which can be attributed to their strengths as non-parametric machine learning classifiers effective in handling any numerical data without assuming the distribution of the data (Pu *et al.*, 2018). The RF classifier performed better than SVM classifier due to its ability to successfully select and rank variables that have supreme efficiency in discriminating between the classes (Belgiu and Drăguţ, 2016). The RF achieved higher

user's and producer's accuracy values than SVM (Tables 4.5a and 4.5b) due to its robustness to outliers and noise which results from its distribution and casting of a unit vote for the most prominent class input (Breiman, 2001). The misclassifications for the five common urban trees using both RF and SVM classifiers (Tables 4.5a and 4.5b) could be attributed to errors in ground reference data and congregation of neighbouring tree crowns during the segmentation process because of their crown size (Le Louarn *et al.*, 2017). The misclassifications resulted in variations in the area of coverage for the tree species classified by both the RF and SVM classifiers (Table 4.4).

Results from this study show that RF and SVM classifiers can insight into the spatial distribution of common urban trees and other LULC's valuable in the management of urban trees, urban forest or urban greenspace (Roy *et al.*, 2012). This study provides a basis for the incorporation of satellite imagery and baseline data for sustainable urban tree management programmes (Schäffler and Swilling, 2013). The findings from this study could be useful for identifying potential planting spaces, informing policymakers on the increase and maintenance of existing canopy cover and quantifying urban forest ecosystem services such as carbon storage and sequestration (Roy *et al.*, 2012). Moreover, this study could be valuable in determining costs and expenditures related to planting, establishment, maintenance and management of urban trees (Roy *et al.*, 2012). According to Schäffler and Swilling (2013), proper management of ecological assets such as urban trees can boost ecosystem provision, economic attractiveness and create employment.

When using VHR imagery, the OBIA effectively deals with challenges encountered using pixel-based approaches which include the presence of shadows near features (Jombo *et al.*, 2020), mixed pixels or high spectral variability existing within tree classes (Myint *et al.*, 2011; Alonzo *et al.*, 2014). The aforementioned challenges encountered in previous studies were overcome by the object-based approach used in this study. In this study, the OBIA approach produced good accuracy results as it categorized the pixels into objects, which reduced the variance within the same LULC type by averaging pixels within IOs. The use of an object-based approach with shape/geometric and contextual information that is calculated from every single IO assists in urban LULC classification, especially using high spatial resolution imagery (Pu *et al.*, 2011). Moreover, as objects were used in this study, expert knowledge about the study area and additional spatial relations such as the nearest neighbour technique in the classification procedure was useful in discriminating the different urban trees and other LULC classes.

4.5 Conclusions

This study has shown the capability of OBIA in the classification and mapping of urban trees using VHR WV-2 multispectral data. Classification using SVM and RF classifiers enabled accurate discrimination of urban trees and other LULC classes as both obtained high overall accuracies. The RF classifier with an overall accuracy of 91.9% performed better than SVM (87.3%) in classification and mapping urban trees and other LULC classes. This study is of great importance to urban managers and other stakeholders on the use of OBIA in the mapping of urban trees. This study provided information on the spatial distribution of the common urban trees, useful in managing urban landscapes. A single WV-2 image was used in this study to classify urban trees and other LULC classes due to the availability of data in the vegetation growing season. It is thus recommended that future research compares WV-2 with other satellite images such as WorldView-3/4, Sentinel-2 and Landsat 8 acquired on the same date in the classification of urban trees and other LULC classes in the study area. Future studies can map urban trees using OBIA of high-resolution multispectral data and LiDAR, which incorporates tree height and measurement of crown spread in the analysis which can increase the accuracy levels obtained in this study.

Chapter Five

Urban tree classification using point cloud LiDAR data and WorldView-2 satellite imagery in a heterogeneous environment

This chapter is based on **Jombo, S**., E. Adam and Tesfamichael, S. Urban tree classification using point cloud LiDAR data and WorldView-2 satellite imagery in a heterogeneous environment. *International Society for Photogrammetry and Remote Sensing*. (Under review).

Abstract

Feature complexity and heterogeneity of land use and land cover (LULC) in urban areas pose a challenge for tree species classification. Recent developments in very high spatial resolution (VHSR) satellite imagery, Light Detection and Ranging (LiDAR) point-cloud data and vegetation indices combined with machine learning classifiers provide an opportunity for improved urban tree and LULC classification efforts. The classification of tree species in a complex urban environment is a challenge using optical data alone as they can be confused with man-made structures. The inclusion of structural data such as LiDAR assists in the classification and mapping of tree species producing high accuracies. The first objective of this study was to examine the effectiveness of the fused dataset (VHSR WV-2 bands, vegetation indices and normalised digital surface model (nDSM)) in mapping common urban trees and other LULC classes in the City of Johannesburg, South Africa. The second objective was to rank the importance of WV-2 bands, vegetation indices and nDSM in the classification of common urban trees and LULC classes in the study area. The results indicate that the fused dataset was effective in mapping common urban trees and LULC classes in the study area. This was shown by high classification accuracies of 97% for the Random Forest (RF) and 94% for Support Vector Machines (SVM) classifiers. The nDSM, near-infrared 1 (NIR1), NIR2 were the top-ranked variables in the classification of common urban trees and LULC classes with high Mean Decrease in Accuracy (MDA) and Mean Decrease in Gini (MDG) values. The nDSM had high scores of 0.98 for MDA and 0.61 (MDG), whereas the Green Normalized Difference Vegetation Index (GNDVI) had low MDA and MDG values of 0.18 and 0.01, respectively. Overall, this study's results indicate that data fusion of WV-2 bands, vegetation indices, and nDSM is applicable in mapping urban trees and LULC classes in a heterogeneous environment. This research provides information to municipalities on the methods and data that can be used for sustainable urban tree management in urban areas.

5.1 Introduction

Urban tree management is important to enhance the benefits provided by the ecosystem services, which improve the environment for the urbanites (Pu and Landry, 2020). These benefits include surface and air temperature reduction (Alonzo *et al.*, 2014), maintain environmental health, prevent soil erosion (Shojanoori *et al.*, 2016), energy conservation (Azeez *et al.*, 2019) and increase property values (Hartling *et al.*, 2019). The diversity of urban trees is a vital parameter in the characterization of urban ecosystems, which is crucial for sustainable urban planning (Hartling *et al.*, 2019). Accordingly, well-detailed urban trees maps are vital to understand the distribution and extend of tree species which assists municipalities and policymakers in sustainable urban development (Jombo *et al.*, 2020).

Compared to traditional approaches such as field surveys and manual interpretation of aerial maps which is labour intensive, time-consuming and costly, remote sensing technologies such as very high-resolution imagery, can provide a quick, easy, repeatable and convenient alternative to obtain urban tree canopy and species information (Pu and Landry, 2020; Jombo *et al.*, 2020). Initially, tree species mapping was limited to vegetation cover at a large scale using low spatial resolution imagery such as Moderate-Resolution Imaging Spectroradiometer (MODIS), Satellite pour l'Observation de la Terre (SPOT) and Landsat (Hartling *et al.*, 2019). However, mapping urban tree species in a heterogeneous urban environment is challenging when using low spatial resolution imagery due to the complexity of features, species diversity and spatial variations (Alonzo *et al.*, 2014). The low spatial resolution images are not suitable for urban tree classification because of their ground instantaneous field of view, e.g. 30m for Landsat, which is larger than the characteristic scale of spatial variation in urban areas, which is approximately 5 to 10m (Alonzo *et al.*, 2016).

Recent developments in remote sensing techniques and the advent of very high spatial resolution (VHSR) satellite imagery such as GeoEye, Quickbird and WorldView (WV) have improved the classification of trees in heterogeneous urban environments (Pu and Landry, 2012; Li *et al.*, 2015; Hartling *et al.*, 2019). While sensors such as GeoEye and Quickbird provide imagery with a spatial resolution of < 2.5m, their spatial and spectral range does not allow for accurate discrimination of the structural variation among tree species (Clark *et al.*, 2005). Compared to the traditional four bands of GeoEye and Quickbird, the DigitalGlobe's WorldView-2 (WV-2) satellite launched in 2009 has four additional bands (red-edge, coastal, yellow, near-infrared 2), which proved to be capable of discriminating tree species in previous studies (Li *et al.*, 2015; Alonso-Benito *et al.*, 2016; Karlson *et al.*, 2016). However, the classification of urban trees using VHSR imagery such as WV-

2 in a heterogeneous area is still sub-optimal due to various factors such as shadow effects, crown brightness and background noise which pose challenges to extruding valuable information on urban trees (Liu *et al.*, 2017). This suggests that non-spectral data may be required to assist in the discrimination and classification of tree species to get high accuracies.

The integration of Light Detection and Ranging (LiDAR) and optical data can improve classification accuracies in urban tree species mapping (Hartling *et al.*, 2019). This is attributed to the integration of textural and spatial information obtained from optical and LiDAR data, respectively (Pu and Landry, 2020). In general, LiDAR sensors scan objects on the ground by emitting high-density pulses and record the backscattered or reflected light (Wehr and Lohr, 1999). The distance to the object is measured by recording the time between emitted and backscattered pulses and using the speed of light to convert the time to distance (Heritage and Large, 2009). Each pulse contains x, y and z records which represent highly accurate 3-dimensional (3D) position of ground or non-ground features (Hyyppa, 2000). This enables the sensors to capture fundamental structural attributes of tree species such as height, crown depth, and other vegetation's biophysical characteristics (Zhang *et al.*, 2015).

Previous studies have used LiDAR data to map fuel types (e.g. Alonso-Benito *et al.*, 2016), extraction of buildings and trees (e.g. Demir *et al.*, 2008), individual tree segmentation (e.g. Li *et al.*, 2012; Zhang *et al.*, 2015), mapping forest structural types (e.g. Ruiz *et al.*, 2016) and urban tree classification (e.g. Alonzo *et al.*, 2014; Alonzo *et al.*, 2016; Azeez *et al.*, 2019; Hartling *et al.*, 2019). The focus on the classification of trees has been on environments with homogeneous species composition, and there is still a growing interest in tree classification in heterogeneous urban environments. Moreover, previous studies have been conducted in America, Europe, and Asian countries, and a few have been carried out in Africa (Kaszta *et al.*, 2016). This is because the availability of LiDAR infrastructure in Africa is still limited (Kaszta *et al.*, 2016). Therefore, it is vital to map trees in a heterogeneous urban landscape in Africa using LiDAR and optical remote sensing data to provide timely and useful information for sustainable urban forest management and urban planning.

Several studies (e.g., Cho *et al.*, 2012; Colgan *et al.*, 2012; Naidoo *et al.*, 2012) have classified tree species using integrated optical and LiDAR data. For example, Cho *et al.* (2012) used WV-2, Quickbird, LiDAR and hyperspectral datasets to map common savanna tree species in the Kruger National Park, South Africa. The study produced an overall accuracy of 79% using the maximum

likelihood classifier. Colgan *et al.* (2012) mapped savanna tree species using the Support Vector Machines (SVM) classifier and bidirectional reflectance distribution (BRDF) correction on LiDAR and hyperspectral data in the Kruger National Park. The study produced an overall prediction accuracy of 76%. Naidoo *et al.* (2012) classified savanna tree species by integrating LiDAR, hyperspectral data, and vegetation indices in the Kruger National Park. The study produced an overall accuracy of 87.68% using the Random Forest (RF) classifier and highlighted the importance of vegetation indices in the classification of trees. However, other studies (Wu *et al.*, 2018; Pu and Landry, 2020) found that the addition of LiDAR data might not be that helpful in the classification of tree species or can improve the classification accuracies only slightly. It is not clear whether these varying accuracies were due to similar tree height, crowns, shape, or low LiDAR point cloud density. Thus, it is necessary to carry out studies that classify and map trees in a heterogeneous environment by integrating high-density LiDAR and optical data to assess the additional ability of the LiDAR sensor in improving urban tree classification.

The classification of urban trees faces several challenges, including the complexity of the environment, the spatial heterogeneity of tree species, and differences in the shape and structure of trees (Zhang *et al.*, 2015). Urban areas consist of various land use and land cover (LULC) classes which include built-up, roads, trees, bare soil and water bodies, which makes the filtering process (distinguish ground and non-ground points) of LiDAR data more difficult (Yan *et al.*, 2015). Unlike trees in forest plantations, which in most cases have the same canopy characteristics, the spatial heterogeneity of urban trees is a challenge due to their differences in treetops, crown widths and height (Zhang *et al.*, 2015). Urban trees' classification also faces challenges because the vegetation in these environments co-exists with different man-made land cover types (Alonzo *et al.*, 2014). These challenges have made the establishment and updating of urban tree inventories much more difficult for proper planning and sustainable urban tree management (Pu and Landry, 2012).

The City of Johannesburg (CoJ) is complex and consists of, amongst others, tall buildings, roads, water bodies, grasslands and is considered one of the largest man-made urban forests in the world (Schäffler and Swilling, 2013; Jombo *et al.*, 2020). The classification of urban trees in the city using optical remote sensing data alone is a problem, as they can be confused with man-made structures (Jombo *et al.*, 2020). To overcome this problem, the fusion of LiDAR data and VHSR imagery can produce high accuracies in the classification of urban trees and LULC classes. It is against this background that this study assessed the ability of fused data (WV-2 bands, vegetation indices and normalised digital surface model (nDSM)) in mapping trees species and other LULC classes in a

heterogeneous urban environment. The specific objectives of this study were to (1) examine the effectiveness of the fused dataset in mapping common urban trees and LULC classes in Randburg municipality, Johannesburg, and (2) rank the importance of WV-2 bands, vegetation indices and nDSM in the classification of common urban trees and LULC classes in the study area. This research seeks to provide information that can be used to promote sustainable urban tree management.

5.2 Methods

5.2.1 Study area

Randburg municipal area is in the CoJ, Gauteng province, South Africa (Figure 5.1). The study area covers 167.9km^2 and has a warm climate consisting of high temperatures and rainfall in summer and low temperatures in winter (Goldreich, 1992). The mean monthly temperature ranges from 17°C in July to 25°C in January, and average monthly rainfall values range from 6mm in July to 107mm in January (City of Johannesburg, 2009). The annual rainfall varies between 700 and 720mm (Knight, 2018). The study area lies at an altitude above 1700m and has hard and resistant quartzite rocks (Knight, 2018). These rocks weather over time to produce thin soils with high biodiversity, especially vegetation species (Knight, 2018).

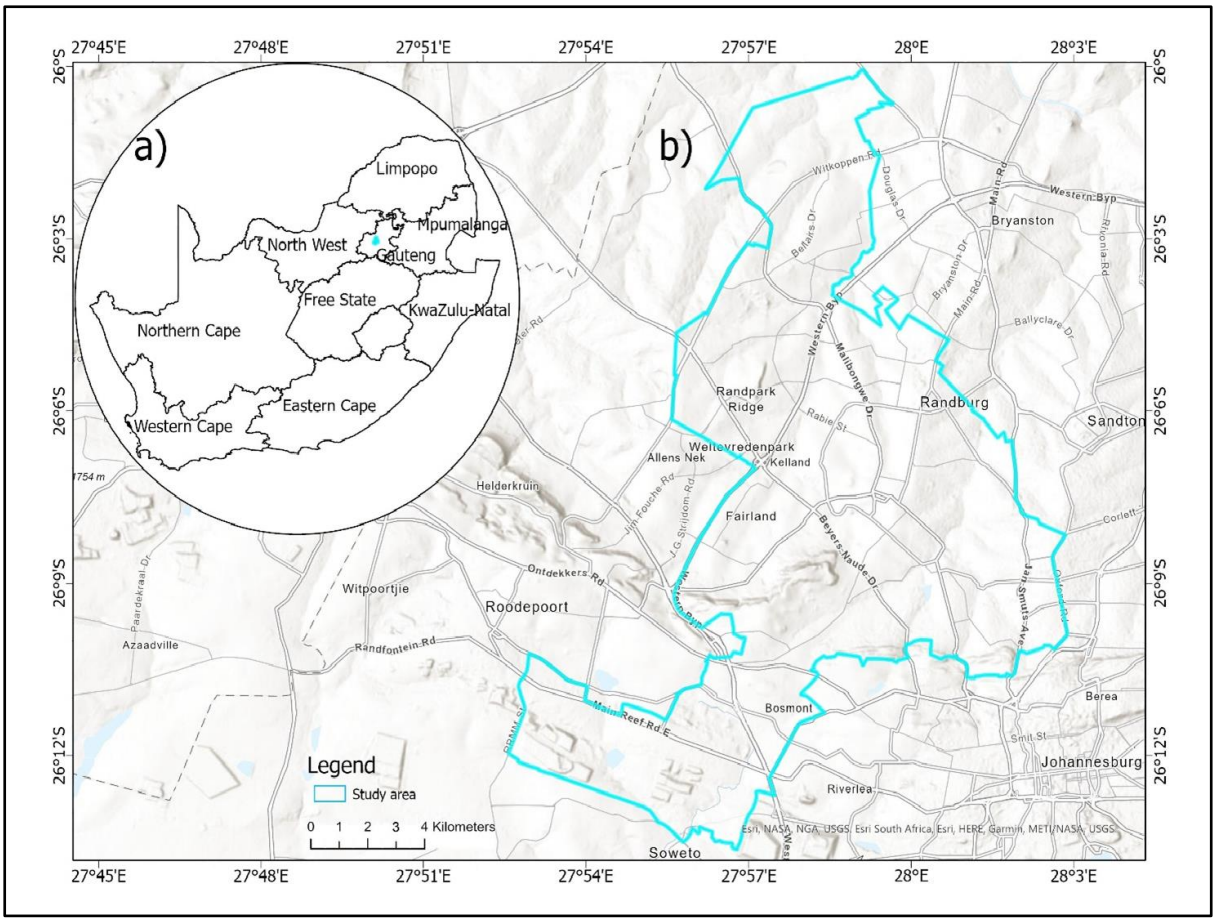


Figure 5.1 The map shows a) South African provinces and b) ESRI's basemap showing Randburg municipal area.

The CoJ, which includes the study area, is reported to be amongst the most street-lined cities globally and comprises a human-made tropical forest (Johannesburg City Parks and Zoo, 2021). The area is in the grassland biome dominated by a single stratum of vegetation and herbaceous plants with short stems and perennating organs near the ground (Rutherford and Westfall, 1994). Large tracts of land have been transformed from grassland to urban woodland due to urbanisation which led to the planting of invasive tree species (Symes *et al.*, 2017). The most common alien trees growing in the study area include jacaranda, oaks, gum, pine and London plane (Turton *et al.*, 2006; Schäffler and Swilling, 2013; Mudede *et al.*, 2020). The study area is heterogeneous, with different LULC classes, including water bodies, trees, roads, grasslands, bare land, residential and industrial buildings (Symes *et al.*, 2017; Knight, 2018; Jombo *et al.*, 2021).

5.2.2 LiDAR data

LiDAR data for the present study was obtained from the municipality of Johannesburg's Corporate Geo-Informatics, Development Planning and Urban Management (DP&UM). The

survey was carried out by the LiDAR department of the African Consulting Surveyors (www.africansurveyors.com) between 7 and 9 August 2019 using a Cesna 210 (ZS-MBU) aircraft with an average point density of 3-4 points per m^2. The characteristics of the LiDAR survey are shown in Table 5.1. The time of the survey was regarded to be corresponding to the field data collection, aerial photograph and the WV-2 imagery used in this study. The time difference between the data collection times used in this study was ≤ 4 months. A total of 228 blocks, measuring 1000m x 1000m per block in size, covered the study area. The data were collected in the Hartebeesthoek WG29 coordinate system. The LiDAR point clouds were grouped into the ground and non-ground points by the data provider.

Table 5.1 Summary of flight and sensor characteristics of the LiDAR survey used in this study.

Parameter	**Value**
Average flying height	2200m (above mean sea level) and 500m (above ground level)
Sensor	Reigl Litemapper 5600
Flight side overlap	35%
Wavelength	1064nm
Pulse rate	66KHz
Scan angle	60°
Scan width	577m
Beam divergence	0.5mrad
Vertical accuracy	+/-20mm
Horizontal accuracy	+/-20mm

A Digital Terrain Model (DTM) with a spatial resolution of 2m was derived using the ground points to match the spatial resolution of the WV-2 image used in this study. The DTM was produced using the Inverse Distance Weighting (IDW) method as described in Xiaoye (2008). The IDW method was considered to be an appropriate method due to the high density of the point clouds used in this study (Xiaoye, 2008; Azeez *et al.*, 2019). The resultant DTM had a maximum elevation value of 1805m and a minimum of 1305m (Figure 5.2a). A nDSM was generated by subtracting the DTM from the Digital Surface Model (DSM) with maximum and minimum values of the nDSM being 0 and 555m, respectively (Figure 5.2b). This layer showed the top of reflective surfaces such as tree canopy and building tops.

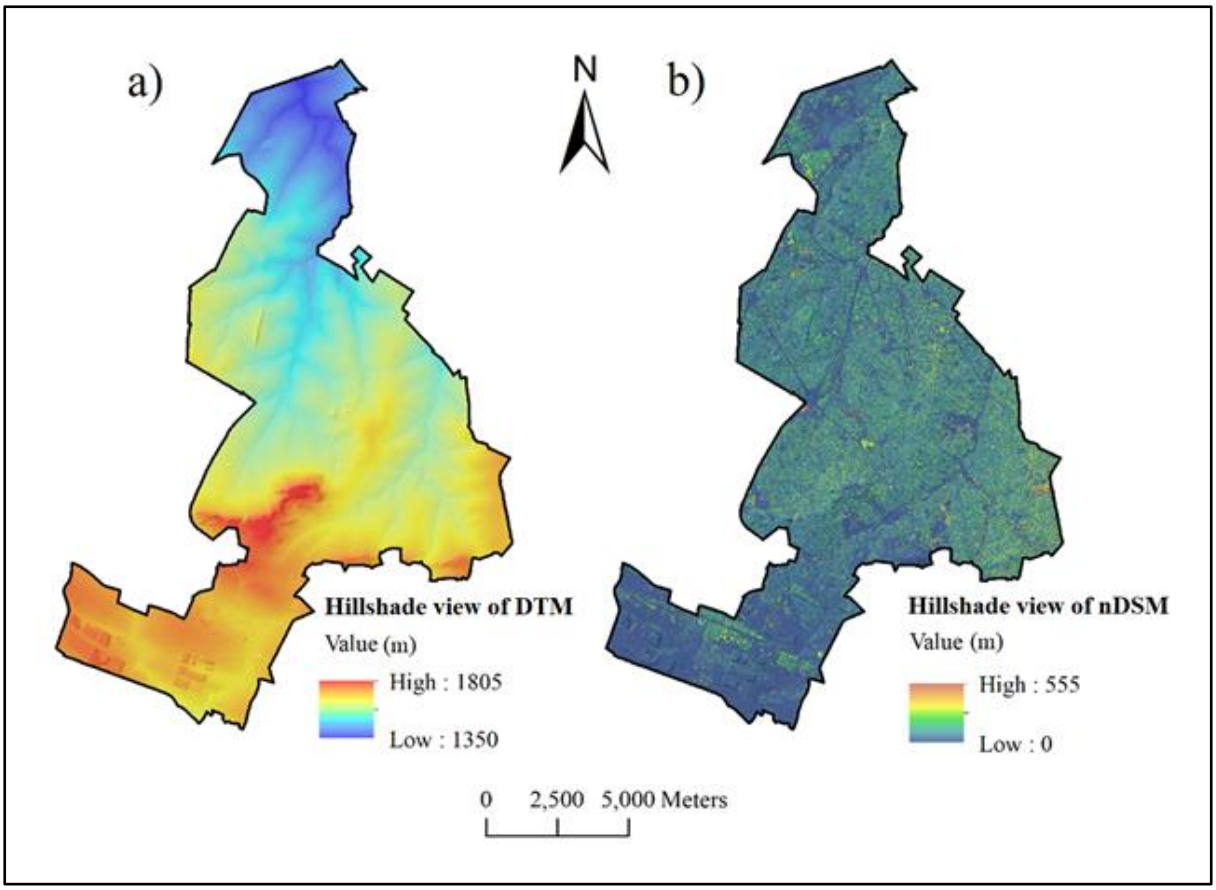


Figure 5.2 a) Hillshade view of Digital Terrain Model (DTM) and b) Normalised Digital Surface Model (nDSM) for the study area.

5.2.3 Multispectral data

Cloud-free WV-2 satellite imagery created from 36 scenes was used in the present study. The municipality of Johannesburg's Corporate Geo-Informatics, Development Planning and Urban Management (DP&UM) unit provided the WV-2 satellite imagery acquired on 10 November 2019. The geometric and radiometric anomalies were already corrected on the WV-2 scenes, and they were projected to Hartebeesthoek WG29 coordinate system to match with the LiDAR data used in this study. The WV-2 satellite imagery has a spatial resolution of 2m, with eight multispectral bands, including the traditional four bands, namely: blue (450 to 510nm), green (510 to 580nm), yellow (585 to 625nm) and red (630 to 690nm). The imagery has four additional bands: coastal (400 to 450nm), red edge (705 to 745nm), near-infrared 1 (NIR1) (770 to 895nm) and NIR2 (860 to 1040nm). The imagery was orthorectified using the Digital Elevation Model (DEM) derived from the ground LiDAR point clouds, with a 2m spatial resolution. The orthorectification of the imagery had a Root Mean Square Error of less than one pixel. The pre-processing was done using ArcGIS (ESRI ® ArcGIS Desktop: Release 10.6.1, Redlands, California, USA).

5.2.4 Vegetation indices

In this study, a total of seven vegetation indices were calculated using six WV-2 multispectral bands (Table 5.2). Previous studies (Mustafa *et al.*, 2015; Shojanoori *et al.*, 2016; Jombo *et al.*, 2021) found that vegetation indices are important in the classification of urban trees and LULC classes using WV-2 imagery. Vegetation indices using the visible and the NIR bands improve the sensitivity of the detection of green vegetation, which results in high classification accuracies (Xue and Su, 2017). Vegetation indices such as NDVI have successfully been used in previous studies to distinguish urban trees from non-vegetated features and produced high classification accuracies (Mustafa *et al.*, 2015; Li *et al.*, 2015; Shojanoori *et al.*, 2016; Jombo *et al.*, 2021). The vegetation indices used in this study have successfully classified vegetation species in previous studies shown in Table 5.2.

Table 5.2 Vegetation indices used in this study.

Index name	Abbreviation	Bands	Formula	Application examples
Normalized Difference Vegetation Index	NDVI	NIR1, red	$\frac{NIR1 - red}{NIR1 + red}$	(Demir *et al.*, 2008; Omer *et al.*, 2016; Fang *et al.*, 2018)
Normalized Difference Vegetation Index—NDVI2	NDVI2	NIR2, red	$\frac{NIR2 - red}{NIR2 + red}$	(Hartling *et al.*, 2019; Varin *et al.*, 2020)
Normalized Difference Vegetation Index—Green/Red Ratio	NDVI-GR	NIR1, green, red	$\frac{NIR1 - (green + red)}{NIR1 + (green + red)}$	(Gitelson *et al.*, 1996; Hartling *et al.*, 2019)
Normalized Difference Vegetation Index—Yellow	NDVI-Y	NIR1, yellow	$\frac{NIR1 - yellow}{NIR1 + yellow}$	(Waser *et al.*, 2014; Hartling *et al.*, 2019)
Normalized Difference Red Edge Index	NDRE	NIR1, red edge	$\frac{NIR1 - red\ edge}{NIR1 + red\ edge}$	(Wężyk *et al.*, 2019)
Normalized Difference Red Edge Index 2	NDRE2	NIR2, red edge	$\frac{NIR2 - red\ edge}{NIR2 + red\ edge}$	(Hartling *et al.*, 2019)
Green Normalized Difference Vegetation Index	GNDVI	NIR1, green	$\frac{NIR1 - green}{NIR1 + green}$	(Omer *et al.*, 2016; Wężyk *et al.*, 2019)

5.2.5 Reference data

Fieldwork was conducted in September 2019, and coordinates for common urban trees were uploaded into a handheld Global Positioning System (GPS) Garmin eTrex 20 X (GPS; Garmin International Inc., Kansas, USA). A stratified purposeful sampling method was used to identify the common urban trees in the study area due to its ability to capture different tree types rather than identifying tree species in the same class (Patton, 2002). The study area was partitioned into four equal sections, each measuring roughly 42km^2. In each section, the samples for the common urban trees were selected using the zigzag sampling technique (Paulo *et al.*, 2005; Almeida and Tomé, 2009). This technique involves inserting points along a zigzag transect inside the zone

segments, and the trees closest to the points are chosen for analysis (Paulo *et al.*, 2005). The sampling method was used mostly on the streets where urban tree species coordinates were delineated on the WV-2 satellite imagery. A total of 472 samples were used to classify the five common urban trees, which are Oak (*Quercus* spp.), Pine (*Pinus* spp.), London plane (*Platanus* spp.), Jacaranda (*Jacaranda* spp.) and Gum (*Eucalyptus* spp.) as shown in Table 5.2. The samples for the classes were georeferenced using a high resolution (0.5m) aerial photograph acquired on 6 November 2019. A total of 1540 samples for the common urban trees and the LULC classes were used in this study. These samples were randomly split into 70% training (n = 1078) and 30% test (n = 462) as shown in Table 5.3.

Table 5.3 Total number of training and test datasets for common trees and land use and land cover (LULC) classes used in this study.

Category	**Common name**	**Latin name**	**Code**	**Training dataset**	**Test dataset**	**Total number of samples**
Common trees	Gum	*Eucalyptus* spp.	ES	72	31	103
	Jacaranda	*Jacaranda* spp.	JS	63	27	90
	London plane	*Platanus* spp.	PL	49	21	70
	Oak	*Quercus* spp.	QS	46	20	66
	Pine	*Pinus* spp.	PN	100	43	143
LULC	Bare soil	-	BS	75	32	107
	Grassland	-	GL	147	63	210
	Other vegetation	-	OV	166	71	237
	Road	-	RD	112	48	160
	Urban built-up	-	UB	152	65	217
	Waterbody	-	WB	96	41	137
Total				1078	462	1540

5.2.6 Image data fusion and classification

Following data attainment and pre-processing, the nDSM was fused with the WV-2 imagery and vegetation indices images using ENVI (5.4) software suite (Harris Geospatial Solutions, Broomfield, CO, USA). The Image Stack (IS) fusion was used to integrate the bands from the WV-2 imagery, seven vegetation indices and nDSM into a single file. The IS fusion combines separate referenced image bands into a single image file (Milewski *et al.*, 2009). The IS fusion has

successfully been used to integrate optical multispectral bands, vegetation indices and nDSM to classify urban trees at high accuracy (Forzieri *et al.*, 2010; Luo *et al.*, 2015; Hartling *et al.*, 2019).

5.2.7 Image segmentation

Prior to the object-based classification, image segmentation was done to produce image objects (IOs) that were used to classify common urban trees and LULC classes in this study. The multi-resolution segmentation (MRS) algorithm, a bottom-up region merging process, was used to segment the fused dataset. The eight multispectral bands of WV-2 were given a band weight coefficient of 1, and the nDSM was assigned a weight coefficient of 2. Previous studies indicated that assigning a higher band weight coefficient for the nDSM at the segmentation stage effectively extracts more meaningful objects, such as tree species and built-up features (Pu and Landry, 2012; Pu and Landry, 2020). The band weight coefficients used in this study were derived from previous studies which used similar classes and VHSR data in heterogeneous urban environments (Pu and Landry, 2012, 2020; Jombo *et al.*, 2021). The colour criterion was assigned a weight of 0.8, and the shape feature variable was allocated the remaining value of 0.2. Previous studies (e.g. Pu and Landry, 2020; Jombo *et al.*, 2021) indicated that desired results are produced in the classification of urban trees and LULC classes when the shape feature variable is given less weight than the colour criterion. The scale factor is one of the vital MRS algorithm parameters, and its value controls the relative sizes of the IOs, which impacts the classification accuracy (Benz *et al.*, 2004). A scale factor controls the internal heterogeneity of the IOs and is consequently correlated with their average size, *viz.*, a large scale factor value enables high internal heterogeneity while increasing the number of pixels per IO (Benz *et al.*, 2004). Seven different scale settings (10, 15, 20, 25, 30, 35, 40, 45 and 50) were tested in this study, and the final segmentation scale factor was chosen based on assessing the shape of the IOs. The degree to which the resulting IOs match most individual tree crowns' feature boundaries was visually compared and these IOs were used in the object-based classification analysis.

5.2.8 Feature selection

In selecting segments used for the classification of common urban trees and LULC classes, shape and spectral information were used. The determination of the features to use in object-based classification is a challenge because it is time-consuming to select the perfect features to use from the hundreds or thousands of spectral, textural, contextual and geometrical feature variables available in the Definiens eCognition Developer software (Zhou *et al.*, 2012). To reduce the aforementioned challenge, the Feature Space Optimization (FSO) tool was used to identify the

optimal feature variables to use in the classification of the common urban trees and LULC classes. The FSO helps distinguish classes using the nearest neighbour method on the selected features (Zhou *et al.*, 2012). The shape and spectral variables used in selecting IOs include the spectral, geometry and textural variables. The mean and brightness values for the 8 multispectral bands of WV-2 imagery were used to select IOs. The use of shape and spectral information in selecting IOs has produced satisfactory results in previous studies (Mustafa *et al.*, 2015; Fang *et al.*, 2018; Hartling *et al.*, 2019).

5.2.9 Classification methods

The classification of common urban trees and LULC classes on the IOs derived from the fused dataset was done using eCognition Developer (Version 9.3.1, Definiens AG, Munich, Germany) software. Two machine learning classifiers were applied to the IOs to classify common urban trees and LULC classes; these are RF and SVM. The two classifiers were used due to their powerful performance in urban trees classification (Le Louarn *et al.*, 2017; Pu *et al.*, 2018; Jombo *et al.*, 2020).

5.2.9.1 Random Forest classifier

The RF developed by Breiman (2001) is a powerful machine learning algorithm built on the classification and regression trees (CART). The trees are made from the training samples by drawing out a subset through a bagging approach. The algorithm is governed by three parameters which are *mtry*, nodesize and *ntree*. The *mtry* is the number of the sampled variables that range from 1 to *n* (total number of variables). In classification, the default *mtry* is $\sqrt{(n)}$, which plays a role in reducing the calculation time required to run the model (Breiman, 2001; Collins *et al.*, 2018). The nodesize is the minimal size of terminal seeds that have to be split, and the *ntree* is the number of trees chosen in the RF ensemble (Breiman, 2001). In the RF classifier, the binary classification *ntrees* are built with replacement drawn from the training samples. These *ntrees* contribute a unit vote, and the correct classification from all the trees is determined by the majority votes (Breiman, 2001). The samples that are not in the bootstrap sample are used for validating the tree performance and are known as the out-of-bag (OOB) data. The RF classifier uses the input variables' explanatory power, known as variable importance (VI). The VI has two metrics, namely, the Mean Decrease in Accuracy (MDA) and a Mean Decrease in Gini (MDG) (Breiman, 2001). The most important variables are the ones with high MDA and MDG values. The 10-fold cross-validation method was used to find the optimum *ntree* and *mtry* parameters. In this study, the *mtry* value of 6, *ntree* value of 2500 and node size of 5 were used. The classification was done using eCognition Developer (Version 9.3.1, Definiens AG, Munich, Germany) software.

5.2.9.2 Support Vector Machines

The Support Vector Machines (SVM) classifier is a supervised method that uses a hyperplane to separate features into different classes (Vapnik, 1995). If classes are not linearly separable, the SVM algorithm uses the kernel functions to transform non-linear observations into linear ones. The common kernel functions used for vegetation classification are sigmoid, linear, radial basis function (RBF) and polynomial (Azeez *et al.*, 2019). Previous studies that used the kernel functions highlighted that the RBF performs better than other kernels due to various factors, which include its efficiency in an infinite-dimensional feature space, and it only requires the tuning of two parameters which are cost (C) and gamma (γ) (Xu *et al.*, 2012; Omer *et al.*, 2015; Azeez *et al.*, 2019). The C determines the trade-off between the margin maximization and minimization of the training error (Vapnik, 1995). A large C value accepts a smaller margin hyperplane if the decision function correctly classifies the training samples. A lower C value causes the optimizer to search for a larger-margin separating hyperplane, even if the hyperplane misclassifies more samples (Vapnik, 1995). The γ parameter influences the shape or curvature of the hyperplane separating the training data. If the γ is small, the decision boundary is close to linear, which affects the non-linear classification data; on the other hand, when the γ is high, this results in overfitting (Vapnik, 1995). In this study, the classification of common urban trees and LULC classes using SVM was done using eCognition Developer (Version 9.3.1, Definiens AG, Munich, Germany) software.

5.2.10 Accuracy assessment

The accuracy of the RF and SVM maps was done using confusion matrices computed using the test dataset. The observed and the predicted data were compared to assess the user's and producer's accuracy. The user's accuracy is the total number of correctly classified samples in a class divided by the total number of classified samples in that class (Congalton, 1991). On the other hand, the probability that a sample belongs to a certain class and the classifier accurately assigns it to such a class is the user's accuracy (Congalton, 1991). The overall accuracy was calculated by averaging the correctly classified samples among all classes (Congalton, 1991). Cohen's kappa index of agreement (KIA) was also calculated to evaluate if there is an agreement between reference data and the classifier (Congalton, 1991). The KIA statistic ranges from -1 to +1, where 1 represents a perfect agreement, -1 indicates an agreement that is worse than the one expected by chance, and 0 shows agreement by random chance (Cohen, 1960). The most effective classifier between RF and SVM was found by comparing the accuracies and the KIA statistic values.

5.2.11 McNemar's test

The McNemar's test was used in this study to determine the significance and statistical reliability of the RF and SVM classifiers. This test is non-parametric and shows differences among the classifiers' confusion matrices (Foody and Mathur, 2004). The test was applied in this study due to its ability to compare thematic maps with the same test samples used for validation. The McNemar's test was calculated starting with figuring out the Z value as follows:

$$Z = \frac{f_{12} + f_{21}}{\sqrt{f_{12} - f_{21}}} \quad \text{Equation 5.1}$$

in which f_{12} denotes the correctly classified test samples by the SVM classifier and incorrectly classified by RF. The incorrectly classified samples by the SVM classifier but correctly classified by the RF classifier are represented by f_{21}. The Z value can be referred to as the chi-squared distribution table with a single degree of freedom (Congalton *et al.*, 1983). At a 95% confidence interval, the Z value should be greater than 1.96 for the test to be statistically significant (Dwyer, 1991). The McNemar's test was expressed using a chi-squared (χ^2), computed as follows:

$$\chi^2 = (f_{12} - f_{21})^2 / (f_{12} + f_{21}) \quad \text{Equation 5.2}$$

In order to imply that the performance of the RF and SVM classifiers was significantly different, the χ^2 value obtained from equation (5.2) was supposed to be greater than 3.84 based on the chi-squared table at a 95 % confidence interval.

5.2.12 Variable selection

The variable importance calculated by both the RF and SVM classifiers was used to rank the WV-2 bands, vegetation indices and nDSM according to their ability to classify common urban trees and LULC classes in the study area. Subsequently, a forward variable selection method (Sutter and Kalivas, 1993) was employed to identify the least number of variables with high accuracy. Numerous RFs were iteratively fitted consecutively utilizing the ranked variables. Initially, new RF models were built using the top-ranked variables, and for the next iteration, the second top-ranked variables were added. This process was done repeatedly until all the variables (n = 16) were considered. Lastly, the subsets with the lowest OOB error rate for the RF classifier were taken as the optimum classification variables. The variable's ranking was done, and the variables that led to a decrease in the OOB rate were selected. The variables that did not decrease the OOB error rate

and those that led to its increase were not chosen for the final classification model. The importance of the variables using the SVM classifier was ranked by generating a Receiver Operating Characteristic (ROC) curve and calculating the area under the ROC curve (Guyon and Elisseeff, 2003). The variables with high ROC curve variable importance were chosen to classify and map common urban trees and LULC classes using the SVM algorithm.

5.3 Results

5.3.1 Segmentation of used dataset

The fused dataset (WV-2 bands, vegetation indices and nDSM) was segmented using the multiresolution segmentation (MRS) algorithm. After conducting trial and error on the fused image, the optimum MRS scale parameter of 20 was used; this scale produced 15,457,579 objects. The IOs tend to be over-segmented, and this was done deliberately to keep the relatively small tree objects identifiable (Puissant *et al.*, 2014). A subsection of the fused dataset and a segmented portion of the study area are shown in Figure 5.3.

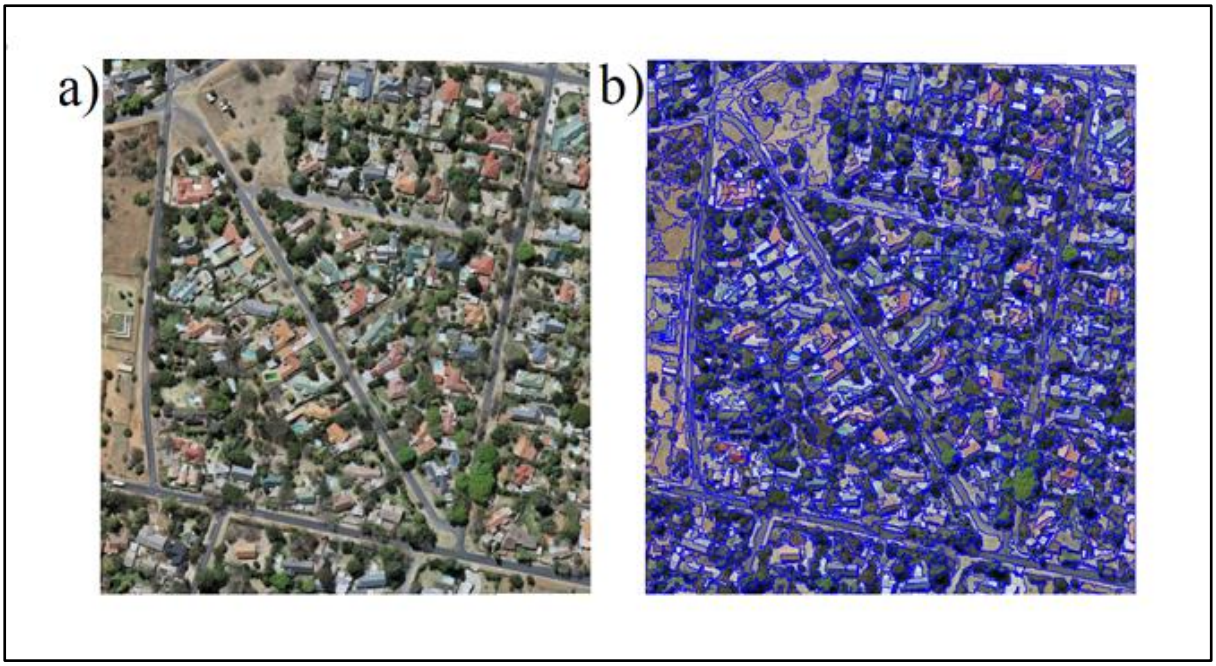


Figure 5.3 a) Subsection of the fused dataset (WV-2 bands, vegetation indices and nDSM) and b) segmented subsection of the fused dataset.

5.3.2 Classification of the common urban tree species and LULC classes

The IOs were classified using RF and SVM classifiers and the images had a total of 11 classes consisting of five common urban tree species (*Eucalyptus*, *Jacaranda*, *Platanus*, *Pinus* and *Quercus* spp.) and six LULC classes (bare land, built up, grassland, other vegetation, road, and waterbody) (Figure

5.4). The classification maps showed that the built-up was spread all over the study area, and most of the common trees are situated along the streets (Figure 5.4). There is more built-up and bare land in the southern part than the northern part of the study area (Figure 5.4). The common urban trees were mainly located along the streets and close to built-up features (Figure 5.4).

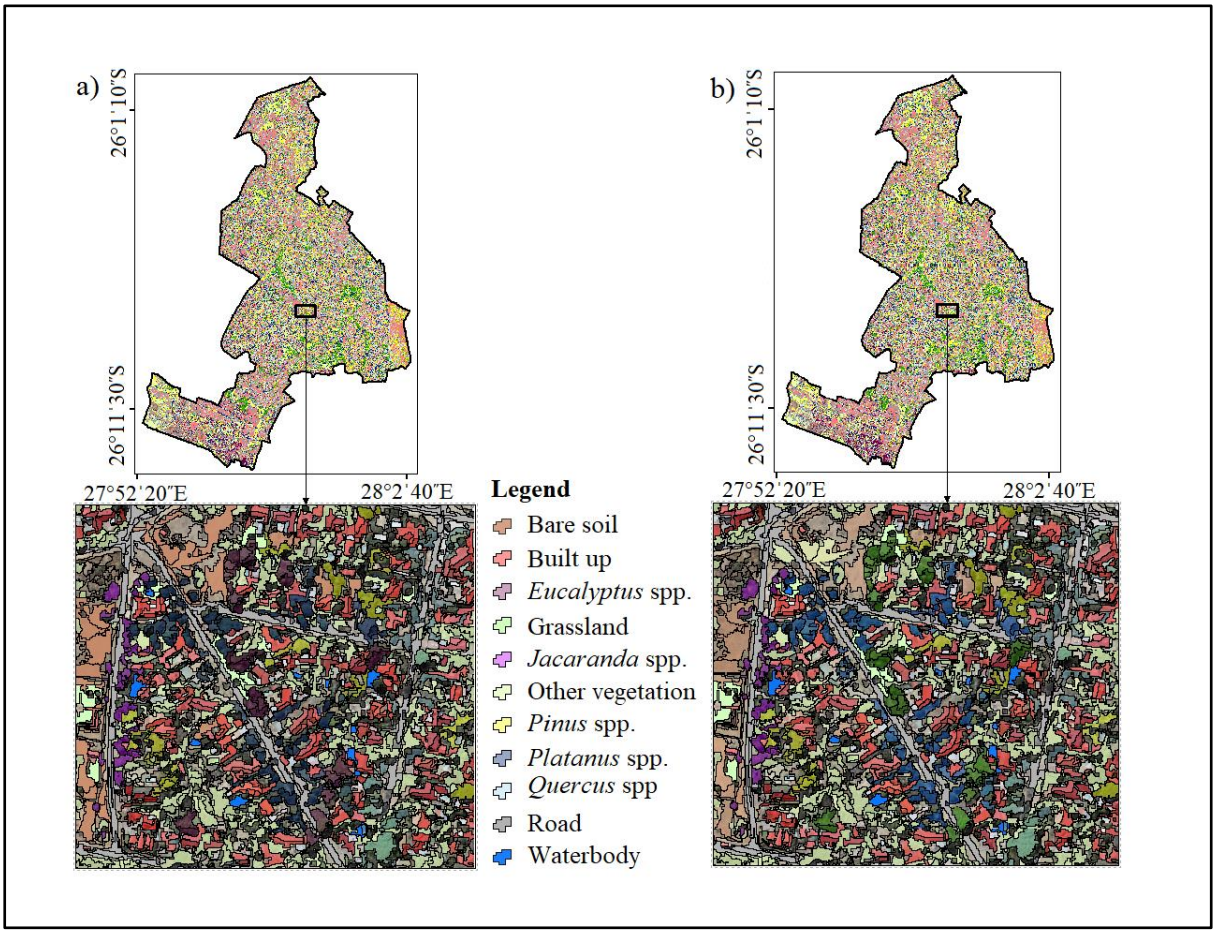


Figure 5.4 Classification maps for common urban trees and land use and land cover (LULC) classes using a) RF and b) SVM classifiers.

5.3.3 Validation

The classified fused imageries with WV-2 bands, vegetation indices and nDSM using RF and SVM classifiers were validated using the test dataset (Tables 5.3 and 5.4). All the variables (n = 16) and the most important variables (n = 12) were used to classify the common urban trees and the LULC classes. The RF classifier produced an overall accuracy value of 96%, and SVM produced 93%. using all the variables (n = 16). Cohen's KIA for RF (0.95) was greater than the one for the SVM classifier (0.92) (Table 5.4).

Both the user's and producer's accuracies for the common urban trees and LULC classes using the RF classifier were above 85% (Table 5.4a). The highest user's accuracy for the RF classifier was 100% for the road and waterbody classes, while the lowest was for *Platanus* spp. class (86%). The producer's accuracies for the RF classifier were all above 85%, with the highest being 100% for the built-up, *Platanus* spp., *Quercus* spp., road, and waterbody classes (Table 5.4a). The lowest user's accuracy was 88% for other vegetation class where some of the samples in this were misclassified as *Jacaranda* spp., *Platanus* spp., *Quercus* spp., grassland, and *Eucalyptus* spp. (Table 5.4a). The user's accuracies for the SVM classifier ranged from 85% for *Jacaranda* and *Quercus* spp. to 100% for the road and waterbody classes (Table 5.4b). The producer's accuracies for the SVM classifier ranged from 84% for bare land to 100% for built-up, *Quercus* spp., road, and the waterbody class (Table 5.4b). The user's accuracies for the common urban trees based on the RF classifier were greater than or equal to the ones for SVM. The producer's accuracies for the common urban trees based on the RF classifier were all greater than the one for the SVM classifier, except the value for the *Jacaranda* spp. class (Table 5.4a and 5.b).

Table 5.4 Confusion matrix for a) Random Forest (RF) classifier and b) Support Vector Machines (SVM) using all the variables (n =16). The classes namely, *Jacaranda* spp. (JC), built-up (BU), Bare land (BL), *Platanus* spp. (PL), *Quercus* spp. (QS), other vegetation (OV), *Pinus* spp. (PN), road (RD), grassland (GL), waterbody (WB) and *Eucalyptus* spp. (EC). Cohen's Kappa Index of Agreement (KIA), user's accuracy (UA), producer's accuracy (PA) and overall accuracy (OA) were calculated. The total (TL) number of the test samples in the rows and columns are also shown.

a) RF using all the variables (n = 16)

Class	JC	BU	BL	PL	QS	OV	PN	RD	GL	WB	EC	TL	UA
JC	26	0	0	0	0	1	0	0	0	0	0	27	96
BU	0	64	3	0	0	0	0	0	0	0	0	67	96
BL	0	0	30	0	0	0	0	0	1	0	0	31	97
PL	0	0	0	18	0	2	0	0	0	0	1	21	86
QS	0	0	0	0	19	1	0	0	0	0	0	20	95
OV	2	0	0	0	0	66	3	0	0	0	0	71	93
PN	0	0	0	0	0	0	42	0	1	0	0	43	98
RD	0	0	0	0	0	0	0	48	0	0	0	48	100
GL	0	0	0	0	0	3	0	0	59	0	0	62	95
WB	0	0	0	0	0	0	0	0	0	41	0	41	100
EC	0	0	0	0	0	2	0	0	0	0	29	31	94
TL	28	64	33	18	19	75	45	48	61	41	30	462	
PA	93	100	91	100	100	88	93	100	97	100	97		

OA = 96
KIA = 0.95

b) SVM using all the variables (n = 16)

Class	JC	BU	BL	PL	QS	OV	PN	RD	GL	WB	EC	TL	UA
JC	23	0	0	1	0	3	0	0	0	0	0	27	85
BU	0	59	6	0	0	0	0	0	0	0	0	65	91
BL	0	0	31	0	0	0	0	0	1	0	0	32	97
PL	0	0	0	18	0	2	0	0	0	0	1	21	86
QS	0	0	0	0	17	3	0	0	0	0	0	20	85
OW	1	0	0	0	0	63	4	0	0	0	3	71	89
PN	0	0	0	0	0	0	42	0	1	0	0	43	98
RD	0	0	0	0	0	0	0	48	0	0	0	48	100
GL	0	0	0	0	0	1	0	0	62	0	0	63	98
WB	0	0	0	0	0	0	0	0	0	41	0	41	100
EC	0	0	0	0	0	4	0	0	0	0	27	31	87
TL	24	59	37	19	17	76	46	48	64	41	31	462	
PA	96	100	84	95	100	83	91	100	97	100	87		

OA = 93
KIA= 0.92

The RF classifier outperformed SVM in the classification of common urban trees and LULC classes in this study using the selected variables (n = 12). The RF classifier produced an overall accuracy of 97%, while SVM generated a value of 94% (Figures 5.5a and 5.5b). The Cohen's KIA values for both classifiers improved from 0.95 for RF and 0.92 for SVM to 0.96 and 0.93 for RF and SVM classifiers, respectively (Tables 5.4 and 5.5). The user's accuracy for the RF classifier for the built-up class (98%) using the selected variables (n = 12) improved from 96% using all the variables (n = 16). All the user's and producer's accuracies for both classifiers (RF and SVM) using the selected variables (n = 16) were greater than or equal to the values produced using all the variables (n =16) in this study (Tables 5.4 and 5.5).

Table 5.5 Confusion matrix for a) Random Forest (RF) classifier and b) Support Vector Machines (SVM) using the selected variables (n =12). The classes namely, *Jacaranda* spp. (JC), built-up (BU), Bare land (BL), *Platanus* spp. (PL), *Quercus* spp. (QS), other vegetation (OV), *Pinus* spp. (PN), road (RD), grassland (GL), waterbody (WB) and *Eucalyptus* spp. (EC). Cohen's Kappa Index of Agreement (KIA), user's accuracy (UA), producer's accuracy (PA) and overall accuracy (OA) were calculated. The total (TL) number of the test samples in the rows and columns are also shown.

a) RF using all the variables (n = 12)

Class	JC	BU	BL	PL	QS	OV	PN	RD	GL	WB	EC	TL	UA
JC	26	0	0	0	0	1	0	0	0	0	0	27	96
BU	0	64	1	0	0	0	0	0	0	0	0	65	98
BL	0	0	32	0	0	0	0	0	1	0	0	33	97
PL	0	0	0	21	0	0	0	0	0	0	0	21	100
QS	0	0	0	0	19	1	0	0	0	0	0	20	95
OV	2	0	0	0	0	66	3	0	0	0	0	71	93
PN	0	0	0	0	0	0	42	0	1	0	0	43	98
RD	0	0	0	0	0	0	0	48	0	0	0	48	100
GL	0	0	0	0	0	3	0	0	59	0	0	62	95
WB	0	0	0	0	0	0	0	0	0	41	0	41	100
EC	0	0	0	0	0	2	0	0	0	0	29	31	94
TL	28	64	33	21	19	73	45	48	61	41	29	462	
PA	93	100	97	100	100	90	93	100	97	100	100		

OA = 97

KIA = 0.96

b) SVM using all the variables (n = 12)

Class	JC	BU	BL	PL	QS	OV	PN	RD	GL	WB	EC	TL	UA
JC	24	0	0	1	0	3	0	0	0	0	0	28	86
BU	0	59	6	0	0	0	0	0	0	0	0	65	91
BL	0	0	31	0	0	0	0	0	1	0	0	32	97
PL	0	0	0	18	0	2	0	0	0	0	1	21	86
QS	0	0	0	0	17	3	0	0	0	0	0	20	85
OW	0	0	0	0	0	63	4	0	0	0	3	70	90
PN	0	0	0	0	0	0	42	0	1	0	0	43	98
RD	0	0	0	0	0	0	0	48	0	0	0	48	100
GL	0	0	0	0	0	1	0	0	62	0	0	63	98
WB	0	0	0	0	0	0	0	0	0	41	0	41	100
EC	0	0	0	0	0	4	0	0	0	0	27	31	87
TL	24	59	37	19	17	76	46	48	64	41	31	462	
PA	100	100	84	95	100	83	91	100	97	100	87		

OA = 94

KIA= 0.93

5.3.4 Statistical comparisons

McNemar's test was applied to both the RF and SVM classified maps using 462 samples (Table 5.6). The test was calculated using the classified maps generated using the selected variables (n = 12). The correctly classified samples by both the RF and SVM were 457, while the incorrectly classified samples by both classifiers were 3 (Table 5.6). The incorrectly classified samples by RF but correctly classified by SVM were 0, whilst the correctly classified samples by RF and incorrectly classified by SVM were 2 (Table 5.6). The test indicated no significant differences in the accuracy of RF and SVM classifiers, as shown by the p-value (0.16), which is greater than 0.05 at a 95 % confidence interval. The Z value (1.42) was less than 1.96 and the χ^2 (2.00) was less than 3.84, which shows no significant differences in the accuracy of the two classifiers.

Table 5.6 The comparison of classification accuracies for RF and SVM classifiers using McNemar's test. The McNemar's chi-squared value is represented by χ^2 and Σ is for summation.

Classifier		**RF**		
		Correct	Incorrect	Σ
SVM	Correct	457	0	457
	Incorrect	2	3	5
	Σ	459	3	462
	χ^2 = 2.00	p-value = 0.16	Z value = 1.42	

5.3.5 Variable importance and ranking

The nDSM variable was the most important in classifying the common urban trees and LULC classes, as shown by a high MDA and MDG scores of 0.98 and 0.61, respectively, using the RF classifier (Figure 5.5). The NIR2 band followed by the NIR1, NDVI-GR had higher MDA values (Figure 5.5). The NIR1 band followed by NIR2, NDVIGR, red and red edge bands had high MDG values. The GNDVI and NDRE2 had the lowest MDA and MDG values (Figure 5.5), which indicated that they were the least important variables in the classification of the common urban trees and LULC classes in this study (Figure 5.5).

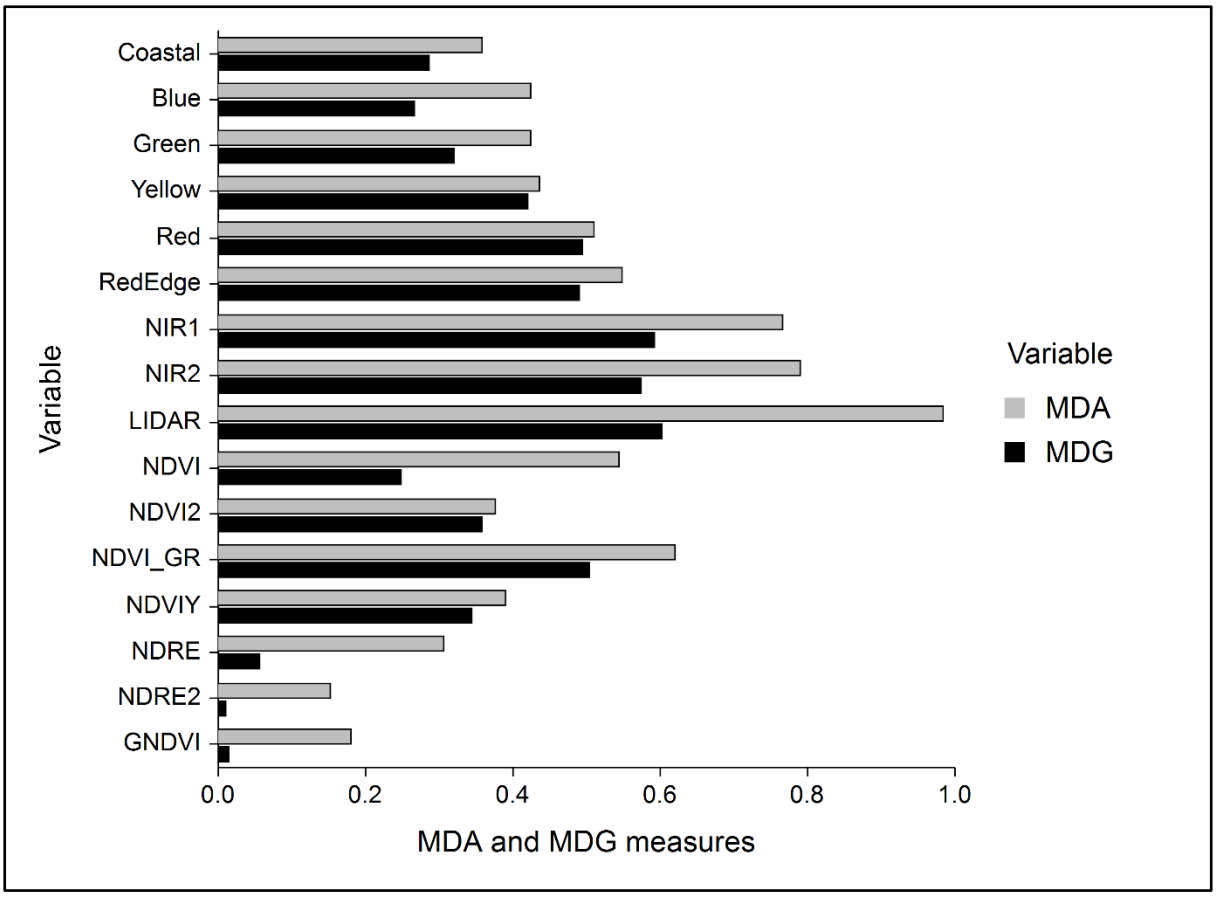


Figure 5.5 Mean Decrease in Accuracy (MDA) and Mean Decrease in Gini (MDG) values for the variables used in the classification of common urban trees and land use and land cover (LULC) based on the Random Forest (RF) classifier.

The forward feature selection using the RF classifier indicates that a subset with 12 variables produced the lowest OOB error rate of 4% (Figure 5.6). The use of all the variables (n = 16) yielded an OOB error rate of 20.01% (Figure 5.6). The OOB error rate increased from 4% to 16.82% when the 13th variable was added (Figure 5.6). The RF algorithm was used to classify common urban trees and LULC classes using a) all the variables (n = 16) and b) the selected variables (n = 12).

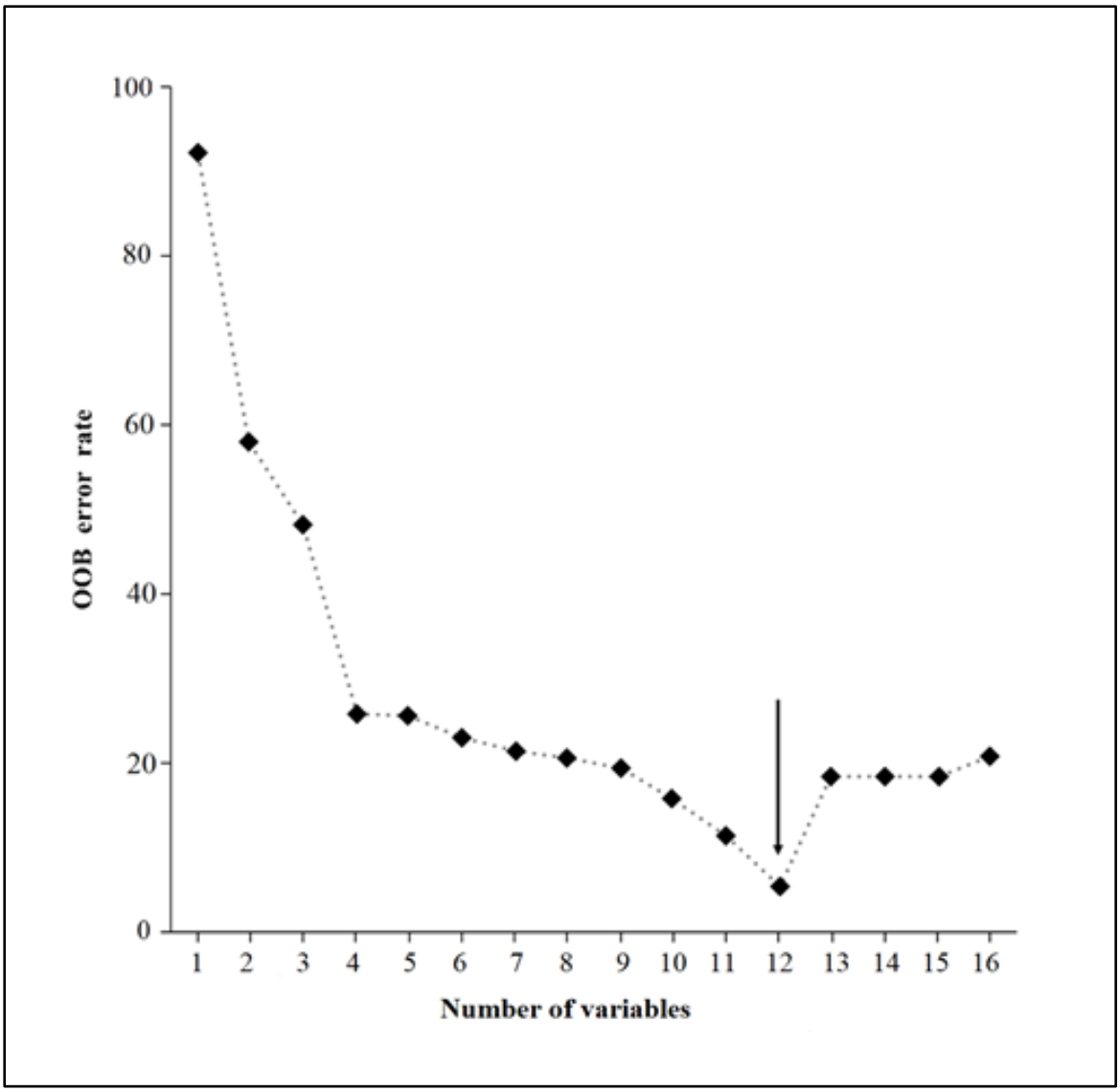


Figure 5.6 Forward feature selection results for identifying the optimal subset of variables using the OOB error rate in the RF classifier. A black arrow shows the optimal subset of variables with the lowest OOB error rate.

Figure 5.7 plots the ROC curve variable importance considered in SVM classification. The analysis showed that 12 variables produced high ROC variable importance ranging from 83% to 96%, as shown in Figure 5.7. The variables with high ROC variable importance were used for classification using the SVM algorithm. The variables with less ROC curve variable importance were removed when the classification was done using 12 variables. It is evident from the plots (Figures 5.6 and 5.7) that the variables selected by both RF and SVM were the same in the classification of common urban trees and LULC classes in this study. The classifications were done using a) all the variables

(n = 16) and b) the selected variables (n = 12). The classifications were done using both the RF and SVM classifiers.

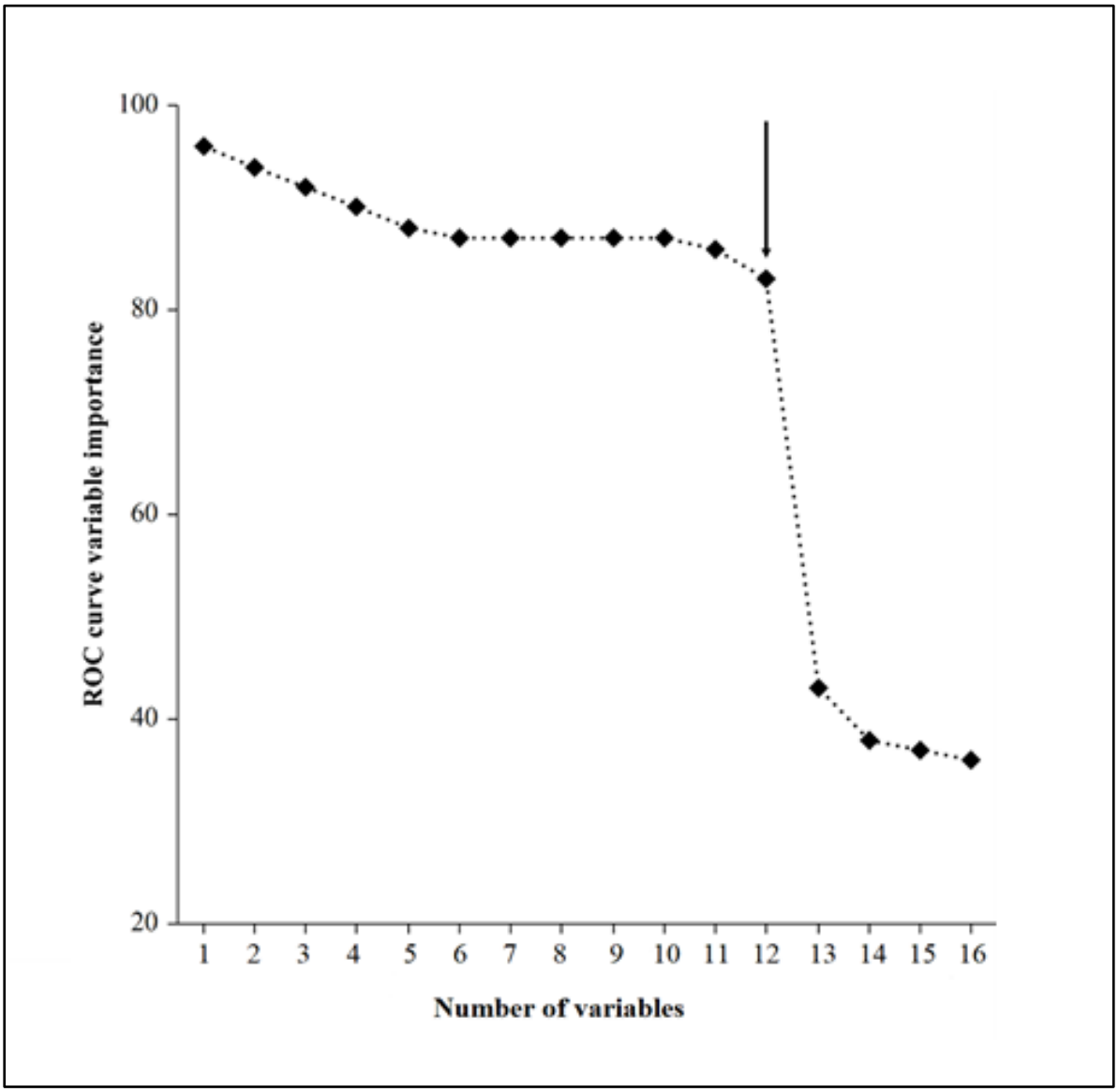


Figure 5.7 ROC curve importance for identifying the optimal variables based on the SVM classifier. A black arrow shows the optimal variables with the highest ROC curve variable importance end.

5.4 Discussion

5.4.1 Effectiveness of fused data

Several studies have indicated LiDAR data's success combined with VHSR imagery and vegetation indices in the classification of trees in areas with homogeneous species composition. In contrast, this study was undertaken in a heterogeneous urban landscape that includes high rise buildings, grassland and trees with varying treetops, crown widths and height. Accordingly, the classification

of tree species in a heterogeneous urban environment is challenging due to the spectral similarity between classes, the complexity of features and spatial variations. Such classification is needed, particularly in South Africa, where there is a dearth of urban tree information vital to municipalities for sustainable urban tree management. This study aimed to classify common tree species and LULC classes by integrating WV-2 bands, vegetation indices, and nDSM in a heterogeneous urban area to assist in urban tree management.

In complex urban environments, object-based ensemble analysis produces high accuracies due to its ability to account for differences of illumination gradients in individual tree crowns, which affects the spectral response (Hartling *et al.*, 2019). Segmentation is important in object-based ensemble analysis, and its scale parameter size has a substantial influence on classification accuracy (Benz *et al.*, 2004; Colgan *et al.*, 2012; Alonzo *et al.*, 2014; Azeez *et al.*, 2019). In this study, the MRS algorithm with a small-scale parameter of 20 was used, and it assisted in the provision of shapes at the exact location which matched the individual tree crowns and LULC classes. This algorithm also reduced the amount of time needed in the classification and analysis process whilst keeping vital spectral information on the IOs, which played a role in producing high accuracies. This is in line with previous studies (Alonzo *et al.*, 2014; Azeez *et al.*, 2019; Pu and Landry, 2020), which indicated that small segmentation scale parameter is important in distinguishing urban tree and LULC classes with high classification accuracies. The use of object-based segmentation on fused data (nDSM, VHSR imagery bands and vegetation indices) has been proven to be effective in producing high accuracies, and this is comparable to other studies (e.g. Hellesen and Matikainen, 2013; Hamedianfar *et al.*, 2014; Hartling *et al.*, 2019).

5.4.2 Accuracies and Mcnemar's test

The results using both RF and SVM classifiers using the selected variables (n = 12) produced overall accuracies of 97% and 94%, respectively (Tables 5.5a and 5.5b). These accuracies were higher than the ones produced in the studies by Le Louarn *et al.* (2017), Pu *et al.* (2018) and Jombo *et al.* (2021), in which similar urban trees and LULC features were classified using the same classifiers. Jombo *et al.* (2021) used object-based ensemble analysis to classify common urban trees and LULC classes at the accuracy of 91.9% for RF and 87.3% for SVM using WV-2 imagery and NDVI. The accuracies in our study were higher with the addition of nDSM and seven vegetation indices which played a role in the classification. This corroborates the findings of Hartling *et al.* (2019), Fang *et al.* (2020) and Varin *et al.* (2020), which show that the use of fused nDSM and optical remote sensing data improves classification accuracies. This is due to the ability of the

nDSM data to detect the structural attributes of trees and LULC features in combination with the textural/spatial information from WV-2 imagery (Zhang *et al.*, 2015).

In this study, high Cohen's KIA, user's, and producer's accuracies were obtained, which indicates that the use of fused data (WV-2 bands, vegetation indices and nDSM) produces good results in the classification of trees in a heterogeneous urban environment. The user's and producer's accuracies using the selected variables (n = 12) for both RF and SVM algorithms were above 80%, with Cohen's KIA values of 0.96 (RF) and 0.93 (SVM) (Table 5.5). This is in line with previous studies (Hellesen and Matikainen, 2013; Azeez *et al.*, 2019) in which similar results were attained in classifying tree species using both multispectral and nDSM data. Hellesen and Matikainen (2013) used the object-based ensemble analysis to map shrub and tree cover using nDSM and optical remote sensing data in Denmark at an accuracy of 96.7% with varying user's accuracies ranging from 74.9% to 98.5% and 92.6% to 97.4% for the producer's accuracy. Hamedianfar *et al.* (2014) also used object-based ensemble analysis to classify urban LULC using fused data (WV-2 bands, vegetation indices and nDSM) at an overall accuracy of 92.84% and varying user's accuracies from 81.3% to 100% and 76% to 100% for the producer's accuracies. In this study, the lowest producer's accuracy for RF was 90% due to the spectral similarity between other vegetation, *Jacaranda* spp., *Quercus* spp., grassland, and *Eucalyptus* spp. classes (Table 5.5a). Moreover, the other vegetation class produced low producer's accuracy of 83% using the SVM classifier and this was because of its spectral similarity with *Jacaranda* spp., *Platanus* spp., *Quercus* spp., grassland, and *Eucalyptus* spp. (Table 5.5b). This might be because the tree species had a similar phenological timing and they shared the same spectral characteristics expressing the leaf emergence and senescence stages (Fang *et al.*, 2020).

5.4.3 Importance of WV-2 bands, vegetation indices and nDSM

The nDSM data, NIR1 and NIR2 bands had high MDA and MDG values showing that they played a critical role in classifying the common urban trees and LULC classes using the RF classifier in this study (Figures 5.5 and 5.6). Both SVM and RF selected the same important variables in the classification of common urban trees and LULC classes in this study (Figures 5.5 and 5.6). These findings are in accord with recent studies (Fang *et al.*, 2018; Hartling *et al.*, 2019; Varin *et al.*, 2020), which highlight that nDSM data is important in the classification of trees because it shows differences in the crown structure, while the multispectral bands located in the visible region such as NIR1 and NIR2 assist in depicting the unique phenology of leaf pigments and function of leaf area development. In this study, feature variables such as the vegetation indices helped separate

vegetated areas (e.g., tree classes and grassland) from non-vegetated areas such as built-up and bare land classes. This is supported by Zhou *et al.* (2012), Hellesen and Matikainen (2013) and Loozen *et al.* (2020), who highlighted that the NIR spectral region and indices based on this region are vital in the classification of trees due to their usefulness in separating tree species from non-vegetated features.

5.4.4 Importance of the study

This study's results can offer information to municipalities, urban forest managers, and other stakeholders involved in urban tree management. This can help formulate urban tree inventories essential in decision-making and policy formulation to promote urban sustainable resource management (Klobucar *et al.*, 2020). This study was conducted at the municipality level, and it would be of greater value to be investigated at a district or national level to improve the understanding of methods and data used in the formulation of urban tree inventories. The use of remote sensing techniques shows the spatial distribution of urban trees, helping municipalities reduce problems faced in cities. These problems emanate from less tree canopy cover, including rising air and land surface temperature, air pollution, and noise pollution (Wang *et al.*, 2018). These problems can be reduced by proper monitoring, classification, mapping, and management of urban trees using information acquired from remote sensing technology such as LiDAR and VHSR imagery.

5.5 Conclusions

This study shows the effectiveness of fused data (WV-2 bands, vegetation indices and nDSM) in the classification and mapping of common urban trees and LULC classes. To that end, the fused data were effective in the classification of common urban trees and LULC classes in this study, as shown by high accuracies of 97% for the RF classifier and 94% for the SVM classifier. These results corroborate the ability of the fused dataset in the classification of tree species and LULC classes in a heterogeneous urban environment. Object-based ensemble analysis also contributed to high accuracies due to its use of objects, spatial information, including their location, shape, area, and textural pattern to produce sensible classifications. The nDSM was the most effective variable, and the inclusion of the vegetation indices also assisted in the classification of common urban trees and LULC classes using the two machine learning algorithms. This study's results can be relevant to other cities across the world where similar heterogeneous environments can adapt data fusion methods of this study. Such information is vital for tree planting programmes and encourages municipalities to acquire high point-cloud LiDAR data that can assist in urban tree

management, reducing problems such as the growth of urban heat islands, pollution, and increased energy consumption.

Chapter Six

Assessing the spatiotemporal dynamics of vegetation coverage and land surface temperature in a heterogeneous urban area

This chapter is based on **Jombo, S**., Adam, E., Byrne, M.J. and Newete, S.W. Assessing the spatiotemporal dynamics of vegetation coverage and land surface temperature in a heterogeneous urban area. *Remote Sensing*. (Under review)

Abstract

Urban trees play a critical role in alleviating land surface temperatures in cities. In remote sensing studies, vegetation indices are widely used to examine the relationship between Land Surface Temperature (LST) and vegetation cover. The vegetation cover can be measured using the Normalised Difference Vegetation Index (NDVI). In this study, the LST-NDVI relationship was assessed in each of the seven city-regions (A-G) in Johannesburg using Moderate-Resolution Imaging Spectroradiometer (MODIS) datasets to provide a basis for urban ecological planning and environmental protection. This study's specific objective was to determine the spatiotemporal dynamics of vegetation coverage and LST in the seven city-regions over 19 years, between 2001 and 2020. The relationship between LST and NDVI was also examined over the years of study. The results showed a significant spatiotemporal difference in LST and NDVI values in the city-regions with a negative correlation between them, ranging from -0.03 to -0.76. The LST values increased in all the city-regions with the highest value of 20.1°C in city-region G, followed by 19.6°C in city-region E. The vegetation cover decreased over the years, with the lowest NDVI value in city-region G (0.39), followed by city-regions F (0.43) and D (0.48). The city-regions with high LST and low vegetation cover include the city-centre and highly populated suburbs. This indicates that areas with greater vegetation cover have low LSTs and vice versa. These findings provide useful information for municipal authorities and other stakeholders to undertake appropriate decisions to tackle Urban Heat Island (UHI) effects by adopting effective urban planning and management interventions.

6.1 Introduction

Rapid urbanization and urban climate changes are critical global problems and require fundamental considerations for urban planning in the 21st century (Amani-Beni *et al.*, 2019). Urban Heat Island (UHI) is one of the consequences of rapid urbanisation (Ahmed *et al.*, 2020), and it is described as an urban area that is significantly warmer, as opposed to nearby rural areas (Howard, 1833). The UHI is caused by replacing vegetation with paved surfaces in the process of urbanisation (Aina *et al.*, 2017). The presence of vegetation helps regulate the urban climate through its evaporative cooling effect by which reduces air and land surface temperatures (Baris *et al.*, 2009). Urban vegetation provides several ecosystem services, and among these are moderating temperatures by providing shade, reducing wind speed and cooling through evapotranspiration, and thus decreasing the risk of heat-related diseases for urban dwellers (Ferrini *et al.*, 2020). Trees and other green spaces within built-up structures can reduce air temperatures by 3°C (McPherson and Simpson, 2003). Consequently, finding effective measures to reduce and mitigate the UHI effects has drawn much attention in urban ecology and planning studies for sustainable urban development (Zhou *et al.*, 2017; Amani-Beni *et al.*, 2019; Alexander, 2020).

In many countries, meteorological departments measure air temperature at weather stations or airports (Aina *et al.*, 2017). Although the data collected from weather stations are more accurate than those acquired from remote sensing satellite data, this on-site data collection procedure is more costly and time-consuming for large areas (Odindi *et al.*, 2015). In addition, the arrangement of landcover structures and different land uses in urban environments makes it difficult to obtain accurate temperature results using data from weather stations. Therefore, thermal spatial distribution is better described using remote sensing satellite data (Alexander, 2020). The advent of remotely-sensed satellite data has provided cost-effective and dependable data acquired regularly at varying spatial resolutions and extents (Odindi *et al.*, 2015). Remote sensing data have been used in various studies such as forest ecology (Lechner *et al.*, 2020), biology (Nimit *et al.*, 2020) and thermal remote sensing (Guha and Govil, 2020) over large spatial extents. The popularity of RS data emanates from its good quality and availability, accompanied by continual improvements in processing algorithms (Odindi *et al.*, 2015).

Most previous studies have focussed on the relationship between Normalised Difference Vegetation Index (NDVI) and Land Surface Temperature (LST) in European and Asian cities (Yue *et al.*, 2007; Huang and Ye, 2015; Alexander, 2020; Guha and Govil, 2020). NDVI is an indicator or measure of vegetation abundance (Lechner *et al.*, 2020), while LST is the temperature at the

interface between air and the ground surface (Rao *et al.*, 2021). Huang and Ye (2015) spatially modelled urban vegetation and LST in Beijing, China. They found that NDVI is negatively correlated with LST, suggesting that urban vegetation is capable of reducing LST. Alexander (2020) examined the spatial pattern of LST and its relationship with spectral indices and land cover in Aarhus Kommune municipality, Denmark. The study found a high negative correlation between the percentage of tree cover and LST, ranging from -0.68 to -0.75. Guha and Govil (2020) assessed the spatiotemporal variation of the NDVI-LST relationship from 2012 to 2018 using Landsat imagery in Raipur city in India. The results showed an LST increase of 11.62°C between 2012 and 2018, and it was negatively correlated with NDVI. The three aforementioned studies noted a negative correlation between LST and NDVI, suggesting that vegetation can reduce LST. Therefore, it is necessary to examine the NDVI-LST relationship in African cities focussing on different city-regions with varying climate conditions, which has not been addressed in previous studies.

A few such studies have been conducted in African cities (e.g., Odindi *et al.*, 2015; Hardy and Nel, 2015; Adeyemi *et al.*, 2015; Mudede *et al.*, 2020; Ngie, 2020; Magidi and Ahmed, 2020). Hardy and Nel (2015) examined the UHI in Johannesburg using ASTER and Landsat data. They found typically high LST values in informal settlements due to low vegetation cover. Odindi *et al.* (2015) highlighted the importance of vegetation in mitigating UHI effects by reducing LSTs using Moderate-Resolution Imaging Spectroradiometer (MODIS) and Landsat data in the Ethekwini municipal area. Both studies (Hardy and Nel, 2015; Odindi *et al.*, 2015) highlighted that the use of night-time satellite imagery is better than the daytime scenes as most of them are not usable due to the presence of clouds. Mudede *et al.* (2020) determined the LST-NDVI relationship in two suburbs of the city of Johannesburg, namely Sandton and Rosebank, using Landsat 8 satellite data. The results showed a negative correlation of -0.90 between LST and NDVI. These studies were conducted at a municipal and suburb level, but not at a city-regional extent, which can help forest managers identify city-regions where tree planting can be done to reduce air and LSTs.

The City of Johannesburg is heterogeneous, with various land use and cover classes, including tall buildings, impervious surfaces, trees, grass, and water bodies (Knight, 2018). The spatial distribution of vegetation in the city shows a wide disparity, with many trees located in the wealthy northern suburbs and fewer trees in the poor southern suburbs (Storie, 2014). This wide disparity of trees was due to the apartheid town planning and socio-cultural divide, where the northern suburbs were dominated by white people and the southern suburbs, which had lower property

prizes, were designed for black residents in the city (Mabin, 2014). The city's climatic conditions differ, where rainfall and temperature are slightly higher in the north than in the southern city-regions (Storie, 2014). With a high number of trees, the northern part of the city is believed to have lower temperatures. There has been rapid urbanization over the years in Johannesburg due to population growth and in-migration of people from places in South Africa and other countries (City of Johannesburg Metropolitan Municipality, 2020). As the population continues to increase in the city, the spatiotemporal dynamics of vegetation coverage and its relationship with LST need to be examined. The relationship between population and LST has produced inconsistent results across different cities and countries over the years, requiring further research (Adeyeri *et al.*, 2017; Ahmed *et al.*, 2020; Jung *et al.*, 2021). The heterogeneity of the landscape due to rapid urbanization, population rise, vegetation presence (Guha and Govil, 2020) and varying climatic variations in the city-regions influence the spatiotemporal dynamics of vegetation coverage and LST. It is, therefore, essential to examine the spatiotemporal dynamics of vegetation coverage and LST in the city-regions of Johannesburg.

To the best of our knowledge, there has not been any study undertaken in South Africa that focussed on the spatiotemporal dynamics of vegetation coverage and LST at a city-regional level using night-time MODIS data. The choice of MODIS data for this study was because it is available and easy to access over large areas. Furthermore, the data can be acquired daily, after every 8 and 16 days (Hong *et al.*, 2011). This study determines the spatiotemporal dynamics of vegetation coverage and LST in the seven city-regions of the city of Johannesburg. This study's first objective was to determine changes in the spatial distribution of vegetation and LST across the seven regions of the city with a five-year interval from 2001-2020 (2001, 2005, 2010, 2015 and 2020). The second objective was to analyse the variances of mean LST and NDVI values in the study area. This was investigated to determine the vegetation coverage and LST changes over the study period in the seven city-regions. This has the potential to guide the municipality to find ways that can promote urban greening whilst reducing air and surface temperatures. The third objective was to examine the relationship between NDVI and LST, which could be important to municipalities, policymakers, local and regional urban planners in finding ways to reduce the effects of LST for sustainable urban development.

6.2 Materials and methods

6.2.1 Study area

The study was conducted in the City of Johannesburg, in South Africa, situated in Gauteng Province with a total area of 1 645km² (Deshpande *et al.*, 2017). The city centre is located at latitudes 26° 20' 41" S and longitude 28° 04' 73" E (Figure 6.1). The study area has a population of approximately 5.05 million people, and it is growing due to the high birth rate and inflow of people from other provinces and countries (City of Johannesburg Metropolitan Municipality, 2020). The study area has a seasonal climate with wet summers and dry winters, and the warmest month is January, with an average annual temperature of 20.6°C (Nana *et al.*, 2019).

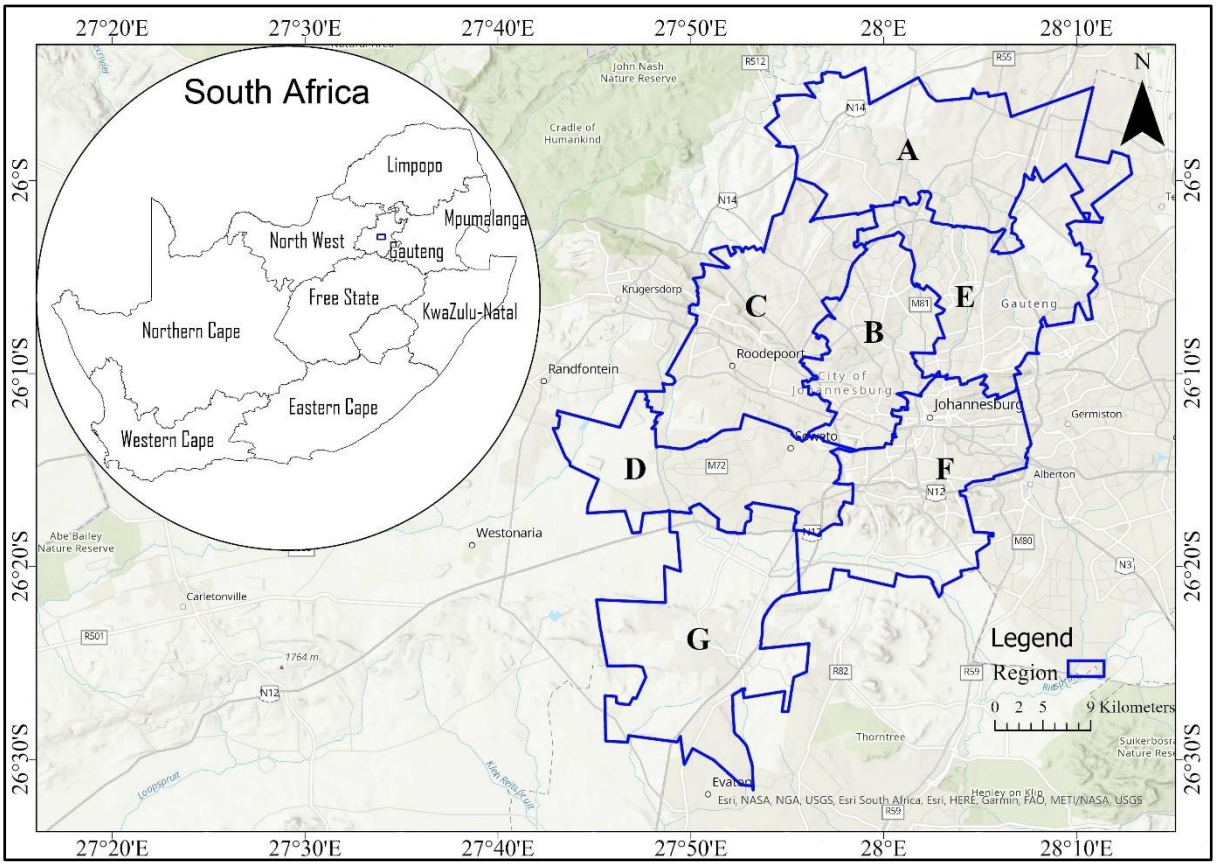


Figure 6.1 Map of South Africa and the study area with the seven city-regions (A-G) of the City of Johannesburg.

The study area has seven city-regions (A-G), as shown in Figure 6.1. Each municipal city-region is responsible for delivering health services, social development, housing, libraries, sports and other community-based programs to improve people's livelihoods (Wapwera and Egbu, 2013). Some of the areas in the city-regions are shown in Table 6.1. The city is often referred to as an urban forest due to its vast number of tree species which may exceed 10 million (Schäffler and Swilling, 2013).

Urbanization in the study area has contributed to a rise in UHI intensity where it has been shown that the city centre can be 11°C warmer in the summer season with lower relative humidity (< 43%) in comparison to surrounding areas (Knight, 2018).

Table 6.1 Some of the suburbs located in the seven city-regions of the City of Johannesburg (CoJ).

City-region	Areas
A	Kya Sands, Fourways, Lanseria, Dainfern, Diepsloot and Midrand
B	Rosebank, Randburg, Parktown, Melville, Mayfair and Emmarentia
C	Constantia Kloof, Roodepoort, Florida and Northgate
D	Soweto, Protea Glen, Dobsonville and Doornkop
E	Houghton, Alexandra, Sandton, Orange Grove and Wynberg
F	Johannesburg South and Inner City
G	Protea South, Orange Farm, Ennerdale, Eldorado Park and Lenasia

6.2.2 Multispectral remote sensing data

The study used the Terra MODIS (MOD11A2) eight-day data to retrieve LST and MOD13A2 data for NDVI. Both the MODIS LST and NDVI were obtained from the United States Geological Survey (USGS) website (https://earthexplorer.usgs.gov). The MODIS LST and NDVI datasets were downloaded from the Land Processes Distributed Active Archive Centre (LP DAAC), which partners with USGS and the National Aeronautics and Space Administration (NASA). The MODIS products were used in this study due to their simplicity and robustness (Ramon Solano *et al.*, 2010; El Kenawy *et al.*, 2019), and the LSTs and NDVIs were calibrated for atmospheric noise in the NASA labs. The images were downloaded from the warmest month (January) in the study area (Ngigi, 2009; Adeleke *et al.*, 2020). The datasets were collected on the 1st and 17th of January in 2001, 2005, 2010, 2015 and 2020. A total of twenty MODIS images were downloaded, with two for each year. Both the MODIS LST and NDVI have 1 km (actual 0.928 km) spatial resolution, and they are generated every 8 days and 16 days, respectively (Wan, 2006; Ramon Solano *et al.*, 2010). Using the random points function in ArcMap, 50 random points in each city-region were created, and the same points were used to extract both LST and NDVI values for all the years of study (2001, 2005, 2010, 2015 and 2020).

6.2.2.1 Image preprocessing

The thermal values for the MOD11A2 were converted from Kelvin x 200 to degrees Celsius (°C). The digital numbers were converted to temperature in °C using the equation:

$$LST_c = DN * 0.02 - 273.15 \quad \text{Equation 6.1}$$

where LST_c is the converted LST image and DN is the digital number (Zhang *et al.*, 2013). The MOD13A2 images for the NDVI were converted to real values using the equation:

$$NDVI_C = DN * 0.001 \quad \text{Equation 6.2}$$

where $NDVI_C$ is the converted NDVI image, DN stands for digital number, and 0.001 is the scale factor. This was done to convert the data to give real values between -1 and 1 for the NDVI. The LST and NDVI values were converted using the raster calculator in ArcMap 10.6 software (Esri ArcGIS, 2018).

6.2.2.2 Land Surface Temperature

The MOD11A2 Terra eight-day LST datasets were acquired on the 1st and the 17th to match the MOD13A2 16-day 1-km images acquired on the same dates. A total of ten MOD11A2 images were downloaded in January, with two for each year. The MOD11A2 night mode was used in this study due to its reliability and avoid contamination by atmospheric aerosols and clouds that affect Terra daytime mode (Odindi *et al.*, 2015; El Kenawy *et al.*, 2019). The MOD11A2 datasets have increasingly been used and produced satisfactory results in various thermal research and remote sensing studies (Imhoff *et al.*, 2010; Odindi *et al.*, 2015; Rotem-Mindali *et al.*, 2015; Islam and Ma, 2018; El Kenawy *et al.*, 2019).

6.2.2.3 Meteorological data

The validation of derived MODIS LST data was done using in-situ measurements from weather stations. This study used the atmospheric and meteorological data collected from Johannesburg-Botanical Gardens weather station in city-region B of the study area (Table 6.2). The atmospheric and meteorological data were obtained from the South African Weather Service (SAWS). The SAWS provided data from a single weather station due to the unavailability of atmospheric and meteorological data from the other weather stations in the study area. The weather station's average values were used to verify the MODIS LST on the same day the satellite images were acquired. Pearson's correlation and linear regression analysis were performed to measure the correlation between average MODIS LST values and average temperature values obtained from the study area's weather station.

Table 6.2 Temperature, wind and humidity readings collected at Johannesburg-Botanical Gardens weather station at the time of MODIS LST imagery overpass.

Date	Minimum temperature (°C)	Maximum temperature (°C)	Mean temperature (°C)	Average wind speed (m/s)	Humidity
01/01/2001	13	24.3	18.7	4.6	87
17/01/2001	13.6	25.9	19.8	1.6	100
01/01/2005	16.8	29	22.9	1.8	86
17/01/2005	16.5	29.5	21.2	1.2	76
01/01/2010	17.2	29.6	23.4	0	58
17/01/2010	16.3	27.7	22	1.5	93
01/01/2015	14.1	25.7	19.9	1.3	77
17/01/2015	16.8	30.4	23.6	1.4	45
01/01/2020	14.8	30.2	22.2	1.7	56
17/01/2020	13.9	28.5	21.2	2.5	62

6.2.2.4 Normalised Difference Vegetation Index (NDVI)

The MOD13A2 16-day 1-km datasets from the 1st and the 17th of January in the years 2001, 2005, 2010, 2015 and 2020 were used. The two datasets for each year were integrated to derive a map with mean NDVI values. This was achieved by adding the mean NDVI values for the two MOD13A2 datasets and dividing them by 2 using the raster calculator in ArcMap 10.6 software (Esri ArcGIS, 2018). The MOD13A2 datasets were used to determine the level of greenness in the study area. These datasets have produced high accuracies in previous studies (Song *et al.*, 2013; Soto-Mardones and Maldonado-Ibarra, 2015; Marzban *et al.*, 2017).

6.2.3 Statistical analysis

The LST and NDVI datasets were first put on a data screening procedure to scan and identify any unexpected or cells with missing data. Both the MODIS LST and NDVI datasets were tested using the One-Sample Kolmogorov-Smirnov test over the years (2001, 2005, 2010, 2015 and 2020). The One-Sample Kolmogorov-Smirnov test revealed that the data were normally distributed. A two-way Analysis of variance (ANOVA) was used to ascertain whether there were differences in the LST and NDVI values in the study area over the years (2001, 2005, 2010, 2015 and 2020). The null hypothesis data analysis was carried out using the Number Cruncher Statistical System (NCSS) statistical software (Version 20.0.2).

6.2.3.1 Pearson's correlation analysis

The Pearson's correlation analysis was performed between LST and NDVI to determine the influence of vegetated areas on LST in the study area's seven city-regions. The correlation coefficients were produced showing the relationship between LST and NDVI in all the city-regions

were produced. An assumption that LST values are negatively correlated with NDVI values was considered before performing Pearson's correlation test.

6.3 Results

6.3.1 Spatiotemporal distribution and variations of LST

Descriptive statistics showing the LST values for each of the study periods were generated (Table 6.3). The minimum LST, maximum LST and standard deviation (SD) values for city-regions A to G for 2001, 2005, 2010, 2015 and 2020 are shown in Table 6.3. The highest maximum LST value (20.1°C) was in city-region G in 2020 (Table 3). The minimum LST (13.0°C) was recorded in city-region B in 2001(Table 6.3). The SD varied across the city-regions during the study period, the highest SD (1.0) was in city-region G in 2020, whilst the lowest was 0.3 in city-region A (2015) (Table 6.3).

Table 6.3 Minimum (Min), maximum (Max) and standard deviation (SD) land surface temperature (LST) values for city-region A to G for the years 2001, 2005, 2010, 2015 and 2020 in the study area.

	2001			2005			2010			2015			2020		
City-region	Min	Max	SD	Min	Max	SD	Min	Max	SD	Min	Max	SD	Min	Max	SD
A	13.2	16.3	0.7	14.2	16.6	0.6	15.6	16.7	0.5	16.6	16.7	0.3	15.1	16.9	0.6
B	13.0	16.6	0.6	13.9	17.0	0.5	16.2	17.6	0.7	17.5	18.6	0.4	14.2	18.7	0.6
C	14.3	17.0	0.6	14.2	17.9	0.4	15.4	18.2	0.7	16.6	18.3	0.5	16.6	18.6	0.7
D	15.1	17.6	0.8	15.2	17.8	0.6	15.6	17.9	0.4	16.6	18.9	0.6	16.3	19.5	0.9
E	15.7	17.4	0.9	14.3	17.7	0.8	15.7	17.8	0.7	16.1	18.1	0.7	16.4	19.6	0.8
F	15.6	17.9	0.8	16.1	18.1	0.5	15.8	18.2	0.6	15.2	18.5	0.8	16.0	19.5	0.7
G	15.0	18.3	1.0	15.8	18.7	0.6	16.4	18.7	0.6	16.1	18.6	0.5	16.2	20.1	0.7

The mean LST maps retrieved from 2001, 2005, 2010, 2015 and 2020 in city-region A to G of the study area are shown in Figure 6.2. The highest LST values were found in the southern part of the study area, and low LST values were in the city's northern part (Figure 6.2). There has been an increase in LST values over the years in all the city-regions.

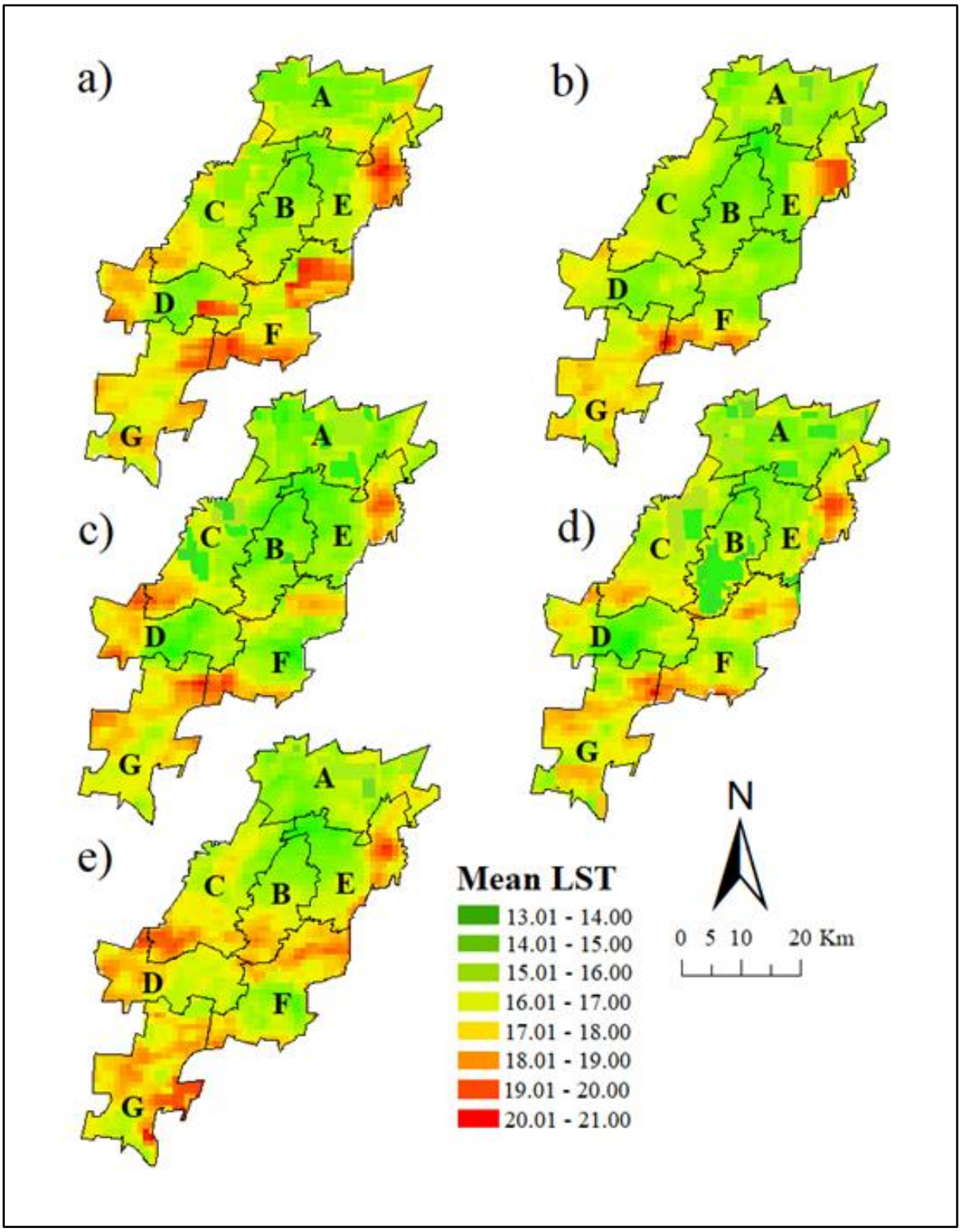


Figure 6.2 Maps with mean LST values for city-regions A to G in the city of Johannesburg over the study periods of a) 2001, b) 2005, c) 2010, d) 2015, and e) 2020.

The maximum MODIS LST values in all the city-regions are shown in 2020 (Figure 6.3). The highest mean MODIS LST value (20.1°C) was recorded in city-region G (2020), whilst the lowest maximum LST value (16.3 °C) was recorded in city-region A in 2001.

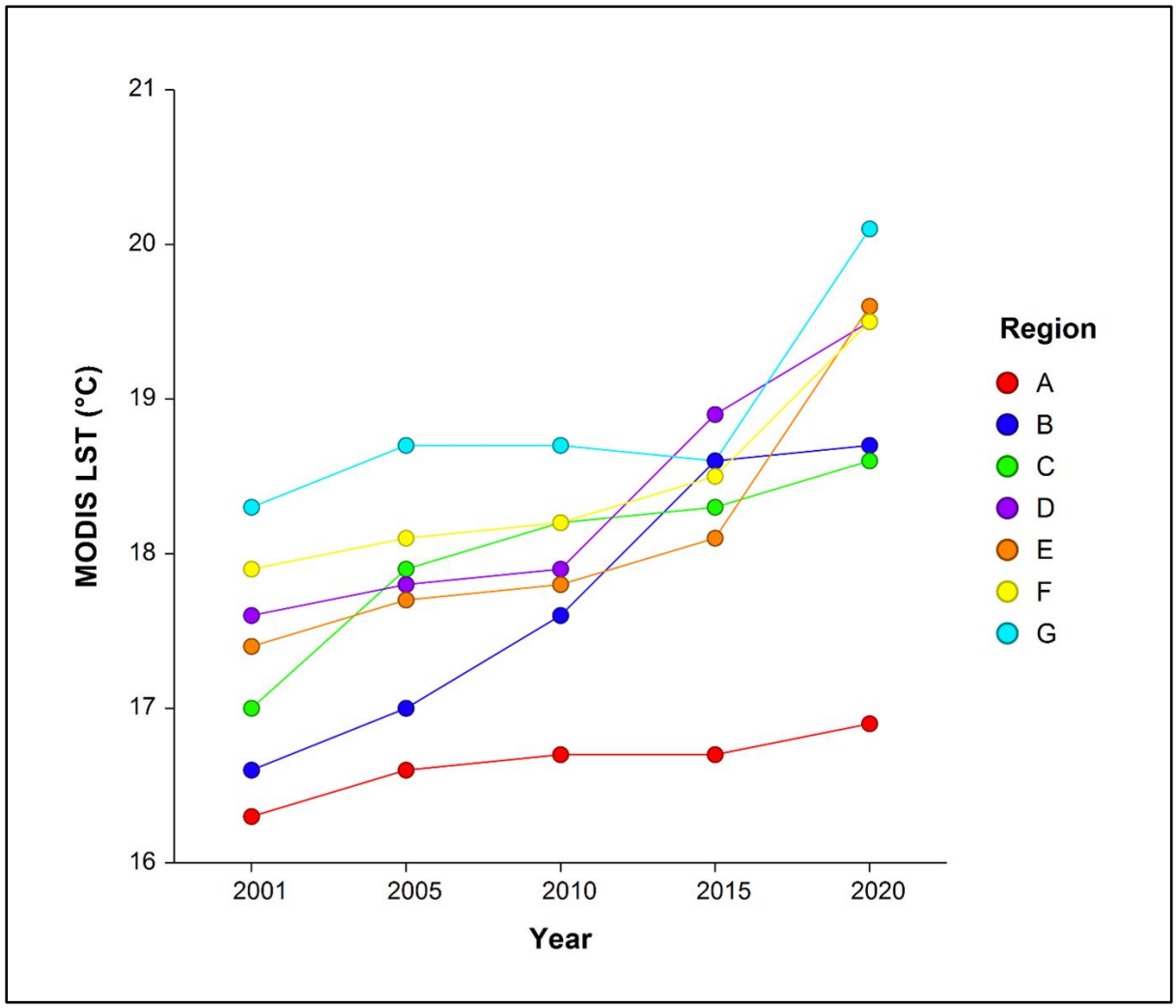


Figure 6.3 Mean MODIS LST values for city-regions A to G in the years: 2001, 2005, 2010, 2015 and 2020.

6.3.2 Validation of MODIS LST data

There was a significant positive relationship between the MODIS LST values and temperature obtained from the weather station. This was indicated by Pearson's correlation analysis ($\alpha = 0.05$) and linear regression, which produced a correlation coefficient of 0.94. The coefficient of determination (R^2) between MODIS LST values and in-situ weather station temperature data values for the years of study (2001, 2005, 2010, 2015 and 2020) was 0.89 (Figure 6.4). This indicates that the MODIS LST data correlate well with in-situ weather station temperature data.

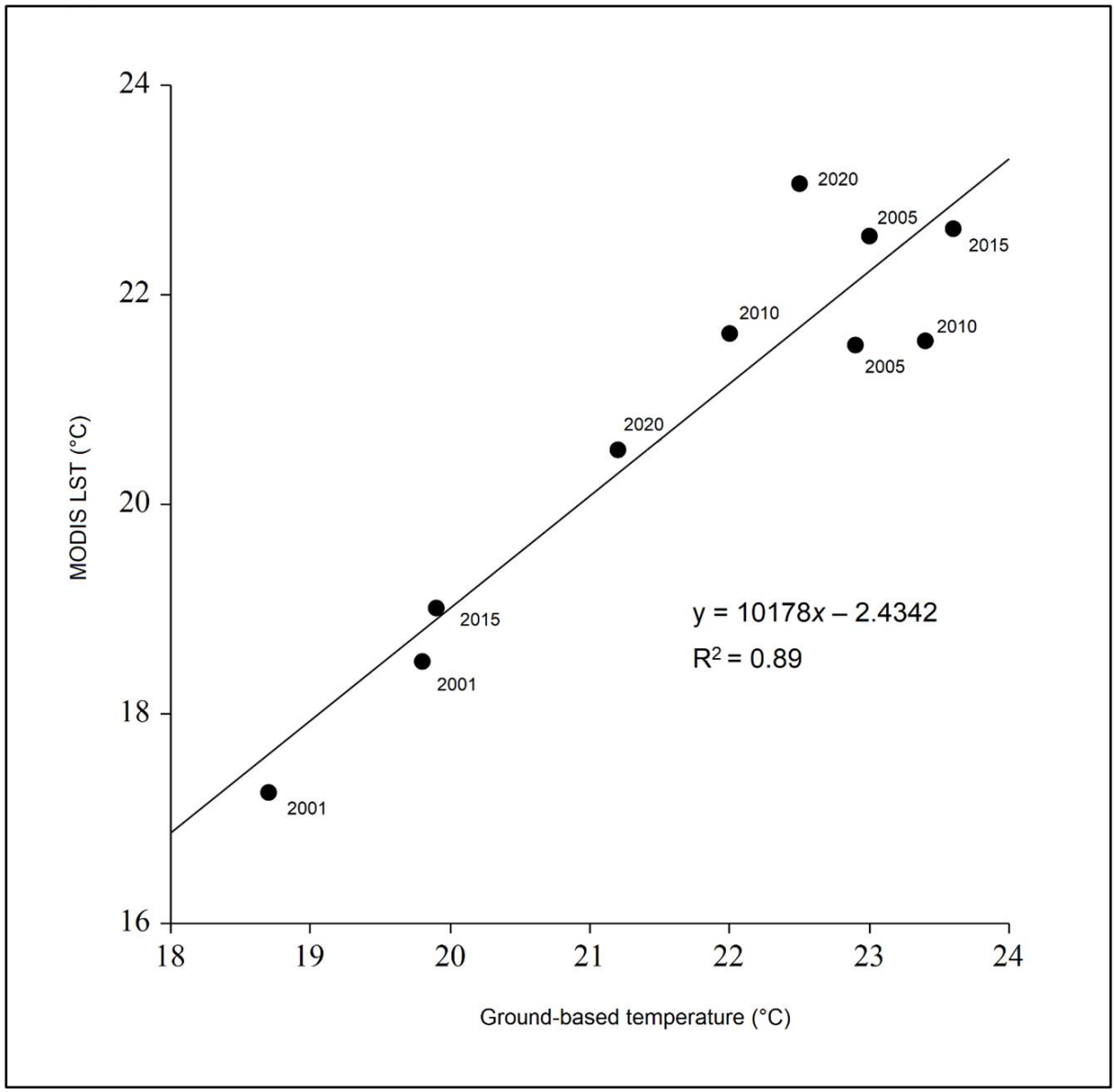


Figure 6.4 Ground-based weather station vs MODIS LST values in degrees Celsius (°C) for the years: 2001, 2005, 2010, 2015 and 2020.

6.3.3 Spatiotemporal distribution and variations of NDVI

Descriptive statistics showing the NDVI values for each of the study periods were generated. The minimum NDVI, maximum NDVI and standard deviation (SD) values for city-regions A to G for the years 2001, 2005, 2010, 2015 and 2020 are shown in Table 6.4. The highest value for the NDVI (0.69) was recorded in city-region A in 2001 (Table 6.4). The minimum NDVI value (0.13) was recorded in city-region G in 2020 (Table 6.4). The SD varied across the city-regions in the years of study, and the highest SD value (0.16) was for city-region F in 2010 (Table 6.4).

Table 6.4 Minimum (Min), maximum (Max) and standard deviation (SD) values for NDVI in city-regions A to F for 2001, 2005, 2010, 2015 and 2020 in the study area.

	2001			2005			2010			2015			2020		
City-region	Min	Max	SD	Min	Max	SD	Min	Max	SD	Min	Max	SD	Min	Max	SD
A	0.21	0.69	0.08	0.25	0.67	0.07	0.21	0.65	0.12	0.22	0.63	0.12	0.16	0.65	0.11
B	0.30	0.67	0.05	0.23	0.65	0.09	0.25	0.63	0.10	0.28	0.60	0.09	0.15	0.64	0.08
C	0.20	0.65	0.08	0.20	0.61	0.10	0.17	0.60	0.11	0.18	0.52	0.11	0.18	0.58	0.07
D	0.18	0.54	0.10	0.19	0.52	0.12	0.18	0.51	0.10	0.24	0.50	0.12	0.20	0.48	0.11
E	0.22	0.57	0.08	0.24	0.55	0.13	0.22	0.53	0.13	0.25	0.52	0.11	0.20	0.50	0.09
F	0.20	0.52	0.12	0.22	0.50	0.15	0.19	0.48	0.16	0.19	0.45	0.15	0.22	0.43	0.14
G	0.14	0.49	0.07	0.19	0.45	0.09	0.19	0.43	0.08	0.15	0.44	0.09	0.13	0.39	0.07

The NDVI maps retrieved for the years 2001, 2005, 2010, 2015 and 2020 for city-regions A to G are shown in Figure 6.5. The high NDVI values were found in city-regions A, B and C (Figure 6.5).

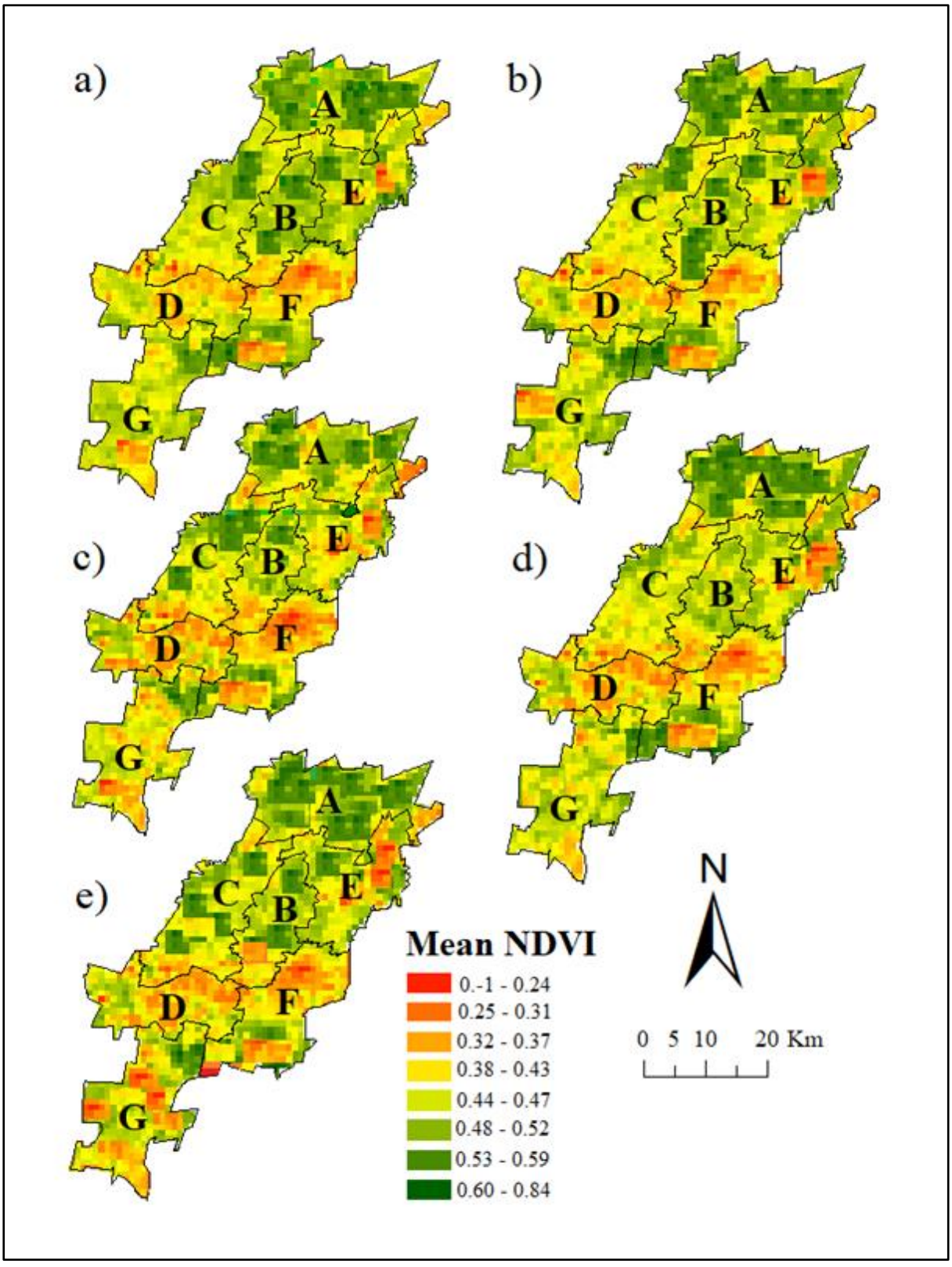


Figure 6.5 Maps with mean NDVI values for city-regions A to G in the years: a) 2001, b) 2005, c) 2010, d) 2015 and e) 2020.

The maximum NDVI values showed a progressively decreasing trend from 2001 to 2020 across the city except for city-regions A, B and C (Figure 6.6). The highest mean NDVI value (0.69) was in city-region A in 2001, and the lowest was 0.39 in city-region G in 2020 (Figure 6.6).

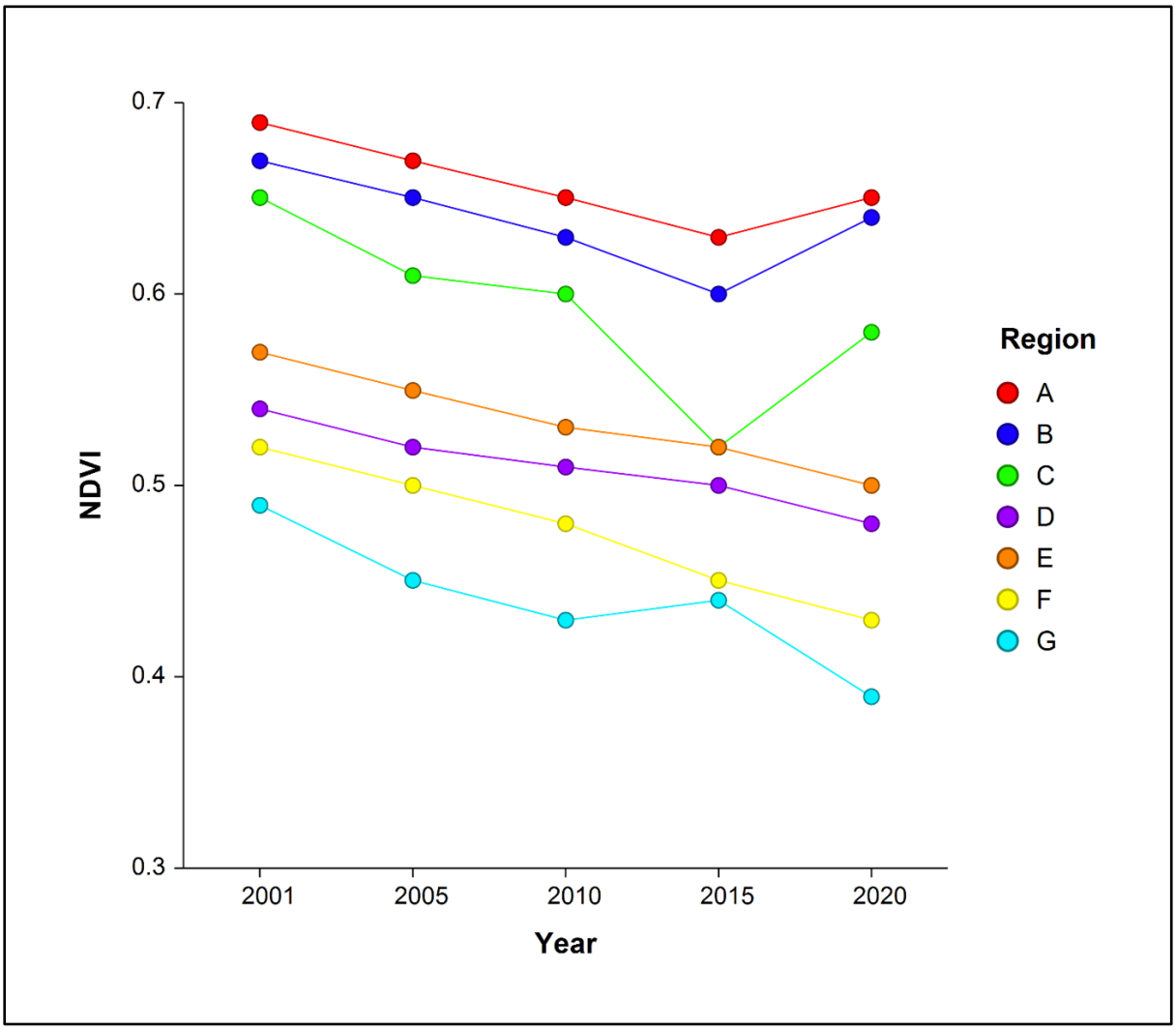


Figure 6.6 The mean NDVI values for city-regions A to G in the study area for the years: 2001, 2005, 2010, 2015 and 2020.

6.3.4 Analysis of variance on MODIS LST and NDVI data

The results with their significance level for LST mean values in each city-region are shown below (Table 6.5). There was a significant difference between mean LST values for city-region B with city-regions (C, D, E, F and G). The differences in mean LST values for the other city-regions were non-significant ($p>0.05$), meaning that there were no significant differences in the LST mean values (Table 6.5).

Table 6.5 Two-way ANOVA test results with Tukey's post hoc test in the city-regions for LST values for the years: 2001, 2005, 2010, 2015 and 2020.

City-region	A	B	C	D	E	F	G
A	..						
B	0.30**	..					
C	1.00**	0.01*	..				
D	1.00**	0.04*	0.99**	..			
E	1.00**	0.03**	0.97**	1.00**	..		
F	0.99**	< .001*	0.98**	0.75**	0.59**	..	
G	0.95**	< .001*	0.82**	0.34**	0.20**	1.00**	..

p< 0.05 = *, Not significant = **

The results with their significance level for NDVI mean values in each city-region are shown below (Table 6.6). The results showed a significant difference between mean NDVI values for city-region D with city-regions A, E, F and G. The differences in mean NDVI values for the other city-regions were non-significant, meaning that there were no significant differences in the NDVI values (Table 6.6).

Table 6.6 Two-way ANOVA test results with Tukey's post hoc test in the city-regions for NDVI values for the years: 2001, 2005, 2010, 2015 and 2020.

City-region	A	B	C	D	E	F	G
A	..						
B	0.34**	..					
C	0.13**	1.00**	..				
D	0.14**	0.14**	0.37**	..			
E	1.00**	0.33**	0.12**	< .001*	..		
F	0.93**	0.94**	0.72**	0.01*	0.93**	..	
G	1.00**	0.67**	0.35**	< .001*	1.00**	1.00**	..

p< 0.05 = *, Not significant = **

6.3.5 Relationship between LST and NDVI

The NDVI was derived from MOD13A2 images to establish a quantifiable relationship with MODIS LST data (MOD11A2). The Pearson correlation coefficients between MODIS LST and NDVI were calculated for the study area in all the city-regions (A to G). The correlation coefficients were all negative, with the lowest value of -0.76 (city-region A) in 2020 (Table 6.7). The highest change (-0.58) was in city-region C between 2015 and 2020, whilst the least change (-0.01) was in city-region B between 2001 and 2005 (Table 6.7).

Table 6.7 The Pearson correlation coefficients between MODIS LST and NDVI for the seven city-regions over the study periods: 2001, 2005, 2010, 2015 and 2020.

	Correlation coefficient				
Year / City-region	2001	2005	2010	2015	2020
A	-0.57	-0.52	-0.16	-0.41	-0.76
B	-0.18	-0.19	-0.05	-0.33	-0.44
C	-0.12	-0.19	-0.03	-0.10	-0.68
D	-0.40	-0.28	-0.07	-0.52	-0.63
E	-0.49	-0.33	-0.28	-0.38	-0.58
F	-0.57	-0.46	-0.40	-0.13	-0.23
G	-0.59	-0.45	-0.43	-0.35	-0.62

6.4 Discussion

The study assessed the impact of vegetation on land surface temperature (LST) in the seven city-regions (A to G) of Johannesburg. The mean LST maps (Figure 6.2) shows that there has been an increase in the LST over the years and a decline in vegetation coverage in all the city-regions (Figure 6.5). The highest mean LST value was 20.1°C in city-region G in 2020 (Table 6.3). This city-region includes areas such as Orange Farm and Lenasia (Table 6.1 above). The other high LSTs were in city-regions E (19.6°C), D and F (19.5°C), and these include areas such as Alexandra, Soweto and Inner City in city-regions E, D and F, respectively (Table 6.3). The rise in LST was due to the presence of bare land and built-up areas, whereas low LST values are associated with vegetated areas. This is in line with Mudede *et al.* (2020), who highlighted that there are high LST values in areas such as Soweto and Alexandra, for which they believed it was due to the occurrence of more open spaces and bare lands that are known as poor absorbers of solar radiation. This is supported by Ahmed *et al.* (2013) and Odindi *et al.* (2015), who asserted that high-temperature values are associated with built-up areas and bare land, whereas areas of low temperatures are associated with water bodies and vegetated areas. The rise in LST values is also caused by structures made of metal sheets made by people who stay in informal settlements in areas such as Soweto and Alexandra, located in city-regions D and E, respectively (Ngie, 2020). The high LST values in city-region F, which includes the Inner-city, can be associated with the expansion of the city where several buildings have and are still being constructed. This is supported in previous studies (Ranagalage *et al.*, 2019; Mudede *et al.*, 2020; Das and Angadi, 2020) that the expansion of cities increases LST through the conversion of urban forests and open green spaces to industrial, commercial and housing spaces.

The vegetation cover decreased progressively over the study periods except for city-regions A, B and C from 2015 to 2020 (Figure 6.6). The rise in mean NDVI values in city-regions A, B and from 2015 to 2020 might be due to an increase in trees through tree planting programmes such as the Annual Arbour Week or Month, Champion Tree Project and the Million Trees Programme (Department of Environment Forestry and Fisheries, Forestry and Fisheries, 2020). The high vegetation cover was mainly in city-regions A and B in 2020 with areas such as Fourways, Diepsloot and Rosebank whilst low vegetation cover was in city-regions D, F and G with areas such as Soweto, Inner City and Orange Farm (Figure 6.6). Higher NDVI values are associated with areas with abundant vegetation, such as green residential areas and vegetated public parks in the northern part of Johannesburg. This is in line with findings in the literature (Yue *et al.*, 2007; Ahmed *et al.*, 2013; Rotem-Mindali *et al.*, 2015) which highlighted that high NDVI and low LST values are associated with vegetated urban land use and land cover areas such as parks, crop fields and urban forests. This is also supported by Maree and Khanyile (2017), who indicated that high NDVI values in the city of Johannesburg are associated with suburban areas having green leafy trees, lawns, gardens and irrigated farms. The vegetated areas with high NDVI values maintain low temperatures due to their ability to reflect more radiation compared to built-up surfaces that absorb and re-emit the solar energy at night (Adeyeri *et al.*, 2017).

This study shows that LST values (Table 6.5) and NDVI values (Table 6.6) varied in some city-regions. There was an increase in LST over the study periods (Figure 6.3). The lowest maximum NDVI value of 0.39 (Table 6.4) and the highest LST value of 20.1°C were in city-region G in 2020 (Table 6.3). This may be due to population growth where it rose from 3 226 055 in 2001 to 4 434 827 in 2011 (Statistics South Africa, 2020). The rise in population in Johannesburg is at a rate of approximately 3% after every five years (Statistics South Africa, 2020). A rise in population in urban areas also increase the housing demands. An increase in population is associated with a loss of vegetation cover to expand suburban areas, which increase LST (Mudede *et al.*, 2020). Statistics South Africa (2020) highlight that population growth in the suburbs of Soweto and Rosebank increases the demand for decent accommodation. This in turn exacerbates the UHI intensity if no measures are taken to increase the vegetation cover.

To understand the relationship between LST and vegetation cover, Pearson's correlation analysis was carried out between LST and NDVI values in all the seven city-regions of the study area. The results show that LST and NDVI exhibited a negative correlation in all the city-regions over the years of study (2001, 2005, 2010, 2015 and 2020). The strongest negative correlation was -0.76 in city-region A, followed by -0.68 in city-region C in 2020 (Table 6.7). This indicates that in all the

city-regions when LST increased, NDVI decreased. The high LST values are due to low vegetation cover resulting in low evapotranspiration. Evapotranspiration occurs when sun rays hit tree canopies which cause evaporative cooling (Adeyeri *et al.*, 2017). The presence of vegetation reduces LST because it creates an albedo 15% more than impervious surfaces due to lower heat absorption and higher longwave radiation reflection (Adeyeri *et al.*, 2017). The negative relationship between LST and NDVI in urban areas is in line with previous studies (Ahmed *et al.*, 2013; Adeyeri *et al.*, 2017; Mudede *et al.*, 2020), where they found that LST values increase with a decrease in vegetation cover, and vice versa.

Urbanisation due to population growth and economic development are amongst the main drivers of a high rise in LST and a decline in vegetation cover due to the continuous cutting down of trees in urban centres (Mudede *et al.*, 2020). The municipalities, the health care sector and stakeholders involved in urban planning and management can use LST and NDVI maps to assess the UHI across the seven city-regions of the city of Johannesburg (Ngie, 2020). This study is important to policymakers in making decisions to reduce LST in the most affected areas and implementing tree planting schemes for urban greening and sustainable urban development for future years (Mudede *et al.*, 2020). The spatial distribution and relationship between LST and NDVI aspects are vital to researchers focussing on urban ecosystem studies, urban tree management and city temperature studies (Mushore *et al.*, 2017).

This study provides information on the spatiotemporal dynamics of vegetation coverage and its relationship with LST to municipal authorities and other stakeholders to facilitate decision making for management intervention to mitigate UHI effects. It should be noted that the findings obtained from MODIS datasets are coarser than other multispectral sensors (e.g. Landsat, Sentinel and SPOT data) and are suitable for mapping over large areas. The spatial resolution of 1000m for both MOD11A2 and MOD13A2 may produce inaccurate results due to their failure to perfectly determine the thermal and vegetation characteristics in a smaller heterogeneous urban environment. Therefore, it is recommended to use higher spatial resolution imagery such as Landsat and ASTER when high accuracies are required. However, as aforementioned, the weather data from SAWS was only for a single weather station (Johannesburg-Bot Tuine), the lack of ground validation data from all the weather stations in the city affect the accuracy of the results obtained. This problem could be resolved by ensuring the weather stations in all the city-regions measure all the appropriate atmospheric and meteorological data for validation purposes.

6.5 Conclusions

In this study, we examined the spatiotemporal dynamics of vegetation coverage and LST at a city-regional level in Johannesburg, over 19 years, between 2001 and 2020. The spatial distribution of both LST and NDVI provides essential information for understanding the city's local temperature variations, which can help introduce effective ways to minimise the adverse impacts of high temperatures. The LST was negatively correlated to NDVI, which suggests that the presence of vegetation reduces LST. Therefore, urban planners should maximise their effort to adopt effective urban greening plans to minimise the negative impacts of high LST. It is recommended that the municipality and other stakeholders in urban planning and management advise residents, companies, and all inhabitants in all the city-regions to stop tree removal and start tree-planting programmes to reduce LST that would eventually reduce the UHI effects. These measures will ultimately contribute towards global warming mitigation and climate change impacts in areas where most people live.

Chapter Seven

Synthesis

7.1 Introduction

Accurate identification and classification of urban tree species are crucial in urban forest management (Ajewole, 2010). This is important for developing sustainable management programmes, which include the identification of potential planting spaces, the increase and maintenance of existing tree canopy cover and informing policymakers (Roy *et al.*, 2012). Urban forest managers require information on the status, spatial distribution, changes, and ecosystem services they bring to the urbanites (Escobedo *et al.*, 2011). However, the monitoring and mapping of urban trees are challenging due to various factors that include the landscape's heterogeneity and image resolution (Agarwal *et al.*, 2013). Remote sensing uses various image processing methods to identify, classify, map, and monitor urban trees (Alonzo *et al.*, 2016). Therefore, precise techniques for urban tree classification are required to capture information using airborne and spaceborne sensors (Le Louarn *et al.*, 2017; Brabant *et al.*, 2019; Li *et al.*, 2019).

This thesis mapped urban trees using different remote sensing datasets, including hyperspectral data from field spectroscopy, Light Detection and Ranging (LiDAR) point-cloud data, WorldView-2 (WV-2) and Moderate Resolution Imaging Spectroradiometer (MODIS) satellite imagery. Chapter 2 explored the potential of feature selection methods in classifying urban trees using field spectroscopy data. It revealed that feature selection methods can reduce the high dimensionality and classify urban trees, with accuracies ranging from 64% to 95.3%. The study did not show the spatial distribution of the common urban trees in the study area. We found the necessity of using very high spatial resolution (VHSR) multispectral data to classify the common urban trees and show their spatial distribution. Chapter 3 assessed the capability of remote sensing to map and classify urban tree species using WV-2 imagery. The study used pixel-based classification methods to classify the common urban trees and other land use and land cover (LULC) classes. The results indicated that pixel-based classification methods can classify common urban trees and LULC classes, showing their spatial distribution, with accuracies of 84.2% and 81.2% for random forest (RF) and support vector machines (SVM) classification algorithms, respectively. The need to reduce misclassifications due to factors such as "mixed pixel problem" encouraged the use of an object-based classification method that considers among others, the shape, location and textural properties of a feature. Chapter 4 examined SVM and RF classification algorithms' performance in the object-based mapping of common urban trees and other LULC classes using WV-2 multispectral imagery. It shows that the RF and SVM classifiers perform well in classifying the common urban trees and other LULC classes in the study area, with accuracies of 91.9% for RF and 87.3% for SVM. Structural data such as LiDAR can improve the accuracies

in the classification and mapping of urban trees and LULC classes. Chapter 5 examined the effectiveness of the fused dataset (WV-2 bands, vegetation indices and normalised Digital Surface Model (nDSM)) in mapping common urban trees and the LULC classes. It revealed that the fused dataset was effective in the classification, with accuracies of 97% and 94% for the RF and SVM classification algorithms, respectively. The information from the classification using VHR data alone and fused data are essential for urban forest managers and municipalities in tree planting programmes that can reduce problems such as the emergence and growth of Urban Heat Islands (UHIs). Chapter 6 assessed the spatiotemporal dynamics of vegetation coverage and land surface temperature (LST) in the seven city-regions of the City of Johannesburg (CoJ) over 19 years, between 2001 and 2020. It revealed a decrease in vegetation cover and an increase in LSTs in all the seven city-regions of the CoJ over the years of study. The study indicated that areas with a high amount of vegetation cover had low LSTs and vice versa.

The study area used in Chapters 2, 3, 4 and 5 is Randburg municipal area. Chapter 6 used the CoJ as the study area. The fieldwork was carried out in September 2017 and March 2019. However, due to differences in the datasets used in some of the chapters, the training and test samples of the common urban trees and other LULC classes differ from each chapter.

7.2 Summary of the findings

A summary of the findings for each objective and research question in this study is provided below.

7.2.1 The potential of feature selection methods in the classification of urban trees using field spectroscopic data.

Hyperspectral data can accurately classify urban trees in heterogeneous urban environments (Alonzo *et al.*, 2014; Liu *et al.*, 2017; Aval *et al.*, 2019). However, due to the exorbitant cost and high data dimensionality of hyperspectral data, its application in urban classification is still limited. The "Hughes effect" is the major problem in applying hyperspectral data in tree species classification (Liu *et al.*, 2017). The "Hughes effect" occurs when the number of samples is less than the number of features dataset used, and this results in low accuracies, especially when using the classification algorithms that were designed for low-dimensional data (Kiala *et al.*, 2019). The high data dimensionality and high volume of hyperspectral data have been reduced by using feature selection methods to select key wavelengths to produce high accuracies in the classification (Serpico and Bruzzone, 2001; Mureriwa *et al.*, 2016). The feature selection methods include Support Vector Machines (SVM) wrapper, Partial Least Squares Discriminant Analysis (PLS-DA), Guided

Regularized Random Forest (GRRF), Principal Component Analysis (PCA) and Genetic Algorithm (GA). The use of feature selection methods in the classification of urban trees using hyperspectral data has often been overlooked in South Africa and remains largely unexplored.

The potential of feature selection methods is essential for effectively classifying urban trees using field spectroscopic data. Chapter 2 explored the potential of feature selection methods to classify six common urban trees using field hyperspectral data. The feature selection methods used in this chapter were PCA-DA, PLS-DA and GRRF. The objectives were to identify the optimal wavelengths (i.e. from 350 to 2500 nm) using the three feature selection methods and compare their effectiveness in identifying the key wavelengths that precisely classify the common urban trees. The RF and SVM performance was assessed in the classification of the selected key wavelengths by each of the feature selection methods. The results revealed that the three feature selection methods were able to identify the key wavelengths that precisely classify the common urban trees. The GRRF method selected 13 wavelengths, whilst both the PCA-DA and PLS-DA selected 10 wavelengths. The feature selection methods selected wavelengths mostly in the Short-Wave Infrared (SWIR) region of the electromagnetic spectrum. The wavelengths located in the SWIR region of the electromagnetic spectrum were 10 for the PCA-DA, 9 for the PLS-DA and 8 by the GRRF. The SVM classifier produced overall accuracies of 95.3%, 93.3% and 86% using the GRRF, PLS-DA and PCA-DA techniques, respectively. Moreso, the RF classifier produced 88.7%, 72% and 64% for the GRRF, PLS-DA and PCA-DA techniques, respectively. The study revealed that the GRRF method was the most effective and efficient feature selection tool compared to PCA-DA and PLS-DA in reducing the high dimensionality of field hyperspectral data. Although this study was conducted using field spectroscopic data, it did not show how the spatial distribution of the species in the study area. It was recommended that very high-resolution multispectral data such as WV-2 could assist in showing the spatial distribution of trees and increase accuracies in the study area. This would assist municipalities and stakeholders in urban tree planning and management.

7.2.2 The capability of remote sensing to classify and map urban alien tree species using high-resolution multispectral data.

The classification and mapping of urban trees have long been done using traditional field-based surveys or interpretation of aerial photographs, which are tedious, costly and challenging to use in large areas (Alonzo *et al.*, 2016). Remote sensing techniques offer solutions to the aforementioned problems by offering robust, repeatable and efficient ways of classifying and mapping tree species

(Myeong *et al.*, 2006). The use of hyperspectral data has overcome labour problems in classifying trees, but it is costly and requires more computer processing time due to the high dimensionality of data. The hyperspectral data used in chapter 2 did not show the spatial distribution of the tree species as field spectroscopic data were used. To save time and show the spatial distribution of the tree species, VHSR imagery was used in this chapter. The WV-2 imagery has successfully been used in the classification of urban trees, producing good accuracies due to its good geometric, radiometric and spectral resolution (Li *et al.*, 2015; Shojanoori *et al.*, 2016; Yan *et al.*, 2018). The classification method and image appropriateness are fundamental requirements in classification to produce high accuracies (Lu and Weng, 2007). Machine learning algorithms such as RF and SVM have been used to classify urban trees and produced high accuracies (Puissant *et al.*, 2014; Li *et al.*, 2015; Le Louarn *et al.*, 2017). The RF and SVM machine learning algorithms were used in this study to classify the common urban trees and other LULC classes on WV-2 imagery.

The use of VHSR satellite imagery is vital in the classification of tree species and LULC classes in a heterogeneous urban environment. Chapter 3 assessed the capability of pixel-based analysis methods using VHSR satellite imagery to map and classify urban alien tree species and other LULC classes in the Randburg municipal area. The study examined RF and SVM machine learning algorithms' effectiveness in the classification of common urban alien tree species and other LULC classes in the study area. The study also tested the utility of WV-2 spectral bands and compared RF and SVM's effectiveness in the classification of the common urban trees and LULC classes in the study area. The study revealed that the RF and SVM algorithms effectively classified common urban alien trees and LULC classes in the study area, with overall accuracies of 84.2% for RF and 81.2% for SVM. The red, red-edge, NIR1 and NIR2 bands were the most effective in the classification with Mean Decrease Accuracy (MDA) values ranging from 0.14 (red edge) to 0.16 (red). The RF classifier outperformed the SVM algorithm by 3%, though there were no significant differences in their confusion matrices at a 5% significance level as they produced a Z value of -1.64, which was less than 1.96. However, there were some misclassifications in the study, and these were due to various factors, which include spectral signature overlap, "mixed pixel problem", and the reference points' location errors. These misclassifications can be solved using object-based ensemble analysis to produce high accuracies (Le Louarn *et al.*, 2017). Therefore object-based ensemble analysis was worth considering for the classification of the urban trees and LULC classes to improve the accuracies whilst reducing the problems encountered using pixel-based classification techniques.

7.2.3 The ability of object-based ensemble analysis in classifying common urban trees using high-resolution multispectral data.

Pixel-based classification methods have been used to classify urban trees and LULC classes using WV-2 imagery (Immitzer *et al.*, 2012; Liu and An, 2019; Jombo *et al.*, 2020). The methods have been affected by various factors, including the "mixed pixel" problem, urban complexity, and shadow effect, resulting in low accuracy (Le Louarn *et al.*, 2017). These problems were proven to be overcome by object-based classification techniques as they consider several properties such as the object's location, area, shape and texture (Agarwal *et al.*, 2013). The CoJ has a heterogeneous landscape that includes high rise buildings, roads, trees, water bodies and bare land (Schäffler and Swilling, 2013). This heterogeneity makes it difficult to classify urban trees and LULC classes using pixel-based techniques. Therefore, it was necessary to examine whether object-based analysis can be used to classify urban trees and other LULC classes in the study area.

Object-based methods in the classification of tree species in a heterogeneous urban environment are crucial as they can produce higher accuracies than pixel-based techniques (Le Louarn *et al.*, 2017). Chapter 4 examined whether object-based ensemble analysis can improve the accuracies in classifying common urban trees and other LULC classes using VHR satellite imagery. The study examined RF and SVM classification algorithms' performance in the object-based mapping of common urban trees and LULC classes using WV-2 imagery in the Randburg municipal area. The study showed that RF and SVM algorithms are capable of classifying urban trees and LULC classes in a heterogeneous environment. The classification algorithms produced accuracies of 91.9% for RF and 87.3% for SVM. This illustrated an improvement in the overall accuracies from the ones produced using the pixel-based classification techniques. The RF classification accuracy increased from 84.2% to 91.9%, and SVM accuracy increased from 81.2% to 87.3%. The increases for both classification algorithms were more than 5%, showing a significant improvement. The RF classification algorithm performed better than SVM using both pixel-based and object classification techniques. The study recommended the use of the object-based classification technique of fused WV-2 imagery with structural data such as Light Detection and Ranging (LiDAR) that incorporates several properties such as tree height and measurement of crown spread that can increase the accuracy levels.

7.2.4 The ability of a combination of airborne LiDAR point-cloud data and very high-resolution imagery in the classification and mapping of common urban trees.

The integration of VHR imagery with LiDAR data can improve the accuracies in mapping urban tree species and LULC classes (Hartling *et al.*, 2019). This is due to the integration of spatial/textural information from VHR imagery, and LiDAR data provides structural/vertical information, which is vital in the classification of tree species (Pu and Landry, 2020). The classification of urban trees in heterogeneous environments faces challenges because the vegetation in these environments co-exists with man-made LULC features (Alonzo *et al.*, 2014). The study area (Randburg municipality) is complex, and it was, therefore, necessary to assess the ability of fused LiDAR data and WV-2 imagery in the classification of the common urban trees and LULC classes.

In Chapter 5, the study examined the effectiveness of fused data (nDSM, WV-2 bands and vegetation indices) in mapping common urban trees and LULC classes in the Randburg municipal area. The importance of the nDSM, WV-2 bands and vegetation indices in the classification of the common urban trees and LULC classes was ranked. The results revealed that the fused dataset effectively classified the common urban trees and LULC classes in the study area, with high accuracies of 97% for RF and 94% for the SVM classifier. The study also highlighted that the nDSM, NIR2, NIR1 and Normalized Difference Vegetation Index Green/Red Ratio (NDVIGR) were the top-ranked variables in classifying the common urban trees and LULC classes in the study area. The results from the study are essential to municipalities to promote tree planting programmes in areas with less tree cover and encourage the purchase of high-point cloud LiDAR data that can help reduce problems such as the emergence of Urban Heat Islands (UHIs) in the CoJ. Therefore, there was a necessity to determine how the city-regions in the CoJ have lost tree coverage over the years and how this was related to LST in the city.

7.2.5 The spatiotemporal dynamics of vegetation coverage and LST in a heterogeneous urban area.

The presence of vegetation such as trees is an effective way to regulate the urban climate by adding air moisture content which reduces LSTs (Baris *et al.*, 2009). Trees can moderate temperatures by reducing wind speed, cooling through evapotranspiration and providing shade, which can lower the risk of heat-related illnesses for urban dwellers (Ferrini *et al.*, 2020). Consequently, research on effective measures to mitigate the UHI effects is crucial in urban ecology and planning for sustainable development (Alexander, 2020). The CoJ has a heterogeneous landscape with various

LULC classes that include buildings, grasslands, water bodies and trees (Knight, 2018). The spatial distribution of trees in the CoJ shows a wide disparity, with a low amount of trees in the southern part of the CoJ and a high amount of trees in the wealthy northern suburbs of the city (Storie, 2014). Various factors influence vegetation coverage and LST's spatiotemporal dynamics, including rapid urbanisation and population growth (Guha and Govil., 2020). To the best of my knowledge, there has not been any study that has focussed on the spatiotemporal dynamics of vegetation coverage and LST at a city-regional level in South Africa using night-time MODIS data. Therefore, it was necessary to determine the spatiotemporal dynamics of vegetation coverage and LST at a city-regional level in the CoJ.

In this research, chapter 6 determined the changes in the spatiotemporal dynamics of vegetation coverage and LST across the seven regions of the city with a five-year interval from 2001-2020 (2001, 2005, 2010, 2015 and 2020). In the study, the relationship between LST and NDVI values were analysed. The vegetation coverage decreased over the years in all the city-regions, whilst LST values increased. The highest LST increase was 20.1°C, whilst the lowest NDVI value was 0.39, and they were all in city-region G in 2020. The results also revealed a significant spatiotemporal difference in LST and NDVI in the city-regions with a negative correlation between them, and the values ranged from -0.03 to -0.76. This study indicated that city-regions with a high amount of vegetation cover have low LSTs and vice versa. The findings of this study provide important information to the municipalities to carry out appropriate programmes that help reduce the emergence of UHIs.

7.3 Conclusions

The following conclusions can be drawn based on the objectives of this study:

- Several studies used field spectroscopic data to classify tree species in South Africa and produced high accuracy results. However, few studies have classified tree species in a heterogeneous urban environment. The majority of studies that used field spectroscopic data to classify trees were conducted in commercial forests and savanna environments. The use of field spectroscopic data in classifying urban trees in Southern African urban environments has not been well examined. The outcomes of the study indicated that field spectroscopic data can be used to classify urban trees in a heterogeneous urban environment, with accuracies ranging from 64% to 95.3%, though the spatial distribution of the species in the study area was not

shown. These outcomes triggered the desire to test VHSR WV-2 imagery to show the common urban trees' spatial distribution in the study area.

- The classification of common urban trees and other LULC classes using RF and SVM classification algorithms produced accuracies of 84.2% and 81.2%, respectively on VHSR WV-2 multispectral imagery. The outcomes indicated that urban trees can be classified and mapped using pixel-based classification methods on VHR images. The results also indicated that the NIR1, NIR2, red and red edge bands were the most influential in the classification of urban tree species.
- The classification of common urban trees using object-ensemble analysis produced high accuracies of 91.9% and 87.3% using RF and SVM classification algorithms, respectively, on VHSR WV-2 imagery. The high accuracies were due to spatial information, which includes shape, directional pattern, area and location of the image objects in the object-based analysis. These results indicated that object-based ensemble analysis performs better than pixel-based classification methods in the classification of urban trees and LULC in a heterogeneous urban environment. The classification accuracies for both RF and SVM classification algorithms using pixel-based classification methods increased by 7.7% and 6.1%, respectively, when the object-based ensemble analysis was used.
- A combination of airborne LiDAR point cloud data and VHSR produced high accuracies in mapping common urban trees. The incorporation of vegetation indices also assisted in the classification of trees and other LULC classes. As a result, the combination of WV-2 satellite imagery, nDSM and vegetation indices produced accuracies of 97% for RF and 94% for SVM in the classification and mapping of tree species in a heterogeneous urban environment. This indicated an increase in the RF and SVM algorithms' accuracies using object-based ensemble analysis and when LiDAR data was incorporated in the classification of the common urban trees and LULC classes in the study area. The overall accuracies for both the RF and SVM classifiers increased by 5.1% and 6.7%, respectively.
- The spatiotemporal dynamics of vegetation coverage and LST can be obtained using remote sensing data. The results of the study showed that vegetation has been decreasing over the years with the lowest NDVI value of 0.39, whilst LST has been increasing over the years, with the highest increase of 20.1°C in city-region G in 2020. The findings of this study can assist urban planners in finding areas that need tree planting to reduce LST and increase NDVI values.

In conclusion, this study indicated the efficiency of various techniques in the classification and monitoring of tree species in a heterogeneous urban environment. The findings contribute to the establishment of a comprehensive urban tree inventory for sustainable urban tree management. While remote sensing multispectral imagery alone is inadequate to address all the needs of urban tree management, the use of information generated through image analysis is a step towards creating a comprehensive urban inventory that supports urban greening programmes for conservation, development and management of tree resources.

7.3 Research limitations and future directions

Several limitations were encountered in this study, and these include:

- The use of MODIS data in assessing the spatiotemporal dynamics of vegetation coverage and LST (Chapter 6) have several challenges. The MODIS data were particularly important to the study because of their easy availability and coverage of the historical data for the study periods required. However, the data's low spatial resolution makes it difficult to extract detailed information from the mapping. The spatial resolution of both MOD11A2 and MOD13A2 were 1 km which might have produced low accuracy results in this study due to their failure to account for thermal and vegetation changes in small landcover classes. Chapter 6 also depended on data from the South African Weather Service (SAWS) to validate the MODIS LST data. However, the weather data used in this study was only from a single weather station which might have reduced the validity.

- The ability to classify urban trees in urban environments shows an advancement in remote sensing science. However, successful urban tree classification depends on understanding the spatial, spectral, and temporal resolution limitations, which can hinder tree species classification and mapping in different environments. Future studies should focus on identifying and employing biochemical and biophysical traits of trees per species type to enhance the interpretability of remote sensing data used to produce tree species maps.

- Recent advancements in hyperspectral imaging, small-format cameras on unmanned aerial vehicles (UAVs) have been used to classify urban trees. In comparison to the data acquisition using airborne and satellite methods, UAVs data collection approaches have several advantages, which include, ability to collect data under unfavourable imaging situations, e.g. under high cloud coverage. The UAVs also do not depend on airports to take off and the availability of satellite sensors in an area of interest. They are also cost-efficient and can provide

data with a high temporal and spatial resolution (Jang *et al.*, 2020). However, UAVs have limited flight duration, and they can be unstable in windy conditions, which makes them difficult to use in large scale areas(Wang *et al.*, 2019).

References

Abbasi, M., Verrelst, J., Mirzaei, M., Marofi, S., and Riyahi Bakhtiari, H.R. (2019). Optimal Spectral Wavelengths for Discriminating Orchard Species Using Multivariate Statistical Techniques. *Remote Sensing,* 12(1): 63.

Abdel-Rahman, E.M., Mutanga, O., Adam, E., and Ismail, R. (2014). Detecting Sirex noctilio grey-attacked and lightning-struck pine trees using airborne hyperspectral data, random forest and support vector machines classifiers. *ISPRS Journal of Photogrammetry and Remote Sensing,* 88: 48-59.

Abiye, T. (2015). The Role of Wetlands Associated to Urban Micro-Dams in Pollution Attenuation, Johannesburg, South Africa. *Wetlands,* 35(6): 1127-1136.

Abiye, T., Masindi, K., Mengistu, H., and Demlie, M. (2018). Understanding the groundwater-level fluctuations for better management of groundwater resource: A case in the Johannesburg region. *Groundwater for Sustainable Development,* 7: 1-7.

Adam, E., Mureriwa, N., and Newete, S. (2017). Mapping Prosopis glandulosa (mesquite) in the semi-arid environment of South Africa using high-resolution WorldView-2 imagery and machine learning classifiers. *Journal of Arid Environments,* 145: 43-51.

Adam, E., and Mutanga, O. (2009). Spectral discrimination of papyrus vegetation (Cyperus papyrus L.) in swamp wetlands using field spectrometry. *ISPRS Journal of Photogrammetry and Remote Sensing,* 64(6): 612-620.

Adam, E., Mutanga, O., and Ismail, R. (2013). Determining the susceptibility of Eucalyptus nitensforests to Coryphodema tristis (cossid moth) occurrence in Mpumalanga, South Africa. *International Journal of Geographical Information Science,* 27(10): 1924-1938.

Adelabu, S., Mutanga, O., Adam, E.E., and Cho, M.A. (2013). Exploiting machine learning algorithms for tree species classification in a semiarid woodland using RapidEye image. *Journal of Applied Remote Sensing,* 7(1): 073480.

Adeleke, O., Akinlabi, S.A., Hassan, S., and Jen, T. (2020). Predicting the Effect of Seasonal Variation on the Physical Composition of Municipal Solid Waste: A Case Study of the City of Johannesburg. Advances in Manufacturing Engineering. Springer.

Adeyemi, A., Botai, J., Ramoelo, A., Van Der Merwe, F., and Tsela, P. (2015). Effect of impervious surface area and vegetation changes on mean surface temperature over Tshwane metropolis, Gauteng Province, South Africa. *South African Journal of Geomatics,* 4(4): 351.

Adeyeri, O.E., Akinsanola, A.A., and Ishola, K.A. (2017). Investigating surface urban heat island characteristics over Abuja, Nigeria: Relationship between land surface temperature and multiple vegetation indices. *Remote Sensing Applications: Society and Environment,* 7: 57-68.

African Green City Index (2011). Assessing the environmental performance of Africa's major cities. Economist Intelligence Unit. Munich, Germany.

Agarwal, S., Vailshery, L., Jaganmohan, M., and Nagendra, H. (2013). Mapping Urban Tree Species Using Very High Resolution Satellite Imagery: Comparing Pixel-Based and Object-Based Approaches. *ISPRS International Journal of Geo-Information,* 2(1): 220-236.

Ahmed, B., Kamruzzaman, M., Zhu, X., Rahman, M., and Choi, K. (2013). Simulating Land Cover Changes and Their Impacts on Land Surface Temperature in Dhaka, Bangladesh. *Remote Sensing,* 5(11): 5969-5998.

Ahmed, H.A., Singh, S.K., Kumar, M., Maina, M.S., Dzwairo, R., and Lal, D. (2020). Impact of urbanization and land cover change on urban climate: Case study of Nigeria. *Urban Climate,* 32.

Aina, Y.A., Adam, E.M., and Ahmed, F. (2017). Spatiotemporal Variations in the Impacts of Urban Land Use Types on Urban Heat Island Effects: The Case of Riyadh, Saudi Arabia. *ISPRS - International Archives of the Photogrammetry, Remote Sensing and Spatial Information Sciences,* XLII-3/W2: 9-14.

Ajewole, O.I. (2010). Prospects and challenges for incorporating trees into urban infrastructural developments in Nigeria. *International Journal of Sustainable Development & World Ecology,* 15(5): 419-429.

Alexander, C. (2020). Normalised difference spectral indices and urban land cover as indicators of land surface temperature (LST). *International Journal of Applied Earth Observation and Geoinformation,* 86.

Almeida, A.M., and Tomé, M. (2009). Field sampling of cork value before extraction in Portuguese 'montados'. *Agroforestry systems,* 79(3): 419-430.

Alonso-Benito, A., Arroyo, L., Arbelo, M., and Hernández-Leal, P. (2016). Fusion of WorldView-2 and LiDAR Data to Map Fuel Types in the Canary Islands. *Remote Sensing,* 8(8).

Alonzo, M., Bookhagen, B., and Roberts, D.A. (2014). Urban tree species mapping using hyperspectral and lidar data fusion. *Remote Sensing of Environment,* 148: 70-83.

Alonzo, M., Mcfadden, J.P., Nowak, D.J., and Roberts, D.A. (2016). Mapping urban forest structure and function using hyperspectral imagery and lidar data. *Urban Forestry & Urban Greening,* 17: 135-147.

Amani-Beni, M., Zhang, B., Xie, G.-D., and Shi, Y. (2019). Impacts of Urban Green Landscape Patterns on Land Surface Temperature: Evidence from the Adjacent Area of Olympic Forest Park of Beijing, China. *Sustainability,* 11(2).

Anderson, K., and Gaston, K.J. (2013). Lightweight unmanned aerial vehicles will revolutionize spatial ecology. *Frontiers in Ecology and the Environment,* 11(3): 138-146.

Asner, G.P. (1998). Biophysical and biochemical sources of variability in canopy reflectance. *Remote Sensing of Environment,* 64(3): 234-253.

Aval, J., Fabre, S., Zenou, E., Sheeren, D., Fauvel, M., and Briottet, X. (2019). Object-based fusion for urban tree species classification from hyperspectral, panchromatic and nDSM data. *International Journal of Remote Sensing,* 40(14): 5339-5365.

Azeez, O.S., Pradhan, B., and Jena, R. (2019). Urban tree classification using discrete-return LiDAR and an object-level local binary pattern algorithm. *Geocarto International*: 1-19.

Baris, M.E., Sahin, S., and Yazgan, M.E. (2009). The contribution of trees and green spaces to the urban climate: The case of Ankara. *African Journal of Agricultural Research,* 4(9): 791-800.

Barker, M., and Rayens, W. (2003). Partial least squares for discrimination. *Journal of Chemometrics,* 17(3): 166-173.

Bartesaghi-Koc, C., Osmond, P., and Peters, A. (2019). Mapping and classifying green infrastructure typologies for climate-related studies based on remote sensing data. *Urban Forestry & Urban Greening,* 37: 154-167.

Belgiu, M., and Drăguţ, L. (2016). Random forest in remote sensing: A review of applications and future directions. *ISPRS Journal of Photogrammetry and Remote Sensing,* 114: 24-31.

Benz, U.C., Hofmann, P., Willhauck, G., Lingenfelder, I., and Heynen, M. (2004). Multi-resolution, object-oriented fuzzy analysis of remote sensing data for GIS-ready information. *ISPRS Journal of Photogrammetry and Remote Sensing,* 58(3-4): 239-258.

Brabant, C., Alvarez-Vanhard, E., Laribi, A., Morin, G., Thanh Nguyen, K., Thomas, A., and Houet, T. (2019). Comparison of Hyperspectral Techniques for Urban Tree Diversity Classification. *Remote Sensing,* 11(11): 1269.

Breiman, L. (2001). Random forests. *Machine learning,* 45(1): 5-32.

Calviño-Cancela, M., and Martín-Herrero, J. (2016). Spectral Discrimination of Vegetation Classes in Ice-Free Areas of Antarctica. *Remote Sensing,* 8(10): 856.

Campomanes, F., Pada, A.V., and Silapan, J. (2016). Mangrove classification using support vector machines and random forest algorithm: a comparative study. GEOBIA 2016 : Solutions and Synergies.

Cao, J., Liu, K., Zhu, Y., Li, J., and He, Z. (2018). Identifying Mangrove Species Using Field Close-Range Snapshot Hyperspectral Imaging and Machine-Learning Techniques. *Remote Sensing,* 10(12): 2047.

Chen, W., Huang, H., Dong, J., Zhang, Y., Tian, Y., and Yang, Z. (2018). Social functional mapping of urban green space using remote sensing and social sensing data. *ISPRS Journal of Photogrammetry and Remote Sensing,* 146: 436-452.

Cherrington, E.A. (2016). *Towards ecologically consistent remote sensing mapping of tree communities in French Guiana.* PhD Thesis. Technische Universität Dresden.

Chivasa, W., Mutanga, O., and Biradar, C. (2019). Phenology-based discrimination of maize (Zea mays L.) varieties using multitemporal hyperspectral data. *Journal of Applied Remote Sensing,* 13(01): 017504.

Cho, M.A., Mathieu, R., Asner, G.P., Naidoo, L., Van Aardt, J., Ramoelo, A., Debba, P., Wessels, K., Main, R., Smit, I.P.J., and Erasmus, B. (2012). Mapping tree species composition in South African savannas using an integrated airborne spectral and LiDAR system. *Remote Sensing of Environment,* 125: 214-226.

City of Johannesburg (2009). Climate Change Adaptation Plan. City of Johannesburg.

City of Johannesburg Metropolitan Municipality (2020). 2019/20 IDP Review: The City of Johannesburg. City of Johannesburg.

Clark, M., Roberts, D., and Clark, D. (2005). Hyperspectral discrimination of tropical rain forest tree species at leaf to crown scales. *Remote Sensing of Environment,* 96(3-4): 375-398.

Cleve, C., Kelly, M., Kearns, F.R., and Moritz, M. (2008). Classification of the wildland–urban interface: A comparison of pixel- and object-based classifications using high-resolution aerial photography. *Computers, Environment and Urban Systems,* 32(4): 317-326.

Cocchi, M., Biancolillo, A., and Marini, F. (2018). Chemometric Methods for Classification and Feature Selection. Data Analysis for Omic Sciences: Methods and Applications.

Cohen, J. (1960). A Coefficient of Agreement for Nominal Scales. *Educational and Psychological Measurement,* 20(1): 37-46.

Colgan, M., Baldeck, C., Féret, J.-B., and Asner, G. (2012). Mapping Savanna Tree Species at Ecosystem Scales Using Support Vector Machine Classification and BRDF Correction on Airborne Hyperspectral and LiDAR Data. *Remote Sensing,* 4(11): 3462-3480.

Collins, L., Griffioen, P., Newell, G., and Mellor, A. (2018). The utility of Random Forests for wildfire severity mapping. *Remote Sensing of Environment,* 216: 374-384.

Congalton, R.G. (1991). A review of assessing the accuracy of classifications of remotely sensed data. *Remote Sensing of Environment,* 37(1): 35-46.

Congalton, R.G., Oderwald, R.G., and Mead, R.A. (1983). Assessing Landsat classification accuracy using discrete multivariate analysis statistical techniques. *Photogrammetric engineering and remote sensing,* 49(12): 1671-1678.

Czaja, M., Kołton, A., and Muras, P. (2020). The Complex Issue of Urban Trees—Stress Factor Accumulation and Ecological Service Possibilities. *Forests,* 11(9): 932.

Dalponte, M., Bruzzone, L., and Gianelle, D. (2012). Tree species classification in the Southern Alps based on the fusion of very high geometrical resolution multispectral/hyperspectral images and LiDAR data. *Remote Sensing of Environment,* 123: 258-270.

Das, S., and Angadi, D.P. (2020). Land use-land cover (LULC) transformation and its relation with land surface temperature changes: A case study of Barrackpore Subdivision, West Bengal, India. *Remote Sensing Applications: Society and Environment,* 19.

De Santana, F.B., Borges Neto, W., and Poppi, R.J. (2019). Random forest as one-class classifier and infrared spectroscopy for food adulteration detection. *Food Chem,* 293: 323-332.

Degerickx, J., Roberts, D.A., and Somers, B. (2019). Enhancing the performance of Multiple Endmember Spectral Mixture Analysis (MESMA) for urban land cover mapping using airborne lidar data and band selection. *Remote Sensing of Environment,* 221: 260-273.

Demir, N., Poli, D., and Baltsavias, E. (2008). Extraction of buildings and trees using images and LiDAR data. *International Archives of the Photogrammetry, Remote Sensing and Spatial Information Sciences,* 37(B4): 313-318.

Deng, H., and Runger, G. (2013). Gene selection with guided regularized random forest. *Pattern Recognition,* 46(12): 3483-3489.

Department of Agriculture Forestry and Fisheries. (2011). *State of Forest Report.* [Online]. Available: www.gdard.gpg.gov.za/Documents1/Gauteng_State%20of%20Environment%20Report_2011.pdf. [Accessed 10 January 2021].

Department of Environment Forestry and Fisheries. (2020). *South Africa Yearbook 2019/20.* [Online]. Available: https://www.gcis.gov.za/sites/default/files/docs/resourcecentre/yearbook/Yearbook2020-6-Environment%20and%20Tourism.pdf [Accessed 04 February 2021].

Deshpande, S., Verma, P., Yadav, P., Gubbi, J., and Balamurali, P. (2017). Urban Growth Studies for Johannesburg City Using Remotely Sensed data. *Asian Journal of Geoinformatics,* 16(3).

Dizdaroglu, D., Yigitcanlar, T., and Dawes, L.A. (2009). Sustainable urban futures: An ecological approach to sustainable urban development. In Proceedings of The Second Infrastructure Theme Postgraduate Conference 2009: Rethinking Sustainable

Development-Planning, Infrastructure Engineering, Design and Managing Urban Infrastructure.

Duryea, M.L., and Kampf, E. (2007). *Wind and trees: lessons learned from hurricanes.* University of Florida, IFAS Extension Gainesville, FL.

Dwyer, A. (1991). Matchmaking and McNemar in the comparison of diagnostic modalities. *Radiology,* 178(2): 328-330.

El Kenawy, A.M., Hereher, M.E., and Robaa, S.M. (2019). An Assessment of the Accuracy of MODIS Land Surface Temperature over Egypt Using Ground-Based Measurements. *Remote Sensing,* 11(20).

Ellis, E.A., and Mathews, A.J. (2019). Object-based delineation of urban tree canopy: assessing change in Oklahoma City, 2006–2013. *Computers, Environment and Urban Systems,* 73: 85-94.

Escobedo, F.J., Kroeger, T., and Wagner, J.E. (2011). Urban forests and pollution mitigation: analyzing ecosystem services and disservices. *Environ Pollut,* 159(8-9): 2078-2087.

Esri Arcgis. (2018). Version 10.6. *ESRI: Redlands, CA, USA.*

Fang, F., Mcneil, B.E., Warner, T.A., and Maxwell, A.E. (2018). Combining high spatial resolution multi-temporal satellite data with leaf-on LiDAR to enhance tree species discrimination at the crown level. *International Journal of Remote Sensing,* 39(23): 9054-9072.

Fang, F., Mcneil, B.E., Warner, T.A., Maxwell, A.E., Dahle, G.A., Eutsler, E., and Li, J. (2020). Discriminating tree species at different taxonomic levels using multi-temporal WorldView-3 imagery in Washington D.C., USA. *Remote Sensing of Environment,* 246.

Farrugia, B. (2019). WASP (write a scientific paper): Sampling in qualitative research. *Early Hum Dev,* 133: 69-71.

Fassnacht, F.E., Latifi, H., Stereńczak, K., Modzelewska, A., Lefsky, M., Waser, L.T., Straub, C., and Ghosh, A. (2016). Review of studies on tree species classification from remotely sensed data. *Remote Sensing of Environment,* 186: 64-87.

Fassnacht, F.E., Neumann, C., Forster, M., Buddenbaum, H., Ghosh, A., Clasen, A., Joshi, P.K., and Koch, B. (2014). Comparison of Feature Reduction Algorithms for Classifying Tree Species With Hyperspectral Data on Three Central European Test Sites. *IEEE Journal of Selected Topics in Applied Earth Observations and Remote Sensing,* 7(6): 2547-2561.

Ferreira, M.P., Zortea, M., Zanotta, D.C., Féret, J.B., Shimabukuro, Y.E., and Souza Filho, C.R. (2015). On the Use of Shortwave Infrared for Tree Species Discrimination in Tropical Semideciduous Forest. *ISPRS - International Archives of the Photogrammetry, Remote Sensing and Spatial Information Sciences,* XL-3/W3: 473-476.

Ferrini, F., Fini, A., Mori, J., and Gori, A. (2020). Role of Vegetation as a Mitigating Factor in the Urban Context. *Sustainability,* 12(10).

Foody, G.M., and Mathur, A. (2004). A relative evaluation of multiclass image classification by support vector machines. *IEEE Transactions on Geoscience and Remote Sensing,* 42(6): 1335-1343.

Forestry and Agricultural Biotechnology Institute. (2019). *The Polyphagous Shothole Borer (PSHB) And Its Fungus In South Africa.* [Online]. Available: https://www.fabinet.up.ac.za/index.php/research/7 [Accessed 10 October 2019].

Forsyth, G., Richardson, D., Brown, P., and Van Wilgen, B. (2004). A rapid assessment of the invasive status of Eucalyptus species in two South African provinces: working for water. *South African Journal of Science,* 100(1-2): 75-77.

Forzieri, G., Moser, G., Vivoni, E.R., Castelli, F., and Canovaro, F. (2010). Riparian Vegetation Mapping for Hydraulic Roughness Estimation Using Very High Resolution Remote Sensing Data Fusion. *Journal of Hydraulic Engineering,* 136(11): 855-867.

Ghiyamat, A., Shafri, H.Z.M., Amouzad Mahdiraji, G., Shariff, A.R.M., and Mansor, S. (2013). Hyperspectral discrimination of tree species with different classifications using single- and multiple-endmember. *International Journal of Applied Earth Observation and Geoinformation,* 23: 177-191.

Gholizadeh, H., Gamon, J.A., Zygielbaum, A.I., Wang, R., Schweiger, A.K., and Cavender-Bares, J. (2018). Remote sensing of biodiversity: Soil correction and data dimension reduction methods improve assessment of α-diversity (species richness) in prairie ecosystems. *Remote Sensing of Environment,* 206: 240-253.

Ginsburg, S.B., Viswanath, S.E., Bloch, B.N., Rofsky, N.M., Genega, E.M., Lenkinski, R.E., and Madabhushi, A. (2015). Novel PCA-VIP scheme for ranking MRI protocols and identifying computer-extracted MRI measurements associated with central gland and peripheral zone prostate tumors. *J Magn Reson Imaging,* 41(5): 1383-1393.

Gitelson, A.A., Kaufman, Y.J., and Merzlyak, M.N. (1996). Use of a green channel in remote sensing of global vegetation from EOS-MODIS. *Remote Sensing of Environment,* 58(3): 289-298.

Godinho, S., Gil, A., Guiomar, N., Neves, N., and Pinto-Correia, T. (2016). A remote sensing-based approach to estimating montado canopy density using the FCD model: a contribution to identifying HNV farmlands in southern Portugal. *Agroforestry systems,* 90(1): 23-34.

Goldreich, Y. (1992). Urban climate studies in Johannesburg, A sub-tropical city located on a ridge—A review. *Atmospheric Environment. Part B. Urban Atmosphere,* 26(3): 407-420.

Grobler, C.H., Bredenkamp, G.J., and Brown, L.R. (2002). Natural woodland vegetation and plant species richness of the urban open spaces in Gauteng, South Africa. *Koedoe,* 45(1): 19-34.

Guha, S., and Govil, H. (2020). An assessment on the relationship between land surface temperature and normalized difference vegetation index. *Environment, Development and Sustainability*: 1-20.

Guyon, I., and Elisseeff, A. (2003). An introduction to variable and feature selection. *Journal of machine learning research,* 3(Mar): 1157-1182.

Hamedianfar, A., Shafri, H.Z.M., Mansor, S., and Ahmad, N. (2014). Improving detailed rule-based feature extraction of urban areas from WorldView-2 image and lidar data. *International Journal of Remote Sensing,* 35(5): 1876-1899.

Hardy, C., and Nel, A. (2015). Data and techniques for studying the urban heat island effect in Johannesburg. *The International Archives of Photogrammetry, Remote Sensing and Spatial Information Sciences,* 40(7): 203.

Hartling, S., Sagan, V., Sidike, P., Maimaitijiang, M., and Carron, J. (2019). Urban Tree Species Classification Using a WorldView-2/3 and LiDAR Data Fusion Approach and Deep Learning. *Sensors,* 19(6): 1284.

Hellesen, T., and Matikainen, L. (2013). An Object-Based Approach for Mapping Shrub and Tree Cover on Grassland Habitats by Use of LiDAR and CIR Orthoimages. *Remote Sensing,* 5(2): 558-583.

Henderson, H. (1990). Jacaranda. *Farming in South Africa. Weeds A,* 30: 2132-2134.

Henderson, L. (2001). *Alien weeds and invasive plants.* Plant Protection Research Institute, Agricultural Research Council.

Henry, A., and Flood, M.G. (1919). The history of the London plane, Platanus acerifolia, with notes on the genus Platanus. Proceedings of the Royal Irish Academy. Section B: Biological, Geological, and Chemical Science.

Heritage, G., and Large, A. (2009). *Laser scanning for the environmental sciences.* John Wiley & Sons.

Hill, R.A., Wilson, A.K., George, M., and Hinsley, S.A. (2010). Mapping tree species in temperate deciduous woodland using time-series multi-spectral data. *Applied Vegetation Science,* 13(1): 86-99.

Holmström, H. (2002). Estimation of single-tree characteristics using the kNN method and plotwise aerial photograph interpretations. *Forest ecology and management,* 167(1-3): 303-314.

Hong, S.-H., Hendrickx, J.M.H., and Borchers, B. (2011). Down-scaling of SEBAL derived evapotranspiration maps from MODIS (250 m) to Landsat (30 m) scales. *International Journal of Remote Sensing,* 32(21): 6457-6477.

Howard, L. (1833). *The climate of London: deduced from meteorological observations made in the metropolis and at various places around it.* Harvey and Darton, J. and A. Arch, Longman, Hatchard, S. Highley and R. Hunter.

Huang, C., and Ye, X. (2015). Spatial Modeling of Urban Vegetation and Land Surface Temperature: A Case Study of Beijing. *Sustainability,* 7(7): 9478-9504.

Hyyppa, J. (2000). Feasibility for estimation of single tree characteristics using laser scanner. IGARSS 2000. IEEE 2000 International Geoscience and Remote Sensing Symposium. Taking the Pulse of the Planet: The Role of Remote Sensing in Managing the Environment. Proceedings (Cat. No.00CH37120).

Imhoff, M.L., Zhang, P., Wolfe, R.E., and Bounoua, L. (2010). Remote sensing of the urban heat island effect across biomes in the continental USA. *Remote Sensing of Environment,* 114(3): 504-513.

Immitzer, M., Atzberger, C., and Koukal, T. (2012). Tree species classification with random forest using very high spatial resolution 8-band WorldView-2 satellite data. *Remote Sensing,* 4(9): 2661-2693.

Islam, S., and Ma, M. (2018). Geospatial Monitoring of Land Surface Temperature Effects on Vegetation Dynamics in the Southeastern Region of Bangladesh from 2001 to 2016. *ISPRS International Journal of Geo-Information,* 7(12).

Izquierdo-Verdiguier, E., Zurita-Milla, R., and Rolf, A. (2017). On the use of guided regularized random forests to identify crops in smallholder farm fields. 2017 9th International Workshop on the Analysis of Multitemporal Remote Sensing Images (MultiTemp).

Jaenson, R., Bassuk, N., Schwager, S., and Headley, D. (1992). A statistical method for the accurate and rapid sampling of urban street tree populations. *Journal of Arboriculture,* 18(4): 171-183.

Jang, G., Kim, J., Yu, J.-K., Kim, H.-J., Kim, Y., Kim, D.-W., Kim, K.-H., Lee, C.W., and Chung, Y.S. (2020). Review: Cost-Effective Unmanned Aerial Vehicle (UAV) Platform for Field Plant Breeding Application. *Remote Sensing,* 12(6): 998.

Jarocińska, A., Białczak, M., and Sławik, Ł. (2018). Application of aerial hyperspectral images in monitoring tree biophysical parameters in urban areas. *Miscellanea Geographica,* 22(1): 56-62.

Jebur, M.N., Mohd Shafri, H.Z., Pradhan, B., and Tehrany, M.S. (2014). Per-pixel and object-oriented classification methods for mapping urban land cover extraction using SPOT 5 imagery. *Geocarto International,* 29(7): 792-806.

Jim, C.Y. (2013). Sustainable urban greening strategies for compact cities in developing and developed economies. *Urban Ecosystems,* 16(4): 741-761.

Johannesburg City Parks and Zoo. (2018). *The city that's a rain forest.* [Online]. Available: http://www.jhbcityparks.com/index.php/street-trees-contents-29 [Accessed 20 September 2018].

Johannesburg City Parks and Zoo. (2021). *The city that's a rain forest.* [Online]. Available: https://www.jhbcityparksandzoo.com/services-facilities/ecological-services/trees [Accessed 12 January 2021].

Jombo, S., Adam, E., Byrne, M.J., Ali, K.A., and Newete, S.W. (2020). Exploring the Potential of Feature Selection Methods in the Classification of Urban Trees using Field Spectroscopy Data. *International Journal of Geospatial and Environmental Research,* 7(3): 3.

Jombo, S., Adam, E., Byrne, M.J., and Newete, S.W. (2020). Evaluating the capability of Worldview-2 imagery for mapping alien tree species in a heterogeneous urban environment. *Cogent Social Sciences,* 6(1): 1754146.

Jombo, S., Adam, E., and Odindi, J. (2017). Quantification of landscape transformation due to the Fast Track Land Reform Programme (FTLRP) in Zimbabwe using remotely sensed data. *Land Use Policy,* 68: 287-294.

Jombo, S., Adam, E., and Odindi, J. (2021). Classification of tree species in a heterogeneous urban environment using object-based ensemble analysis and World View-2 satellite imagery. *Applied Geomatics*.

Jovanovic, G., Romanic, S.H., Stojic, A., Klincic, D., Saric, M.M., Letinic, J.G., and Popovic, A. (2019). Introducing of modeling techniques in the research of POPs in breast milk - A pilot study. *Ecotoxicol Environ Saf,* 172: 341-347.

Jovanović, M.M., and Milanović, M.M. (2017). Remote Sensing and Forest Conservation: Challenges of Illegal Logging in Kursumlija Municipality (Serbia). Forest Ecology and Conservation.

Jung, M.C., Dyson, K., and Alberti, M. (2021). Urban Landscape Heterogeneity Influences the Relationship between Tree Canopy and Land Surface Temperature. *Urban Forestry & Urban Greening,* 57: 126930.

Karlson, M., Ostwald, M., Reese, H., Bazié, H.R., and Tankoano, B. (2016). Assessing the potential of multi-seasonal WorldView-2 imagery for mapping West African agroforestry tree species. *International Journal of Applied Earth Observation and Geoinformation,* 50: 80-88.

Karlson, M., Ostwald, M., Reese, H., Sanou, J., Tankoano, B., and Mattsson, E. (2015). Mapping tree canopy cover and aboveground biomass in Sudano-Sahelian woodlands using Landsat 8 and random forest. *Remote Sensing,* 7(8): 10017-10041.

Kaszta, Ż., Van De Kerchove, R., Ramoelo, A., Cho, M., Madonsela, S., Mathieu, R., and Wolff, E. (2016). Seasonal Separation of African Savanna Components Using Worldview-2 Imagery: A Comparison of Pixel- and Object-Based Approaches and Selected Classification Algorithms. *Remote Sensing,* 8(9): 763.

Ke, Y., and Quackenbush, L.J. (2011). A review of methods for automatic individual tree-crown detection and delineation from passive remote sensing. *International Journal of Remote Sensing,* 32(17): 4725-4747.

Kiala, Z., Mutanga, O., Odindi, J., and Peerbhay, K. (2019). Feature Selection on Sentinel-2 Multispectral Imagery for Mapping a Landscape Infested by Parthenium Weed. *Remote Sensing,* 11(16).

Klobucar, B., Östberg, J., Jansson, M., and Randrup, T.B. (2020). Long-Term Validation and Governance Role in Contemporary Urban Tree Monitoring: A Review. *Sustainability,* 12(14).

Knight, J. (2018). Transforming the Physical Geography of a City: An Example of Johannesburg, South Africa. Urban Geomorphology.

Konijnendijk, C.C., Nilsson, K., Randrup, T.B., and Schipperijn, J. (2005). *Urban forests and trees: a reference book*. Springer.

Korpela, I., Ørka, H., Maltamo, M., Tokola, T., and Hyyppä, J. (2010). Tree species classification using airborne LiDAR – effects of stand and tree parameters, downsizing of training set, intensity normalization, and sensor type. *Silva Fennica,* 44(2).

Krahwinkler, P., and Rossman, J. (2011). Using decision tree based multiclass support vector machines for forest mapping. IEEE Int. Geoscience and Remote Sensing Symp., Vancouver, Canada.

Kuser, J.E. (2006). *Urban and community forestry in the northeast*. Springer Science & Business Media.

Le Louarn, M., Clergeau, P., Briche, E., and Deschamps-Cottin, M. (2017). "Kill Two Birds with One Stone": Urban Tree Species Classification Using Bi-Temporal Pléiades Images to Study Nesting Preferences of an Invasive Bird. *Remote Sensing,* 9(9): 916.

Lechner, A.M., Foody, G.M., and Boyd, D.S. (2020). Applications in Remote Sensing to Forest Ecology and Management. *One Earth,* 2(5): 405-412.

Leckie, D.G., Tinis, S., Nelson, T., Burnett, C., Gougeon, F.A., Cloney, E., and Paradine, D. (2005). Issues in species classification of trees in old growth conifer stands. *Canadian journal of remote sensing,* 31(2): 175-190.

Lee, L.C., Liong, C.Y., and Jemain, A.A. (2018). Partial least squares-discriminant analysis (PLS-DA) for classification of high-dimensional (HD) data: a review of contemporary practice strategies and knowledge gaps. *Analyst,* 143(15): 3526-3539.

Li, D., Ke, Y., Gong, H., and Li, X. (2015). Object-based urban tree species classification using bi-temporal WorldView-2 and WorldView-3 images. *Remote Sensing,* 7(12): 16917-16937.

Li, W., Guo, Q., Jakubowski, M.K., and Kelly, M. (2012). A New Method for Segmenting Individual Trees from the Lidar Point Cloud. *Photogrammetric Engineering & Remote Sensing,* 78(1): 75-84.

Li, X., Chen, W.Y., Sanesi, G., and Lafortezza, R. (2019). Remote Sensing in Urban Forestry: Recent Applications and Future Directions. *Remote Sensing,* 11(10): 1144.

Liu, H., and An, H. (2019). Urban Greening Tree Species Classification Based on HSV Colour Space of WorldView-2. *Journal of the Indian Society of Remote Sensing,* 47(11): 1959-1967.

Liu, L., Coops, N.C., Aven, N.W., and Pang, Y. (2017). Mapping urban tree species using integrated airborne hyperspectral and LiDAR remote sensing data. *Remote Sensing of Environment,* 200: 170-182.

Loozen, Y., Rebel, K.T., De Jong, S.M., Lu, M., Ollinger, S.V., Wassen, M.J., and Karssenberg, D. (2020). Mapping canopy nitrogen in European forests using remote sensing and environmental variables with the random forests method. *Remote Sensing of Environment,* 247: 111933.

Love, S.L., Wimpfheimer, R., and Noble, K. (2009). *Selecting, planting, and caring for trees, shrubs, and vines.* University of Idaho Extension.

Lu, D., and Weng, Q. (2007). A survey of image classification methods and techniques for improving classification performance. *International Journal of Remote Sensing,* 28(5): 823-870.

Luo, S., Wang, C., Xi, X., Zeng, H., Li, D., Xia, S., and Wang, P. (2015). Fusion of Airborne Discrete-Return LiDAR and Hyperspectral Data for Land Cover Classification. *Remote Sensing,* 8(1): 3.

Mabin, A. (2014). In the forest of transformation. Changing Space, Changing City. Wits University Press.

Magidi, J., and Ahmed, F. (2020). Spatio-temporal variations of land surface temperature using Landsat and MODIS: case study of the City of Tshwane, South Africa. *South African Journal of Geomatics,* 9(2): 379-396.

Malvern Panalytical. (2019). *ASD FieldSpec 4 Standard-Res Spectroradiometer.* [Online]. Available: https://www.malvernpanalytical.com/en/products/product-range/asd-range/fieldspec-range/fieldspec-4-standard-res-spectroradiometer [Accessed 10 December 2019].

Manickathan, L., Defraeye, T., Allegrini, J., Derome, D., and Carmeliet, J. (2018). Parametric study of the influence of environmental factors and tree properties on the transpirative cooling effect of trees. *Agricultural and Forest Meteorology,* 248: 259-274.

Marcinkowska-Ochtyra, A., Zagajewski, B., Ochtyra, A., Jarocińska, A., Wojtuń, B., Rogass, C., Mielke, C., and Lavender, S. (2017). Subalpine and alpine vegetation classification based on hyperspectral APEX and simulated EnMAP images. *International Journal of Remote Sensing,* 38(7): 1839-1864.

Maree, G., and Khanyile, S. (2017). *Green vegetation and impervious surfaces in the Gauteng Province.* [Online]. Available: https://www.gcro.ac.za/outputs/map-of-the-month/detail/green-vegetation-and-impervious-surfaces-in-the-gauteng-province/ [Accessed 22 September 2020.

Marzban, F., Sodoudi, S., and Preusker, R. (2017). The influence of land-cover type on the relationship between NDVI–LST and LST-Tair. *International Journal of Remote Sensing,* 39(5): 1377-1398.

Masetic, Z., and Subasi, A. (2016). Congestive heart failure detection using random forest classifier. *Computer Methods and Programs in Biomedicine,* 130: 54-64.

Matasci, G., Coops, N.C., Williams, D.a.R., and Page, N. (2018). Mapping tree canopies in urban environments using airborne laser scanning (ALS): a Vancouver case study. *Forest Ecosystems,* 5(1): 31.

Mavimbela, L.Z., Sieben, E.J.J., and Procheş, Ş. (2018). Invasive alien plant species, fragmentation and scale effects on urban forest community composition in Durban, South Africa. *New Zealand Journal of Forestry Science,* 48(1).

Maxwell, A.E., Warner, T.A., and Fang, F. (2018). Implementation of machine-learning classification in remote sensing: an applied review. *International Journal of Remote Sensing,* 39(9): 2784-2817.

Mcpherson, E.G., and Simpson, J.R. (2003). Potential energy savings in buildings by an urban tree planting programme in California. *Urban Forestry & Urban Greening,* 2(2): 73-86.

Milewski, A., Sultan, M., Jayaprakash, S.M., Balekai, R., and Becker, R. (2009). RESDEM, a tool for integrating temporal remote sensing data for use in hydrogeologic investigations. *Computers & Geosciences,* 35(10): 2001-2010.

Motsatsi, G. (2010). *The role of urban forestry with special emphasis on work carried out by Johannesburg City Parks.* [Online]. Available: http://web.vdw.co.za/Portals/19/Documents/Convention%202010/The%20Role%20Of%20Urban%20Forestry%20-%20Gabriel%20Motsatsi.pdf [Accessed 11 January 2021].

Mountrakis, G., Im, J., and Ogole, C. (2011). Support vector machines in remote sensing: A review. *ISPRS Journal of Photogrammetry and Remote Sensing,* 66(3): 247-259.

Mudede, M.F., Newete, S.W., Abutaleb, K., and Nkongolo, N. (2020). Monitoring the urban environment quality in the city of Johannesburg using remote sensing data. *Journal of African Earth Sciences,* 171.

Mureriwa, N., Adam, E., Sahu, A., and Tesfamichael, S. (2016). Examining the Spectral Separability of Prosopis glandulosa from Co-Existent Species Using Field Spectral Measurement and Guided Regularized Random Forest. *Remote Sensing,* 8(2): 144.

Mushore, T.D., Mutanga, O., Odindi, J., and Dube, T. (2017). Linking major shifts in land surface temperatures to long term land use and land cover changes: A case of Harare, Zimbabwe. *Urban Climate,* 20: 120-134.

Mustafa, Y.T., Habeeb, H.N., Stein, A., and Sulaiman, F.Y. (2015). Identification and mapping of tree species in urban areas using WorldView-2 imagery. *ISPRS Annals of Photogrammetry, Remote Sensing and Spatial Information Sciences,* II-2/W2: 175-181.

Mutanga, O., Adam, E., and Cho, M.A. (2012). High density biomass estimation for wetland vegetation using WorldView-2 imagery and random forest regression algorithm. *International Journal of Applied Earth Observation and Geoinformation,* 18: 399-406.

Mutanga, O., Skidmore, A.K., and Prins, H.H.T. (2004). Predicting in situ pasture quality in the Kruger National Park, South Africa, using continuum-removed absorption features. *Remote Sensing of Environment,* 89(3): 393-408.

Myeong, S., Nowak, D.J., and Duggin, M.J. (2006). A temporal analysis of urban forest carbon storage using remote sensing. *Remote Sensing of Environment,* 101(2): 277-282.

Myint, S.W., Gober, P., Brazel, A., Grossman-Clarke, S., and Weng, Q. (2011). Per-pixel vs. object-based classification of urban land cover extraction using high spatial resolution imagery. *Remote Sensing of Environment,* 115(5): 1145-1161.

Naicker, K., Cukrowska, E., and Mccarthy, T.S. (2003). Acid mine drainage arising from gold mining activity in Johannesburg, South Africa and environs. *Environmental Pollution,* 122(1): 29-40.

Naidoo, L., Cho, M.A., Mathieu, R., and Asner, G. (2012). Classification of savanna tree species, in the Greater Kruger National Park region, by integrating hyperspectral and LiDAR data in a Random Forest data mining environment. *ISPRS Journal of Photogrammetry and Remote Sensing,* 69: 167-179.

Nana, M., Coetzer, K., and Vogel, C. (2019). Facing the heat: initial probing of the City of Johannesburg's heat-health planning. *South African Geographical Journal,* 101(2): 253-268.

Ngie, A. (2020). Thermal Remote Sensing of Urban Climates in South Africa through the Mono-Window Algorithm. *ISPRS - International Archives of the Photogrammetry, Remote Sensing and Spatial Information Sciences,* XLII-3/W11: 117-123.

Ngigi, S.M. (2009). *Establishing effective, appropriate and applicable technologies in treating contaminated surface water as part of a rehabilitation strategy for the Princess dump in Roodepoort, West of Johannesburg.* (Doctoral dissertation). University of the Witwatersrand, Johannesburg.

Nilsson, K., Konijnendijk, C.C., and Nielsen, A.B. (2013). Urban Forest Function, Design and Management. In: Loftness, V. & Haase, D. (eds.). Sustainable Built Environments. New York, NY: Springer New York.

Nimit, K., Masuluri, N.K., Berger, A.M., Bright, R.P., Prakash, S., Tvs, U., T, S.K., Rohit, P., A, T., Ghosh, S., and Varghese, S.P. (2020). Oceanographic preferences of yellowfin tuna (Thunnus albacares) in warm stratified oceans: A remote sensing approach. *International Journal of Remote Sensing,* 41(15): 5785-5805.

Niska, H., Skon, J.-P., Packalen, P., Tokola, T., Maltamo, M., and Kolehmainen, M. (2010). Neural networks for the prediction of species-specific plot volumes using airborne laser scanning and aerial photographs. *IEEE Transactions on Geoscience and Remote Sensing,* 48(3): 1076-1085.

Nordin, S.A., Abd Latif, Z., and Omar, H. (2018). Individual tree crown segmentation in tropical peat swamp forest using airborne hyperspectral data. *Geocarto International*: 1-19.

Novack, T., Esch, T., Kux, H., and Stilla, U. (2011). Machine Learning Comparison between WorldView-2 and QuickBird-2-Simulated Imagery Regarding Object-Based Urban Land Cover Classification. *Remote Sensing,* 3(10): 2263-2282.

Nowak, D.J., Crane, D.E., Stevens, J.C., Hoehn, R.E., Walton, J.T., and Bond, J. (2008). A ground-based method of assessing urban forest structure and ecosystem services. *Arboriculture and Urban Forestry,* 34(6): 347-358.

Odebiri, O., Mutanga, O., Odindi, J., Peerbhay, K., and Dovey, S. (2020). Predicting soil organic carbon stocks under commercial forest plantations in KwaZulu-Natal province, South Africa using remotely sensed data. *GIScience & Remote Sensing*: 1-14.

Odindi, J., Bangamwabo, V., and Mutanga, O. (2015). Assessing the Value of Urban Green Spaces in Mitigating Multi-Seasonal Urban Heat using MODIS Land SurfaceTemperature (LST) and Landsat 8 data. *International Journal of Environmental Research,* 9(1): 9-18.

Odindi, J., Mutanga, O., Abdel-Rahman, E.M., Adam, E., and Bangamwabo, V. (2015). Determination of urban land-cover types and their implication on thermal characteristics in three South African coastal metropolitans using remotely sensed data. *South African Geographical Journal,* 99(1): 52-67.

Odindi, J., Mutanga, O., Rouget, M., and Hlanguza, N. (2016). Mapping alien and indigenous vegetation in the KwaZulu-Natal Sandstone Sourveld using remotely sensed data. *Bothalia,* 46(2).

Odindi, J.O., Adam, E.E., Ngubane, Z., Mutanga, O., and Slotow, R. (2014). Comparison between WorldView-2 and SPOT-5 images in mapping the bracken fern using the random forest algorithm. *Journal of Applied Remote Sensing,* 8(1): 083527.

Oldeland, J., Große-Stoltenberg, A., Naftal, L., and Strohbach, B. (2017). The potential of UAV derived image features for discriminating savannah tree species. The roles of remote sensing in nature conservation. Springer.

Omer, G., Mutanga, O., Abdel-Rahman, E., and Adam, E. (2016). Empirical Prediction of Leaf Area Index (LAI) of Endangered Tree Species in Intact and Fragmented Indigenous Forests Ecosystems Using WorldView-2 Data and Two Robust Machine Learning Algorithms. *Remote Sensing,* 8(4): 324.

Omer, G., Mutanga, O., Abdel-Rahman, E.M., and Adam, E. (2015). Performance of Support Vector Machines and Artificial Neural Network for Mapping Endangered Tree Species Using WorldView-2 Data in Dukuduku Forest, South Africa. *IEEE Journal of Selected Topics in Applied Earth Observations and Remote Sensing,* 8(10): 4825-4840.

Ordóñez, C., Threlfall, C.G., Kendal, D., Hochuli, D.F., Davern, M., Fuller, R.A., Van Der Ree, R., and Livesley, S.J. (2019). Urban forest governance and decision-making: A systematic review and synthesis of the perspectives of municipal managers. *Landscape and Urban Planning,* 189: 166-180.

Paap, T., Burgess, T.I., and Wingfield, M.J. (2017). Urban trees: bridge-heads for forest pest invasions and sentinels for early detection. *Biological Invasions,* 19(12): 3515-3526.

Paap, T., De Beer, Z.W., Migliorini, D., Nel, W.J., and Wingfield, M.J. (2018). The polyphagous shot hole borer (PSHB) and its fungal symbiont Fusarium euwallaceae: a new invasion in South Africa. *Australasian Plant Pathology,* 47(2): 231-237.

Pal, M. (2005). Random forest classifier for remote sensing classification. *International Journal of Remote Sensing,* 26(1): 217-222.

Palinkas, L.A., Horwitz, S.M., Green, C.A., Wisdom, J.P., Duan, N., and Hoagwood, K. (2015). Purposeful sampling for qualitative data collection and analysis in mixed method implementation research. *Administration and Policy in Mental Health and Mental Health Services Research,* 42(5): 533-544.

Patton, M.Q. (2002). Qualitative research and evaluation methods. Thousand Oaks. *Cal.: Sage Publications*.

Paulo, M.J., Tomé, M., Otten, A., and Stein, A. (2005). Comparison of three sampling methods in the characterization of cork oak stands for management purposes. *Canadian Journal of Forest Research,* 35(10): 2295-2303.

Pautasso, M., Schlegel, M., and Holdenrieder, O. (2015). Forest Health in a Changing World. *Microbial Ecology,* 69(4): 826-842.

Peerbhay, K.Y., Mutanga, O., and Ismail, R. (2013). Commercial tree species discrimination using airborne AISA Eagle hyperspectral imagery and partial least squares discriminant analysis (PLS-DA) in KwaZulu–Natal, South Africa. *ISPRS Journal of Photogrammetry and Remote Sensing,* 79: 19-28.

Pretzsch, H., Biber, P., Uhl, E., Dahlhausen, J., Rötzer, T., Caldentey, J., Koike, T., Van Con, T., Chavanne, A., Seifert, T., Toit, B.D., Farnden, C., and Pauleit, S. (2015). Crown size and growing space requirement of common tree species in urban centres, parks, and forests. *Urban Forestry & Urban Greening,* 14(3): 466-479.

Pu, R. (2011). Mapping urban forest tree species using IKONOS imagery: preliminary results. *Environmental monitoring and assessment,* 172(1-4): 199-214.

Pu, R., and Landry, S. (2012). A comparative analysis of high spatial resolution IKONOS and WorldView-2 imagery for mapping urban tree species. *Remote Sensing of Environment,* 124: 516-533.

Pu, R., and Landry, S. (2020). Mapping urban tree species by integrating multi-seasonal high resolution pléiades satellite imagery with airborne LiDAR data. *Urban Forestry & Urban Greening,* 53.

Pu, R., Landry, S., and Yu, Q. (2011). Object-based urban detailed land cover classification with high spatial resolution IKONOS imagery. *International Journal of Remote Sensing,* 32(12): 3285-3308.

Pu, R., Landry, S., and Yu, Q. (2018). Assessing the potential of multi-seasonal high resolution Pléiades satellite imagery for mapping urban tree species. *International Journal of Applied Earth Observation and Geoinformation,* 71: 144-158.

Puissant, A., Rougier, S., and Stumpf, A. (2014). Object-oriented mapping of urban trees using Random Forest classifiers. *International Journal of Applied Earth Observation and Geoinformation,* 26: 235-245.

Qian, Y., Zhou, W., Yan, J., Li, W., and Han, L. (2014). Comparing machine learning classifiers for object-based land cover classification using very high resolution imagery. *Remote Sensing,* 7(1): 153-168.

Qin, Y., Xiao, X., Dong, J., Zhang, G., Roy, P.S., Joshi, P.K., Gilani, H., Murthy, M.S.R., Jin, C., Wang, J., Zhang, Y., Chen, B., Menarguez, M.A., Biradar, C.M., Bajgain, R., Li, X., Dai, S., Hou, Y., Xin, F., and Moore Iii, B. (2016). Mapping forests in monsoon Asia with ALOS PALSAR 50-m mosaic images and MODIS imagery in 2010. *Scientific Reports,* 6: 20880.

Raczko, E., and Zagajewski, B. (2017). Comparison of support vector machine, random forest and neural network classifiers for tree species classification on airborne hyperspectral APEX images. *European Journal of Remote Sensing,* 50(1): 144-154.

Ramon Solano, R., Didan, K., Jacobson, A., and Huete, A. (2010). Modis Vegetation Index User's Guide. *The University of Arizona: Tucson, AZ, USA.*

Ranagalage, M., Murayama, Y., Dissanayake, D., and Simwanda, M. (2019). The Impacts of Landscape Changes on Annual Mean Land Surface Temperature in the Tropical Mountain City of Sri Lanka: A Case Study of Nuwara Eliya (1996–2017). *Sustainability,* 11(19).

Rani, D. (2019). Jacaranda Mimosifolia. D.Don: A powerful solution for environmental degradation caused by urbanization in urban greening. *International Journal for Research in Applied Science and Engineering Technology,* 7: 695-699.

Rao, Y., Dai, J., Dai, D., and He, Q. (2021). Effect of urban growth pattern on land surface temperature in China: A multi-scale landscape analysis of 338 cities. *Land Use Policy,* 103: 105314.

Räsänen, A., Rusanen, A., Kuitunen, M., and Lensu, A. (2013). What makes segmentation good? A case study in boreal forest habitat mapping. *International Journal of Remote Sensing,* 34(23): 8603-8627.

Republic of South Africa. (1996). Constitution of the republic of South Africa. *Cape Town,* 230(38): 1241-1331.

Richardson, J.J., and Moskal, L.M. (2014). Uncertainty in urban forest canopy assessment: Lessons from Seattle, WA, USA. *Urban Forestry & Urban Greening,* 13(1): 152-157.

Roman, L.A., Conway, T.M., Eisenman, T.S., Koeser, A.K., Ordóñez Barona, C., Locke, D.H., Jenerette, G.D., Östberg, J., and Vogt, J. (2020). Beyond 'trees are good': Disservices, management costs, and tradeoffs in urban forestry. *Ambio.*

Rossi, J.-P., Garcia, J., Roques, A., and Rousselet, J. (2015). Trees outside forests in agricultural landscapes: spatial distribution and impact on habitat connectivity for forest organisms. *Landscape Ecology,* 31(2): 243-254.

Rotem-Mindali, O., Michael, Y., Helman, D., and Lensky, I.M. (2015). The role of local land-use on the urban heat island effect of Tel Aviv as assessed from satellite remote sensing. *Applied Geography,* 56: 145-153.

Roy, S., Byrne, J., and Pickering, C. (2012). A systematic quantitative review of urban tree benefits, costs, and assessment methods across cities in different climatic zones. *Urban Forestry & Urban Greening,* 11(4): 351-363.

Ruiz, L.Á., Recio, J.A., Crespo-Peremarch, P., and Sapena, M. (2016). An object-based approach for mapping forest structural types based on low-density LiDAR and multispectral imagery. *Geocarto International,* 33(5): 443-457.

Rutherford, M.C., and Westfall, R.H. (1994). *Biomes of southern Africa: an objective categorization.* National Botanical Institute.

Ryan, J., Estefan, G., and Rashid, A. (2007). Soil and plant analysis laboratory manual. ICARDA Aleppo. Syria.

Salehi, B., Zhang, Y., Zhong, M., and Dey, V. (2012). Object-based classification of urban areas using VHR imagery and height points ancillary data. *Remote Sensing,* 4(8): 2256-2276.

Salih, A.a.M., Ganawa, E.-T., and Elmahl, A.A. (2017). Spectral mixture analysis (SMA) and change vector analysis (CVA) methods for monitoring and mapping land degradation/desertification in arid and semiarid areas (Sudan), using Landsat imagery. *The Egyptian Journal of Remote Sensing and Space Science,* 20: S21-S29.

Schäffler, A., and Swilling, M. (2013). Valuing green infrastructure in an urban environment under pressure — The Johannesburg case. *Ecological Economics,* 86: 246-257.

Scholz, T., Hof, A., and Schmitt, T. (2018). Cooling Effects and Regulating Ecosystem Services Provided by Urban Trees—Novel Analysis Approaches Using Urban Tree Cadastre Data. *Sustainability,* 10(3): 712.

Seiferling, I., Naik, N., Ratti, C., and Proulx, R. (2017). Green streets − Quantifying and mapping urban trees with street-level imagery and computer vision. *Landscape and Urban Planning,* 165: 93-101.

Serpico, S.B., and Bruzzone, L. (2001). A new search algorithm for feature selection in hyperspectral remote sensing images. *IEEE Transactions on Geoscience and Remote Sensing,* 39(7): 1360-1367.

Shackelford, A.K., and Davis, C.H. (2003). A hierarchical fuzzy classification approach for high-resolution multispectral data over urban areas. *IEEE Transactions on Geoscience and Remote Sensing,* 41(9): 1920-1932.

Shackleton, C.M. (2006). Urban forestry–A cinderella science in South Africa? : Taylor & Francis.

Shi, Y., Skidmore, A.K., Wang, T., Holzwarth, S., Heiden, U., Pinnel, N., Zhu, X., and Heurich, M. (2018). Tree species classification using plant functional traits from LiDAR and hyperspectral data. *International Journal of Applied Earth Observation and Geoinformation,* 73: 207-219.

Shojanoori, R., Shafri, H.Z.M., Mansor, S., and Ismail, M.H. (2016). The Use of WorldView-2 Satellite Data in Urban Tree Species Mapping by Object-Based Image Analysis Technique. *Sains Malaysiana,* 45(7): 1025-1034.

Song, C., Jia, L., and Menenti, M. (2013). Retrieving high-resolution surface soil moisture by downscaling AMSR-E brightness temperature using MODIS LST and NDVI data. *IEEE Journal of Selected Topics in Applied Earth Observations and Remote Sensing,* 7(3): 935-942.

Sothe, C., Dalponte, M., Almeida, C.M.D., Schimalski, M.B., Lima, C.L., Liesenberg, V., Miyoshi, G.T., and Tommaselli, A.M.G. (2019). Tree Species Classification in a Highly Diverse Subtropical Forest Integrating UAV-Based Photogrammetric Point Cloud and Hyperspectral Data. *Remote Sensing,* 11(11): 1338.

Soto-Mardones, L., and Maldonado-Ibarra, I. (2015). Spatio-temporal variability of NDVI and land surface temperature in the Maule and Biobío Regions (2000-2012). *Chilean journal of agricultural research,* 75(4): 434-442.

Statistics South Africa. (2011). *City of Johannesburg.* [Online]. Available: http://www.statssa.gov.za/?page_id=4286&id=11307 [Accessed 10 January 2020].

Statistics South Africa. (2020). *City of Johannesburg.* [Online]. Available: http://www.statssa.gov.za/?page_id=993&id=city-of-johannesburg-municipality [Accessed 22 September 2020.

Storie, M. (2014). Changes in the natural landscape. Changing Space, Changing City. Wits University Press.

Sun, C., Cao, S., and Sanchez-Azofeifa, G.A. (2019). Mapping tropical dry forest age using airborne waveform LiDAR and hyperspectral metrics. *International Journal of Applied Earth Observation and Geoinformation,* 83: 101908.

Suppers, A., Van Gool, A.J., and Wessels, H. (2018). Integrated Chemometrics and Statistics to Drive Successful Proteomics Biomarker Discovery. *Proteomes,* 6(2): 20.

Sutter, J.M., and Kalivas, J.H. (1993). Comparison of Forward Selection, Backward Elimination, and Generalized Simulated Annealing for Variable Selection. *Microchemical Journal,* 47(1-2): 60-66.

Symes, C.T., Roller, K., Howes, C., Lockwood, G., and Van Rensburg, B.J. (2017). Grassland to Urban Forest in 150 Years: Avifaunal Response in an African Metropolis. Ecology and Conservation of Birds in Urban Environments.

Thanh Noi, P., and Kappas, M. (2017). Comparison of Random Forest, k-Nearest Neighbor, and Support Vector Machine Classifiers for Land Cover Classification Using Sentinel-2 Imagery. *Sensors,* 18(1): 18.

Thomsen, P., Bühler, O., and Kristoffersen, P. (2016). Diversity of street tree populations in larger Danish municipalities. *Urban Forestry & Urban Greening,* 15: 200-210.

Timilsina, S., Aryal, J., and Kirkpatrick, J.B. (2020). Mapping Urban Tree Cover Changes Using Object-Based Convolution Neural Network (OB-CNN). *Remote Sensing,* 12(18): 3017.

Tochon, G., Féret, J.B., Valero, S., Martin, R.E., Knapp, D.E., Salembier, P., Chanussot, J., and Asner, G.P. (2015). On the use of binary partition trees for the tree crown segmentation of tropical rainforest hyperspectral images. *Remote Sensing of Environment,* 159: 318-331.

Turton, A., Schultz, C., Buckle, H., Kgomongoe, M., Malungani, T., and Drackner, M. (2006). Gold, scorched earth and water: the hydropolitics of Johannesburg. *Water Resources Development,* 22(2): 313-335.

Tyrväinen, L., Pauleit, S., Seeland, K., and De Vries, S. (2005). Benefits and uses of urban forests and trees. Urban forests and trees. Berlin, Heidelberg: Springer.

Tyson, P.D., and Wilcocks, J.R.N. (1971). Rainfall variation over Johannesburg—the local climate over Johannesburg. *University of Witwatersrand: Johannesburg, South Africa.*

Tzotsos, A., and Argialas, D. (2006). MSEG: A generic region-based multi-scale image segmentation algorithm for remote sensing imagery. Proceedings of ASPRS 2006 Annual Conference, Reno, Nevada.

United Nations Publications. (2019). *World Urbanization Prospects: The 2018 Revision.* UN.

Van Wilgen, B.W. (2012). Evidence, Perceptions, and Trade-offs Associated with Invasive Alien Plant Control in the Table Mountain National Park, South Africa. *Ecology and society,* 17(2).

Van Wilgen, B.W., and Richardson, D.M. (2014). Challenges and trade-offs in the management of invasive alien trees. *Biological Invasions,* 16(3): 721-734.

Vapnik, V. (1995). *The nature of statistical learning theory.* Springer New York.

Varin, M., Chalghaf, B., and Joanisse, G. (2020). Object-Based Approach Using Very High Spatial Resolution 16-Band WorldView-3 and LiDAR Data for Tree Species Classification in a Broadleaf Forest in Quebec, Canada. *Remote Sensing,* 12(18).

Vidhya, R., Vijayasekaran, D., and Ramakrishnan, S.S. (2017). Mapping invasive plant Prosopis juliflora in arid land using high resolution remote sensing data and biophysical parameters. *INDIAN J. MAR. SCI.,* 46(06): 10.

Wan, Z. (2006). MODIS land surface temperature products users' guide. *Institute for Computational Earth System Science, University of California: Santa Barbara, CA, USA.*

Wang, B.H., Wang, D.B., Ali, Z.A., Ting Ting, B., and Wang, H. (2019). An overview of various kinds of wind effects on unmanned aerial vehicle. *Measurement and Control,* 52(7-8): 731-739.

Wang, K., Wang, T., and Liu, X. (2018). A Review: Individual Tree Species Classification Using Integrated Airborne LiDAR and Optical Imagery with a Focus on the Urban Environment. *Forests,* 10(1).

Wang, L., Sousa, W.P., and Gong, P. (2004). Integration of object-based and pixel-based classification for mapping mangroves with IKONOS imagery. *International Journal of Remote Sensing,* 25(24): 5655-5668.

Wapwera, S., and Egbu, C. (2013). Planning authorities: A review of roles, functions and responsibilities in Jos Metropolis, Nigeria. *The Built & Human Environment Review,* 6(1): 55-70.

Waser, L.T., Küchler, M., Jütte, K., and Stampfer, T. (2014). Evaluating the potential of WorldView-2 data to classify tree species and different levels of ash mortality. *Remote Sensing,* 6(5): 4515-4545.

Wehr, A., and Lohr, U. (1999). Airborne laser scanning—an introduction and overview. *ISPRS Journal of Photogrammetry and Remote Sensing,* 54(2-3): 68-82.

Wen, D., Huang, X., Liu, H., Liao, W., and Zhang, L. (2017). Semantic Classification of Urban Trees Using Very High Resolution Satellite Imagery. *IEEE Journal of Selected Topics in Applied Earth Observations and Remote Sensing,* 10(4): 1413-1424.

Wężyk, P., Hawryło, P., Szostak, M., Zięba-Kulawik, K., Winczek, M., Siedlarczyk, E., Kurzawiński, A., Rydzyk, J., Kmiecik, J., and Gilewski, W. (2019). Using LiDAR Point Clouds in Determination of the Scots Pine Stands Spatial Structure Meaning in the Conservation of Lichen Communities in "Bory Tucholskie" National Park. *Archives of Photogrammetry, Cartography and Remote Sensing,* 31(1): 85-103.

World Bank (2019). Urban population - South Africa. The World Bank Group.

Wu, J., Yao, W., and Polewski, P. (2018). Mapping Individual Tree Species and Vitality along Urban Road Corridors with LiDAR and Imaging Sensors: Point Density versus View Perspective. *Remote Sensing,* 10(9).

Xiao, Q., and Mcpherson, E.G. (2005). Tree health mapping with multispectral remote sensing data at UC Davis, California. *Urban Ecosystems,* 8(3-4): 349-361.

Xiaoye, L. (2008). Airborne LiDAR for DEM generation: some critical issues. *Progress in Physical Geography: Earth and Environment,* 32(1): 31-49.

Xu, C., Dai, F., Xu, X., and Lee, Y.H. (2012). GIS-based support vector machine modeling of earthquake-triggered landslide susceptibility in the Jianjiang River watershed, China. *Geomorphology,* 145-146: 70-80.

Xu, F., Hao, Z., Huang, L., Liu, M., Chen, T., Chen, J., Zhang, L., Zhou, H., and Yao, M. (2020). Comparative identification of citrus huanglongbing by analyzing leaves using laser-induced breakdown spectroscopy and near-infrared spectroscopy. *Applied Physics B,* 126(3): 1-7.

Xue, J., and Su, B. (2017). Significant Remote Sensing Vegetation Indices: A Review of Developments and Applications. *Journal of Sensors,* 2017: 1-17.

Yan, J., Zhou, W., Han, L., and Qian, Y. (2018). Mapping vegetation functional types in urban areas with WorldView-2 imagery: Integrating object-based classification with phenology. *Urban Forestry & Urban Greening,* 31: 230-240.

Yan, W.Y., Shaker, A., and El-Ashmawy, N. (2015). Urban land cover classification using airborne LiDAR data: A review. *Remote Sensing of Environment,* 158: 295-310.

Yu, Q., Gong, P., Tian, Y.Q., Pu, R., and Yang, J. (2008). Factors affecting spatial variation of classification uncertainty in an image object-based vegetation mapping. *Photogrammetric Engineering & Remote Sensing,* 74(8): 1007-1018.

Yuan, X., King, D., and Vlcek, J. (1991). Sugar maple decline assessment based on spectral and textural analysis of multispectral aerial videography. *Remote Sensing of Environment,* 37(1): 47-54.

Yue, W., Xu, J., Tan, W., and Xu, L. (2007). The relationship between land surface temperature and NDVI with remote sensing: application to Shanghai Landsat 7 ETM+ data. *International Journal of Remote Sensing,* 28(15): 3205-3226.

Zengeya, T., Ivey, P., Woodford, D.J., Weyl, O., Novoa, A., Shackleton, R., Richardson, D., and Van Wilgen, B. (2017). Managing conflict-generating invasive species in South Africa: Challenges and trade-offs. *Bothalia-African Biodiversity & Conservation,* 47(2): 1-11.

Zhang, C., Chen, Y.L., and Lu, D.S. (2015). Mapping the land-cover distribution in arid and semiarid urban landscapes with Landsat Thematic Mapper imagery. *International Journal of Remote Sensing,* 36(17): 4483-4500.

Zhang, C., and Qiu, F. (2012). Mapping Individual Tree Species in an Urban Forest Using Airborne Lidar Data and Hyperspectral Imagery. *Photogrammetric Engineering & Remote Sensing,* 78(10): 1079-1087.

Zhang, C., Zhou, Y., and Qiu, F. (2015). Individual Tree Segmentation from LiDAR Point Clouds for Urban Forest Inventory. *Remote Sensing,* 7(6): 7892-7913.

Zhang, L.-W., Huang, J.-F., Guo, R.-F., Li, X.-X., Sun, W.-B., and Wang, X.-Z. (2013). Spatio-temporal reconstruction of air temperature maps and their application to estimate rice growing season heat accumulation using multi-temporal MODIS data. *Journal of Zhejiang University SCIENCE B,* 14(2): 144-161.

Zhou, W., Wang, J., and Cadenasso, M.L. (2017). Effects of the spatial configuration of trees on urban heat mitigation: A comparative study. *Remote Sensing of Environment,* 195: 1-12.

Zhou, X., Jancso, T., Chen, C., and Verone, M. (2012). Urban land cover mapping based on object oriented classification using WorldView 2 satellite remote sensing images. International scientific conference on sustainable development & ecological footprint.

Zhou, Z., Morel, J., Parsons, D., Kucheryavskiy, S.V., and Gustavsson, A.-M. (2019). Estimation of yield and quality of legume and grass mixtures using partial least squares and support vector machine analysis of spectral data. *Computers and Electronics in Agriculture,* 162: 246-253.

Zhu, G., and Blumberg, D.G. (2002). Classification using ASTER data and SVM algorithms: The case study of Beer Sheva, Israel. *Remote Sensing of Environment,* 80(2): 233-240.

Zovko, M., Žibrat, U., Knapič, M., Kovačić, M.B., and Romić, D. (2019). Hyperspectral remote sensing of grapevine drought stress. *Precision Agriculture,* 20(2): 335-347.